

FINITE AMPLITUDE HARBOR OSCILLATIONS:
THEORY AND EXPERIMENT

by

STEVEN R. ROGERS

S.B., Massachusetts Institute of Technology
(1972)

Submitted in partial fulfillment
of the requirements for the degree of
Doctor of Science
at the
Massachusetts Institute of Technology
(January, 1977)

Signature redacted

Signature of Author Department of Physics, January, 1977

Signature redacted

Certified by Thesis Supervisor

Signature redacted

Accepted by Chairman, Department of Physics



FINITE AMPLITUDE HARBOR OSCILLATIONS:
THEORY AND EXPERIMENT

by

STEVEN R. ROGERS

Submitted to the Department of Physics
on January 13, 1977 in partial fulfillment of the requirements
for the Degree of Doctor of Science

ABSTRACT

A nonlinear theory of finite amplitude, time-periodic oscillations in a narrow harbor is developed, starting from the Boussinesq equations for shallow water waves. The narrowness of the harbor permits a linear treatment of radiation damping and a one-dimensional treatment of the nonlinear harbor response. The wave field in the harbor is expanded in harmonics, whose spatial dependence is governed by a set of coupled, nonlinear ordinary differential equations, subject to two-point boundary conditions. Solutions are obtained by analytical perturbation techniques and by an iterative numerical procedure. Results indicate significant nonlinear effects at large amplitudes.

Harbor resonance experiments were carried out using a model harbor placed in a large, shallow wave basin. The effects of boundary layer dissipation, flow separation, and spurious reflections in the wave basin are analyzed. The experimental observations are found to agree reasonably well with the proposed nonlinear theory.

Finally, the nonlinear theory is applied to large-scale harbors and some theoretical predictions are presented.

Thesis Supervisor: Chiang C. Mei, Professor of Civil Engineering

ACKNOWLEDGEMENTS

The author wishes to express his appreciation to the Fannie and John Hertz Foundation for a generous fellowship which enabled him to devote full time to his studies, and to the Fluid Dynamics Branch of the Office of Naval Research (Contract N062-228) for providing funds for laboratory supplies and computer time.

Many members of the Ralph M. Parsons Laboratory for Water Resources and Hydrodynamics gave of their time and knowledge to assist in this endeavor. Among them are Mr. Edward F. McCaffrey (Research Engineer) and Mr. Stanley M. White, who designed the data acquisition system used in the experiments, and Mr. Roy G. Milley, who helped with the construction of the experimental apparatus. Mrs. Elizabeth A. Quivey did a superb job typing the manuscript.

I would especially like to thank Mr. Dick K.-P. Yue and Mr. Demosthenes C. Angelides for many valuable discussions, and for their enthusiasm and fine sense of humor.

Professor Chiang C. Mei, who supervised this work, has been a constant source of inspiration and guidance. I am deeply grateful for his time, his encouragement, and, most of all, his friendship.

To my parents, who have taught me the importance of education, I am eternally grateful.

Finally, I should like to dedicate this work to my wife, Rahel, whose patience, understanding, and devotion have really made it all possible.

TABLE OF CONTENTS

	<u>Page</u>
TITLE PAGE	1
ABSTRACT	2
ACKNOWLEDGEMENTS	4
TABLE OF CONTENTS	5
LIST OF FIGURES	7
LIST OF TABLES	12
CAST OF CHARACTERS	13
1. INTRODUCTION	15
1.1 Description of the Problem and Review of Literature	15
1.2 Elements of Water Wave Theory	17
1.3 Linearized Theory of the Long, Narrow Bay	26
1.4 Scope of this Investigation	30
2. WAVE SYSTEM OF THE OCEAN	32
2.1 Motivation for a Linear Treatment	32
2.2 The Radiated Wave	33
2.3 The Impedance Boundary Condition	36
2.4 On the Validity of the Linear Approximation	40
3. RESONANT OSCILLATIONS OF A LONG, NARROW BAY	42
3.1 Reduction to One Space Dimension	42
3.2 Equations Governing Time-Periodic Solutions	44
3.3 Regular Perturbation Analysis for the Lowest Resonant Modes or for Very Small Amplitude Waves	48
3.4 An Energy Theorem and Relation to the Korteweg-de Vries Equation	61

	<u>Page</u>
3.5 Numerical Solution by Iteration	68
4. EXPERIMENTAL STUDY OF THE LONG, NARROW BAY	75
4.1 Equipment and Procedures	75
4.1.1 Wave Basin	75
4.1.2 Wave Gauges	77
4.1.3 On-line Digital Computer	77
4.1.4 Model Harbor	79
4.2 Multiple Reflections from Wavemaker	80
4.3 Real Fluid Effects	89
4.3.1 Viscous Dissipation in Wall Boundary Layers	89
4.3.2 Separation Loss at the Entrance	93
5. EXPERIMENTAL AND THEORETICAL RESULTS	101
5.1 Comparison of Theory with Experiment	101
5.2 Some Theoretical Predictions for a Large Scale Harbor	131
6. CONCLUDING REMARKS	162
6.1 Validity of the Various Approximations	162
6.2 On the Importance of Nonlinear and Frictional Effects	163
6.3 Suggestions for Future Research	164
LIST OF REFERENCES	167
APPENDIX A: Numerical Iteration Procedure for Solving a Nonlinear, Two-Point Boundary Value Problem	171
APPENDIX B: Fourier Analysis of Experimental Data	182
BIOGRAPHY	184

LIST OF FIGURES

<u>Figure</u>	<u>Page</u>
1.1	Geometry of long, narrow bay. 27
3.1	Regular perturbation theory: Frequency response of large-scale harbor ($h = 20$ m., $2a = 100$ m., $L = 1000$ m., $A_1 = .03$).
(a)	First harmonic amplitude at the back wall. 52
(b)	Second harmonic amplitude at the back wall. 53
(c)	Zeroth harmonic amplitude at the back wall. 54
3.2	Regular perturbation theory: First resonant mode of large scale harbor ($h = 20$ m., $2a = 100$ m., $L = 1000$ m., $A_1 = .03$, $\lambda = 1.41$).
(a)	Spatial variation of the harmonics. 55
(b)	Surface profiles at times $t = m\pi/4$, $m = 0,1,2\dots7$. 56
3.3	Regular perturbation theory: Second resonant mode of large-scale harbor ($h = 20$ m., $2a = 100$ m., $L = 1000$ m., $A_1 = .03$, $\lambda = 4.36$).
(a)	Spatial variation of the harmonics. 57
(b)	Surface profiles at times $t = m\pi/4$, $m = 0,1,2\dots7$. 58
3.4	Regular perturbation theory: Third resonant mode of large-scale harbor ($h = 20$ m., $2a = 100$ m., $L = 1000$ m., $A_1 = .03$, $\lambda = 7.36$).
(a)	Spatial variation of the harmonics. 59
(b)	Surface profiles at times $t = m\pi/4$, $m = 0,1,2\dots7$. 60
4.1	Experimental set-up. 76
4.2	Typical calibration curves of a wave gauge, at two attenuator settings. 78

<u>Figure</u>		<u>Page</u>
4.3	Theoretical study of multiple reflections from wavemaker: Placement of images.	83
4.4	Experiment (·) vs. theory (-) for the wave amplitude in the ocean ($h = .5$ ft., $2a = .33$ ft., $L = 1.211$ ft., $\omega = 4.067$ sec ⁻¹ , $L_m = 31.17$ ft.). Top: harbor closed. Middle: harbor open. Bottom: the radiated wave.	
	(a) $A_1 = .015$	86
	(b) $A_1 = .027$	87
	(c) $A_1 = .040$	88
4.5	Entrance loss: Normalized first harmonic amplitude, $ T/T_0 $, vs. normalized friction factor, α .	100
5.1	Experiment vs. inviscid nonlinear theory ($\bar{f} = 0$). ($\Delta, +, x$): measured, first, second, and third harmonic amplitudes. (—): nonlinear theory. (----): linear theory for first harmonic amplitude.	
	(a) $L = 1.211$ ft., $A_1 = .015$	107
	(b) $L = 1.211$ ft., $A_1 = .027$	108
	(c) $L = 1.211$ ft., $A_1 = .040$	109
	(d) $L = 4.173$ ft., $A_1 = .015$	110
	(e) $L = 4.173$ ft., $A_1 = .027$	111
	(f) $L = 4.173$ ft., $A_1 = .040$	112
	(g) $L = 7.136$ ft., $A_1 = .015$	113
	(h) $L = 7.136$ ft., $A_1 = .027$	114
	(i) $L = 7.136$ ft., $A_1 = .040$	115
5.2	Experiment vs. inviscid nonlinear theory ($\bar{f} = 0$) with exact dispersion relation. ($\Delta, +, x$): measured first, second, and third harmonic amplitudes. (—): nonlinear theory. (----): linear theory for first harmonic amplitude.	
	(a) $L = 4.173$ ft., $A_1 = .015$	116

<u>Figure</u>		<u>Page</u>
5.2	(b) $L = 4.173$ ft., $A_1 = .027$	117
	(c) $L = 4.173$ ft., $A_1 = .040$	118
5.3	Experiment vs. nonlinear theory with separation loss ($\bar{f} = .35$). ($\Delta, +, x$): measured first, second, and third harmonic amplitudes. (—): nonlinear theory. (----): linear theory for first harmonic amplitude.	
	(a) $L = 1.211$ ft., $A_1 = .015$	119
	(b) $L = 1.211$ ft., $A_1 = .027$	120
	(c) $L = 1.211$ ft., $A_1 = .040$	121
	(d) $L = 4.173$ ft., $A_1 = .015$	122
	(e) $L = 4.173$ ft., $A_1 = .027$	123
	(f) $L = 4.173$ ft., $A_1 = .040$	124
	(g) $L = 7.136$ ft., $A_1 = .015$	125
	(h) $L = 7.136$ ft., $A_1 = .027$	126
	(i) $L = 7.136$ ft., $A_1 = .040$	127
5.4	Experiment vs. nonlinear theory with separation loss ($\bar{f} = .35$) and exact dispersion relation. ($\Delta, +, x$): measured first, second and third harmonic amplitudes. (—): nonlinear theory. (----): linear theory for first harmonic amplitude.	
	(a) $L = 4.173$ ft., $A_1 = .015$	128
	(b) $L = 4.173$ ft., $A_1 = .027$	129
	(c) $L = 4.173$ ft., $A_1 = .040$	130
5.5	Inviscid nonlinear theory ($\bar{f} = 0$): Frequency response of large-scale harbor ($h = 20$ m., $2a = 100$ m., $L = 1000$ m., $A_1 = .03$).	
	(a) Number of harmonics, N^* , required in the numerical solutions.	137

<u>Figure</u>		<u>Page</u>
5.5	(b) First harmonic amplitude at the back wall according to nonlinear theory (Δ) and regular perturbation theory ($—$).	138
	(c) Second harmonic amplitude at the back wall according to nonlinear theory (+) and regular perturbation theory ($—$).	139
	(d) Third harmonic amplitude at the back wall according to nonlinear theory (x).	140
	(e) Zeroth harmonic at the back wall according to nonlinear theory (Δ) and regular perturbation theory ($—$).	141
5.6	Inviscid nonlinear theory ($\bar{f} = 0$): First resonant mode of large scale harbor ($h = 20$ m., $2a = 100$ m., $L = 1000$ m., $A_1 = .03$, $\lambda = 1.41$).	
	(a) Spatial variation of the lower harmonics.	142
	(b) Spatial variation of the higher harmonics.	143
	(c) Surface profiles at times $t = m\pi/4$, $m = 0,1,2\dots7$.	144
5.7	Inviscid nonlinear theory ($\bar{f} = 0$): Second resonant mode of large-scale harbor ($h = 20$ m., $2a = 100$ m., $L = 1000$ m., $A_1 = .03$, $\lambda = 4.36$).	
	(a) Spatial variation of the lower harmonics.	145
	(b) Spatial variation of the higher harmonics.	146
	(c) Surface profiles at times $t = m\pi/4$, $m = 0,1,2\dots7$.	147
5.8	Inviscid nonlinear theory ($\bar{f} = 0$): Third resonant mode of large-scale harbor ($h = 20$ m., $2a = 100$ m., $L = 1000$ m., $A_1 = .03$, $\lambda = 7.36$).	
	(a) Spatial variation of the lower harmonics.	148
	(b) Spatial variation of the higher harmonics.	149
	(c) Surface profiles at times $t = m\pi/4$, $m = 0,1,2\dots7$.	150

<u>Figure</u>		<u>Page</u>
5.9	First harmonic amplitude at the back wall of the large-scale harbor vs. incident wave amplitude. (----): linear theory. (Δ): inviscid nonlinear theory ($\bar{f} = 0$). (x): nonlinear theory with separation loss ($\bar{f} = .35$).	151
5.10	Nonlinear theory with separation loss ($\bar{f} = .35$): First resonant mode of large-scale harbor ($h = 20$ m., $2a = 100$ m., $L = 1000$ m., $A_1 = .03$, $\lambda = 1.41$).	
	(a) Spatial variation of the lower harmonics.	152
	(b) Spatial variation of the higher harmonics.	153
	(c) Surface profiles at times $t = m\pi/4$, $m = 0,1,2\dots7$.	154
5.11	Nonlinear theory with separation loss ($\bar{f} = .35$): Second resonant mode of large-scale harbor ($h = 20$ m., $2a = 100$ m., $L = 1000$ m., $A_1 = .03$, $\lambda = 4.36$).	
	(a) Spatial variation of the lower harmonics.	155
	(b) Spatial variation of the higher harmonics.	156
	(c) Surface profiles at times $t = m\pi/4$, $m = 0,1,2\dots7$.	157
5.12	Nonlinear theory with separation loss ($\bar{f} = .35$): Third resonant mode of large-scale harbor ($h = 20$ m., $2a = 100$ m., $L = 1000$ m., $A_1 = .03$, $\lambda = 7.36$).	
	(a) Spatial variation of the lower harmonics.	158
	(b) Spatial variation of the higher harmonics.	159
	(c) Surface profiles at times $t = m\pi/4$, $m = 0,1,2\dots7$.	160
5.13	Response of large-scale harbor to nonmonochromatic incident wave ($h = 20$ m., $2a = 100$ m., $L = 1000$ m., $A_2 = .050$, $A_3 = .015$, $\lambda = 1.41$).	161

LIST OF TABLES

<u>Table</u>		<u>Page</u>
2.1	Orders of Magnitude of Incident, Reflected, and Radiated Waves in the Ocean	40
5.1	Composition of the Incident Waves Used in the Experiments	102
5.2	Exact and Approximate (Boussinesq) Wavenumbers in the Experiments	103
5.3	Resonant Modes of the Large Scale Harbor According to Linearized Theory	131

CAST OF CHARACTERS

Symbol

a	Half-width of narrow bay
A	Twice the incident wave amplitude
$e_n(x)$	Basis function in the numerical scheme
E	Energy density averaged over time
f, f_1, f_2 \bar{f}, \tilde{f}	Friction parameters
g	Acceleration of gravity
G	Green's function
h	Depth of water
H	Interval size in finite difference mesh
$H_0^{(1)}$	Zeroth order Hankel function of first kind
k	Wavenumber
k_c	Minimum wavenumber for cross modes
ℓ, L	Dimensionless and dimensional harbor length
ℓ_M, L_M	Dimensionless and dimensional length of model ocean
$()_n$	the n -th harmonic of $()$
\vec{n}_S	A vector normal to surface S
N^*	Number of harmonics present in a numerical solution
NPT	Number of points in the finite difference mesh
p	Pressure
P_R	Radiated power
P_V	Power dissipated in viscous boundary layer
Q	Source strength for radiated wave

Symbol

r	Radial coordinate
R_c	Critical Reynolds number
R_{ns}, S_{ns}	Coupling constants in the nonlinear equations
t	Time coordinate
T, T_0	Coefficient of first harmonic, in linearized theory
\vec{u}	Velocity vector
U	Horizontal velocity in harbor entrance
x	Horizontal coordinate
x^*	Near field x-coordinate
\bar{x}	A slow scale in x , e.g. $\bar{x} = \epsilon x$
y	Horizontal coordinate
y^*	Near field y-coordinate
z	Vertical coordinate
Z	Radiation impedance
α	Normalized separation loss parameter
δ	Dimensionless half-width of narrow bay
δ_v	Boundary layer thickness
$\vec{\nabla}$	Two-dimensional gradient operator = $(\frac{\partial}{\partial x}, \frac{\partial}{\partial y})$
ϵ	Nonlinearity parameter
η	Surface elevation
λ	A relaxation parameter; also wavelength
μ^2	Dispersion parameter
ν	Viscosity
ρ	Fluid density
ϕ	Velocity potential; also a phase angle
ω	Circular frequency

CHAPTER 1
INTRODUCTION

1.1 Description of the Problem and Review of Literature

A harbor is a partially enclosed body of water which is joined to the sea by a relatively narrow entrance. The entrance, which is quite often a man-made system of breakwaters, serves to shield the harbor from the most common disturbances, namely wind-generated waves of the open sea. Because it limits the amount of energy exchange between the harbor and the sea, a narrow entrance occasionally has the damaging effect of trapping long waves, which may be originated by tsunamis, surf beats or other sources, and of creating within the harbor large oscillations which may persist for days. This is the phenomenon of harbor resonance or "seiching." The deleterious effects of these oscillations are well-known--ships are torn loose from their moorings causing damage to dock facilities and neighboring vessels, and strong currents in the harbor entrance prevent the safe passage of incoming and outgoing ships, cf. Wilson (1957).

From a theoretical standpoint, the study of harbor oscillations begins with the determination of the frequencies at which resonance occurs and the wave profiles of the resonant modes. Much of the work to date uses linearized, inviscid wave theory, in which the wave amplitude is presumed so small that nonlinear effects are negligible. Rectangular harbors were studied by Miles and Munk (1961), Ippen and Raichlen (1962), Ippen and Goda (1963), Raichlen and Ippen (1965), and Mei and Unluata

(1976). Miles and Munk discovered the peculiar phenomenon, referred to as the "harbor paradox," that the amplitude of monochromatic resonant oscillations actually increases with decreasing width of the harbor entrance. For harbors of arbitrary shape, numerical solution procedures have been developed by Hwang and Tuck (1970), Lee (1971), and Chen and Mei (1974).

The validity of all treatments based upon linearized wave theory is necessarily limited by the assumption of small wave amplitudes. Frequently, the resonated wave heights predicted by these theories are so large that it is no longer justifiable to neglect nonlinear effects. Some attempt to include nonlinear effects in the analysis of harbor resonance was made by Gaillard (1960) and Biesel (1963), but complete solutions were not obtained. The general properties of nonlinear waves, and of water waves in particular, have been studied extensively by Phillips (1960), Longuet-Higgins (1962), Benney and Luke (1964), Whitham (1965, 1967 a,b), Benjamin and Feir (1967), Chu and Mei (1970), Kim and Hanratty (1971), Mei and Unluata (1972), Bryant (1972), etc. A review article by Phillips (1974) is especially useful. For the most part, these authors restrict their attention to progressive waves traveling in an infinite medium having no obstacles in the path of propagation. Finite amplitude standing waves in a basin have been treated by Tadjbakhsh and Keller (1960), Benney and Niell (1962), and by Verhagen and van Wijngaarden (1965), who also performed several experiments.

Laboratory investigations of harbor resonance have been hampered by several difficulties, among them inadequate modelling of the ocean

domain and Reynolds number dissimilarity. Biesel (1954) discusses the similitude of scale models for the study of harbor oscillations. Ippen and Raichlen (1962) and Raichlen and Ippen (1965) investigate the problem of coupling between a large but finite ocean basin and a smaller harbor basin. Ippen and Goda (1963) and Lee (1971) performed experiments to corroborate their theoretical work on harbor resonance. Much of this experimental work is indirectly predicated on the assumptions of linearized theory. For example, it is assumed that the response of a harbor to monochromatic incident waves is itself monochromatic so that wave records need not be Fourier analyzed. Further, the experiments are often conveniently performed in deep water, because the extrapolation to shallow water is trivial in the context of linearized theory. For nonlinear theory, this extrapolation cannot be made.

1.2 Elements of Water Wave Theory

In a wide variety of water wave problems, the fluid motion is essentially incompressible, inviscid, and irrotational. For constant depth, the governing equations are

$$\begin{aligned}
 \nabla^2 \phi + \phi_{zz} &= 0 && \text{in fluid} && -h \leq z \leq \eta(x,y,t) \\
 \phi_z &= 0 && \text{on } z = -h \\
 \eta_t + \phi_x \eta_x + \phi_y \eta_y &= \phi_z && \text{on } z = \eta(x,y,t) \\
 \phi_t + \frac{1}{2}(\phi_z^2 + (\nabla\phi)^2) + g\eta &= 0 && \text{on } z = \eta(x,y,t) && (1.2.1)
 \end{aligned}$$

where

$\eta(x,y,t)$ = displacement of the free surface from its undisturbed position

$\vec{u}(x,y,z,t) = (\phi_x, \phi_y, \phi_z)$ = fluid velocity

$\phi(x,y,z,t)$ = velocity potential

g = acceleration of gravity

h = water depth

$$\vec{\nabla} = \left(\frac{\partial}{\partial x}, \frac{\partial}{\partial y} \right)$$

Subscripts are used to denote differentiation. (1.2.1a) is the consequence of continuity for an incompressible fluid and irrotationality; (1.2.1b) states that the vertical component of velocity must vanish at the bottom; (1.2.1c) is the kinematic free surface boundary condition which ensures that particles on the free surface move tangentially to it; and (1.2.1d) is the dynamic boundary condition stating that atmospheric pressure is constant (e.g., zero) on the free surface and that surface tension is negligible. Note that the two boundary conditions on the free surface are nonlinear because both ϕ and η are unknown.

In linearized wave theory, the wave amplitude is assumed to be infinitesimal and (1.2.1c,d) are replaced by

$$\begin{aligned} \eta_t - \phi_z &= 0 & \text{on } z = 0 \\ \phi_t + g\eta &= 0 & \text{on } z = 0 \end{aligned} \quad (1.2.2)$$

In an infinite ocean of constant depth h , one solution to (1.2.1a,b) and (1.2.2a,b) is the monochromatic progressive wave

$$\begin{aligned} \eta(x,y,t) &= \text{Re} \{ A e^{i(kx - \omega t)} \} \\ \phi(x,y,z,t) &= \text{Re} \left\{ \frac{-igA}{\omega} \frac{\cosh k(z+h)}{\cosh kh} e^{i(kx - \omega t)} \right\} \end{aligned} \quad (1.2.3)$$

where

$$\omega^2 h/g = kh \tanh kh \equiv \mu^2 \quad (1.2.4)$$

is the dispersion relation. In deep water, $\mu^2 \gg 1$, the dispersion relation is approximately $\omega^2 h/g = kh$, and the phase velocity is twice the group velocity. In shallow water, $\mu^2 \ll 1$,

$$\omega^2 h/g = (kh)^2 [1 - \frac{1}{3}(kh)^2 + O(kh)^4] \approx (kh)^2 \quad (1.2.5)$$

the dispersion relation is approximately linear; the phase and group velocities are both equal to $\sqrt{gh} (1 + O(kh)^2)$; and the waves are said to be non-dispersive. For intermediate values of μ , ω is a transcendental function of kh , and the waves are highly dispersive.

When the assumption of infinitesimal wave amplitudes is removed, the nonlinearity parameter

$$\epsilon \equiv A/h = \text{wave height/water depth}$$

is also needed to characterize the wave. Different wave motions are possible depending on the relative magnitudes of ϵ and μ^2 . In deep water, the combination $\epsilon\mu^2$, which is a measure of the slope of the free surface, is found to be of great importance in determining when a wave will break. In shallow water, the combination ϵ/μ^2 , known as Stokes' number, is used to identify three qualitatively different kinds of waves:

$\epsilon/\mu^2 \ll 1$: Linear, dispersive waves (Linearized theory)

$\epsilon/\mu^2 \sim O(1)$: Nonlinear dispersive waves, including cnoidal and solitary waves (Boussinesq and Korteweg-de Vries equations)

$\epsilon/\mu^2 \gg 1$: Nonlinear, nondispersive waves (Airy's equations)

In treating harbor resonance, we deal almost exclusively with shallow water, or "long" waves. This is because the wavelengths of resonant harbor oscillations are on the scale of the horizontal dimensions of the harbor, which are normally much greater than the water depth. For example, a harbor might be two kilometers long and only twenty meters deep, so that $\mu^2 \sim 10^{-4}$ for the lower resonant modes. It is useful then to have a theory in which the assumption of shallow water is built-in, but the assumption of infinitesimal wave amplitudes is not.

To derive such a theory, we introduce scaled variables so that the relative magnitudes of terms in the equations of motion appear explicitly. For a shallow water wave of frequency ω , an appropriate choice of variables is

$$\begin{aligned}t' &= \omega t \\(x', y') &= \frac{\omega}{\sqrt{gh}} (x, y) \\z' &= z/h \\ \eta' &= \eta/h \\ \vec{u}' &= \vec{u}/\sqrt{gh} \\ \phi' &= \omega\phi/gh\end{aligned} \tag{1.2.6}$$

where primes denote dimensionless variables. Henceforth, all variables are dimensionless, and for convenience, the primes will be omitted. Substituting (1.2.6) into (1.2.1), the equations of motion take the dimensionless form:

$$\nabla^2 + \frac{1}{2} \phi_{zz} = 0 \quad (-1 \leq z \leq \eta)$$

$$\begin{aligned} \phi_z &= 0 && \text{on } z = -1 \\ \eta_t + \phi_x \eta_x + \phi_y \eta_y &= \frac{1}{2} \phi_z && \text{on } z = \eta \end{aligned} \quad (1.2.7)$$

$$\phi_t + \frac{1}{2} (\vec{\nabla} \phi)^2 + \frac{1}{2\mu^2} \phi_z^2 + \eta = 0 \quad \text{on } z = \eta$$

where $\mu^2 \equiv \omega^2 h/g$, $\vec{\nabla} \equiv (\frac{\partial}{\partial x}, \frac{\partial}{\partial y})$, and $\nabla^2 \equiv \frac{\partial^2}{\partial x^2} + \frac{\partial^2}{\partial y^2}$. Expanding

$$\phi(x,y,z,t) = \sum_{n=0}^{\infty} \mu^{2n} \phi^{(n)}(x,y,z,t) \quad (1.2.8)$$

we find from (1.2.7a) that

$$\begin{aligned} \phi_{zz}^{(0)} &= 0 \\ \phi_{zz}^{(n)} &= -\nabla^2 \phi^{(n-1)} \quad n = 1, 2, 3, \dots \end{aligned} \quad (1.2.9)$$

Integrating twice with respect to z and applying the bottom boundary condition (1.2.7b), we have

$$\begin{aligned} \phi^{(0)}(x,y,z,t) &= \phi^{(0)}(x,y,t) \quad \text{independent of } z \\ \phi^{(n)}(x,y,z,t) &= \frac{(-1)^n (z+1)^{2n}}{(2n)!} \nabla^2 \phi^{(0)}(x,y,t) \\ & \quad n = 1, 2, 3, \dots \end{aligned} \quad (1.2.10)$$

where integration constants are independent of z and have been grouped into $\phi^{(0)}$. From (1.2.8)

$$\phi(x,y,z,t) = \sum_{n=0}^{\infty} \frac{(-1)^n \mu^{2n} (z+1)^{2n}}{(2n)!} \nabla^2 \phi^{(0)}(x,y,t) \quad (1.2.11)$$

Note that the leading term in the expansion for the vertical velocity ϕ_z is $O(\mu^2)$.

So far, we have made no assumption as to the magnitude of $\phi^{(0)}$ and

no use of the nonlinear boundary conditions on the free surface, (1.2.7c,d). Denoting the magnitude of $\phi^{(0)}$ by ϵ , several approximations to the free surface boundary conditions are possible, depending on the relative magnitudes of ϵ and μ^2 and the degree of accuracy desired. In Airy's approximation, for example, $\mu^2 \ll \epsilon$ and terms of $O(\mu^2)$ are neglected. In the Boussinesq approximation, $\epsilon \sim \mu^2 \ll 1$ and relative errors of $O(\epsilon^2, \epsilon\mu^2, \mu^4)$ are neglected. A detailed treatment of the various types of approximations and their domains of validity is found in Peregrine (1972).

The Boussinesq approximation has several advantages over Airy's approximation. First, Airy's equations can be formally derived from the Boussinesq equations by taking the limit $\mu^2 \rightarrow 0$. Secondly, it is well known that dispersion tends to counteract the wave steepening effect of nonlinearity, and thus to inhibit wave breaking. Airy's equations contain no dispersive terms and lead to shock formation even in physical situations where shocks are not observed experimentally. By contrast, the Boussinesq equations, which contain the leading order effect of dispersion, are found to agree well with experiments so long as the ratio of peak-to-trough wave height to water depth is less than .5. This is quite close to the onset of breaking, which occurs in shallow water when the above ratio is roughly .7. Thus, the Boussinesq approximation has a greater range of validity, so long as breaking does not occur.

Substituting (1.2.11) into (1.2.7c,d), and neglecting relative errors of $O(\epsilon^2, \epsilon\mu^2, \epsilon^4)$, one arrives, after some algebra, at the following form for the Boussinesq equations:

$$\begin{aligned} \eta_t + \vec{\nabla} \cdot \vec{u} + \vec{\nabla} \cdot (\eta \vec{u}) &= 0 \\ \vec{u}_t + \vec{\nabla} \eta + \frac{1}{2} \vec{\nabla} (\vec{u}^2) + \frac{1}{3} \mu^2 \vec{\nabla} \eta_{tt} &= 0 \end{aligned} \quad (1.2.12)$$

where $\vec{u}(x,y,t)$ is the depth-averaged horizontal velocity, defined by

$$\begin{aligned} \vec{u}(x,y,t) &= \frac{1}{1+\eta} \int_{-1}^{\eta} \vec{\nabla} \phi \, dz \\ &= \vec{\nabla} \phi(0) - \frac{\mu^2}{2} \nabla^2 (\vec{\nabla} \phi(0)) \int_{-1}^0 (z+1)^2 dz \\ &= \nabla \phi(0) - \frac{\mu^2}{6} \nabla^2 (\nabla \phi(0)) \end{aligned} \quad (1.2.13)$$

In the limit $\mu^2 \rightarrow 0$, (1.2.12) reduces to Airy's equations.

The fluid pressure, which is found by integrating the vertical equation over z , is given by $(\rho gh)p$ where ρ is the density of the fluid and

$$p = (\eta - z) + \mu^2 (z + z^2/2) (\vec{\nabla} \cdot \vec{u}_t) \quad (1.2.14)$$

The term $(\eta - z)$ is simply the hydrostatic pressure beneath the wave; the additional term reflects the influence of vertical motion, which is $O(\mu^2)$.

One consequence of the nonlinearity of (1.2.12) is that monochromatic waves are no longer possible solutions. If one begins with a wave of the form $(\eta_1(x,y), \vec{u}_1(x,y))e^{-it}$, one finds that the nonlinear terms generate second harmonics, having the time dependence e^{-2it} . Interaction of the first and second harmonics produces third harmonics, having the time dependence e^{-3it} . This process, if continued, leads to a time periodic wave of the form:

$$\begin{aligned} \begin{bmatrix} \eta(x,y,t) \\ \vec{u}(x,y,t) \end{bmatrix} &= \operatorname{Re} \sum_{n=0}^{\infty} \begin{bmatrix} \eta_n(x,y) \\ u_n(x,y) \end{bmatrix} e^{-int} \\ &\equiv \frac{1}{2} \sum_{n=-\infty}^{\infty} \begin{bmatrix} \eta_n(x,y) \\ \vec{u}_n(x,y) \end{bmatrix} e^{-int} \end{aligned} \quad (1.2.15)$$

where, by convention, $(\eta_{-n}, \vec{u}_{-n}) \equiv (\eta_n^*, \vec{u}_n^*)$. Substituting (1.2.15) into (1.2.12), the n-th harmonic is found to satisfy

$$\begin{aligned} -in\eta_n + \vec{\nabla} \cdot \vec{u}_n + \frac{1}{2} \sum_{s=-\infty}^{\infty} \nabla \cdot (\eta_s \vec{u}_{n-s}) &= 0 \\ -in \vec{u}_n + (1 - \frac{1}{3} \mu^2 n^2) \vec{\nabla} \eta_n + \frac{1}{4} \sum_{s=-\infty}^{\infty} \vec{\nabla} (\vec{u}_s \cdot \vec{u}_{n-s}) &= 0 \end{aligned} \quad (1.2.16)$$

Combining the divergence of (1.2.16b) with (1.2.16a) and neglecting relative errors of $O(\epsilon^2, \epsilon\mu^2, \mu^4)$,

$$(\nabla^2 + k_n^2) \eta_n = \sum_{s=-\infty}^{\infty} \left(\frac{-in}{2} \right) \nabla \cdot (\eta_s \vec{u}_{n-s}) - \frac{1}{4} \nabla^2 (\vec{u}_s \cdot \vec{u}_{n-s}) \quad (1.2.17)$$

where

$$\begin{aligned} k_n^2 &= n^2 / (1 - \frac{1}{3} \mu^2 n^2) \\ &= n^2 \cdot [1 + \frac{1}{3} n^2 \mu^2 + O(n\mu)^4] \end{aligned} \quad (1.2.18)$$

is the dispersion relation in dimensionless form. Note that the dispersion relation may be written as

$$\begin{aligned} n^2 &= k_n^2 (1 - \frac{1}{3} k_n^2 \mu^2 + O(k_n \mu)^4) \\ &= \frac{k_n}{\mu} \tanh k_n \mu + O(k_n \mu)^4 \end{aligned} \quad (1.2.19)$$

which shows clearly its connection to the exact dispersion relation

(1.2.4). The error in the Boussinesq dispersion relation is $O(k_n \mu)^4$ and can be quite large for the higher harmonics.

The near linearity of the dispersion curve when $\mu^2 \ll 1$ leads to the phenomenon of resonant linear interactions, which has been studied by Kim and Hanratty (1971), Mei and Unluata (1972), and Bryant (1972). Consider two plane waves

$$\begin{aligned} \eta_1 &= \text{Re} \{ \epsilon A_1 e^{i(k_1 x - n_1 t)} \} & (n_1, k_1 > 0) \\ \eta_2 &= \text{Re} \{ \epsilon A_2 e^{i(k_2 x - n_2 t)} \} & (n_2, k_2 > 0) \end{aligned} \quad (1.2.20)$$

where, from (1.2.17),

$$\begin{aligned} k_1 &= n_1 + O(\mu^2) \\ k_2 &= n_2 + O(\mu^2) \end{aligned} \quad (1.2.21)$$

Through nonlinear interaction, a third wave is formed

$$\eta_3 = \text{Re} \left\{ \epsilon A_3 e^{i[(k_1+k_2)x - (n_1+n_2)t]} + \epsilon B_3 e^{i[(k_1-k_2)x - (n_1-n_2)t]} \right\} \quad (1.2.22)$$

Since $k_1 \pm k_2 = n_1 \pm n_2 + O(\mu^2)$, η_3 represents a propagating wave which travels with approximately the same phase velocity as η_1 and η_2 ; thus, the three waves maintain the same relative phases as they propagate.

The magnitude of η_3 is found to increase linearly with distance so long as the three waves are in phase and $|\eta_3| \ll |\eta_1|, |\eta_2|$. This is known as a resonant three-wave interaction. Eventually, the influence of dispersion limits the distance of coherent propagation to $O(1/\mu^2)$. The net result is that nonlinear interactions of $O(\epsilon^2)$ add constructively over a distance of $O(1/\mu^2)$, and the magnitudes of ϵA_3 and ϵB_3 are

found to be $\epsilon O(\epsilon/\mu^2)$. The Stokes parameter, ϵ/μ^2 , therefore governs the extent of harmonic generation. The subject of resonant nonlinear interactions is discussed at length in Chapter 3.

When $\epsilon/\mu^2 \ll 1$, higher harmonics are generated in profusion, and the horizontal length scales used in (1.2.6) are no longer appropriate. This is the situation just before breaking. The Boussinesq equations cannot be expected to apply to such cases because the scales used in their derivation are no longer the correct physical scales.

1.3 Linearized Theory of the Long Narrow Bay

The harbor we shall consider is a long, narrow bay of width $2a$, length L , and constant depth h . The geometry of the ocean-harbor system is shown in Fig. 1.1. The coastline and harbor walls are taken to be rigid, impermeable, vertical surfaces along which the normal component of velocity must vanish, viz.

$$\vec{u}(x_S, y_S, t) \cdot \vec{n}_S = 0 \quad (1.3.1)$$

where (x_S, y_S) is a point on the surface, and \vec{n}_S is a vector normal to the surface.

The presence of finite boundaries in the fluid introduces new length scales, in addition to those which characterize the wave length and amplitude. We shall see that the dimensionless parameters

$$\begin{aligned} \ell &\equiv L(\omega/\sqrt{gh}) \\ \delta &\equiv a(\omega/\sqrt{gh}) \end{aligned} \quad (1.3.2)$$

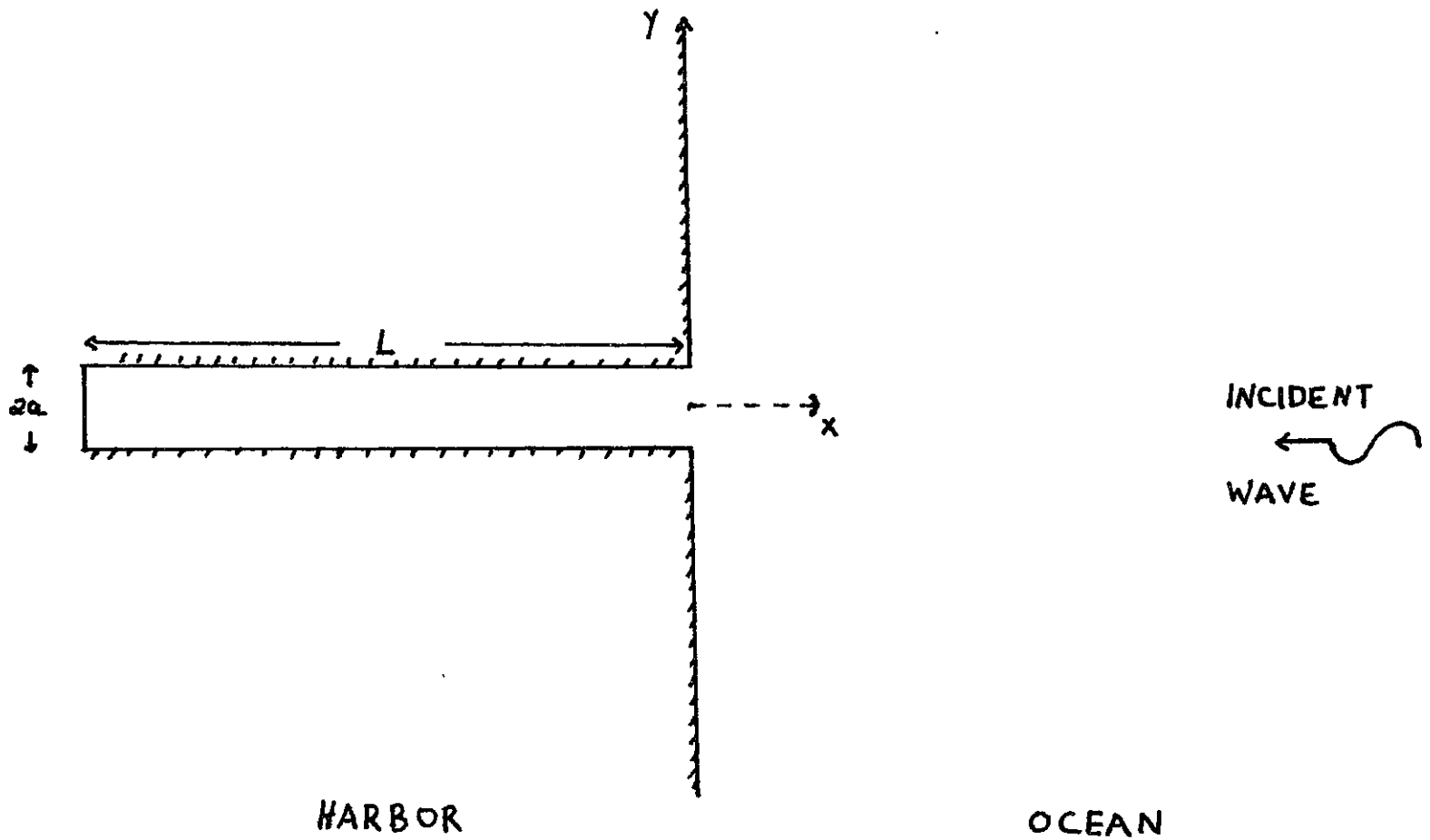


Fig. 1.1. Geometry of long, narrow bay

determine the linear resonance properties of the harbor basin. For a narrow bay ($a/L \ll 1$), resonant oscillations typically occur when $\ell = O(1)$ and $\delta = \ell \cdot (a/L) \ll 1$.

Because $\delta \ll 1$, the ocean-harbor system can be split into three distinct regions: the far field of the ocean, $r = \sqrt{x^2 + y^2} \gg \delta$; the near field of the entrance, $r \sim O(\delta)$; and the far field of the harbor, $-\ell \leq x \ll -\delta$. In the far field of the ocean, the fluid motion varies on the scale of the wavelength and (x,y) are suitable horizontal coordinates. In the near field of the junction, the scale of motion is δ and the coordinates

$$(x^*, y^*) = (x, y) / \delta \quad (1.3.3)$$

are most appropriate. Finally, in the far field of the harbor, the natural choice for coordinates is (x, y^*) .

Before embarking on a nonlinear treatment of the resonance properties of a long, narrow bay, we summarize known results from linearized theory. The geometry of Fig. 1.1 has been studied by Miles and Munk (1960) and Unluata and Mei (1973). Starting from linearized water wave theory, Unluata and Mei obtain asymptotic expansions for the wave field in each of the three regions. By matching the asymptotic solutions in adjacent regions, they determine the response of the harbor in terms of the incident wave amplitude and frequency. For an incident wave of the form

$$\eta^i(x, y, t) = \text{Re} \left(\frac{1}{2} A_1 e^{i(k_1 x - t)} \right) \quad (1.3.4)$$

where k_1 is the dimensionless wave number satisfying the dispersion relation (1.2.19), the response in the far field of the harbor is found

to be

$$\eta^H(x,t) = \text{Re} (T_1 \cos k_1(x + \ell)e^{-it}) \quad (1.3.5)$$

$$u^H(x,t) = \text{Re} \left(\frac{i}{k_1} T_1 \sin k_1(x + \ell)e^{-it} \right)$$

where

$$T_1 \equiv A_1 \left[\cos k_1 \ell - \frac{iZ_1}{k_1} \sin k_1 \ell \right]^{-1} \quad (1.3.6)$$

and

$$\frac{1}{k_1} Z_1 \equiv (k_1 \delta) \left[1 + \frac{2i}{\pi} (\epsilon_n k_1 \delta + \epsilon_n \frac{2\gamma}{\pi e}) \right] \quad (1.3.7)$$

$$\epsilon_n \gamma \equiv .577216 = \text{Euler's constant}$$

Z_1 is the radiation impedance of the harbor entrance; its real and imaginary parts are the radiation damping and mass reactance, respectively.

Letting $Z_1 = Z_{1R} + iZ_{1I}$, we have from (1.3.6),

$$\begin{aligned} \text{Max}_{x,t} \eta^H(x,t) &= |T_1| \\ &= |A_1| \left[\left(\cos k_1 \ell + \frac{Z_{1I}}{k_1} \sin k_1 \ell \right)^2 + \left(\frac{Z_{1R}}{k_1} \sin k_1 \ell \right)^2 \right]^{-1/2} \end{aligned} \quad (1.3.8)$$

When $k_1 \ell$ satisfies the "resonance condition"

$$\cos k_1 \ell + \frac{Z_{1I}}{k_1} \sin k_1 \ell = 0 \quad (1.3.9)$$

(1.3.8) yields

$$\text{Max}_{x,t} \eta^H(x,t) = \frac{|A_1|}{\left| \frac{Z_{1R}}{k_1} \sin k_1 \ell \right|} \quad (1.3.10)$$

so that the incident wave amplitude is amplified by a factor proportional to $1/Z_{1R}$, which is in turn proportional to $1/\delta$. As the width of the harbor entrance is made smaller, δ decreases and the resonant amplification increases; this is the so-called "harbor paradox".

Since $Z_{1I} \sim O(\delta \ln \delta) \ll 1$, the resonance condition (1.3.9) can be written as

$$\cos \left(k_1 \ell - \frac{Z_{1I}}{k_1} \right) \approx 0 \quad (1.3.11)$$

which yields the resonance criterion

$$k_1 \ell = \left(m + \frac{1}{2}\right) \pi + \frac{1}{k_1} Z_{1I} \quad m = 0, 1, 2, \dots \quad (1.3.12)$$

The lowest mode, $m = 0$, is often called the quarter-wave mode because $k_1 \ell \approx \pi/2$ or $\ell \approx \left(\frac{1}{4}\right) \left(\frac{2\pi}{k_1}\right) = \frac{1}{4} \lambda_1$, where λ_1 is the dimensionless wavelength.

Notice that, in (1.3.5), η^H and u^H are independent of y ; that is, the far field of the long, narrow bay is essentially one-dimensional. This allows a great simplification in the nonlinear treatment of the harbor, as will be seen in Chapter 3.

1.4 Scope of this Investigation

The theoretical part of this study analyzes the response of a long

narrow harbor to time-periodic incident waves. In Chapter 2, the wave field of the ocean is shown to be of sufficiently small amplitude that it may be treated as linear. Assuming the entrance width to be small, e.g. $\delta \ll 1$, the interaction of the ocean with the harbor is then approximated by an impedance boundary condition applied at the harbor entrance. The advantage of this approach lies in its mathematical simplicity; its disadvantage is that higher harmonics have larger values of $k_n \delta$ and are therefore less accurately represented. Where greater accuracy is required, a semi-numerical method, such as that of Lee (1971) or Chen and Mei (1974), should be used. In Chapter 3, the nonlinear response of a long, narrow harbor is examined. With the assumption $\delta \ll 1$, the wave field far from the harbor entrance is shown to be essentially one-dimensional, allowing a simplification of the nonlinear equations. The field variables are Fourier analyzed into time harmonics, and an infinite set of coupled, second-order, ordinary differential equations is found to govern the spatial variation of the complex harmonic amplitudes. Perturbation techniques and direct numerical methods are used to solve these equations.

Laboratory experiments were carried out using a model harbor placed in a large shallow wave basin. Chapter 4 deals with the experimental apparatus and procedures, and with the effects of friction and multiple reflections from the walls of the wave basin.

Results of the theoretical and experimental work are compared in Chapter 5. In addition, some theoretical predictions for large scale harbors are presented. A summary of the main conclusions and suggestions for future research are found in Chapter 6.

CHAPTER II
WAVE SYSTEM OF THE OCEAN

2.1 Motivation for a Linear Treatment

The wave field of the ocean consists of three parts: the incident wave, $\eta^i(x,y,t)$; the wave reflected from the coastline, $\eta^r(x,y,t)$; and the wave radiated away from the harbor entrance, $\eta^R(x,y,t)$. To a first approximation, the total wave field, $\eta^T(x,y,t)$, is simply a linear superposition of these three, viz.

$$\eta^T = \eta^i + \eta^r + \eta^R \quad (2.1.1)$$

The total velocity field, $\vec{u}^T(x,y,t)$, satisfies a similar relation.

In analyzing the ocean, we begin with the linear approach of (2.1.1). After the linear solution is obtained, the magnitude of the nonlinear terms will be estimated, and the assumption of linearity will be reexamined. We shall find that, when the harbor entrance is narrow ($\delta \ll 1$), the radiation damping is $O(\delta)$. It is then possible for an incident wave of $O(\epsilon\delta)$ to excite a resonant harbor response of $O(\epsilon)$. To determine a solution that is accurate to $O(\epsilon^2)$, one need only account for nonlinear effects in the harbor, not in the ocean. This is the motivation for a linear treatment of the ocean.

Deleting nonlinear terms in (1.2.16) and (1.2.17), we have for the n -th harmonic

$$\begin{aligned} -in\eta_n + \nabla \cdot \vec{u}_n &= 0 \\ -in\vec{u}_n + \frac{n^2}{k_n^2} \vec{\nabla}\eta_n &= 0 \end{aligned} \quad (2.1.2)$$

and

$$(\nabla^2 + k_n^2)\eta_n = 0 \quad (2.1.3)$$

where $k_n^2 \equiv n^2(1 + \frac{1}{3}n^2\mu^2)$. Note that $\eta_n(x,y)$ is proportional to the velocity potential for $\vec{u}_n(x,y)$. From (2.1.2b), $\vec{\nabla}\eta_n = 0$ so that $\eta_n(x,y)$ is a constant everywhere in the ocean. By properly defining the water depth, the constant can be set to zero, to the leading order, without loss of generality. The term $\vec{u}_0(x,y)$ represents a steady current and will be presumed to be zero, to the leading order. Thus, the zeroth harmonic may be deleted.

2.2 The Radiated Wave

If the harbor entrance were sealed, the boundary condition at the coastline would be

$$\vec{u}_n^T(0,y) \cdot \hat{x} = \left(\frac{-in}{k_n^2}\right) \frac{\partial \eta_n^T(0,y)}{\partial x} = 0 \quad (-\infty < y < \infty) \quad (2.2.1)$$

and the total wave field would be given by

$$\eta_n^T(x,y) = \eta_n^i(x,y) + \eta_n^i(-x,y) \quad (2.2.2)$$

where $\eta_n^i(-x,y)$ is simply the reflection of the incident wave about the y -axis. The function $\eta_n^i(x,y)$ can be any solution of the Helmholtz equation in the domain $x > 0$, $-\infty < y < \infty$. For example, $\eta_n^i(x,y)$ might be an obliquely incident wave

$$\eta_n^i(x,y) = c_n e^{-i\alpha_n x} e^{i\beta_n y} \quad (\alpha_n, \beta_n > 0, \alpha_n^2 + \beta_n^2 = k_n^2) \quad (2.2.3)$$

in which case

$$\eta_n^T(x,y) = 2c_n \cos \alpha_n x e^{i\beta_n y} \quad (2.2.4)$$

represents a standing wave whose amplitude varies sinusoidally in the y direction.

With the harbor entrance open, the boundary condition on the y -axis is more complicated:

$$\vec{u}_n^T(o,y) \cdot \hat{x} = \left(-\frac{in}{k_n^2}\right) \frac{\partial \eta_n^T(o,y)}{\partial x} = \begin{cases} 0 & |y| > \delta \\ U_n(y) & |y| < \delta \end{cases} \quad (2.2.5)$$

where $U_n(y)$ is the unknown velocity distribution in the harbor entrance.

The total wave field

$$\eta_n^T(x,y) = \eta_n^i(x,y) + \eta_n^i(-x,y) + \eta_n^R(x,y) \quad (2.2.6)$$

contains a radiated wave component which is the solution to the following boundary value problem:

$$\begin{aligned} (\nabla^2 + k_n^2) \eta_n^R &= 0 \\ \frac{\partial \eta_n^R(o,y)}{\partial x} &= \begin{cases} 0 & |y| > \delta \\ \frac{ik_n^2}{n} U_n(y) & |y| < \delta \end{cases} \\ \lim_{r \rightarrow \infty} \sqrt{r} \left(\frac{\partial \eta_n^R}{\partial r} - ik_n \eta_n^R \right) &= 0 \end{aligned} \quad (2.2.7)$$

where $r \equiv \sqrt{x^2 + y^2}$. Equation (2.2.7c), known as the radiation condition, ensures that the radiated wave will propagate away from the harbor entrance, as required by causality. In essence, the radiation

condition replaces the initial conditions that would be present in a fully time-dependent treatment of wave scattering. For a detailed derivation of the radiation condition, see Stoker (1957), pp. 174-181.

A formal solution for the radiated wave can be constructed using Green's functions. The appropriate Green's function, which satisfies (2.2.7) with $U_n(y)$ replaced by the unit singularity $\delta(y-y')$, is found to be

$$G_n(x,y,y') = \left(\frac{ik_n^2}{n}\right) \left(\frac{-i}{2} H_0^{(1)}(\sqrt{x^2 + (y-y')^2})\right) \quad (2.2.8)$$

where $H_0^{(1)}$ is the zeroth order Hankel function of the first kind.

Since

$$U_n(y) = \int_{-\delta}^{\delta} U_n(y') \delta(y-y') dy' \quad (2.2.9)$$

the solution for $\eta_n^R(x,y)$ is given by

$$\eta_n^R(x,y) = \frac{k_n^2}{2n} \int_{-\delta}^{\delta} H_0^{(1)}(k_n \sqrt{x^2 + (y-y')^2}) U_n(y') dy' \quad (2.2.10)$$

Let us examine (2.2.10) in the "far field" of the ocean, that is, where $r = \sqrt{x^2 + y^2} \gg \delta$. Substituting the Taylor series

$$H_0^{(1)}(k_n \sqrt{x^2 + (y-y')^2}) = H_0^{(1)}(k_n r) + y' \left[\frac{\partial H_0^{(1)}}{\partial y'} \right]_{y'=0} + \dots \quad (2.2.11)$$

into (2.2.10), we have

$$\eta_n^R(x,y) = \frac{k_n^2}{2n} \left\{ H_0^{(1)}(k_n r) \int_{-\delta}^{\delta} U_n(y') dy' + \left[\frac{\partial H_0^{(1)}}{\partial y'} \right]_{y'=0} \int_{-\delta}^{\delta} y' U_n(y') dy' + \dots \right\} \quad (2.2.12)$$

The first term on the right hand side represents the field of a monopole whose strength is proportional to the total flux, $\int_{-\delta}^{\delta} U_n(y) dy$. The second term is that of a dipole whose strength is proportional to the dipole moment of the velocity distribution, $\int_{-\delta}^{\delta} y U_n(y) dy$. When $\delta \ll 1$, the dipole term is smaller than the monopole term by a factor of δ , and higher terms in the multipole expansion are still smaller. Defining the average velocity by

$$\bar{U}_n \equiv \frac{1}{2\delta} \int_{-\delta}^{\delta} U_n(y') dy' \quad (2.2.13)$$

we have

$$\eta_n^R \approx \left(\frac{k_n}{n}\right) (k_n \delta \bar{U}_n) H_0^{(1)}(k_n r) \cdot [1 + O(\delta)] \quad (2.2.14)$$

Note that, if \bar{U}_n is $O(\epsilon)$, the radiated wave is $O(\epsilon k_n \delta)$ in the far field. We turn our attention now to the near field of the harbor entrance.

2.3 The Impedance Boundary Condition

In the near field of the harbor entrance, r is $O(\delta)$ and, assuming $k_n \delta \ll 1$,

$$H_0^{(1)}(k_n \sqrt{x^2 + (y-y')^2}) \approx 1 + \frac{2i}{\pi} \gamma k_n \left(\frac{r k_n}{2} \sqrt{x^2 + (y-y')^2}\right) + O(k_n \delta \gamma k_n \delta)^2 \quad (2.3.1)$$

where $\gamma \equiv$ Euler's constant = .57722... . Substitution of (2.3.1) into

(2.2.10) yields

$$\eta_n^R(x,y) \approx \frac{k_n^2}{n} \{ \delta \bar{U}_n + \frac{i}{\pi} \int_{-\delta}^{\delta} \ln\left(\frac{\gamma k_n}{2} \sqrt{x^2 + (y-y')^2}\right) U_n(y') dy' \} \quad (2.3.2)$$

Defining the average wave amplitude in the entrance by

$$\bar{\eta}_n^R \equiv \frac{1}{2\delta} \int_{-\delta}^{\delta} \eta_n^R(0,y) dy \quad (2.3.3)$$

we have

$$\begin{aligned} \bar{\eta}_n^R &= \frac{k_n^2}{n} \left\{ \delta \bar{U}_n + \frac{i}{\pi} \frac{1}{2\delta} \int_{-\delta}^{\delta} \int_{-\delta}^{\delta} \ln\left(\frac{\gamma k_n}{2} |y-y'|\right) U_n(y') dy' dy \right\} \quad (2.3.4) \\ &\equiv Z_n \bar{U}_n \end{aligned}$$

where

$$Z_n \equiv \frac{\bar{\eta}_n^R}{\bar{U}_n} = \left(\frac{k_n^2 \delta}{n}\right) \left\{ 1 + \frac{i}{2\pi} \frac{1}{\delta^2} \int_{-\delta}^{\delta} \int_{-\delta}^{\delta} \ln\left(\frac{\gamma k_n}{2} |y-y'|\right) \frac{U_n(y')}{\bar{U}_n} dy' dy \right\} \quad (2.3.5)$$

is called the "radiation impedance" of the ocean-harbor junction. The real and imaginary parts of Z_n are the radiation resistance and mass reactance of the junction, respectively. Note that only the mass reactance depends upon the details of the velocity profile, $U_n(y)$.

Introducing the variable $v = y/\delta$, and using (2.2.13), we arrive at the following expression for the radiation impedance:

$$Z_n = \left(\frac{k_n}{n}\right) (k_n \delta) \left[1 + \frac{2i}{\pi} (\ln k_n \delta + c_n) \right] \quad (2.3.6)$$

where

$$c_n = \ln \frac{\gamma}{2} + \frac{1}{4} \int_{-1}^1 \int_{-1}^1 \ln |v-v'| (U_n(v')/\bar{U}_n) dv' dv \quad (2.3.7)$$

Observe that the radiation resistance and mass reactance are $O(k_n \delta)$ and $O(k_n \delta \ln k_n \delta)$, respectively. In deriving (2.3.6), we assumed that $k_n \delta \ll 1$. This assumption is progressively worse for the higher harmonics, which have larger value of $k_n \delta$. We accept this deterioration of accuracy in the hope that the magnitudes of the higher harmonics are progressively smaller. Where greater accuracy is required in treating the high harmonics, the impedance approach can be abandoned in favor of a semi-numerical method such as that of Lee (1971) or Chen and Mei (1974). To predict the essential features, we choose to avoid these elaborate alternatives.

The form of the velocity profile, $U_n(y)$, depends upon the geometry of the harbor entrance and upon the wave field in the harbor, which is, of course, still undetermined. In the linearized theory of harbor resonance, the wave field in the harbor is expressible as an integral over the Green's function for the harbor, in exact analogy with (2.2.10). The requirement that $\eta_n^T(x,y)$ be continuous at $x=0$ leads to a linear integral equation for $U_n(y)$. The integral equation can then be solved by variational approximation or a numerical quadrature procedure. This approach is only feasible when the harbor is treated as linear, because the use of Green's functions relies upon the principle of superposition. To solve the nonlinear problem, a different approach must be found.

When flow separation at sharp corners is not significant, one may exploit the assumption that $k_n \delta \ll 1$ and determine an approximate form for the velocity profile, without prior knowledge of the wave field of the harbor. This has been recognized long ago by Rayleigh and is easily demonstrated as follows: In the near field of the junction,

the appropriate length scale is δ , and the terms in the Helmholtz equation are in the ratio,

$$(k_n^2 \eta_n) / (\nabla^2 \eta_n) \sim O(k_n \delta)^2 \quad (2.3.8)$$

It follows that

$$\nabla^2 \eta_n = 0 + O(k_n \delta)^2 \quad (2.3.9)$$

so that Laplace's equation governs the motion in the near field with a relative error of $O(k_n \delta)^2$. This is called the "quasi-static" approximation. The name derives from the fact that an observer in the near field sees steady flow and is unaware that it is being driven by oscillatory wave motion.

To solve Laplace's equation, it is only necessary to specify the geometry of the harbor entrance; the details of the adjacent wave fields are irrelevant. For the geometry of Fig. 1.1, the potential flow field can be found by applying a Schwartz-Christoffel transformation. Details are given in Unluata and Mei (1973). The radiation impedance is then found to be

$$Z_n = \left(\frac{k_n}{n}\right) (k_n \delta) \left[1 + \frac{2i}{\pi} \gamma_n k_n \delta + \gamma_n \frac{2\gamma}{\pi e}\right] \quad (2.3.10)$$

where $\gamma_n = \text{Euler's constant} = .5772$.

From (2.2.6), the average total wave amplitude at $x=0$ is given by

$$\bar{\eta}_n^T = 2\bar{\eta}_n^i(0) + \bar{\eta}_n^R = A_n + Z_n \bar{U}_n \quad (2.3.11)$$

where

$$A_n = 2\bar{\eta}_n^i(0) = \frac{1}{2\delta} \int_{-\delta}^{\delta} 2\eta_n^i(o,y) dy \quad (2.3.12)$$

Equation (2.3.11) will be referred to as the "impedance boundary condition." Observe that it was derived without even specifying the geometry of the harbor basin.

2.4 On the Validity of the Linear Approximation

Having obtained the linear solution for the wave field in the ocean, we now estimate the magnitude of the neglected nonlinear terms. The following table shows the orders of magnitude of the n-th harmonic incident, reflected, and radiated waves in both the near and far fields of the ocean.

Table 2.1

	η_n^i	η_n^r	η_n^R
Far Field	A_n	A_n	$k_n \delta \bar{U}_n$
Near Field	A_n	A_n	$(k_n \delta \& n k_n \delta) \bar{U}_n$

The magnitude of \bar{U}_n/A_n is thus far arbitrary.

In section 1.3, Eq. (1.3.6), we have seen that, when the n-th harmonic is resonated,

$$\bar{U}_n/A_n \sim O\left(\frac{1}{k_n \delta}\right) \quad (2.4.1)$$

This result can be anticipated if one thinks of the harbor as a damped

harmonic oscillator, with damping coefficient $k_n \delta$, being driven by an externally applied force of magnitude A_n . The response of the oscillator \bar{U}_n , at its natural frequency, is then given by (2.4.1). Of course, a harbor is a continuous system and therefore has many resonant frequencies, rather than just one.

In analyzing the harbor, we shall require that the maximum value of \bar{U}_n be $O(\epsilon)$. Equation (2.4.1) then constrains A_n to be $O(\epsilon k_n \delta)$. From Table A, the largest wave amplitude in the ocean occurs in the near field, where η_n^R is $O(\epsilon k_n \delta \ln k_n \delta)$. Thus, the largest nonlinear terms are $O(\epsilon k_n \delta \ln k_n \delta)^2$ in the ocean and $O(\epsilon^2)$ in the harbor. It is consistent to treat the harbor as nonlinear and the ocean as linear only if

$$(\epsilon k_n \delta \ln k_n \delta)^2 \ll \epsilon^2 \quad (2.4.2)$$

which is the case whenever $k_n \delta \ll 1$. The conclusion, therefore, is that, so long as $k_n \delta \ll 1$, it is consistent to neglect nonlinear effects in the ocean, and to include leading order nonlinear effects in the harbor.

CHAPTER III
 RESONANT OSCILLATIONS OF A LONG, NARROW BAY

3.1 Reduction to One Space Dimension

The harbor domain, $-\ell \leq x \leq 0$, consists of two regions: the near field, $|x| \sim O(\delta)$, and the far field, $-\ell \leq x \ll -\delta$. We shall show that the waves in the far field are essentially plane waves varying only in the x -direction. Intuitively, this is because oscillations in the y -direction have a minimum cutoff frequency given by $\frac{\omega}{\sqrt{gh}} a = \pi/2$. Since the frequencies under investigation are far below this cutoff, the y -dependence of the near field disturbance cannot propagate outward into the far field of the harbor.

A more rigorous demonstration of the fact that, for low frequency oscillations, the far field of the harbor is one-dimensional, proceeds as follows: Let us define a velocity potential $\phi(x,y,t)$ for the depth-averaged horizontal velocity $\vec{u}(x,y,t)$ by the relation $\vec{u} \equiv \vec{\nabla}\phi$. Integrating the momentum equation (1.2.12b) over space, the Boussinesq equations take the form

$$\begin{aligned} \eta_t + \vec{\nabla} \cdot [(1 + \eta)\vec{\nabla}\phi] &= 0 \\ \phi_t + \eta + \frac{1}{3}\mu^2 \eta_{tt} + \frac{1}{2}(\vec{\nabla}\phi)^2 &= C(t) \end{aligned} \quad (3.1.1)$$

The integration constant $C(t)$ can be absorbed into the term ϕ_t by redefining ϕ ; hence we may set $C(t)$ equal to zero, without loss of generality. The boundary conditions in the far field of the bay are

$$\phi_x(-l, y, t) = 0$$

$$\phi_y(x, \delta, t) = 0 \quad (3.1.2.)$$

$$\phi_y(x, -\delta, t) = 0$$

(3.1.2b,c) suggest that we rescale y , viz.

$$y^* = y/\delta$$

From (3.1.1), with $C(t) = 0$, we then have

$$\begin{aligned} ((1 + \eta)\phi_{y^*})_{y^*} &= -\delta^2 \{ \eta_t + [(1 + \eta)\phi_x]_x \} \\ \frac{1}{2} \phi_{y^*}^2 &= -\delta^2 \{ \phi_t + \eta + \frac{1}{3} \mu^2 \eta_{tt} + \frac{1}{2} \phi_x^2 \} \end{aligned} \quad (3.1.3)$$

Integrating (3.1.3a) over y^* and using the boundary conditions (3.1.2b,c) we find

$$\phi_{y^*}(x, y^*, t) = 0 + O(\delta^2) \quad (3.1.4)$$

so that, to $O(\delta^2)$, $\phi(x, y^*, t)$ is independent of y^* . From (3.1.1b), it follows that $\eta(x, y^*, t)$ is also independent of y^* , to $O(\delta^2)$.

We conclude, therefore, that to $O(\delta^2)$, η , ϕ , and $u = \phi_x$ are independent of y and that the transverse velocity component $v = \phi_y$ is zero. To be consistent with the neglect of $O(\delta^2)$ terms in the quasi-static approximation of the near field (section 2.3), we shall terminate the demonstration of the one-dimensionality of the far field at $O(\delta^2)$.

3.2 Equations Governing Time-Periodic Solutions

The one-dimensionality of the far field of the harbor greatly simplifies the equations governing harmonic interactions. In one dimension, equations (1.2.16) and (1.2.17) reduce to

$$-in\eta_n + u_n' + \frac{1}{2} \sum_{s=-\infty}^{\infty} (\eta_s u_{n-s})' = 0 \quad (3.2.1)$$

$$-inu_n + \left(\frac{n^2}{k_n^2}\right)\eta_n' + \frac{1}{4} \sum_s (u_s u_{n-s})' = 0$$

and

$$\eta_n'' + k_n^2 \eta_n = \frac{-in}{2} \sum_s (\eta_s u_{n-s})' - \frac{1}{4} \sum_s (u_s u_{n-s})'' \quad (3.2.2)$$

where primes denote differentiation with respect to x . From (3.2.1), $u_n' = in\eta_n \cdot (1 + O(\epsilon))$, and $u_n = -\frac{i}{n} \eta_n' (1 + O(\epsilon, \mu^2))$, for $n \neq 0$. To within the accuracy of the Boussinesq approximation

$$\begin{aligned} \sum_s (\eta_s u_{n-s})' &= \sum_s (\eta_s u_{n-s}' + \eta_s' u_{n-s}) \\ &\approx \sum_s (i(n-s)\eta_s \eta_{n-s} - \frac{i}{n-s} \eta_s' \eta_{n-s}') \quad (n \neq s) \end{aligned} \quad (3.2.3)$$

$$\begin{aligned} \frac{1}{2} \sum_s (u_s u_{n-s})'' &= \sum_s (u_{n-s} u_s'' + u_s' u_{n-s}') \\ &\approx \sum_s \frac{s}{n-s} \eta_s' \eta_{n-s}' - \sum_s s(n-s)\eta_s \eta_{n-s} \quad (n \neq s) \end{aligned} \quad (3.2.4)$$

so that (3.2.2) can be written as

$$\eta_n'' + k_n^2 \eta_n = \frac{1}{2} \sum_s (n^2 - s^2) \eta_s \eta_{n-s} - \frac{1}{2} \sum_s \left(\frac{n+s}{n-s} \right) \eta_s' \eta_{n-s}' \quad (3.2.5)$$

(n ≠ s)

(3.2.5) is a second-order ordinary differential equation governing the spatial variation of the n-th harmonic.

To solve (3.2.5), we require two boundary conditions on η_n . The no flux condition at $x = -\ell$ provides one boundary condition:

$$\eta_n'(-\ell) = 0 \quad (3.2.6)$$

The other boundary condition is obtained by requiring that, at $x = 0$, the wave field in the harbor match smoothly with that in the ocean. This matching will only be performed in an average way. Equation (2.3.11), which expresses the average wave amplitude at $x = 0$ in terms of the incident wave amplitude and the horizontal fluid velocity at $x = 0$, yields the "impedance boundary condition,"

$$\eta_n(0) = A_n + Z_n u_n(0) \quad (3.2.7)$$

Since Z_n is $O(k_n \delta \ell n k_n \delta)$ and $u_n = \frac{-in}{k_n^2} \eta_n' + O(\epsilon^2)$, we have

$$\eta_n(0) = A_n - \frac{in}{k_n^2} Z_n \eta_n' + O(\epsilon^2 k_n \delta \ell n k_n \delta) \quad (3.2.8)$$

(3.2.5), (3.2.6), and (3.2.8) comprise the boundary value problem for $\eta_n(x)$.

The zeroth harmonic can be found directly by integrating (3.2.1), viz.

$$u_0(x) = -\frac{1}{2} \sum_s \eta_s(x) u_{-s}(x) + C_0 \quad (3.2.9)$$

$$\eta_0(x) = -\frac{1}{4} \sum_s |u_s(x)|^2 + D_0$$

Since all velocities, $u_s(x)$, vanish at $x = -\ell$, it follows that $C_0 = 0$ and $u_0(x)$ is at most of $O(\epsilon^2)$. In fact, by the following argument, $u_0(x)$ is seen to be at most of $O(\epsilon^3)$: Multiplying (3.2.1a) by η_{-n} and (3.2.1b) by u_{-n} and summing n from $-\infty$ to ∞ , we have:

$$\sum_n -in (\eta_n \eta_{-n} + u_n u_{-n}) + \sum_n (\eta_n u_{-n})' = O(\epsilon^3, \epsilon^2 \mu^2) \quad (3.2.10)$$

where we have used the fact that $k_n^2 = n^2 + O(\mu^2)$. Replacing the summation index n by $-p$, we see that

$$\sum_n -in (\eta_n \eta_{-n} + u_n u_{-n}) = \sum_p ip (\eta_p \eta_{-p} + u_p u_{-p}) = 0 \quad (3.2.11)$$

so that

$$\sum_n (\eta_n u_{-n})' = O(\epsilon^3) \quad (3.2.12)$$

Integrating over x and using the boundary condition $u_n(-\ell) = 0$ for all n , it follows that

$$\sum_n (\eta_n u_{-n}) = O(\epsilon^3) \quad (3.2.13)$$

and, from (3.2.9a), with $C_0 = 0$,

$$u_0(x) = O(\epsilon^3) \quad (3.2.14)$$

The constant D_0 in (3.2.9b) is determined by the impedance condition at the entrance, (3.2.7). In section 2.1, we noted that, by

properly defining the mean depth in the ocean, $A_0 = 0$. From (2.3.5), $Z_0 = 0$, so that $\eta_0(0) = 0$ and

$$D_0 = \frac{1}{4} \sum_S |u_S(0)|^2 \quad (3.2.15)$$

From (3.2.9b), $\eta_0(x)$ is then

$$\eta_0(x) = \frac{1}{4} \sum_S |u_S(0)|^2 - \frac{1}{4} \sum_S |u_S(x)|^2 \quad (3.2.16)$$

Thus η_0 is $O(\epsilon^2)$. At the back wall of the harbor, all velocities $u_S(-\ell)$ vanish and η_0 takes on its maximum value, viz.

$$\eta_0(-\ell) = \frac{1}{4} \sum_S |u_S(0)|^2 > 0 \quad (3.2.17)$$

which shows that there is a mean set-up at the back wall.

Since η_0 and u_0 are strictly $O(\epsilon^2)$ and $O(\epsilon^3)$, they do not have any feedback to other harmonics up to $O(\epsilon^2)$. Thus, they can be calculated after all the other harmonics are obtained. For this reason, we shall discuss the zeroth harmonic separately.

Equation (3.2.5) represents a system of coupled, nonlinear, second-order differential equations for the harmonic amplitudes $\eta_1(x)$, $\eta_2(x)$, $\eta_3(x)$, When $\eta_n(x)$ is $O(\epsilon)$, the coupling terms are $O(\epsilon^2)$ and are thus relatively small. By earlier theories, i.e., Mei and Unluata (1972) and Bryant (1972), it is known that weak nonlinearity does not produce first order effects within a distance of $O(1)$. Therefore, for the first few resonant harbor modes, for which $\ell = O(1)$, the effect of weak nonlinearity may be treated as a perturbation, as in the next section.

3.3 Regular Perturbation Analysis for the Lowest Resonant Modes or for Very Small Amplitude Waves

Substituting the perturbation series

$$\eta_n(x) = \epsilon \eta_n^{(1)}(x) + \epsilon^2 \eta_n^{(2)}(x) + \dots \quad (3.3.1)$$

into (3.2.5), we obtain a sequence of linear problems. At $O(\epsilon)$,

$$\begin{aligned} \eta_n^{(1)''} + k_n^2 \eta_n^{(1)} &= 0 \\ \eta_n^{(1)}(-\ell) &= 0 \\ \eta_n^{(1)}(0) &= A_n - \frac{i n}{k_n} Z_n \eta_n^{(1)}(-0) \end{aligned} \quad (3.3.2)$$

For simplicity, we shall assume that the incident wave is monochromatic, so that only A_1 is nonzero. Then,

$$\begin{aligned} \eta_1^{(1)}(x) &= T_1 \cos k_1(x + \ell) \\ T_1 &\equiv [\cos k_1 \ell - (i/k_1) Z_1 \sin k_1 \ell]^{-1} \cdot A_1 \\ \eta_n^{(1)}(x) &= 0 \quad n = 2, 3, 4, \dots \end{aligned} \quad (3.3.3)$$

This is just the solution of linearized theory, which exhibits resonances whenever $\cos k_1 \ell + (i \text{Im}(Z_1)/k_1) \sin k_1 \ell = 0$.

At $O(\epsilon^2)$,

$$\begin{aligned} \eta_1^{(2)''} + k_1^2 \eta_1^{(2)} &= 0 \\ \eta_2^{(2)''} + k_2^2 \eta_2^{(2)} &= \frac{3}{2} \eta_1^{(1)} \eta_1^{(1)} - \frac{3}{2} \eta_1^{-1(1)} \eta_1^{-1(1)} \\ &= \frac{3}{2} T_1^2 [\cos^2 k_1(x + \ell) - k_1^2 \sin^2 k_1(x + \ell)] \end{aligned} \quad (3.3.4)$$

$$\eta_n^{(2)} + k_n^2 \eta_n^{(2)} = 0 \quad n = 3, 4, 5, \dots$$

with the homogeneous boundary conditions

$$\begin{aligned} \eta_n^{(2)}(-\ell) &= 0 \\ \eta_n^{(2)}(0) + \frac{i n}{k_n^2} Z_n \eta_n^{(2)\prime}(0) &= 0 \end{aligned} \quad (3.3.5)$$

The solution to (3.3.4) and (3.3.5) is

$$\begin{aligned} \eta_n^{(2)} &= 0 \quad n = 1, 3, 4, 5, \dots \\ \eta_2^{(2)} &= \frac{3}{2} T_1^2 \left\{ f(x) - \left(\frac{f(0) + \frac{2i}{k_2} Z_2 f'(0)}{\cos k_2 \ell - \frac{2i}{k_2} Z_2 \sin k_2 \ell} \right) \cos k_2(x + \ell) \right\} \end{aligned} \quad (3.3.6)$$

$$f(x) \equiv \frac{1}{2} \left(\frac{1 + k_1^2}{k_2^2 - 4k_1^2} \right) \cos 2k_1(x + \ell) + \frac{1 - k_1^2}{2k_2^2}$$

The solution for $\eta_2^{(2)}(x)$ is comprised of three parts: a constant term, a forced oscillation having the form $\cos 2k_1(x + \ell)$, and a free oscillation having the form $\cos k_2(x + \ell)$. Since

$$\begin{aligned} k_2^2 - 4k_1^2 &= 4\left(1 + \frac{4}{3} \mu^2\right) - 4\left(1 + \frac{1}{3} \mu^2\right) = 4\mu^2 \\ k_2 - 2k_1 &= 2\left(1 + \frac{2}{3} \mu^2\right) - 2\left(1 + \frac{1}{6} \mu^2\right) = \mu^2 \end{aligned} \quad (3.3.7)$$

it follows that the constant term is $O(\mu^2)$ and the forced term is $O(1/\mu^2)$. Thus, the magnitude of $\epsilon^2 \eta_2^{(2)}(x)$ is generally of order $\epsilon \cdot (\epsilon/\mu^2)$, in which case the perturbation series of (3.3.1) is valid only for $\epsilon/\mu^2 \ll 1$.

For a harbor which is not too long, e.g., one for which $\mu^2 \ell \ll 1$, the perturbation series of (3.3.1) is in fact valid even when ϵ/μ^2 is $O(1)$. To show this, we expand

$$\begin{aligned} \cos 2k_1(x + \ell) &= \cos (k_2 - \mu^2)(x + \ell) \\ &\approx \cos k_2(x + \ell) + \mu^2(x + \ell) \sin k_2(x + \ell) \quad (3.3.8) \end{aligned}$$

and, from (3.3.6),

$$\eta_2^{(2)}(x) = \frac{3}{2} T_1^2 \left\{ g(x) - \left(\frac{g(0) + \frac{2i}{k_2} Z_2 g'(0)}{\cos k_2 \ell - \frac{2i}{k_2} Z_2 \sin k_2 \ell} \right) \cos k_2(x + \ell) \right\} + O(\mu^2)$$

$$g(x) \equiv \frac{1}{4} (x + \ell) \sin k_2(x + \ell) \quad (3.3.9)$$

so that, for a harbor having $\mu^2 \ell \ll 1$, $\epsilon^2 \eta_2^{(2)}(x)$ is $O(\epsilon^2)$.

In summary, the regular perturbation expansion is valid for (i) $\epsilon/\mu^2 \ll 1$ (small amplitudes) and any length harbor, or (ii) $\epsilon/\mu^2 = O(1)$ and "short" harbors having $\mu^2 \ell \ll 1$. To be consistent with the Boussinesq approximation which neglects terms of $O(\epsilon^3)$, we terminate the perturbation series at $O(\epsilon^2)$.

From (3.2.16), the zeroth harmonic first appears at $O(\epsilon^2)$ and is given by

$$\begin{aligned} \eta_0^{(2)}(x) &= \frac{1}{2} (|u_1^{(1)}(0)|^2 - |u_1^{(1)}(x)|^2) \\ &= \frac{1}{2k_1^4} (|\eta_1^{(1)}(0)|^2 - |\eta_1^{(1)}(x)|^2) \quad (3.3.10) \end{aligned}$$

(3.3.3) yields

$$\begin{aligned}\eta_0^{(2)}(x) &= \frac{1}{2k_1^2} |T_1|^2 (\sin^2 k_1 \ell - \sin^2 k_1(x + \ell)) \\ &= \frac{1}{4k_1^2} |T_1|^2 (\cos 2k_1(x + \ell) - \cos 2k_1 \ell)\end{aligned}\quad (3.3.11)$$

Figures 3.1(a), (b), and (c) show the frequency dependence of $|\eta_1|$, $|\eta_2|$, and η_0 evaluated at the back wall of the harbor ($x = -\ell$), for a harbor having the fixed dimensions $a = 50$ m., $h = 20$ m., and $L = 1000$ m. The incident wave is taken to be monochromatic, viz. $A_2 = A_3 = A_4 \dots = 0$, with $A_1 = .03$. The large peaks occurring at $\ell = 1.41, 4.36, \text{ and } 7.36$ correspond to linear resonances of the first harmonic. In Figure 3.1(b), the smaller peaks flanking each of these large peaks correspond to linear resonances of the second harmonic. As frequency increases, dispersion has the effect of shifting the smaller peaks to the right relative to the central peaks. Eventually, the small peak to the left of the central peak overlaps the central peak. When this occurs, the first and second harmonics are resonated simultaneously, and the amplitude of the second harmonic can be a large fraction of the first. As a result of this phenomenon, the peaks in Figure 3.1(b) do not diminish with ℓ as fast as the first harmonic peaks of Figure 3.1(a).

In Figure 3.1(c), the only peaks in η_0 occur at values of ℓ for which the first harmonic is resonated. In contrast with the second harmonic, the zeroth harmonic has no additional peaks because it has no linear resonances of its own. Since η_0 is generated by the square of η_1 , the peaks in Figure 3.1(c) diminish with ℓ more rapidly than the first harmonic peaks of Figure 3.1(a).

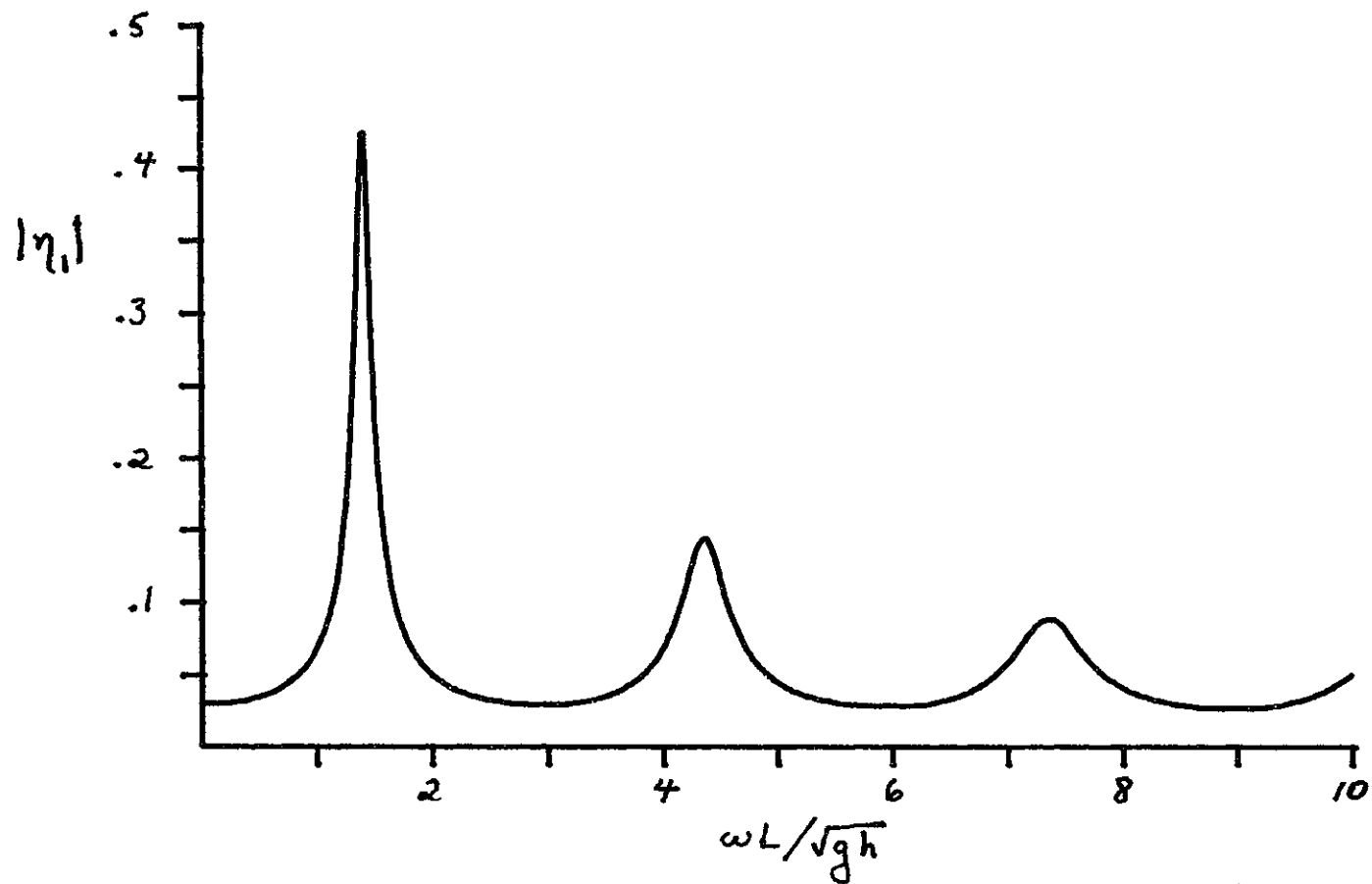


Fig. 3.1a. Regular perturbation theory: Frequency response of large-scale harbor ($h = 20$ m., $2a = 100$ m., $L = 1000$ m., $A_1 = .03$). First harmonic amplitude at the back wall.

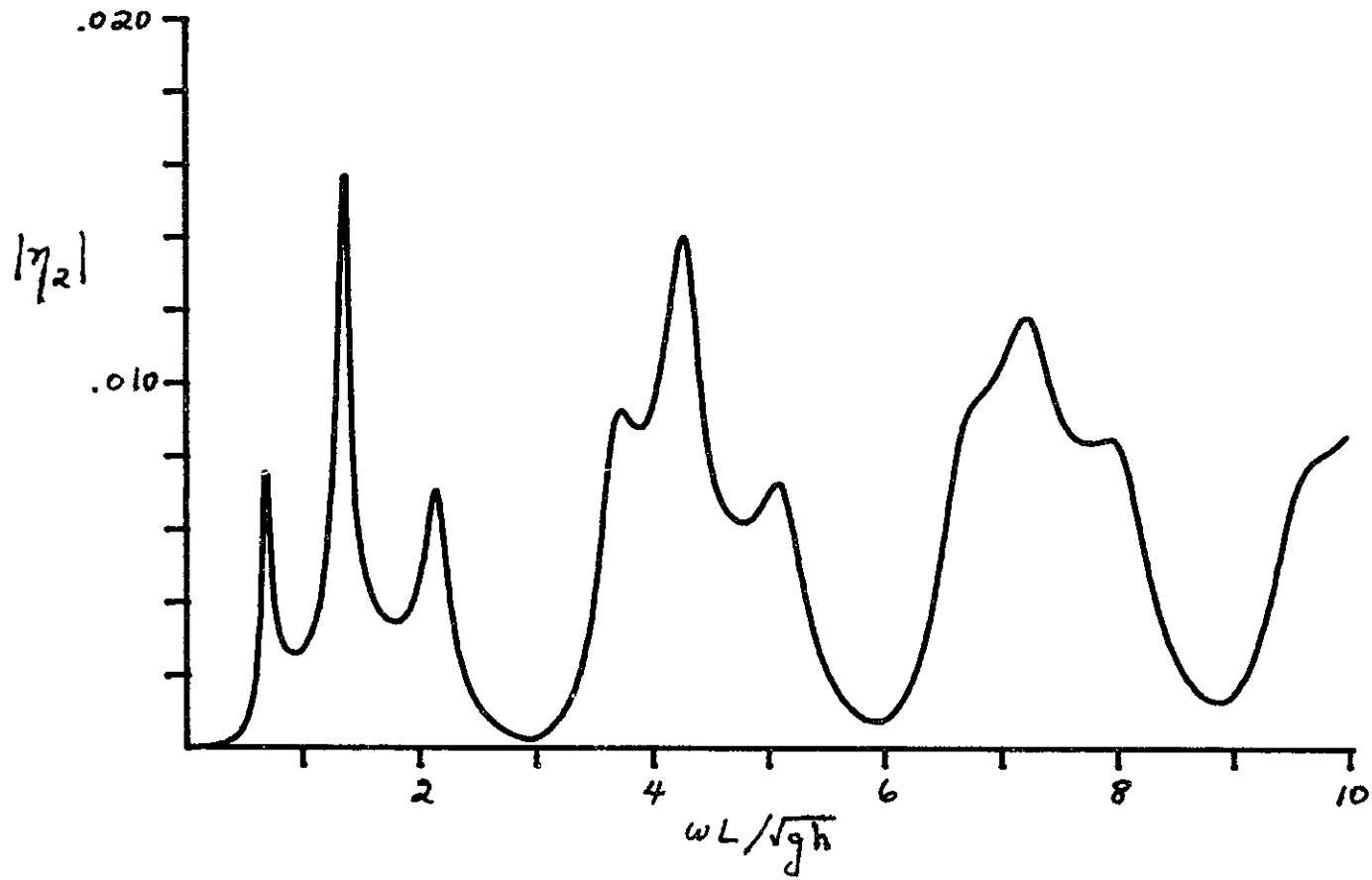


Fig. 3.1b. Regular perturbation theory: Frequency response of large-scale harbor ($h = 20$ m., $2a = 100$ m., $L = 1000$ m., $A_1 = .03$). Second harmonic amplitude at the back wall.

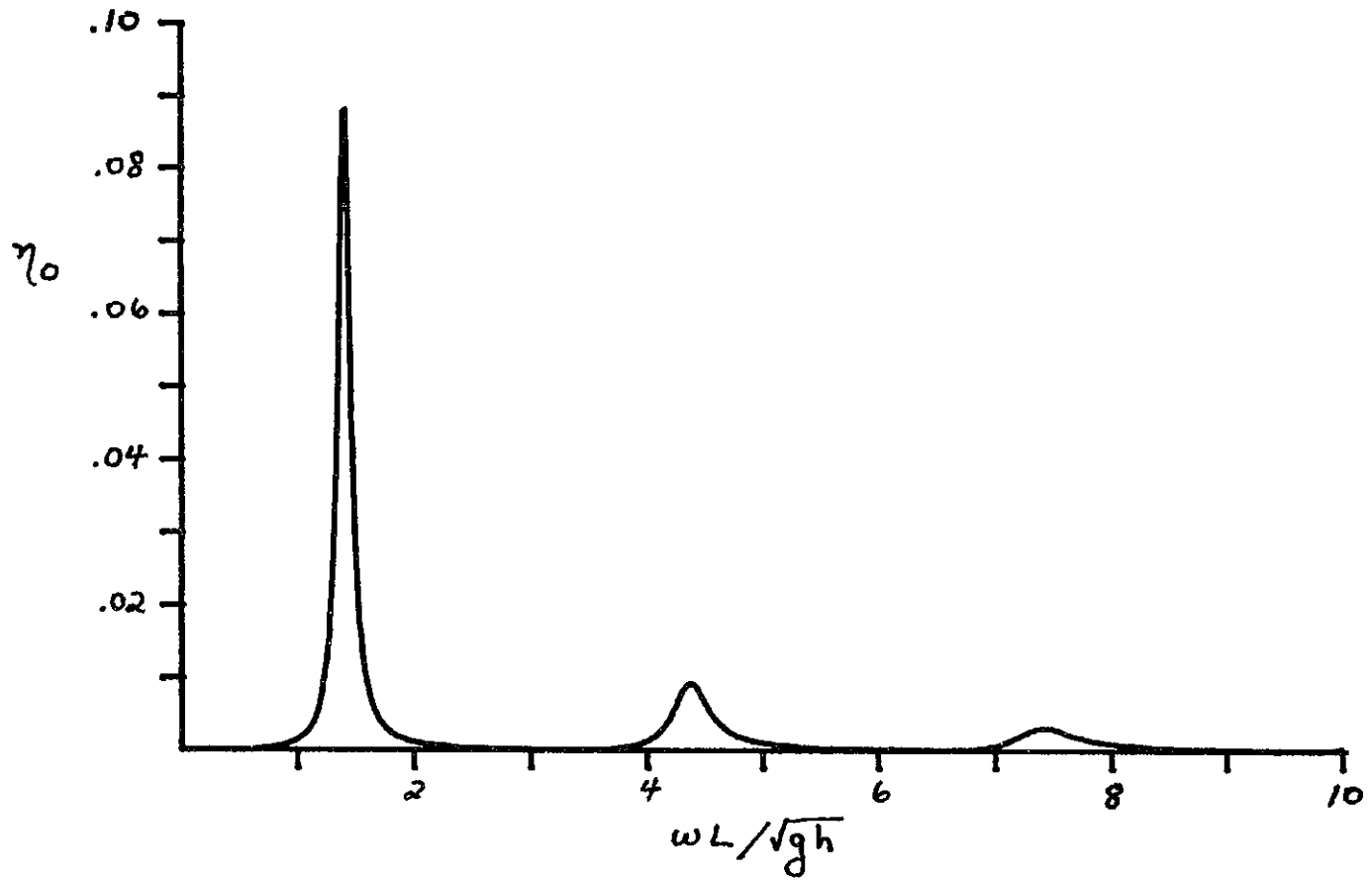


Fig. 3.1c. Regular perturbation theory: Frequency response of large-scale harbor ($h = 20$ m., $2a = 100$ m., $L = 1000$ m., $A_1 = .03$). Zeroth harmonic at the back wall.

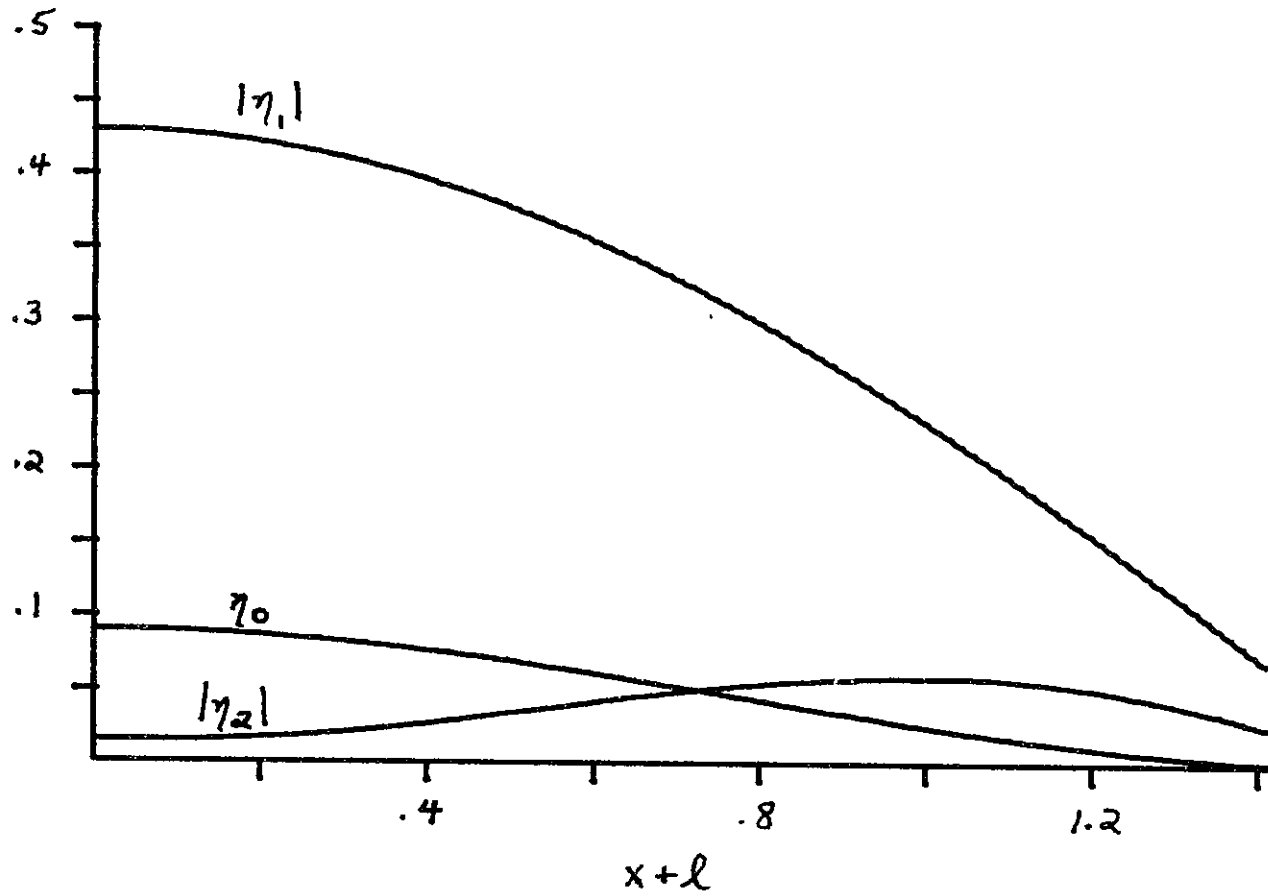


Fig. 3.2a. Regular perturbation theory: First resonant mode of large-scale harbor ($h = 20$ m., $2a = 100$ m., $L = 1000$ m., $A_1 = .03$, $\ell = 1.41$). Spatial variation of the harmonics.

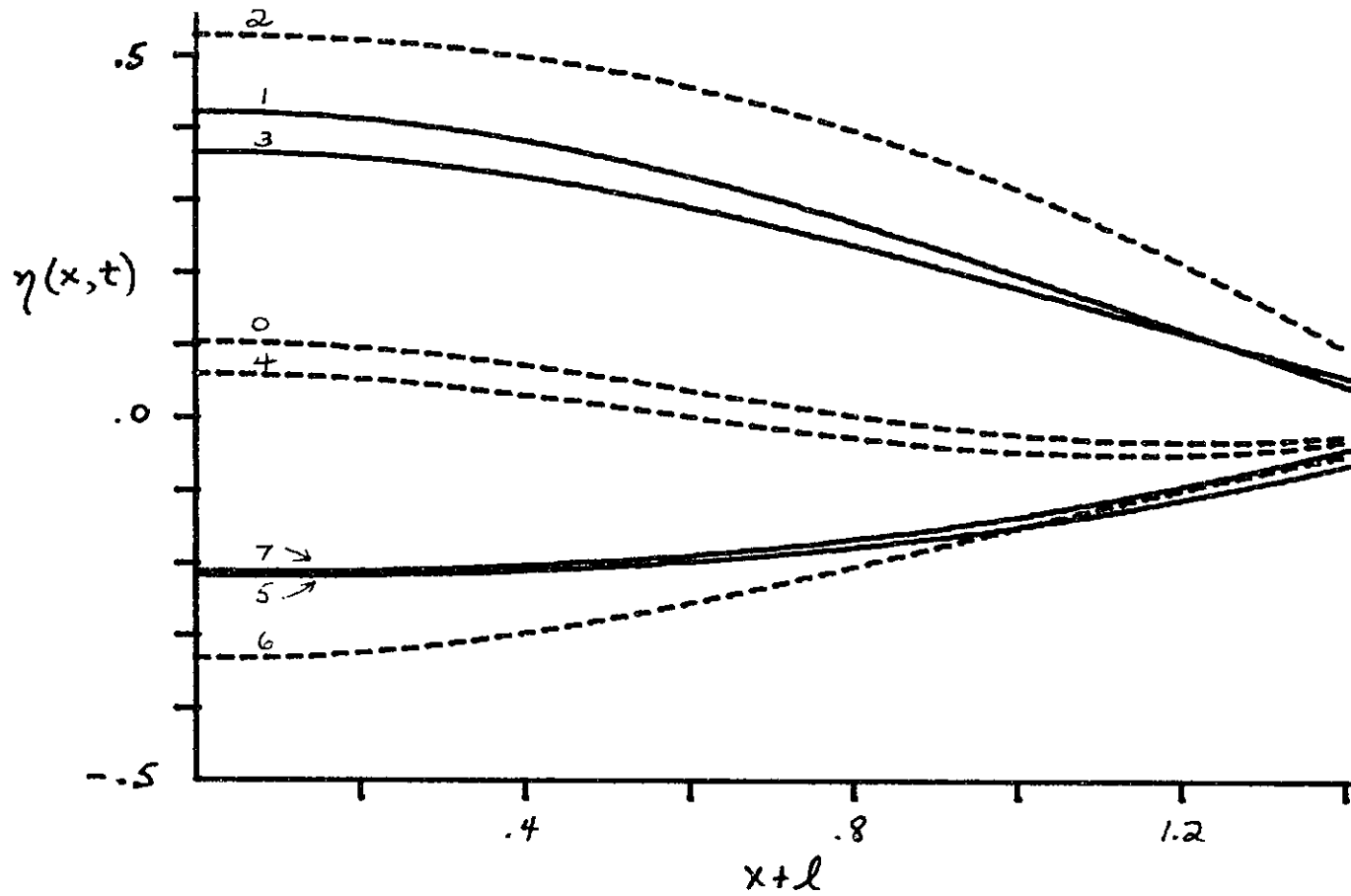


Fig. 3.2b. Regular perturbation theory: First resonant mode of large-scale harbor ($h = 20$ m., $2a = 100$ m., $L = 1000$ m., $A_1 = .03$, $\ell = 1.41$). Surface profiles at times $t = m\pi/4$, $m = 0, 1, 2, \dots, 7$.

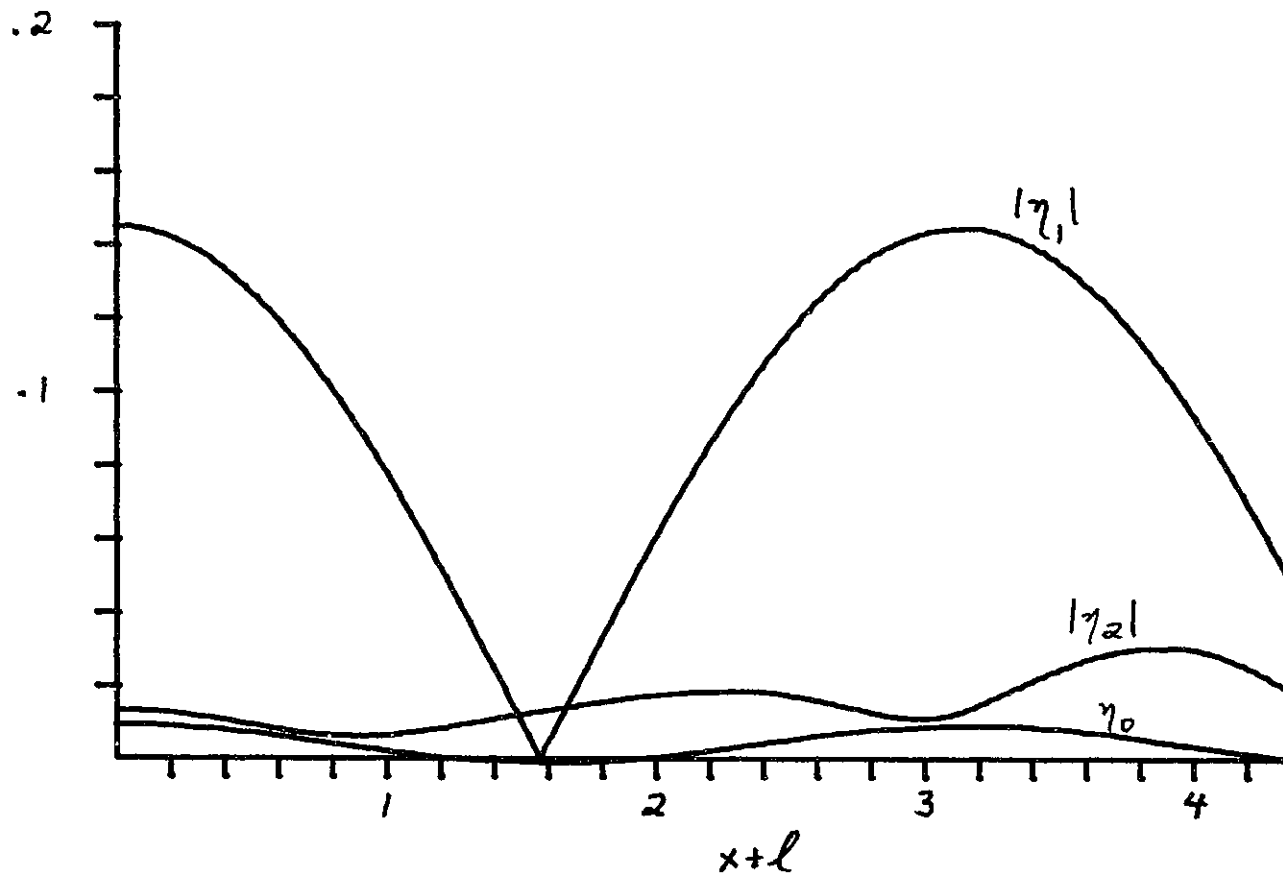


Fig. 3.3a. Regular perturbation theory: Second resonant mode of large-scale harbor ($h = 20$ m., $2a = 100$ m., $L = 1000$ m., $A_1 = .03$, $\epsilon = 4.36$). Spatial variation of the harmonics.

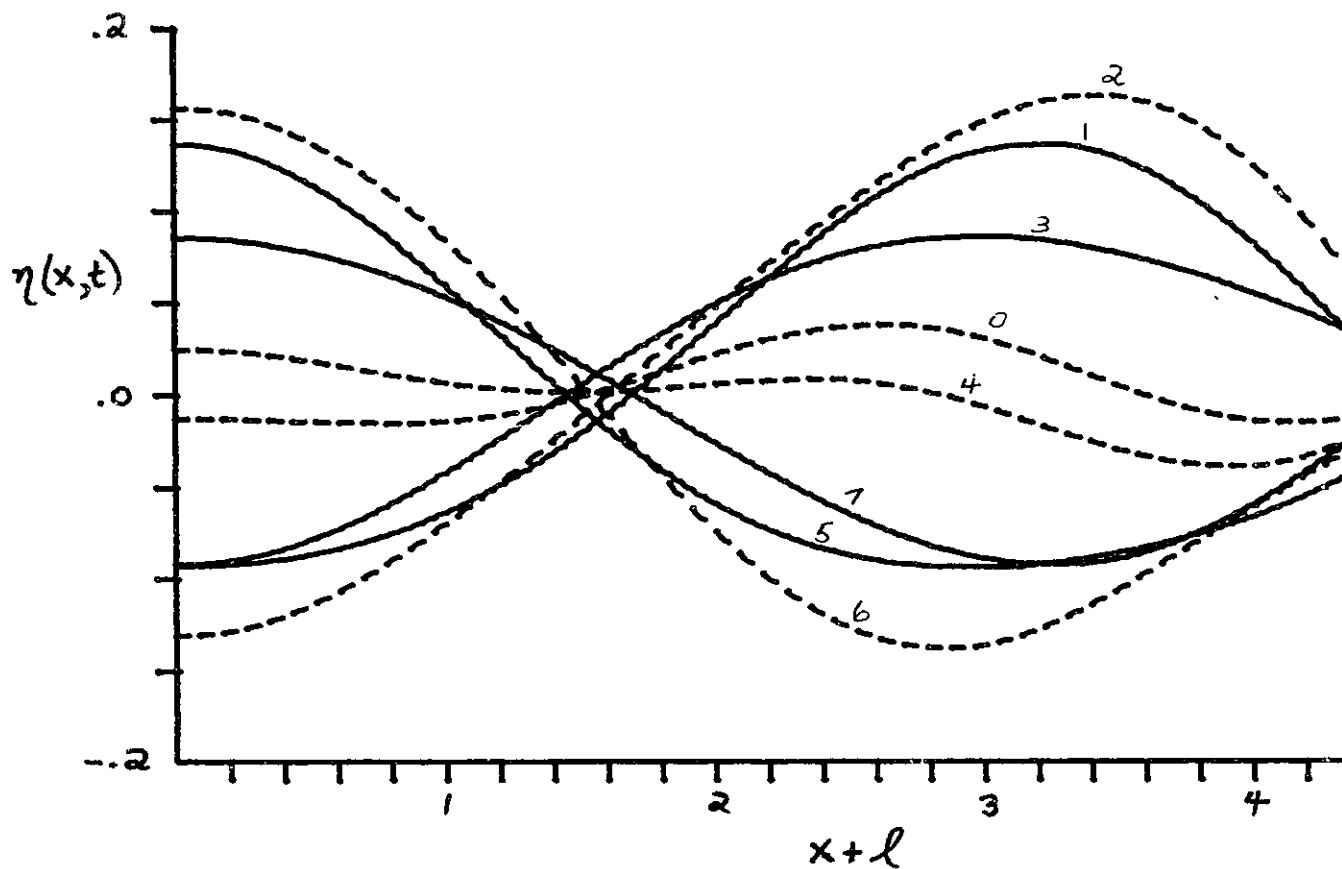


Fig. 3.3b. Regular perturbation theory: Second resonant mode of large-scale harbor ($h = 20$ m., $2a = 100$ m., $L = 1000$ m., $A_1 = .03$, $\ell = 4.36$). Surface profiles at times $t = m\pi/4$, $m = 0,1,2\dots7$.

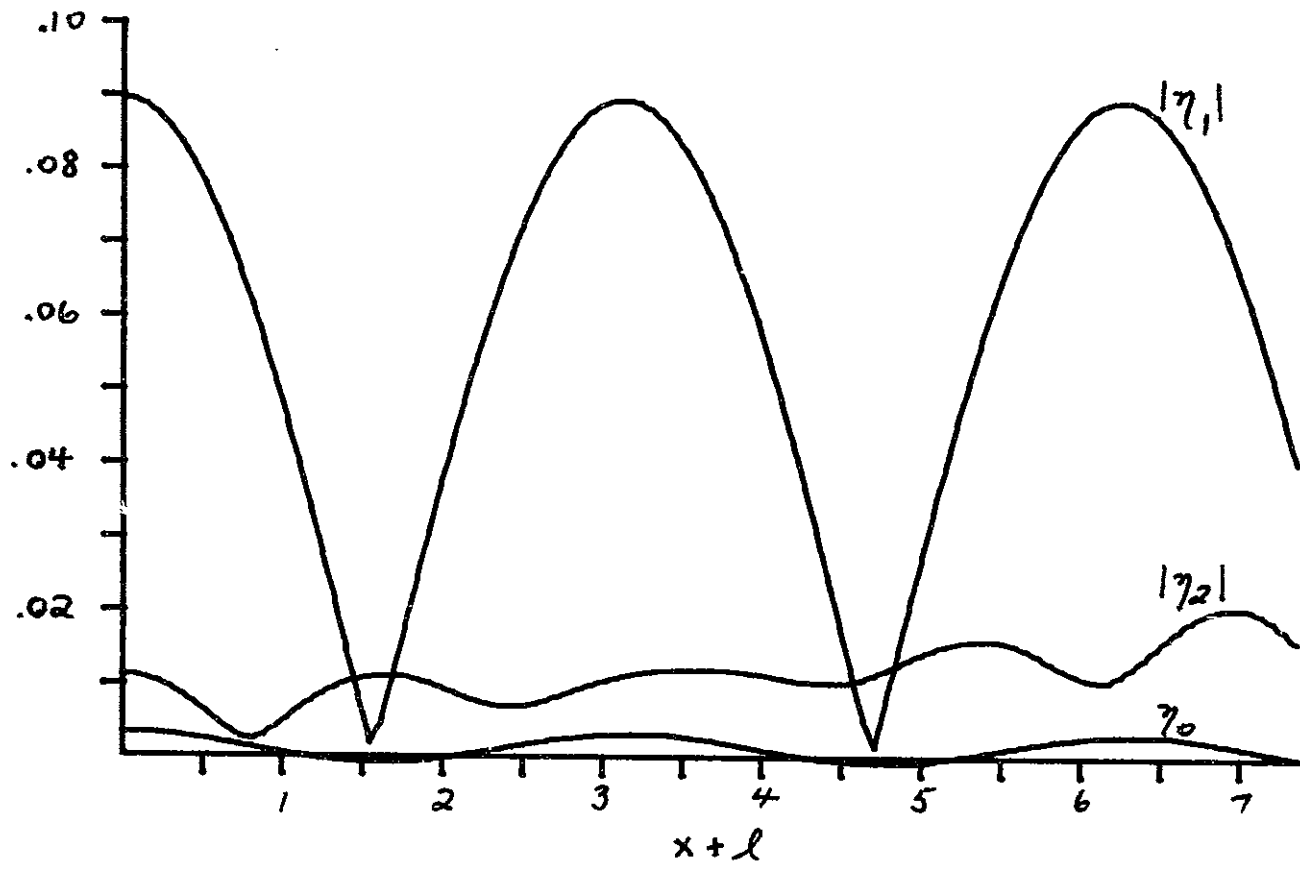


Fig. 3.4a. Regular perturbation theory: Third resonant mode of large-scale harbor ($h = 20$ m., $2a = 100$ m., $L = 1000$ m., $A_1 = .03$, $\ell = 7.36$). Spatial variation of the harmonics.

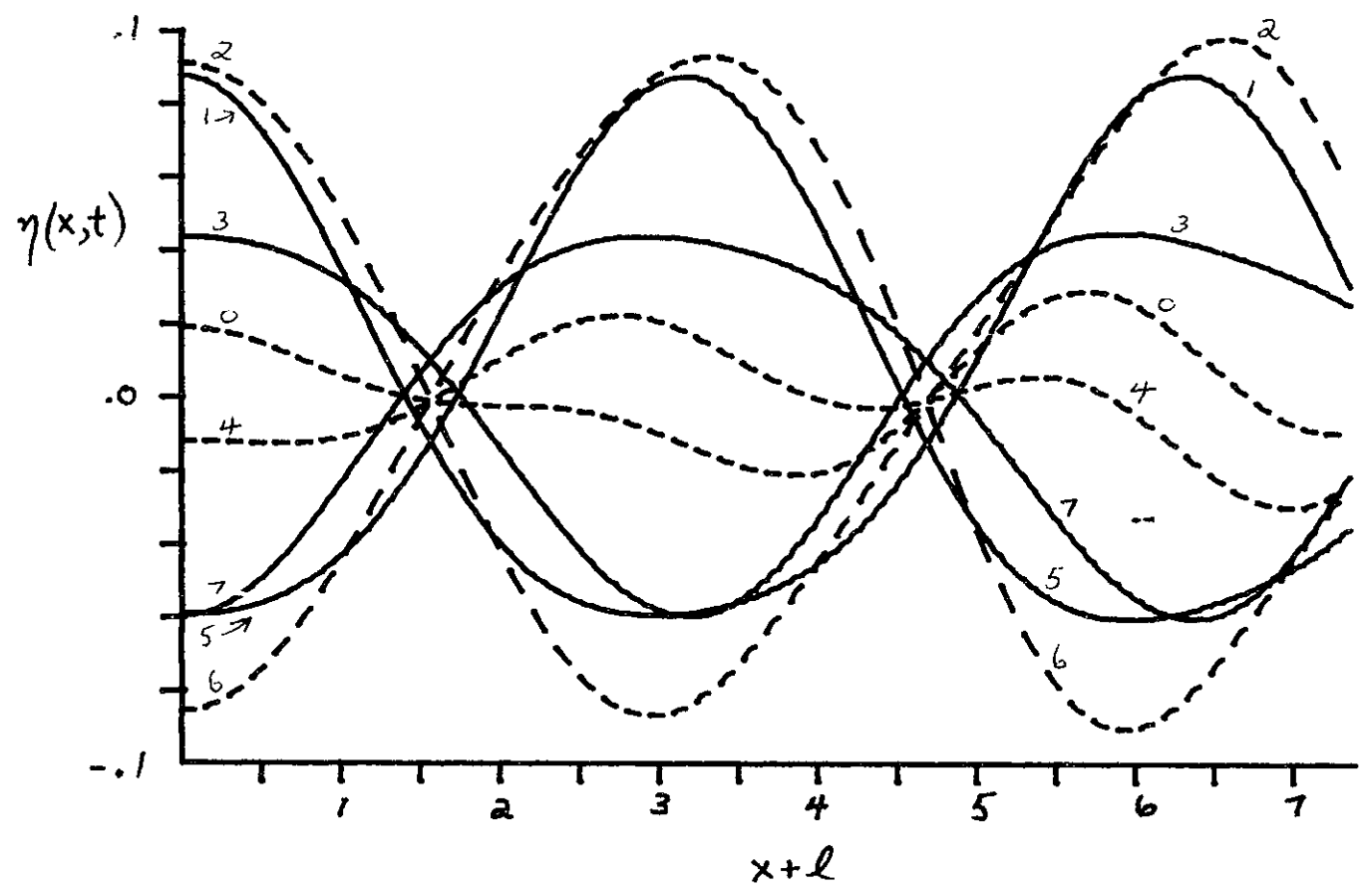


Fig. 3.4b. Regular perturbation theory: Third resonant mode of large-scale harbor ($h = 20$ m., $2a = 100$ m., $L = 1000$ m., $A_1 = .03$, $\ell 7.36$). Surface profiles at times $t = m\pi/4$, $m = 0,1,2\dots7$.

Figures 3.2(a), (b), 3.3(a), (b), and 3.4(a), (b) show the spatial dependence of the harbor response for the first three resonant modes, occurring at $\lambda = 1.41, 4.36, \text{ and } 7.36$, respectively. The (a) figures show the spatial variation of the harmonic amplitudes $|\eta_1(x)|$, $|\eta_2(x)|$, and $\eta_0(x)$. (Recall that η_1 and η_2 are complex quantities whereas η_0 is real.) Observe that the amplitude of the second harmonic increases with increasing distance from the back wall, in accordance with (3.3.9), and that the zeroth harmonic is largest at the back wall and zero at the entrance, in accordance with (3.3.11). In figures 3.3(a) and 3.4(a), the zeroth harmonic is slightly less than zero, indicating a mean set-down, at places where the first harmonic is smallest. This slight set-down, however, is considerably smaller than the mean set-up which exists over most of the harbor.

Figures 3.2(b), 3.3(b) and 3.4(b) show the total surface elevation, $\eta(x,t)$, at times $t = m\pi/4$, $m = 0,1,2\dots7$, for each of the first three resonant modes. Note that, in each figure, maximum height of the wave crest is greater than the maximum depth of the wave trough. Further, in contrast with linearized theory, the free surface has no nodal points and is at no time perfectly flat. These characteristics are also found in the study of finite amplitude standing waves.

3.4 An Energy Theorem and Relation to the Korteweg-de Vries Equation

The regular perturbation method of section 3.3 breaks down when ϵ/μ^2 and ϵx are $O(1)$ because resonant nonlinear interactions lead to significant growth of higher harmonics. The remedy is to include higher

harmonics at $O(\epsilon)$ in the perturbation procedure. Some consequences of physical interest can be deduced by using the technique of "multiple scales." From section 3.3, the spatial growth rate of the second harmonic is $O(\mu^{-2})$ or $O(\epsilon^{-1})$, so we introduce a slow spatial variable $\bar{x} = \epsilon x$ and assume

$$\eta_n(x) = \epsilon \eta_n^{(1)}(x, \bar{x}) + \epsilon^2 \eta_n^{(2)}(x, \bar{x}) + \dots \quad (3.4.1)$$

where x and \bar{x} are treated as separate independent variables. Then

$$\begin{aligned} \frac{d}{dx} &= \frac{\partial}{\partial x} + \epsilon \frac{\partial}{\partial \bar{x}} \\ \frac{d^2}{dx^2} &= \frac{\partial^2}{\partial x^2} + 2\epsilon \frac{\partial^2}{\partial x \partial \bar{x}} + \epsilon^2 \frac{\partial^2}{\partial \bar{x}^2} \end{aligned} \quad (3.4.2)$$

For the sake of clarity in identifying secular terms, we shall take μ^2 to be $O(\epsilon)$ and rewrite (3.2.5) as

$$\eta_n'' + n^2 \eta_n = -\frac{1}{3} \mu^2 n^4 \eta_n + \sum_s \frac{1}{2} (n^2 - s^2) \eta_s \eta_{n-s} - \sum_s \frac{1}{2} \left(\frac{n+s}{n-s} \right) \eta_s' \eta_{n-s}' \quad (3.4.3)$$

Substituting (3.4.1) and (3.4.2) into (3.4.3), we have at $O(\epsilon)$

$$\left(\frac{\partial^2}{\partial x^2} + n^2 \right) \eta_n^{(1)}(x, \bar{x}) = 0 \quad (3.4.4)$$

and at $O(\epsilon^2)$

$$\begin{aligned} \left(\frac{\partial^2}{\partial x^2} + n^2 \right) \eta_n^{(2)}(x, \bar{x}) &= -\frac{1}{3} \frac{\mu^2}{\epsilon} n^4 \eta_n^{(1)} - 2 \frac{\partial^2}{\partial x \partial \bar{x}} \eta_n^{(1)} \\ &+ \sum_s \frac{1}{2} (n^2 - s^2) \eta_s^{(1)} \eta_{n-s}^{(1)} - \frac{1}{2} \left(\frac{n+s}{n-s} \right) \frac{\partial \eta_s^{(1)}}{\partial x} \frac{\partial \eta_{n-s}^{(1)}}{\partial x} \end{aligned} \quad (3.4.5)$$

The general solution to (3.4.4) is

$$\eta_n^{(1)}(x, \bar{x}) = c_n^+(\bar{x})e^{inx} + c_n^-(\bar{x})e^{-inx} \quad (3.4.6)$$

where $c_n^+(\bar{x})$ and $c_n^-(\bar{x})$ are so far arbitrary. The boundary conditions on $\eta_n(x)$ will be imposed at the end of the calculation.

Substituting (3.4.6) into (3.4.5), we have

$$\begin{aligned} \left(\frac{\partial^2}{\partial x^2} + n^2\right)\eta_n^{(2)}(\bar{x}, x) &= f_n^+(\bar{x})e^{inx} + f_n^-(\bar{x})e^{-inx} \\ &+ \text{terms with } e^{\pm i(n-2s)x} \end{aligned} \quad (3.4.7)$$

where

$$f_n^\pm(\bar{x}) = \mp 2in \frac{dc_n^\pm}{d\bar{x}} - \frac{\mu^2}{3\epsilon} n^4 c_n^\pm + \sum_s \left[\frac{1}{2} (n^2 - s^2) + \frac{1}{2} \left(\frac{n+s}{n-s} \right) s(n-s) \right] c_s^\pm c_{n-s}^\pm \quad (3.4.8)$$

In (3.4.7), the forcing terms $f_n^+ e^{inx}$ and $f_n^- e^{-inx}$ are secular, that is, they lead to solutions for $\eta_n^{(2)}(x, \bar{x})$ which are unbounded in x . To eliminate these terms, we set $f_n^\pm(\bar{x}) = 0$, viz.

$$\pm \frac{dc_n^\pm}{d\bar{x}} - \frac{i\mu^2}{6\epsilon} n^3 c_n^\pm + \frac{i}{4} \sum_s (n+s) c_s^\pm c_{n-s}^\pm = 0 \quad (3.4.9)$$

Equation (3.4.9) governs the spatial variation of the coefficients $c_n^\pm(\bar{x})$, which first appeared at $O(\epsilon)$ in the expression for $\eta_n^{(1)}(x, \bar{x})$.

The boundary conditions (3.2.6) and (3.2.8) yield, at $O(\epsilon)$;

$$\begin{aligned} in(c_n^+(-\epsilon\ell)e^{in\ell} - c_n^-(-\epsilon\ell)e^{-in\ell}) &= 0 \\ c_n^+(0) + c_n^-(0) &= A_n + \frac{n^2}{k_n^2} Z_n(c_n^+(0) - c_n^-(0)) \end{aligned} \quad (3.4.10)$$

These two conditions, together with the two first-order differential equations (3.4.9), completely determine $c_n^+(\bar{x})$ and $c_n^-(\bar{x})$.

The system of coupled, nonlinear differential equations (3.4.9) is no easier to solve than the original system (3.2.5). However, without actually solving (3.4.9), we can make several important observations. First, note that the differential equation for $c_n^+(\bar{x})$ does not involve $c_n^-(\bar{x})$ and vice versa. This means that, to $O(\epsilon)$, there is no resonant interaction between the right-going wave $c_n^+(\bar{x})e^{in(x-t)}$ and the left-going wave $c_n^-(\bar{x})e^{-in(x+t)}$. Further, by multiplying (3.4.9) by c_{-n}^\pm and summing from $n = -\infty$ to $n = +\infty$, we obtain

$$\pm \frac{1}{2} \frac{d}{d\bar{x}} \sum_n |c_n^\pm|^2 - \frac{i\mu^2}{6\epsilon} \sum_n n^3 |c_n^\pm|^2 + \frac{i}{4} \sum_n \sum_s (n+s) c_{-n}^\pm c_s^\pm c_{n-s}^\pm = 0 \quad (3.4.11)$$

Replacing the summation indices by $p = -n$ and $q = -s$, we have

$$\sum_n n^3 |c_n^\pm|^2 = - \sum_n p^3 |c_p^\pm|^2 = 0 \quad (3.4.12)$$

$$\sum_n \sum_s (n+s) c_{-n}^\pm c_s^\pm c_{n-s}^\pm = - \sum_p \sum_q (p+q) c_{-q}^\pm c_p^\pm c_{q-p}^\pm = 0$$

so that (3.4.11) leads to

$$\begin{aligned} \sum_n |c_n^+(\bar{x})|^2 &= 2E^+ \\ \sum_n |c_n^-(\bar{x})|^2 &= 2E^- \end{aligned} \quad (3.4.13)$$

where E^+ and E^- are constants, independent of \bar{x} . From (3.4.10a), it follows that $|c_n^+(-\epsilon l)| = |c_n^-(-\epsilon l)|$ for all n , and therefore $E^+ = E^- = E$.

(3.4.13) can be interpreted as a statement of energy conservation: To $O(\epsilon^2)$, the time-averaged energy density at position x is given by

$$\begin{aligned}
E_D(x) &= \frac{1}{2\pi} \int_0^{2\pi} \frac{1}{2} (\eta^2(x,t) + u^2(x,t)) dt \\
&= \frac{\epsilon}{2\pi} \int_0^{2\pi} \frac{1}{8} \{ (\sum_n \eta_n^{(1)}(x) e^{-int})^2 + (\sum_n u_n^{(1)}(x) e^{-int})^2 \} dt \\
&= \frac{\epsilon}{8} \sum_n |\eta_n^{(1)}(x)|^2 + |u_n^{(1)}(x)|^2 + o(\epsilon^3) \tag{3.4.14}
\end{aligned}$$

From (3.4.6)

$$\begin{aligned}
\eta_n^{(1)}(x) &= c_n^+(\bar{x}) e^{inx} + c_n^-(\bar{x}) e^{-inx} \\
u_n^{(1)}(x) &= \frac{1}{in} \frac{\partial \eta_n^{(1)}}{\partial x} = c_n^+(\bar{x}) e^{inx} - c_n^-(\bar{x}) e^{-inx} \tag{3.4.15}
\end{aligned}$$

so that

$$E_D(\bar{x}) = \frac{\epsilon}{4} \sum_n |c_n^+(\bar{x})|^2 + |c_n^-(\bar{x})|^2 = \epsilon^2 E \tag{3.4.16}$$

where, from (3.4.13), $E = E^+ = E^-$ is independent of x . Thus, the total energy, which is a sum of the energies contained in all the harmonics, is independent of x . This means that an increase in the energy content of the higher harmonics must necessarily decrease the energy content of the first harmonic by the same amount.

Next, we shall establish a connection between (3.4.9) and the Korteweg-de Vries equation. Consider the total wave amplitude, at leading order,

$$\eta(x,t) = \frac{1}{2} \sum_{n=-\infty}^{\infty} \eta_n(x) e^{-int}$$

$$\begin{aligned}
&= \frac{\epsilon}{2} \sum_{-\infty}^{\infty} c_n^+(\bar{x}) e^{in(x-t)} + \frac{\epsilon}{2} \sum_{-\infty}^{\infty} c_n^-(\bar{x}) e^{-in(x+t)} \\
&\equiv \epsilon F^+(\bar{x}, x-t) + \epsilon F^-(\bar{x}, x+t)
\end{aligned} \tag{3.4.17}$$

where

$$F^\pm(\bar{x}, \theta) \equiv \frac{1}{2} \sum_{-\infty}^{\infty} c_n^\pm(\bar{x}) e^{\pm in\theta} \tag{3.4.18}$$

Using the fact that

$$\begin{aligned}
\sum_s (n+s) c_s c_{n-s} &= \sum_s (n-s) c_s c_{n-s} + \sum_s 2s c_s c_{n-s} \\
&= 3 \sum_s s c_s c_{n-s}
\end{aligned} \tag{3.4.19}$$

we find from (3.4.9)

$$\frac{\partial F^\pm}{\partial \bar{x}} + \frac{\mu}{6\epsilon} \frac{\partial^3 F^\pm}{\partial \theta^3} + \frac{3}{2} F^\pm \frac{\partial F^\pm}{\partial \theta} = 0 \tag{3.4.20}$$

(3.4.20), which is known as the Korteweg-de Vries (or KdV) equation, describes the propagation of nonlinear, weakly dispersive, shallow water waves progressing in one direction.

In the limit of no dispersion, $\mu^2 \rightarrow 0$, (3.4.20) becomes

$$\frac{\partial F}{\partial \bar{x}} + \frac{3}{2} F \frac{\partial F}{\partial \theta} = 0 \tag{3.4.21}$$

which is a quasi-linear, first order partial differential equation possessing the general solution

$$F = g\left(\theta - \frac{3}{2} F \bar{x}\right) \tag{3.4.22}$$

where g is an arbitrary differentiable function. (3.4.22) is an implicit relation for F . The characteristic curves, along which $F(\bar{x}, \theta)$ is constant, are given by

$$c = g\left(\theta - \frac{3}{2} c\bar{x}\right) \quad (3.4.23)$$

where c is a constant. If the function $g(\theta)$ possesses a maximum at a finite value of θ , then the characteristics of (3.4.23) can be shown to intersect. At the point of intersection, say (\bar{x}_0, θ_0) , F takes on two or more different values. In physical terms, a shock is formed at (\bar{x}_0, θ_0) . Therefore, in the limit of no dispersion, the KdV equation leads to the formation of shocks.

When μ^2 is not zero, (3.4.20) is a third-order partial differential equation, and its solutions are radically different from those of (3.4.21); in fact, no shocks have been found in all the known solutions, analytical or numerical. One special class of solutions, known as permanent waves, is of the form

$$F(\bar{x}, \theta) = G(\theta - \gamma\bar{x}) \quad (3.4.24)$$

where γ is a constant, and, from (3.4.20), $G(\theta)$ satisfies the ordinary differential equation

$$-\gamma \frac{dG}{d\theta} + \frac{\mu^2}{6\epsilon} \frac{d^3 G}{d\theta^3} + \frac{3}{2} G \frac{dG}{d\theta} = 0 \quad (3.4.25)$$

(3.4.25) can be solved exactly in terms of the Jacobi elliptic function "cn"; hence the name "cnoidal waves." These waves typically have sharp crests, shallow troughs, and phase velocities which depend on amplitude.

From (3.4.20), the equation for F^+ does not involve F^- and vice versa. This means that the oppositely directed waves F^+ and F^- do not interact resonantly to $O(\epsilon)$ in our perturbation analysis. Benney and Luke (1964) have used this fact to suggest that nonlinear standing waves can be constructed by superposing two cnoidal waves of equal amplitude travelling in opposite directions. Such waves differ from linear standing waves in that they do not have fixed nodal points and the free surface is at no time perfectly flat.

The solution to (3.4.9), which satisfies the complicated impedance boundary conditions at $x = 0$, in general will bear no simple resemblance to cnoidal waves or nonlinear standing waves. In the next section, we present a numerical procedure for obtaining the solution for the wave field in the harbor.

3.5 Numerical Solution by Iteration

The infinite set of differential equations (3.2.5) is truncated at the N -th harmonic, yielding the system

$$\eta_n'' + k_n^2 \eta_n = \sum_s R_{ns} \eta_s \eta_{n-s} + \sum_s S_{ns} \eta_s' \eta_{n-s}'$$

$$\eta_n'(-l) = 0$$

$$\eta_n'(0) = A_n - \frac{in}{k_n^2} Z_n \eta_n'(0)$$

$$n = 1, 2, 3, \dots, N \quad (3.5.1)$$

where

$$k_n^2 \equiv n^2 \left(1 + \frac{1}{3} \mu^2 n^2 \right)$$

$$R_{ns} = \frac{1}{2} (n^2 - s^2)$$

$$S_{ns} = -\frac{1}{2} \left(\frac{n+s}{n-s} \right)$$

$$Z_n = k_n \delta \left[1 + \frac{2i}{\pi} \left(\ln k_n \delta - \ln \frac{2\gamma}{\pi e} \right) \right] \left(\frac{k_n}{n} \right) \quad (3.5.2)$$

(3.5.1) is as a nonlinear, two-point, boundary value problem. Unlike an initial value problem, which can be solved by direct numerical integration, the solution of (3.5.1) requires an iterative procedure.

At the $(p+1)$ -th iteration, we solve the linear boundary value problem

$$\eta_n^{(p+1)''} + k_n^2 \eta_n^{(p+1)} = \sum_s R_{ns} \eta_s^{(p)} \eta_{n-s}^{(p+1)} + \sum_s S_{ns} \eta_s^{(p)} \eta_{n-s}^{(p+1)}$$

$$\eta_n^{(p+1)}(-\ell) = 0$$

$$\eta_n^{(p+1)}(0) = A_n - \left(\frac{i n}{k_n^2} \right) Z_n \eta_n^{(p+1)}$$

$$n = 1, 2, 3, \dots, N \quad (3.5.3)$$

using finite difference methods. The rate of convergence of successive solutions can be increased by using a relaxation technique, which consists of replacing $\eta_n^{(p+1)}(x)$ by

$$\bar{\eta}_n^{(p+1)}(x) = \lambda \eta_n^{(p+1)}(x) + (1 - \lambda) \eta_n^{(p)}(x) \quad (3.5.4)$$

With $\lambda = 1$, convergence of successive iterates was found to be slow and oscillatory; with $\lambda = .5$, convergence was much faster and, in most cases,

monotonic. The iterative procedure is terminated when successive solutions for $\eta_n(x)$ differ by less than .001, that is, when

$$\begin{aligned} \text{Max}_x |\bar{\eta}_n^{(p+1)}(x) - \eta_n^{(p)}(x)| < .001 \\ n = 1, 2, 3, \dots, N \end{aligned} \quad (3.5.5)$$

If the maximum value of $|\bar{\eta}_N(x)|$ exceeds .001, truncation at the N-th harmonic is deemed inadequate and the system of differential equations is expanded to include the (N + 1) harmonic. The expanded system is then solved by iteration. This procedure is continued until a "penultimate" solution is found, for which

$$\text{Max}_x |\bar{\eta}_{N^*}(x)| < .001 \quad (3.5.6)$$

where N^* is the highest harmonic in the solution.

In the finite difference solution of (3.5.3), the domain $-\ell \leq x \leq 0$ is represented by NPT equally spaced points located at positions $x_j = -\ell + (j - 1) \cdot H$, $j = 1, 2, 3, \dots, \text{NPT}$, where H is the interval size

$$H = \ell / (\text{NPT} - 1) \quad (3.5.7)$$

When the solution requires many harmonics, the choice for H must be made correspondingly small. For example, if we insist that one wavelength of the highest harmonic shall be represented by at least ten points, then the requirement on H is

$$k_{N^*} H \leq \frac{2\pi}{10} = .628 \quad (3.5.8)$$

Since the number of harmonics in the solution, N^* , is not known a priori,

it is necessary to make some initial choice for H, to solve the problem, and then to check to see if (3.5.8) is satisfied. If it is not, the problem must be solved again with a smaller value for H.

The finite difference representation of (3.5.3) is a system of $(N \cdot NPT)$ linear algebraic equations for the complex amplitudes $\eta_n^{(p+1)}(x_j)$, $n = 1, 2, 3, \dots, N$, $j = 1, 2, 3, \dots, NPT$. In principle, the solution can be found by direct Gaussian elimination or matrix inversion, in $O(N \cdot NPT)^3$ operations. A more efficient method is to first calculate N "basis solutions" $e_n(x, q)$ $n = 1, 2, 3, \dots, N$, $q = 1, 2, 3, \dots, N$, which are solutions to the initial value problem for $e_n(x, q)$ defined by

$$e_n'' + k_n^2 e_n = \sum_s R_{ns} \eta_s^{(p)} e_{n-s} + \sum_s S_{ns} \eta_s^{(p)} e_{n-s}'$$

$$e_n'(-l, q) = 0$$

$$e_n(-l, q) = \begin{cases} 1 & \text{if } n = q \\ 0 & \text{if } n \neq q \end{cases}$$

$$n = 1, 2, 3, \dots, N$$

$$q = 1, 2, 3, \dots, N \quad (3.5.9)$$

The solution to (3.5.9) can be rapidly calculated by "stepping" through the difference mesh from x_1 to x_{NPT} . This requires $O(N^2 \cdot NPT)$ operations for each basis solution, using the differencing scheme of (3.5.13) below. Altogether, $O(N^3 \cdot NPT)$ operations are needed to calculate all N basis solutions.

The complete solution to the boundary value problem (3.5.3) is a linear superposition

$$\eta_n^{(p+1)}(x) = \sum_{q=1}^N \alpha_q e_n(x, q) \quad (3.5.10)$$

The boundary condition (3.5.3c) leads to the system of N equations

$$\sum_{q=1}^N [e_n(0, q) + \frac{i n}{k_n^2} Z_n e_n(0, q)] \cdot \alpha_q = A_n$$

$$n = 1, 2, 3 \dots N \quad (3.5.11)$$

which determines the N coefficients α_q , $q = 1, 2, 3 \dots N$. The solution of (3.5.11) by Gaussian elimination requires $O(N^3)$ operations, which is insignificant as compared with the $O(N^3 \cdot NPT)$ operations needed to calculate $e_n(x, q)$.

Thus, by this method, the total number of operations required to solve the boundary value problem for $\eta_n^{(p+1)}(x)$ is $O(N^3 \cdot NPT)$. On the IBM 370 computer at the M.I.T. Information Processing Center, the computation time per iteration was found to be

$$\text{Time (in } \mu \text{ sec)} = 8(NPT) \cdot N^3 \quad (3.5.12)$$

This compares quite favorably with the $O(N \cdot NPT)^3$ operations that would be required if direct Gaussian elimination were used.

The finite difference approximation to (3.5.9) and (3.5.11) was chosen to be

$$\Delta_n^2 e_n(x_J) + \frac{k_n^2}{2} [e_n(x_{J+1}) + e_n(x_{J-1})] =$$

$$\sum_s R_{ns} \eta_s^{(p)}(x_J) e_{n-s}(x_J) + \sum_s S_{ns} \Delta \eta_s^{(p)}(x_J) \Delta e_{n-s}(x_J)$$

$$e_n(x_1) = \begin{cases} 1 & n = q \\ 0 & n \neq q \end{cases}$$

$$e_n(x_2) = e_n(x_1) + \frac{1}{2} H^2 \left[\sum_s R_{ns} n_s^{(p)}(x_1) e_{n-s}(x_1) - k_n^2 e_n(x_1) \right] \quad (3.5.13)$$

and

$$\sum_{q=1}^N [e_n(x_{NPT}, q) + \frac{in}{k_n^2} \Delta e_n(x_{NPT}, q)] \cdot \alpha_q = A_n \quad (3.5.14)$$

where

$$\begin{aligned} \Delta e(x_J) &\equiv \frac{1}{H} [e(x_J) - e(x_{J-1})] = \frac{d}{dx} e(x) \Big|_{x=x_J} + O(H) \\ \Delta^2 e(x_J) &\equiv \frac{1}{H^2} [e(x_{J+1}) - 2e(x_J) + e(x_{J-1})] \\ &= \frac{d^2}{dx^2} \cdot e(x) \Big|_{x=x_J} + O(H^2) \end{aligned} \quad (3.5.15)$$

This finite difference representation was chosen for stability, accuracy, and computation efficiency. In (3.5.13a), the advantage of $\frac{1}{2} k_n^2 [e_n(x_{J+1}) + e_n(x_{J-1})]$ in place of simply $k_n^2 e_n(x_J)$ is that it yields an unconditionally stable scheme for the initial value problem, in which the right hand side of (3.5.13a) is zero. The expression for $e_n(x_2)$ is derived from the Taylor series

$$e_n(x_2) = e_n(x_1) + H e_n'(x_1) + \frac{1}{2} H^2 e_n''(x_1) + \frac{1}{6} H^3 e_n'''(x_1) + O(H^4) \quad (3.5.16)$$

in which $e_n'(x_1) = 0$ by the boundary condition (3.5.9b), and the values of $e_n''(x_1)$ and $e_n'''(x_1)$ are found directly from the differential equation,

(3.5.9a). The relatively high accuracy in $e_n(x_2)$ is desirable for solving initial value problems with $e_n(x_1)$ and $e_n(x_2)$ as starting values. The use of backward rather than central differences for Δ increases the overall truncation error from $O(H^2)$ to $O(H)$, but has the advantage of increased efficiency in the computational algorithm. If central differencing is used, a system of $N \times N$ linear equations for $e_n(x_j)$, $n = 1, 2, \dots, N$ must be solved at each point x_j of the finite difference mesh. This would require an additional $O(N^3 \cdot NPT)$ operations for each basis solution and $O(N^4 \cdot NPT)$ operations for the N basis solutions needed to solve the boundary value problem.

A printout of the computer program, with complete documentation, is found in Appendix A.

CHAPTER IV
EXPERIMENTAL STUDY OF THE LONG, NARROW BAY

4.1 Equipment and Procedures

4.1.1 Wave Basin

The wave basin, schematically shown in Figure 4.1, measures 43 ft. long by 25 ft. wide by 1.5 ft. deep and is made of concrete. Care was taken to make the basin floor horizontal. The interior of the basin is lined with two layers of plastic to prevent leakage and to provide a smooth inner surface.

The wave generator consists of two aluminum plates, each 12.5 ft. long by 1.5 ft. wide by .25 in. thick. The plates are connected to each other by a thin plexiglas strip and are hinged at the bottom to an eight inch wide plate which is bolted to the floor. Each plate is connected to a separate flywheel by a bar whose point of attachment can be adjusted to give different stroke lengths. A rotary drive shaft connects the flywheels to a 1.5 horsepower motor whose maximum output torque is 515 in.-lbs. and whose period is continuously variable from .6 to 3.0 sec. The motor and flywheel assembly are mounted on the basin wall behind the wave generator. A row of closely spaced concrete blocks is placed behind and parallel to the aluminum plates in order to dampen waves generated behind the wave maker.

The open-sea condition is simulated by placing absorbers along the three walls facing the wave generator. The wave absorbers consist of a 4 in. layer of rubberized horsehair mounted on a plywood base

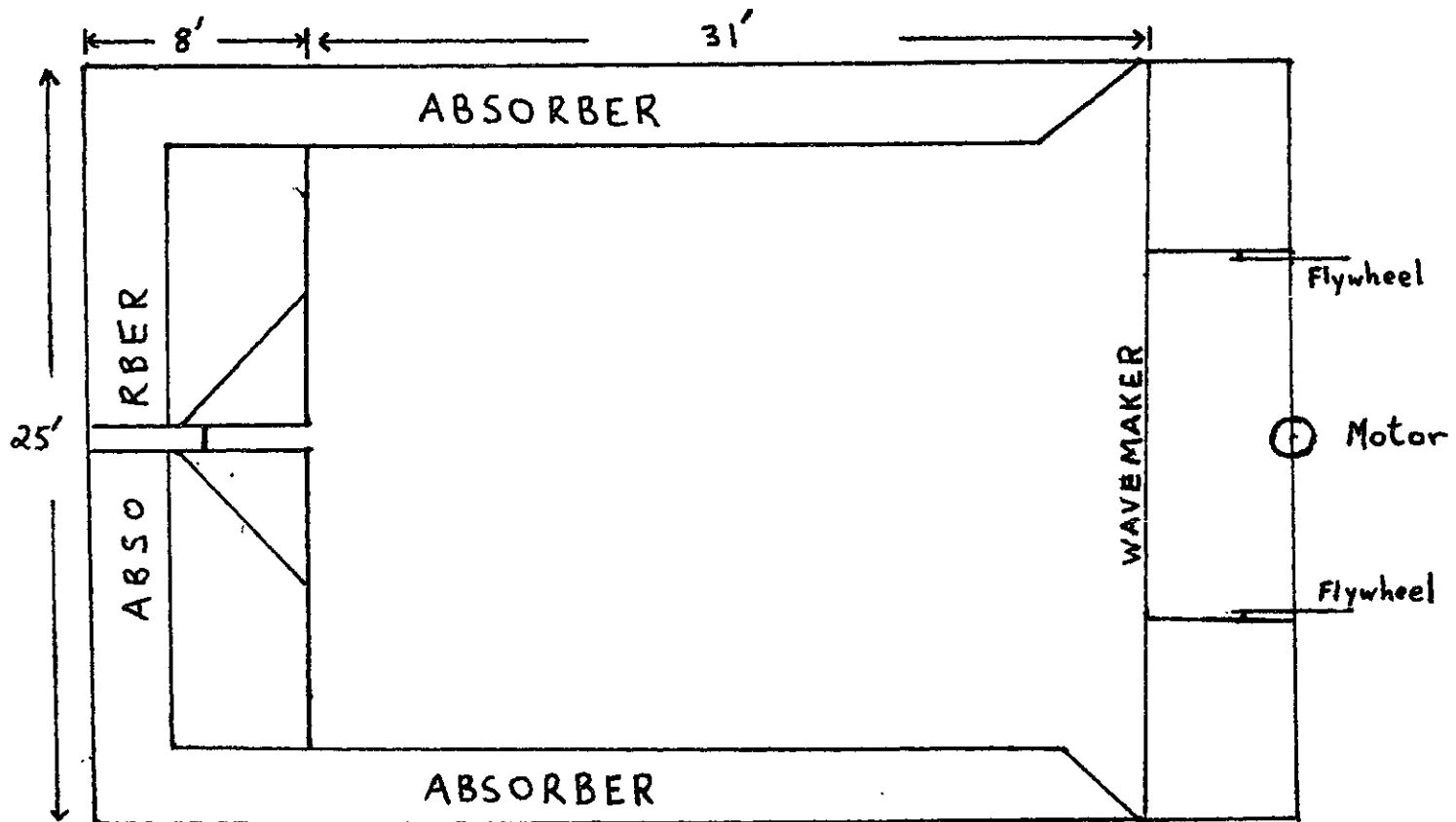


Fig. 4.1. Experimental set-up.

having a 1:5 slope. In preliminary tests, the wave absorbers were found to have a reflection coefficient of 20% for a wave period of 1.5 sec. and a water depth of 6 in.

Two metal rails, mounted on the side walls of the basin, support a movable aluminum carriage. Measuring instruments can be placed on the carriage and swept along the entire length of the basin.

To inhibit the growth of algae, a dilute solution of CuSO_4 was added once every two weeks. The basin was completely emptied every two months; the liner was washed clean; and deposits of aluminum hydroxide were scraped from the wave generator.

4.1.2 Wave Gauges

Resistance wave gauges were used in conjunction with a Model 296 Sanborn recorder. A typical wave gauge consists of two parallel stainless steel wires, measuring $5/64$ " in diameter and 8" long, separated by approximately .5". A bridge circuit is used to measure the resistance between the parallel wires, which is proportional to their depth of immersion in the water, with an error of roughly 3%. The stylus of the Sanborn recorder deflects by an amount proportional to the probe resistance and produces a permanent record on heat-sensitive paper. Typical calibration curves are shown in Fig. 4.2.

4.1.3 On-Line Digital Computer

In order to analyze nonlinear wave profiles, the voltage output terminal of the Sanborn recorder is connected by a long coaxial cable

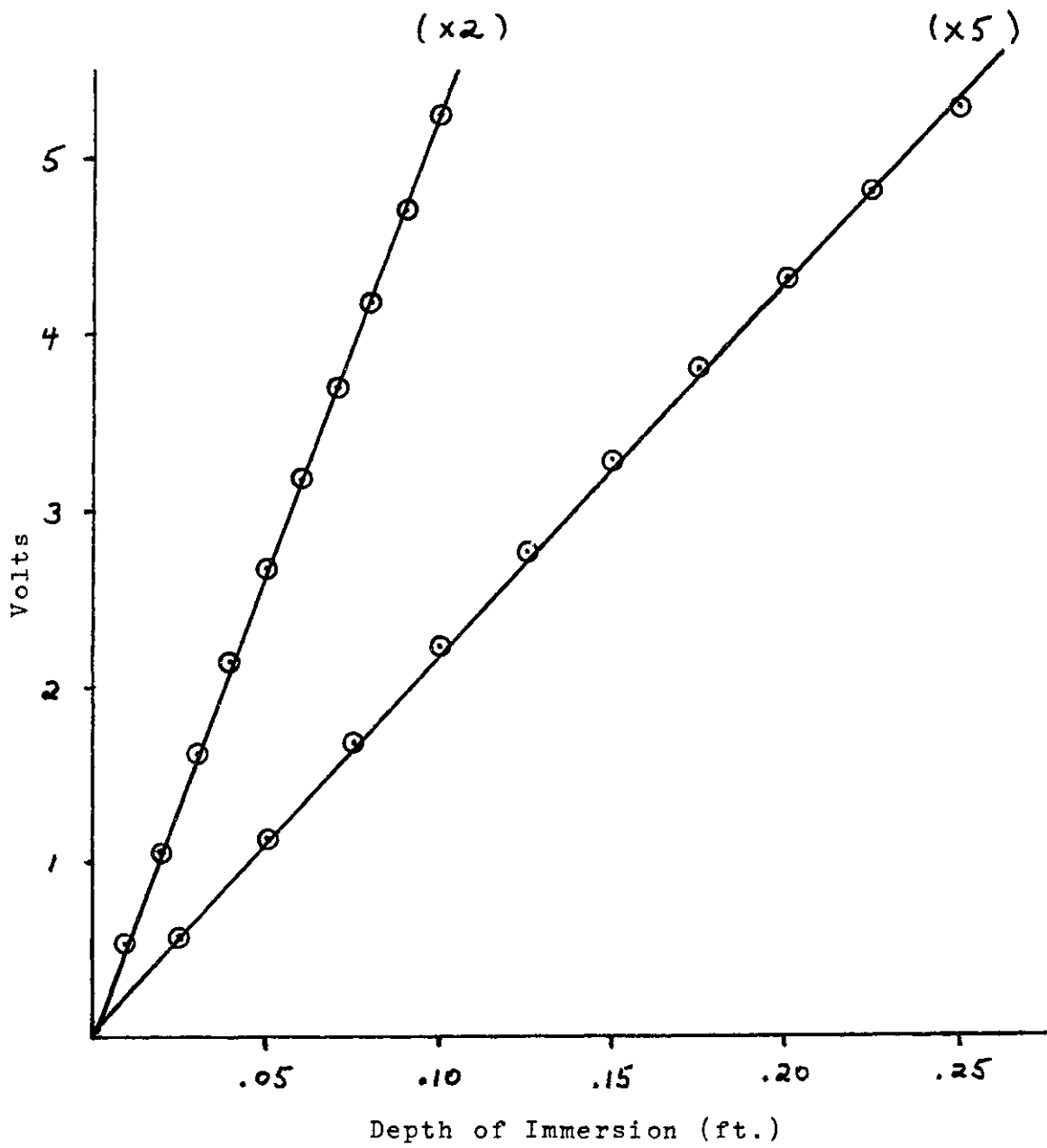


Fig. 4.2. Typical calibration curves of a wave gauge, at two attenuator settings.

to a Hewlett Packard 3450A Multi-Function Meter, which has a maximum sampling rate of 14 counts per sec. The output values of the digital voltmeter are read directly into the central processing unit of the computer, where they are used as input to a BASIC language program.

The computer program is remotely controlled by means of a switch inserted in the coaxial cable joining the recorder to the computer. In one position the switch allows the voltage of the recorder, which is always less than three volts, to pass directly to the computer. In the other position, the voltage across the terminals of a six volt battery is fed into the computer. In each program for data reduction and analysis, a special subroutine directs the execution of the program in accordance with the position of this switch. (See Appendix B.)

4.1.4 Model Harbor

The model harbor consists of two L-shaped sections placed adjacent to each other to form a narrow channel, as shown in Fig. 4.1. Two by four in. beams join the legs of each L for structural rigidity. The model is made of 3/4 in. marine plywood and is coated with epoxy based paint, to increase its durability in water. Each leg of the L's is eight ft. long and consists of a one ft. high wall attached to a six in. wide foundation. Concrete blocks are placed on the foundations to ensure that the model does not move under the action of incident waves. To reduce flow separation, the right angle corner of each L was sanded to a radius of curvature of roughly .5 in. After the harbor was placed in position, strips of sponge rubber were used to seal any gaps

between the basin floor and the harbor walls.

The back wall of the harbor consists of a four in. wide by one ft. high by 3/8 in. thick plexiglas strip which is mounted on a wooden foundation. The back wall is inserted between the two L's at any desired position and clamped into place.

In the harbor resonance experiments, the wave amplitude in the harbor was Fourier analyzed at intervals of two inches along the centerline of the harbor channel. While the flow field in the vicinity of the harbor entrance was observed to be two-dimensional, no lateral variation in the wave amplitude was observed beyond a distance of roughly four inches into the harbor.

4.2 Multiple Reflections from Wavemaker

In the laboratory, the infinite ocean is modelled by a large but finite wave basin. We must therefore consider to what extent reflections from the walls of the basin will perturb the steady-state wave field in the "ocean." Raichlen and Ippen (1965) have found that the effect of wall reflections is quite pronounced when all sides of the basin are perfectly reflective. In our experimental set-up, wave absorbers suppress reflections from three sides of the wave basin. However, the aluminum wavemaker on the fourth side is an almost perfectly reflective surface.

To estimate the effect of multiple reflections from the wavemaker, consider the geometry of Fig. 4.3. We shall treat the ocean as linear and confine our attention to waves of a single frequency, ω . The wave

field in the ocean satisfies the Helmholtz equation

$$(\nabla^2 + k^2)\eta(x,y) = 0 \quad (4.2.1)$$

where

$$\begin{aligned} \eta(x,y,t) &= \text{Re}(\eta(x,y)e^{-it}) \\ k^2 &= 1 + \frac{1}{3}(\omega^2 h/g) \end{aligned} \quad (4.2.2)$$

For simplicity, the harbor entrance will be replaced by a point source located at (0,0), so that

$$\frac{\partial \eta}{\partial x} = 2iQ\delta(y) \quad \text{at } x = 0 \quad (4.2.3)$$

where Q is proportional to the source strength. Denoting the depth-averaged, horizontal velocity of the wavemaker by U_m , we have

$$\frac{\partial \eta}{\partial x} = ik^2 U_m \quad \text{at } x = \ell_m \quad (4.2.4)$$

where $\ell_m \equiv (\omega/\sqrt{gh}) \cdot L_m$. When the harbor is shut ($Q = 0$), the solution to (4.2.1) subject to (4.2.3), (4.2.4) is simply the standing wave

$$\eta^S(x,y) = \left(\frac{-ikU_m}{\sin k\ell_m} \right) \cos kx \quad (4.2.5)$$

Note that η^S is theoretically infinite whenever $k\ell_m = (\text{integer}) \cdot \pi$; in practice, nonlinearity and viscous dissipation will limit η^S to a finite value.

When Q is nonzero, we must add to $\eta^S(x,y)$ the field due to the radiating point source at (0,0). If there were no wall at $x = \ell_m$, the radiated wave would be

$$\eta^R(x,y) = QH_0^{(1)}(kr) \quad (4.2.6)$$

just as it is in the infinite ocean. In order to satisfy the boundary condition

$$\frac{\partial \eta^R}{\partial x} = 0 \quad \text{at } x = \ell_m \quad (4.2.7)$$

we place an "image" source of strength Q at position $(2\ell_m, 0)$. But now, to satisfy the zero flux condition at $x = 0$, we must place another image source of strength Q at position $(-2\ell_m, 0)$. Proceeding in this way, we obtain an infinite string of image sources, all of strength Q , located on the x -axis at $x = \pm 2\ell_m, \pm 4\ell_m, \pm 6\ell_m, \dots$, as shown in Fig. 4.3. The total wave field due to all these image sources is

$$\tilde{\eta}(x,y) = Q \sum_{n=1}^{\infty} H_0^{(1)}(k|\vec{r} - 2n\ell_m \hat{x}|) + H_0^{(1)}(k|\vec{r} + 2n\ell_m \hat{x}|) \quad (4.2.8)$$

Along the x -axis

$$\tilde{\eta}(x,0) = E(-x) + E(+x) \quad (4.2.9)$$

where

$$E(x) \equiv Q \sum_{n=1}^{\infty} H_0^{(1)}(2nk\ell_m + kx) \quad (4.2.10)$$

To approximate $E(x)$, we follow Morse and Feshbach (1953) and assume $k\ell_m \gg 1$, so that, in the domain $0 \leq x \leq \ell_m$, all Hankel functions may be represented by their asymptotic forms. Then

$$E(x) \approx \sqrt{\frac{2i}{\pi}} Q e^{ikx} \sum_{n=1}^{\infty} \frac{e^{2ink\ell_m}}{\sqrt{2nk\ell_m + kx}} \quad (4.2.11)$$

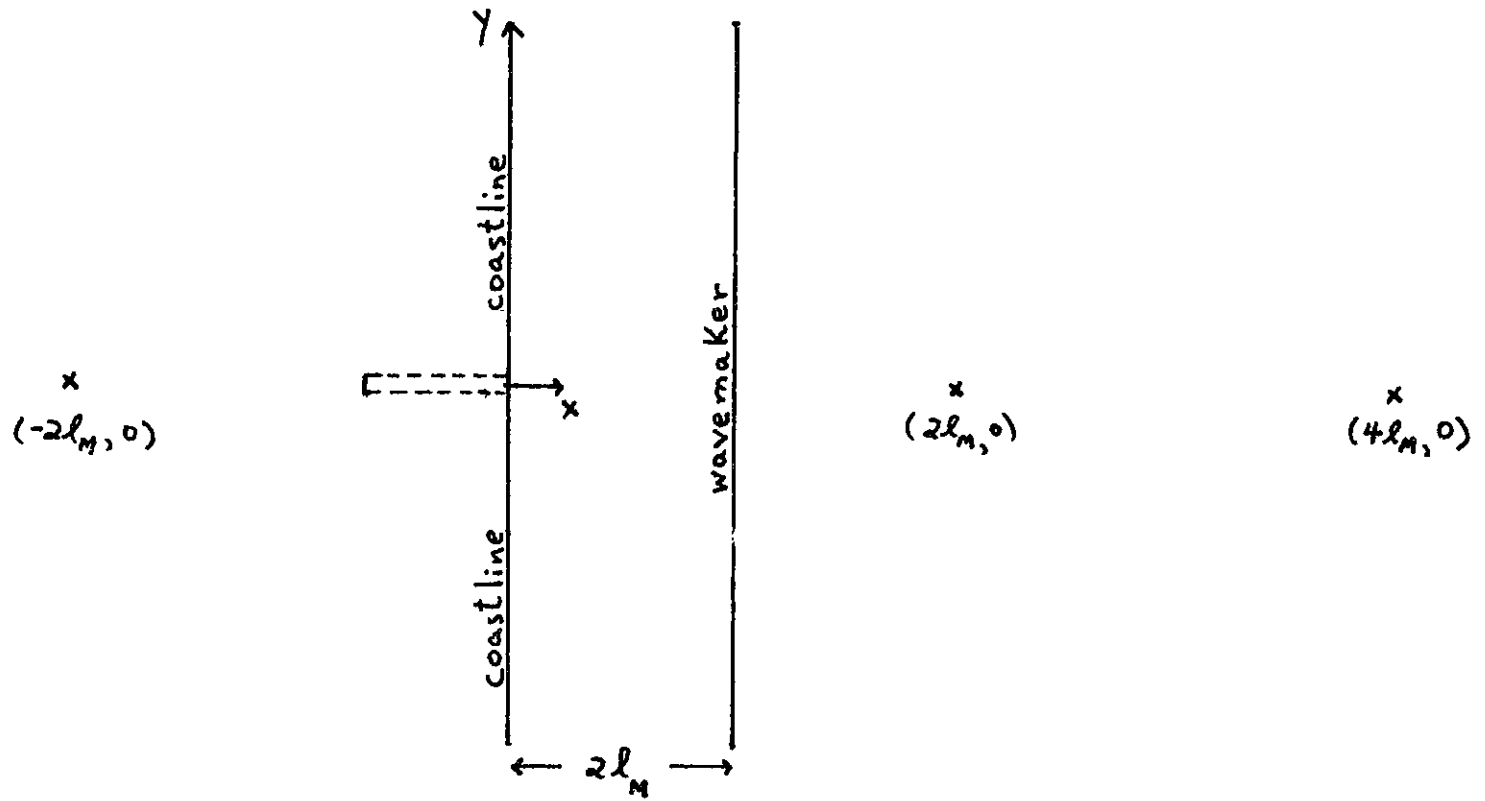


Fig. 4.3. Theoretical study of multiple reflections from wavemaker: Placement of images.

Except in the case $k\ell_m = (\text{integer}) \cdot \pi$, for which the sum in (4.2.11) diverges, we may approximate $E(x)$ by

$$E(x) \approx \sqrt{\frac{2i}{\pi}} Q e^{ikx} \int_1^{\infty} dv \frac{e^{i(2k\ell_m)v}}{\sqrt{2k\ell_m v + kx}} \quad (4.2.12)$$

The integral in (4.2.12) can be evaluated explicitly in terms of Fresnel integrals; but, for the purpose of estimation, we simply integrate once by parts to obtain

$$E(x) \approx \sqrt{\frac{2i}{\pi}} Q e^{ikx} \left\{ \left(\frac{-1}{2ik\ell_m} \right) \frac{e^{2ik\ell_m}}{\sqrt{2k\ell_m + kx}} \right\} + O(k\ell_m)^{-5/2} \quad (4.2.13)$$

From (4.2.9), the net result of all multiple reflections is

$$\tilde{\eta}(x,0) \approx \frac{1}{\sqrt{2i\pi}} \frac{Q}{k\ell_m} \left\{ \frac{e^{i(2k\ell_m + kx)}}{\sqrt{2k\ell_m + kx}} + \frac{e^{i(2k\ell_m - kx)}}{\sqrt{2k\ell_m - kx}} \right\} + O(k\ell_m)^{-5/2} \quad (4.2.14)$$

The interesting feature of (4.2.14) is that, whereas the effect of a single reflected wave is $O(k\ell_m)^{-1/2}$, the combined effect of all reflections is only of $O(k\ell_m)^{-3/2}$.

Our conclusion therefore is that, so long as

$$k\ell_m \gg 1 \quad (4.2.15)$$

$$k\ell_m \neq (\text{integer}) \cdot \pi$$

successive reflections from the wavemaker add destructively to produce a net effect whose magnitude is only $O(k\ell_m)^{-3/2}$. When (4.2.15) is satisfied, the total wave field in the laboratory "ocean" is

$$\eta(x,y) = \left(\frac{-ikU_m}{\sin k\ell_m}\right)\cos kx + QH_0^{(1)}(kr) + O(k\ell_m)^{-3/2} \quad (4.2.16)$$

and the effect of multiple reflections is small.

When either of the conditions in (4.2.15) is violated, the effect of multiple reflections can be quite significant. When this occurs, the harbor basin and ocean basin are said to be strongly coupled. Condition (4.2.15) states that strong coupling will occur unless (a) the ocean basin is very much larger than a wavelength and (b) the frequency of oscillation is not close to a resonant frequency of the ocean basin.

Figs. 4.4 (a),(b),(c) show experimental measurements of the wave field in the model ocean, along the centerline $x = 0$. The experimental values

$$L_m = 31'2''$$

$$\omega = 2\pi/(1.545 \text{ sec}) = 4.067 \text{ sec}^{-1}$$

$$h = .5'$$

yield

$$k\ell_m = 32.96 = 10.49\pi$$

so that (4.2.15) is satisfied. The graph at the top shows the standing wave amplitude $\eta^S(x,0)$ in the ocean, when the harbor entrance is closed; the solid curve is (4.2.5). The middle graph shows the total wave field when the harbor entrance is open, and the first resonant

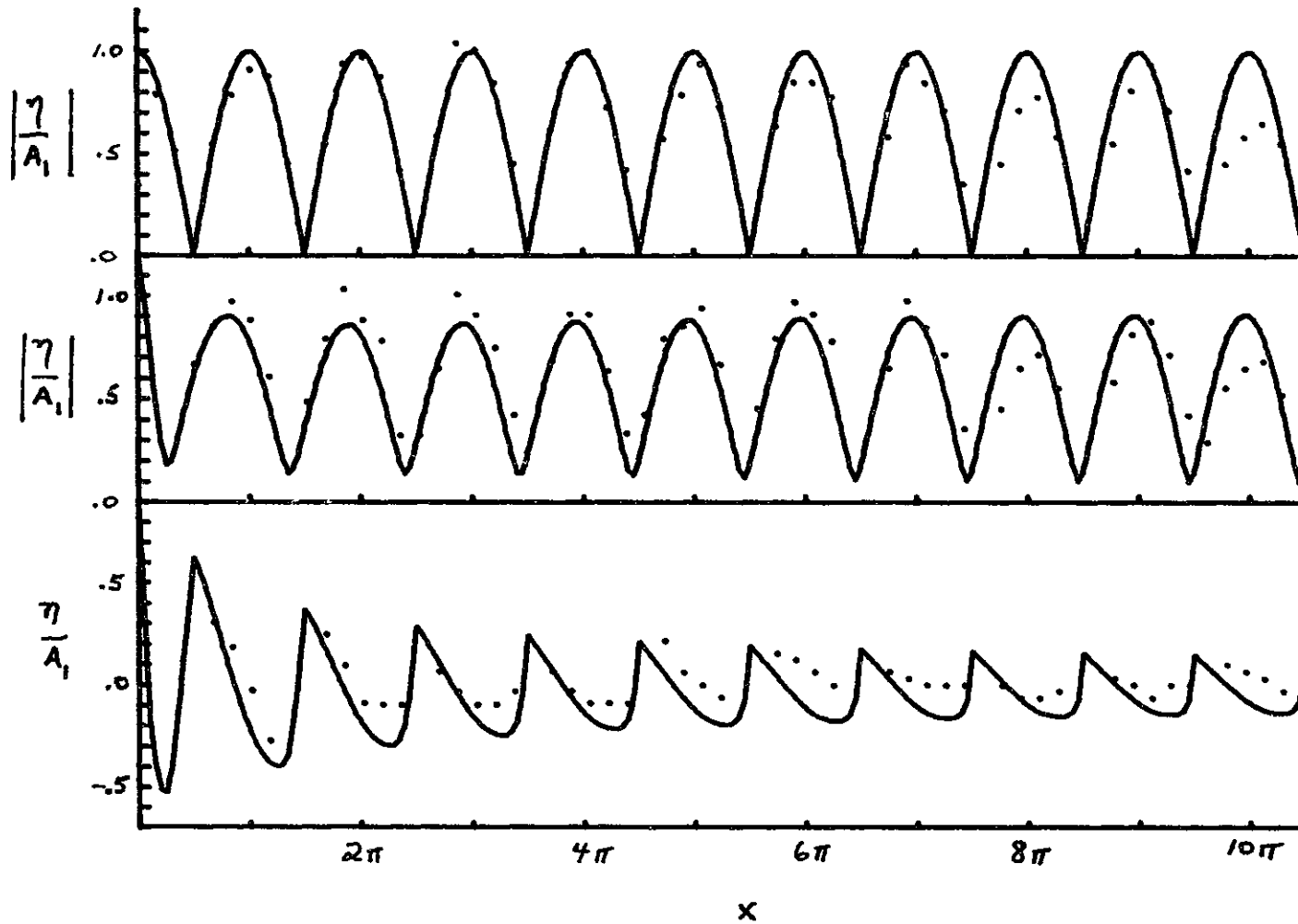


Fig. 4.4a. Experiment (·) vs. theory (—) for the wave amplitude in the ocean ($h = .5$ ft., $2a = .33$ ft., $L = 1.211$ ft., $\omega = 4.067 \text{ sec}^{-1}$, $L_o = 31.17$ ft.). Top: harbor closed. Middle: harbor open. Bottom: the radiated wave. $A_1 = .015$.

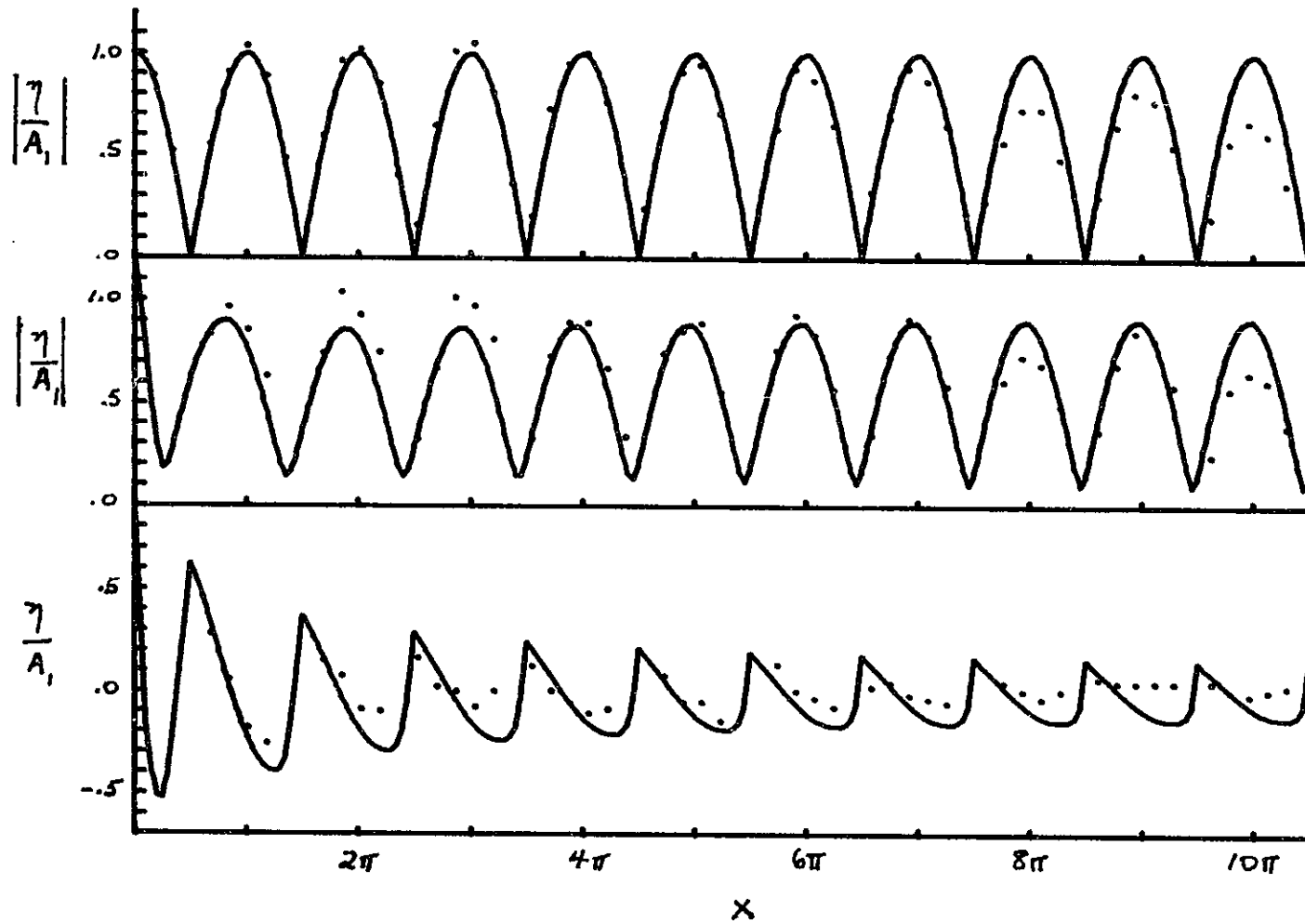


Fig. 4.4b. Experiment (·) vs. theory (—) for the wave amplitude in the ocean ($h = .5$ ft., $2a = .33$ ft., $L = 1.211$ ft., $\omega = 4.067 \text{ sec}^{-1}$, $L_{III} = 31.17$ ft.). Top: harbor closed. Middle: harbor open. Bottom: the radiated wave. $A_1 = .027$.

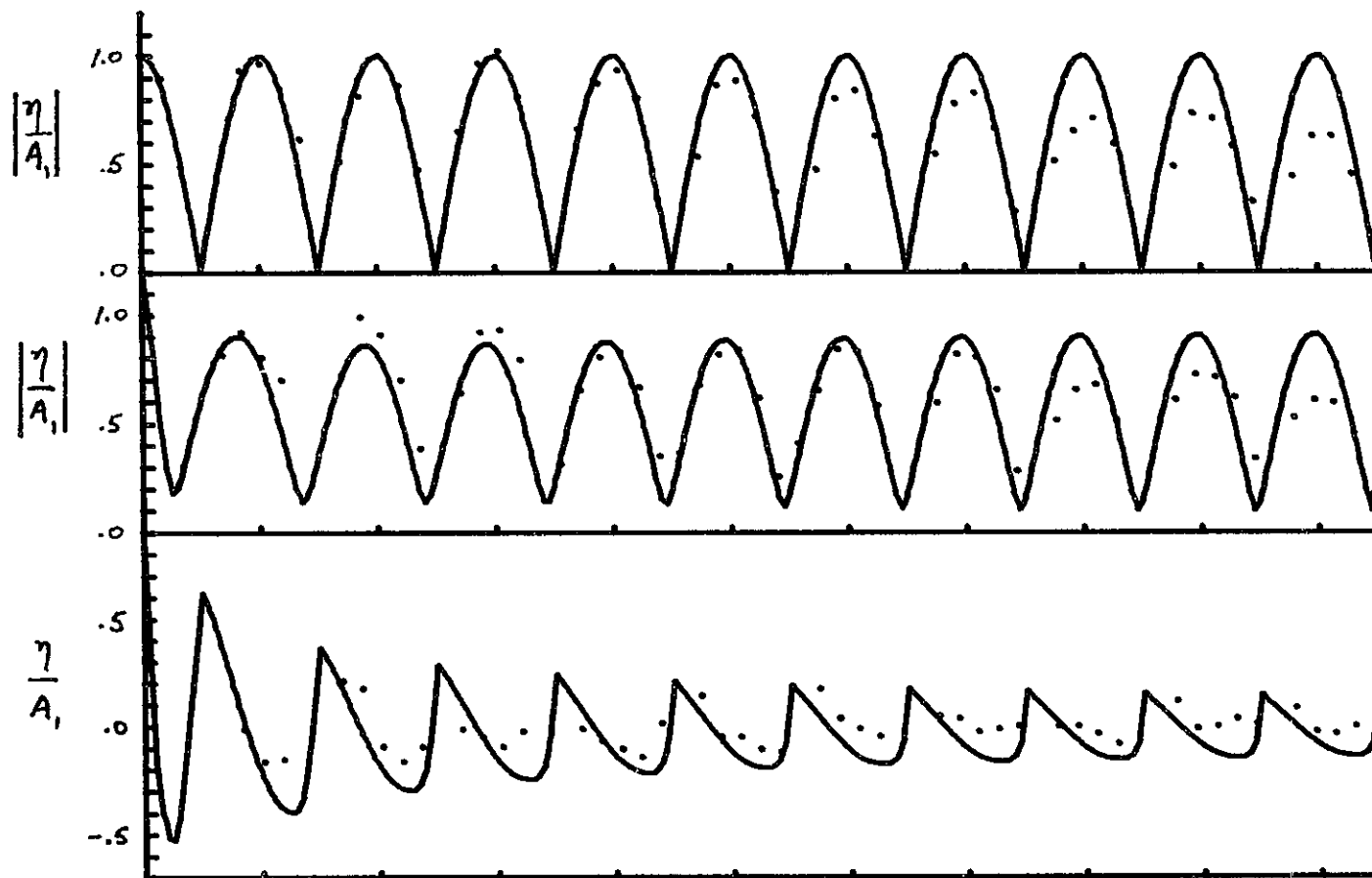


Fig. 4.4c. Experiment (\cdot) vs. theory ($—$) for the wave amplitude in the ocean ($h = .5$ ft., $2a = .33$ ft., $L = 1.211$ ft., $\omega = 4.067$ sec $^{-1}$, $L_m = 31.17$ ft.). Top: harbor closed. Middle: harbor open. Bottom: the radiated wave. $A_1 = .040$.

harbor mode (having $L = 1.211$ ft.) is excited; the solid curve is (4.2.16). The bottom graph shows the component of the total wave field which is the radiated wave, $\eta^R(x,0) = QH_0^{(1)}(kx)$. Since the agreement is fairly good, it confirms experimentally that (i) the ocean can be treated linearly and (ii) reflection from the wavemaker is not significant.

4.3 Real Fluid Effects

In the following two sections, all variables and coordinates are dimensional.

4.3.1 Viscous Dissipation in Wall Boundary Layers

In a laboratory setting, the damping of surface waves in a slightly viscous fluid is a well-known problem. For infinitesimal waves of frequency ω , propagating in a fluid of viscosity ν , the fluid motion is essentially irrotational except near boundaries, where viscous boundary layers of thickness

$$\delta_\nu = \sqrt{2\nu/\omega} \quad (4.3.1.1)$$

are formed. Viscous energy dissipation occurs in (a) the boundary layers near solid walls, (b) the boundary layer near the free surface, and (c) the main body of the fluid. Ursell (1952) has shown that the solid wall boundary layers account for most of the dissipated energy.

For oscillatory boundary layers, the transition from laminar to turbulent flow on a smooth flat surface occurs at the critical

Reynolds number (see Phillips (1966), p. 43)

$$R_c = \frac{\bar{U} \delta_v}{\nu} \approx 160 \quad (4.3.1.2)$$

where \bar{U} is the particle velocity. In shallow water,

$$\bar{U} = \frac{A}{h} \cdot \sqrt{gh} \quad (4.3.1.3)$$

where A is the wave amplitude, and

$$R_c = \left(\frac{A}{h}\right) \sqrt{gh} \sqrt{\frac{2}{\nu \omega}} \quad (4.3.1.4)$$

In the experiments, $h = .5 \text{ ft.}$, $gh = 16 \text{ ft}^2/\text{sec}^2$, $\omega = 4.067 \text{ sec}^{-1}$,
 $\nu = 10^{-5} \text{ ft}^2/\text{sec}$, and

$$R = \left(\frac{A}{h}\right) \cdot 887 \quad (4.3.1.5)$$

so that the transition to turbulence occurs when

$$\left(\frac{A}{h}\right)_c \approx .18 \quad (4.3.1.6)$$

In all but one of the harbor resonance experiments, the value of A/h was below this critical value; therefore, laminar flows prevailed.

Batchelor (1976, pp. 353-358) derives the following expression for the time-averaged power loss per unit area in an oscillatory laminar boundary layer:

$$\frac{dP_v}{dA} = \frac{1}{2\delta_v} \rho \nu |U_T|^2 \quad (4.3.1.7)$$

where $\text{Re}(U_T e^{-i\omega t})$ is the local tangential velocity at the boundary according to inviscid theory and ρ is the fluid density.

To estimate the viscous losses in the far field of the long, narrow bay, we shall use the linear expressions for the wave field,

$$\begin{aligned} \eta(x,y,t) &= \text{Re}(T \cos k(x+L)e^{-i\omega t}) \\ \vec{u}(x,y,t) &= \text{Re}(i \frac{gkT}{\omega} \sin k(x+L)e^{-i\omega t})_x + O(u^2) \end{aligned} \quad (4.3.1.8)$$

where $O(u^2)$ terms include the vertical component of velocity and the depth-dependent terms of the horizontal velocity. The expression for T in terms of the incident wave amplitude is found in Equation (1.3.6). From (4.3.1.7), the power loss per unit area on all surfaces parallel to the x-axis is

$$\frac{dP_v}{dA} = \frac{1}{2\delta_v} \rho v \left| \frac{gkT}{\omega} \right|^2 \sin^2 k(x+L) \quad (4.3.1.9)$$

Integrating over the side walls and bottom of the channel, we obtain for the total power loss

$$\begin{aligned} P_v &= (2a + 2h) \int_{-L}^0 \left(\frac{dP_v}{dA} \right) dx \\ &= \frac{1}{2\delta_v} \rho v \left| \frac{gkT}{\omega} \right|^2 (2a + 2h) \frac{1}{2k} (kL - \frac{1}{2} \sin 2kL) \\ &\approx \frac{1}{2\delta_v} \rho v \left| \frac{gkT}{\omega} \right|^2 (a + h)L \end{aligned} \quad (4.3.1.10)$$

Let us compare P_v with the energy loss due to radiation damping at the harbor entrance. The time-averaged radiated power is given by

$$\begin{aligned} P_R &= (2a \cdot h) \cdot \frac{\omega}{2\pi} \int_0^{2\pi/\omega} dt \rho g \eta(o,t) u(o,t) \\ &= \frac{1}{2} (ah) \rho g \left(\frac{gk}{\omega} \right) |T|^2 \sin 2kL \end{aligned}$$

$$\approx \frac{1}{2}(ah)\rho g\left(\frac{gk}{\omega}\right) |T|^2 \quad (4.3.1.11)$$

and, from (4.3.1.10),

$$\begin{aligned} P_V/P_R &= \frac{\nu}{\delta_V} \left(\frac{k}{\omega}\right) \frac{a+h}{a} \frac{L}{h} \\ &= \left(\frac{a+h}{2a}\right)(kL)\left(\frac{\delta_V}{h}\right) \end{aligned} \quad (4.3.1.11)$$

In the harbor resonance experiments, $a = 2$ in., $h = 6$ in., $\omega = 4.067$ sec^{-1} , $\nu = 10^{-5}$ ft^2/sec and

$$\delta_V = \sqrt{\frac{2\nu}{\omega}} = 2.22 \times 10^{-3} \text{ft.}$$

$$kL \approx \left(n + \frac{1}{2}\right)\pi \quad n = 0,1,2 \quad (4.3.1.12)$$

so that

$$P_V/P_R \approx \left(n + \frac{1}{2}\right) \cdot (2.79 \times 10^{-2}) \quad (4.3.1.13)$$

Thus, the effect of laminar viscous damping is relatively unimportant for the first few modes. It should be noted, however, that a small amount of surface roughness can lead to the formation of turbulent boundary layers, for which ν is effectively much larger than its laminar value. For this reason, care was taken to make the walls of the harbor as smooth as possible.

In a large scale harbor, surface roughness and the Reynolds number in (4.3.1.4) are much greater than in the laboratory, and so, the boundary layers can be turbulent. From the experiments of Jonsson and Carlsen (1976), the effective viscosity ν_e is typically of $O(100\nu)$.

Taking the following typical values for a large scale harbor

$$h = 20 \text{ m}$$

$$2a = 100 \text{ m}$$

$$L = 1 \text{ km}$$

$$v_e = 100v = 10^{-4} \text{ m}^2/\text{sec}$$

$$kL(1/4 \text{ wave mode}) = 1.41$$

$$\omega(1/4 \text{ wave mode}) = .02 \text{ sec}^{-1}$$

we obtain

$$\delta_v = .1 \text{ m}$$

$$P_v/P_R \approx (.7)(1.41)(.005) \approx .005$$

so that the power loss in the turbulent boundary layers is again negligible.

4.3.2 Separation Loss at the Entrance

Except at very low velocities, flow separation occurs at the sharp corners of the harbor entrance, and energy is expended in the production of eddies. The mechanism of flow separation is related to the adverse pressure gradient caused by the sharp curvature of the boundary. If the flow in the entrance is assumed to be quasi-static, then the pressure drop due to flow separation can be described by the hydraulic formula for steady flow

$$h(0^-, t) - h(0^+, t) = \frac{f}{2g} |u(0, t)| u(0, t) \quad (4.3.2.1)$$

where 0^- is on the harbor side of the entrance and 0^+ is on the ocean side. The constant f is an empirical friction factor whose value depends on the Reynolds number and the geometry of the entrance. For an asymmetrical entrance, f may take on different values depending on whether $u(0,t)$ is positive or negative.

An expression similar to (4.3.2.1) was used by Ingard and Ising (1967) and Ingard (1970) in studying nonlinear sound transmission through an orifice, with application to the absorption of sound at high pressure levels. Experimental measurements of both the energy loss and the distortion of the frequency spectrum of the transmitted sound were found to agree with the hydraulic, steady-flow formula. In particular, for a monochromatic wave incident on a symmetrical orifice, only odd harmonics are generated by the nonlinear term $fu|u|$; whereas, for an asymmetrical orifice, both even and odd harmonics are generated. A reduction in the mass reactance, or inertia, of the orifice was also observed by Ingard and Ising (1967), but this is not accounted for in (4.3.2.1). The magnitude of the mass reactance depends on the details of the velocity field, which is difficult to calculate when the flow is separated. Since the inertia of the orifice is associated primarily with the irrotational part of the flow, it is expected to be smaller when flow separation occurs. At high sound pressure levels, the mass reactance is observed to be one half its unseparated value, which suggests that, at any given time, the flow field on one side of the orifice is fully separated.

In water wave problems, separation loss has been studied in connection with the construction of perforated breakwaters; see

Jarlan (1965); Terrett, Osorio, and Lean (1968); and Mei, Liu, and Ippen (1974). The separation loss at a narrow harbor entrance has been studied numerically by Ito (1970) and analytically by Unluata and Mei (1975). The latter show that the higher harmonics generated by the nonlinear term $\frac{f}{2g}|u(0,t)|u(0,t)$ in (4.3.2.1) are not large under usual circumstances; rather, the primary effect of separation is to reduce the amplitude of the fundamental harmonic. We shall therefore present a simplified treatment of flow separation based on a monochromatic entrance velocity, $u(0,t)$.

To allow for an asymmetrical harbor entrance, we shall approximate f by

$$f = \begin{cases} f_1 & \text{when } u(0,t) > 0 \\ f_2 & \text{when } u(0,t) < 0 \end{cases} \quad (4.3.2.2.)$$

This is a mathematical simplification since f is more likely to be a continuous function of time. We then have

$$\frac{f}{2g} u|u| = \frac{\bar{f}}{2g} u|u| + \frac{\tilde{f}}{2g} u^2 \quad (4.3.2.3)$$

where

$$\begin{aligned} \bar{f} &\equiv \frac{1}{2} (f_1 + f_2) \\ \tilde{f} &\equiv \frac{1}{2} (f_1 - f_2) \end{aligned} \quad (4.3.2.4)$$

Next, we Fourier analyze each term of (4.3.2.3):

$$\frac{\bar{f}}{2g} u|u| = \frac{1}{2g} \sum_{-\infty}^{\infty} \bar{f}_n e^{-int}$$

$$\frac{\tilde{f}}{2g} u^2 = \frac{1}{2g} \sum_{-\infty}^{\infty} \tilde{f}_n e^{-int} \quad (4.3.2.5)$$

If we assume that $u(0,t)$ has the simple form

$$u = \frac{1}{2}(Ue^{-it} + U^*e^{it}) = |U| \cos(t-\phi) \quad (4.3.2.6)$$

where ϕ is the phase of U , viz. $U \equiv |U|e^{i\phi}$, then the Fourier coefficients in (4.3.2.5) are found to be

$$\begin{aligned} \bar{f}_n &= \frac{1}{2\pi} \int_0^{2\pi} \bar{f} u |u| e^{int} dt \\ &= \frac{4}{\pi} \frac{\sin(n\pi/2)}{n(4-n^2)} \bar{f} |U|^2 e^{in\phi} \\ \tilde{f}_n &= \frac{1}{2\pi} \int_0^{2\pi} \tilde{f} u^2 e^{int} dt \\ &= \tilde{f} |U|^2 e^{in\phi} \cdot \begin{cases} 1/2 & \text{for } n = 0 \\ 1/4 & \text{for } n = \pm 2 \\ 0 & \text{for all other } n \end{cases} \end{aligned} \quad (4.3.2.7)$$

Observe that \bar{f}_n is zero for even values of n ; thus, we retrieve the known result that, for a symmetric entrance ($\tilde{f}=0$), only odd harmonics are generated by separation. For an asymmetrical entrance, the second and zeroth harmonics are also generated; higher even harmonics would also be generated if $u(0,t)$ were more complicated than in (4.3.2.6).

For steady flow through the entrance of Fig. 1.1, the values of f_1 and f_2 are found to be 1.0 and .4, respectively, according to Daily and Harleman (1966), pp. 314-319. For oscillatory flows, the separation zone on either side of $x = 0$ has only a half wave period during which to develop. It may therefore be expected that the effective friction factors are smaller for oscillatory flow. Moreover, in the experimental

harbor model, the sharp corners at $x = 0$ are slightly rounded, which further reduces flow separation. Thus, the average friction factor $\bar{f} = \frac{1}{2}(f_1 + f_2)$ in the experiments is expected to be smaller than .7. We shall see in section 5.1 that the value of \bar{f} in the experiments is roughly half this value. Taking $f_1 = .5$ and $f_2 = .2$ in the experiments, we have $\bar{f} = .35$, $\tilde{f} = .15$ and

$$\begin{aligned}\bar{f}_1 &= \frac{4}{3\pi} \bar{f}|U|^2 e^{i\phi} = .15|U|U \\ \bar{f}_3 &= \frac{4}{15\pi} \bar{f}|U|^2 e^{3i\phi} = .03 U^3/|U| \\ \tilde{f}_0 &= \frac{1}{2} \tilde{f}|U|^2 = .075|U|^2 \\ \tilde{f}_2 &= \frac{1}{4} \tilde{f}|U|^2 e^{2i\phi} = .0375 U^2\end{aligned}\tag{4.3.2.8}$$

Since U is $O(\epsilon)$, the above coefficients are all $O(\epsilon^2)$. Note that the main effect of separation is to alter the first harmonic, through the coefficient \bar{f}_1 . The term \tilde{f}_0 will lead to a slight increase in the mean set-up, $\eta_0(x)$.

Taking the first harmonic component of (5.3.2.1) and using the impedance condition, $\eta_1(0^+) = A_1 + Z_1 U$, on the ocean side, we obtain

$$\begin{aligned}\eta_1(0^-) &= A_1 + Z_1 U + \bar{f}_1/g \\ &= A_1 + (Z_1 + c_e)U\end{aligned}\tag{4.3.2.9}$$

where

$$c_e \equiv \frac{4}{3\pi} \bar{f}|U|/g\tag{4.3.2.10}$$

The constant c_e is an effective damping constant due to separation. Eq. (4.3.2.9) is an effective harbor boundary condition which includes (i) the forcing of the incident wave, A_i ; (ii) the inertia of the harbor entrance, $\text{Im}(Z_1)$; (iii) the damping due to the radiated wave, $\text{Re}(Z_1)$; and (iv) the damping due to separation loss at the entrance, c_e .

Using (4.3.1.8) for the wave field in the harbor, we have

$$\eta_1(0^-) = T \cos kL \quad (4.3.2.11)$$

$$U = i \frac{gk}{\omega} T \sin kL \quad (4.3.2.12)$$

and, from (4.3.2.9),

$$\begin{aligned} T &= A[\cos kL - i \frac{gk}{\omega} (Z_1 + c_e) \sin kL]^{-1} \\ &= A[(\cos kL + \frac{gk}{\omega} \text{Im}(Z_1) \sin kL) - i \frac{gk}{\omega} (\text{Re}(Z_1) + \frac{4}{3\pi} \frac{k}{\omega} \bar{F}|T|) \sin kL]^{-1} \end{aligned} \quad (4.3.2.13)$$

Resonance occurs, as before, when $\cos kL + \frac{gk}{\omega} \text{Im}(Z_1) \sin kL = 0$. At resonance,

$$\begin{aligned} |T| &= |A| [\frac{gk}{\omega} (\text{Re}(Z_1) + \frac{4}{3\pi} \frac{k}{\omega} \bar{F}|T|) |\sin kL|]^{-1} \\ &= |T_0| [1 + \alpha |T|/|T_0|]^{-1} \quad (\text{at resonance}) \end{aligned} \quad (4.3.2.14)$$

where

$$\begin{aligned} |T_0| &\equiv |A| (\frac{gk}{\omega} \text{Re}(Z_1) |\sin kL|)^{-1} \\ &= |T| \quad \text{when } \bar{F} = 0 \quad (\text{no separation}) \\ \alpha &\equiv \frac{4}{3\pi} \frac{k}{\omega} \bar{F} |T_0| / \text{Re}(Z_1) \end{aligned} \quad (4.3.2.15)$$

Physically, α measures the amount of energy loss due to separation as compared with that due to radiation damping. When $\alpha \gg 1$, separation losses dominate radiation losses.

Solving (4.3.2.14) for $|T|/|T_0|$, we find

$$\begin{aligned} |T|/|T_0| &= \frac{1}{2\alpha} \sqrt{1 + 4\alpha} \\ &\approx \alpha^{-1/2} \quad \text{when } \alpha \gg 1/4 \end{aligned} \quad (4.3.2.16)$$

A plot of $|T|/|T_0|$ vs. α is shown in Fig. 4.5. Suppose we allow $\text{Re}(Z)$ to approach zero while maintaining \bar{f} and A constant (and nonzero). This corresponds to the well-known harbor paradox, in which $\text{Re}(Z_1)$ is made smaller by decreasing the width of the harbor entrance and $|T_0|$ is observed to increase without limit. From (4.3.2.16), we see that $|T|/|T_0| \rightarrow 0$ and that, specifically,

$$\begin{aligned} |T| &\approx |T_0| \alpha^{-1/2} \\ &= \left(\frac{4}{3\pi} \frac{k}{\omega} \bar{f} \right)^{-1/2} (\text{Re}(Z) |T_0|)^{1/2} \\ &= \left(\frac{4}{3\pi} \frac{k}{\omega} \bar{f} \right)^{-1/2} \left(\frac{|A|}{\frac{gk}{\omega} |\sin kL|} \right)^{1/2} \end{aligned} \quad (4.3.2.17)$$

Instead of increasing without limit, $|T|$ approaches a finite value proportional to $(|A|/\bar{f})^{1/2}$. Thus, the presence of separation losses effectively removes the harbor paradox.

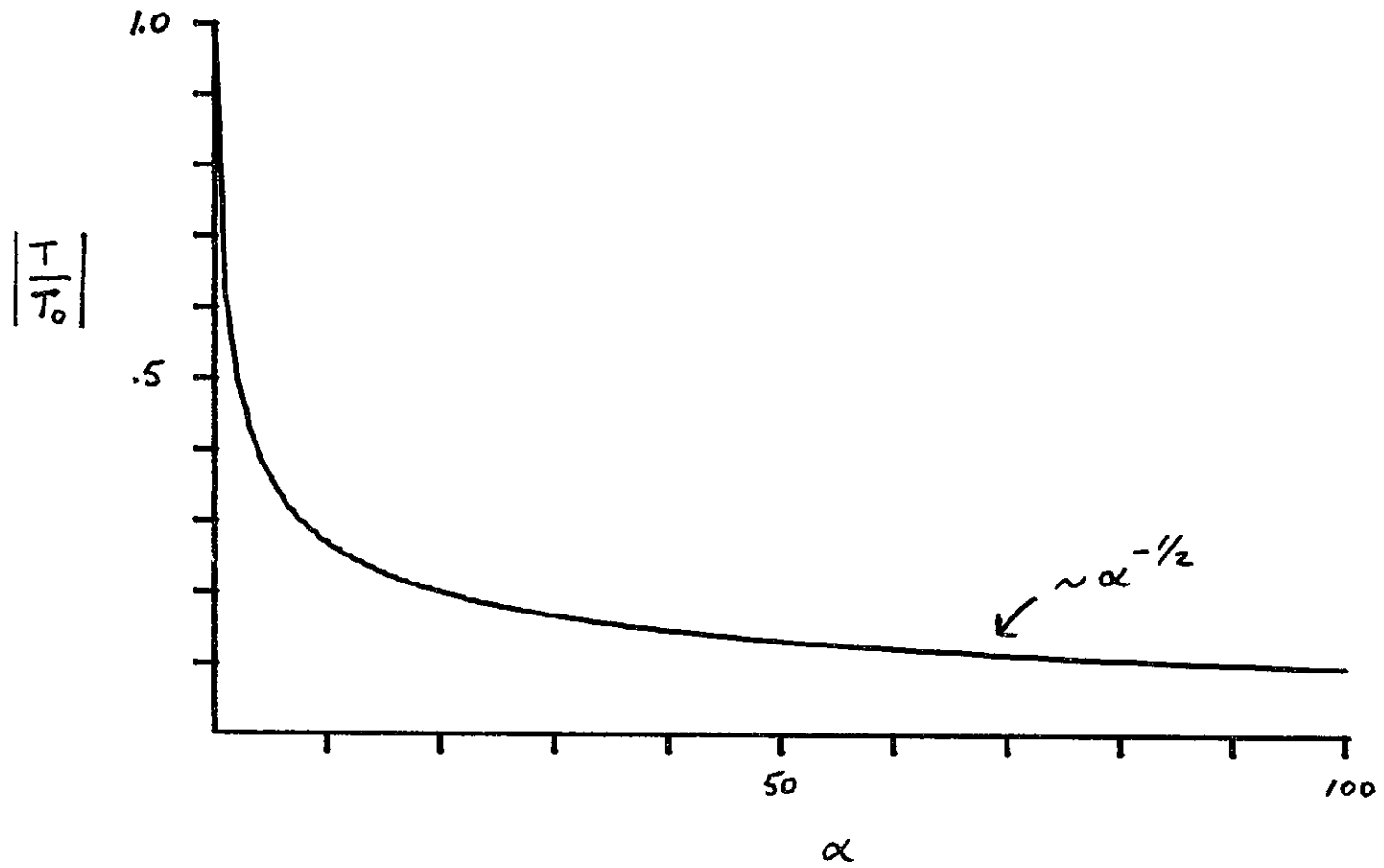


Fig. 4.5. Entrance loss: Normalized first harmonic amplitude, $|T/T_0|$, vs. normalized friction factor, α .

CHAPTER V
EXPERIMENTAL AND THEORETICAL RESULTS

5.1 Comparison of Theory with Experiment

The experimental set-up is shown in Fig. 4.1, where the coordinates are defined.

Five length scales are involved in the study of the long, narrow bay: harbor width, $2a$; mean water depth, h ; harbor length, L ; wavelength of the first harmonic of the incident wave, approximately $\sqrt{gh} \cdot 2\pi/\omega$; and incident wave amplitude, $\frac{1}{2}|A_1|h$. In the experiments, these had the values

$$2a = 1/3 \text{ ft.}$$

$$h = 1/2 \text{ ft.}$$

$$L = 1.211, 4.173, \text{ and } 7.136 \text{ ft.}$$

$$\sqrt{gh} \cdot (2\pi/\omega) = (4.0125 \text{ ft/sec}) (1.545 \text{ sec}) = 6,200 \text{ ft.}$$

$$|A_1| \cdot h = .0075, .0135, \text{ and } .020 \text{ ft.}$$

Three harbor lengths and three incident wave amplitudes were tested.

The corresponding dimensionless parameters are

$$\delta \equiv a \cdot (\omega/\sqrt{gh}) = .169$$

$$\lambda \equiv L \cdot (\omega/\sqrt{gh}) = 1.227, 4.230, \text{ and } 7.233$$

$$\mu^2 \equiv \omega^2 h/g = .257$$

$$|A_1| = .015, .027, \text{ and } .040$$

The values of λ were chosen so as to produce the first three linearly

resonant harbor modes. Each resonant mode was studied for three different values of $|A_1|$; so, altogether, nine resonant harbor oscillations were examined.

The incident waves produced by the wave generator are not perfectly monochromatic. With the harbor entrance closed, the standing wave amplitude in the ocean was measured at $x = y = 0$ and was found to have the harmonic composition given in Table 5.1. The phases, ϕ_n , are defined by $A_n \equiv |A_n|e^{i\phi_n}$ and are given in radians.

Table 5.1

$ A_1 $.015	.027	.040
$ A_2 $.001	.003	.012
$ A_3 $.000 (2)	.001	.003
$\phi_2 - 2\phi_1$	6.210	5.646	5.506
$\phi_3 - 3\phi_1$.671	1.795	5.314

These are used as inputs in the numerical calculations.

Table 5.2 compares the wavenumbers k_n calculated by the approximate Boussinesq dispersion relation

$$(k_n h)^2 = n^2 \mu^2 \left(1 + \frac{1}{3} n^2 \mu^2\right) + O(n\mu)^6$$

where $\mu^2 = \omega^2 h/g = .257$, with those calculated by the exact dispersion relation

$$n^2 \mu^2 = (k_n h) \tanh (k_n h)$$

which is valid for arbitrary depth, e.g. arbitrary ($n\mu$).

Table 5.2

n	Exact k_n (ft. ⁻¹)	Boussinesq k_n (ft. ⁻¹)
1	1.060	1.056
2	2.448	2.350
3	4.710	4.048
4	8.228	6.244
5	12.850	8.986

Note that the error in the Boussinesq values for k_n is quite large for the higher harmonics.

The theoretical assumption that the far field of the harbor is one-dimensional is only valid when transverse modes of oscillation, or "cross modes," are not present. The minimum wavenumber, k_c , for which cross modes are possible, is given by

$$(k_c) \cdot (2a) = \pi$$

so that, with $2a = 1/3$ ft.,

$$k_c = 9.42 \text{ ft.}^{-1}$$

From Table 5.2, we see that cross modes can exist for the fifth harmonic or higher. In the experiments, the amplitudes of these harmonics were negligible, and the far field of the harbor was observed to be approximately one-dimensional.

The wave amplitude in the harbor was Fourier analyzed at intervals of two inches along the centerline of the harbor channel. The zeroth harmonic, or mean set-up, was removed by the Fourier analysis. The variation of the first three harmonic amplitudes with distance from the back wall of the harbor is shown, for each of the nine experimental cases, in Figs. 5.1(a) through 5.1(i). The horizontal dotted line indicates the maximum amplitude of the first harmonic predicted by linearized theory. The solid lines are theoretical curves based on the inviscid nonlinear theory of Chapter 3. These solutions were computed by the numerical procedure of Section 3.5, with the incident wave composition given in Table 5.1 and the Boussinesq values of k_n given in Table 5.2. Convergence of the iteration scheme was achieved in all cases with five harmonics or less.

For the shortest harbor ($L = 1.211$ ft.) the higher harmonics are small, owing to the short distance over which nonlinear interactions take place, and the inviscid nonlinear theory agrees closely with linearized theory. The reduction of the first harmonic amplitude is due primarily to separation loss at the entrance, rather than to nonlinearity, and will be discussed later.

In the two longer harbors ($L = 4.173$ ft. and 7.136 ft.), there is considerable harmonic generation; in some instances, the second harmonic is as large as fifty percent of the first. In such cases, the second harmonic siphons an appreciable amount of energy from the first harmonic, and therefore, the maximum amplitude of the first harmonic is observed to be significantly less than that predicted by linearized theory. For the longest harbor ($L = 7.136$ ft.), the agreement between experiment and

and inviscid theory is fairly good. In particular, the significant reduction of the first harmonic and the presence of higher harmonics are well accounted for by the nonlinear theory. However, for the second harbor ($L = 4.173$ ft.), we note the qualitative feature that the observed second harmonic is higher than calculated, and that the observed reduction of the first harmonic is larger than that calculated. These discrepancies cannot be attributed to harmonic generation by flow separation at the entrance, as this was shown to be quite small, in Section 4.3.2.

We believe that part of the discrepancy between theoretical and experimental values of the higher harmonics is most likely due to errors in the Boussinesq values for k_n , cf. Table 5.2. Errors in the values of k_n lead to corresponding errors in the positions of nodes and anti-nodes of the harmonic amplitudes. These errors increase with increasing distance from the back wall of the harbor. Furthermore, because the harbor response is large at resonant values of $k_n L$, a small error in k_n can significantly alter the absolute magnitude of the n -th harmonic. We suspect that this happens for the second harbor ($L = 4.173$ ft.). In this case, the Boussinesq value of $k_2 L$ is 9.807 which does not lie close to a resonant mode; whereas the exact value of $k_2 L$ is 10.216, which coincides with the fourth resonant mode, having $kL = \frac{7}{2}\pi + \text{Im}(Z)$. Because of this, the second harmonic predicted by Boussinesq theory is expected to be smaller than that observed in the laboratory. The energy conservation theorem of Section 3.4 implies that the first harmonic must also be affected.

Figures 5.2(a), (b), and (c) show the results of a numerical

calculation in which the exact values of k_n are used instead of the Boussinesq values, for the second harbor. Note that the second harmonic is now larger and the first harmonic smaller than that obtained previously (cf. Figs. 5.1(d),(e),(f)). This improves the agreement between theory and experiment, though the quantitative agreement is still not as good as for the long harbor ($L = 7.136$ ft.) case. Of course, this ad hoc correction of the values of k_n must await rigorous justification by a nonlinear theory which is valid for arbitrary depth.

We have used the shortest harbor to determine the average friction factor, $\bar{f} = \frac{1}{2} (f_1 + f_2)$, which appears in the entrance loss theory of Section 4.3.2. The value $\bar{f} = .35$, which is half the upper limit expected on the basis of steady flow values for f_1 and f_2 , was found to give good agreement with the experimental data on the shortest harbor. In Figs. 5.3(a) through 5.3(i), the experimental data for all nine harbor resonances is compared with theoretical curves computed using the entrance loss theory of Section 4.3.2, with $\bar{f} = .35$. Since harmonic generation by separation has been shown to be small, only the main effect of separation, e.g. reduction of the first harmonic, has been included in the numerical computation.

The inclusion of entrance loss does not significantly improve the agreement between experiment and theory for the second and third harbor lengths. In particular, the quantitative agreement is still better for the longest harbor than for the medium length harbor. By using $\bar{f} = .35$ and an ad hoc application of the exact dispersion relation, as explained previously, we obtain the theoretical curves shown in Figs. 5.4(a),(b),(c) for the medium length harbor.

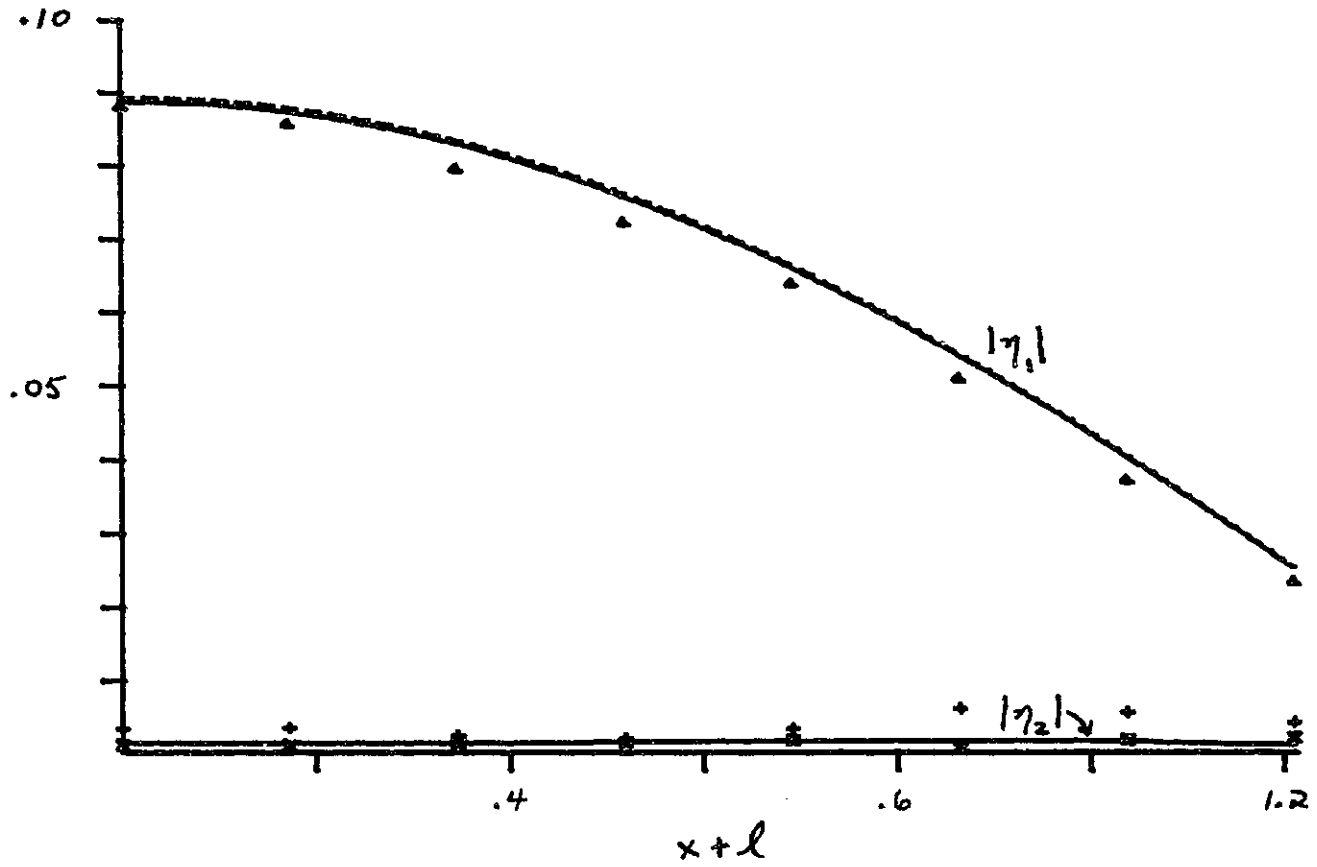


Fig. 5.1a. Experiment vs. inviscid nonlinear theory ($\bar{f} = 0$). ($\Delta, +, x$): measured first, second, and third harmonic amplitudes. (—): nonlinear theory. (----): linear theory for first harmonic amplitude. $L = 1.211$ ft., $A_1 = .015$.

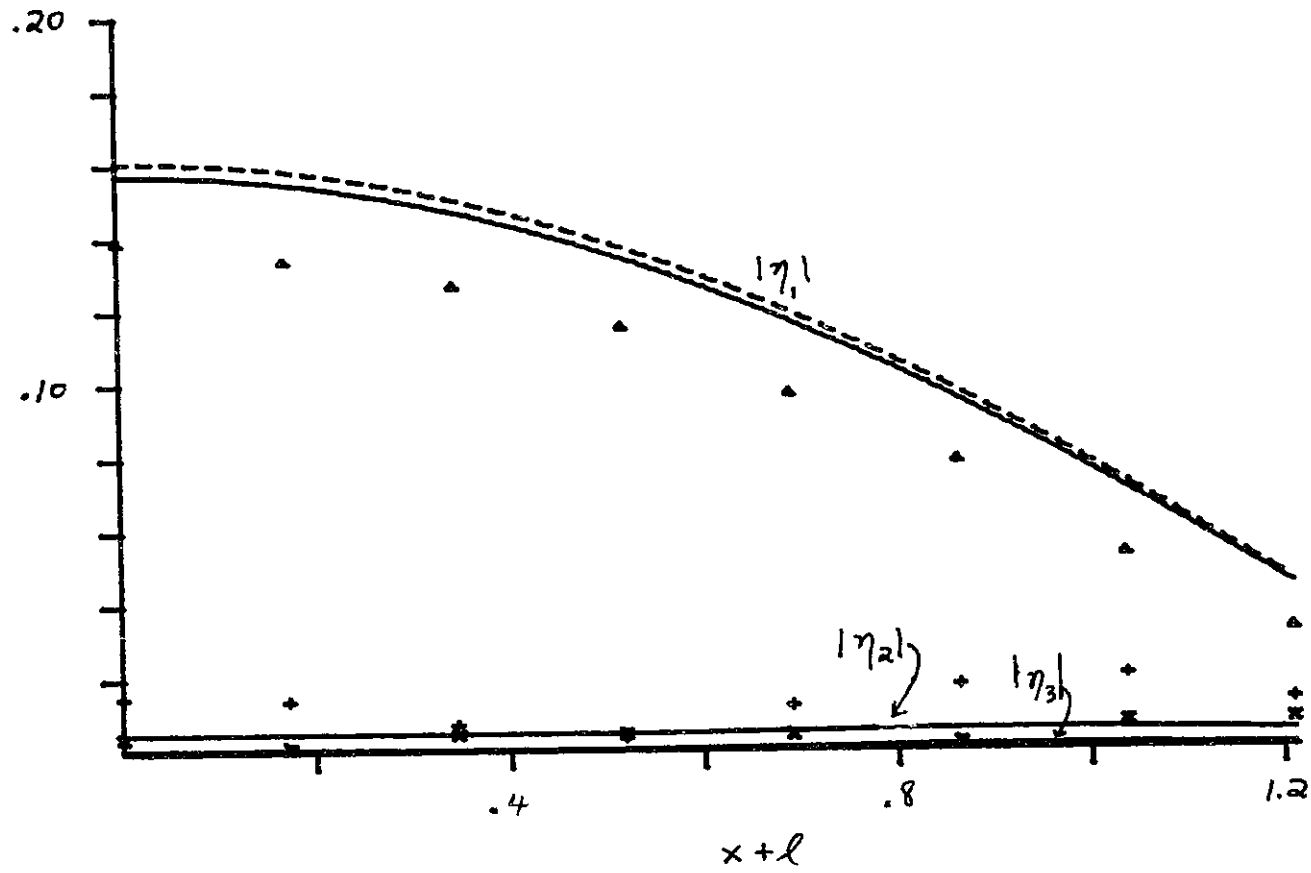


Fig. 5.1b. $L = 1.211$ ft., $A_1 = .027$ (See Fig. 5.1a).

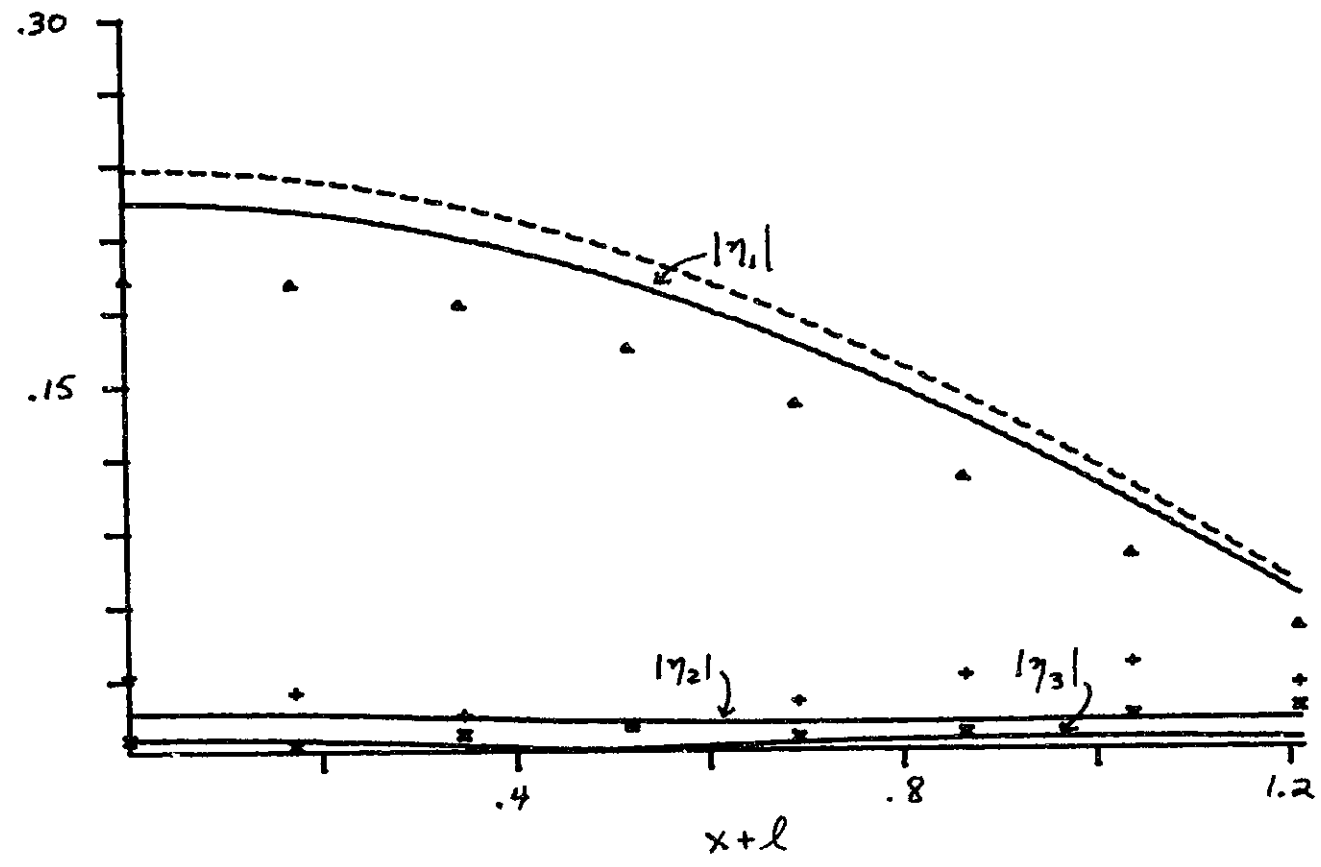


Fig. 5.1c. $L = 1.211$ ft., $A_1 = .040$ (See Fig. 5.1a).

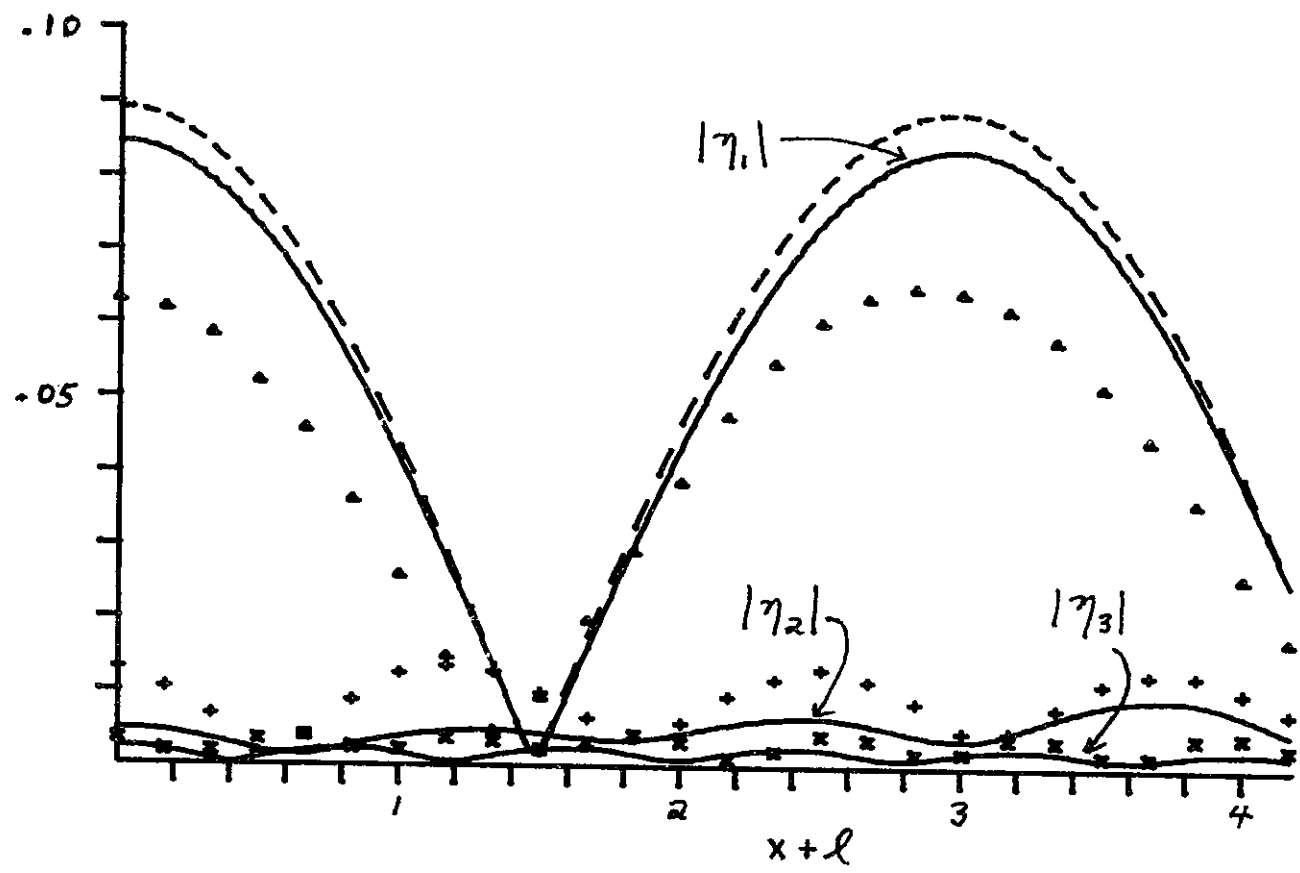


Fig. 5.1d. $L = 4.173$ ft., $A_1 = .015$ (See Fig. 5.1a).

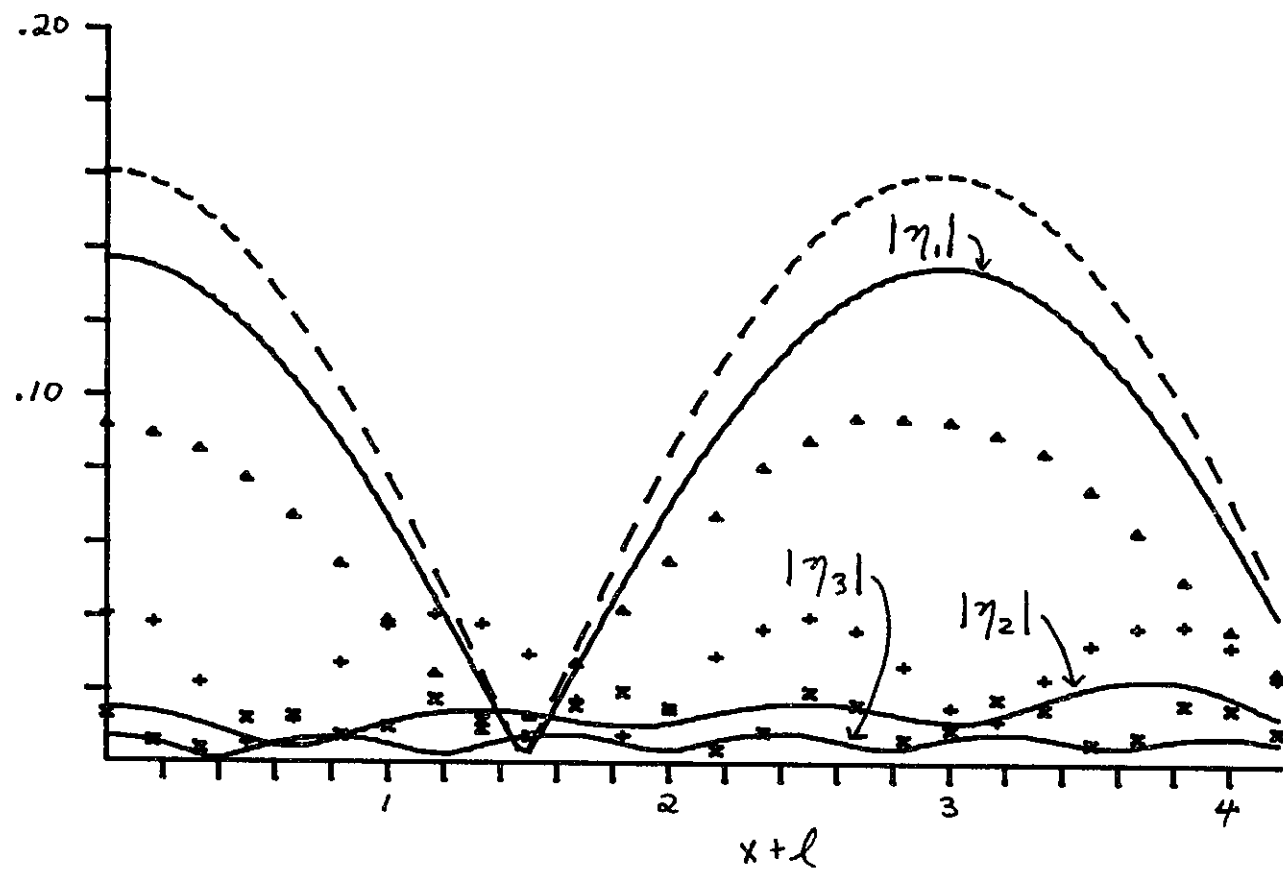


Fig. 5.1e. $L = 4.173$, $A_1 = .027$ (See Fig. 5.1a).

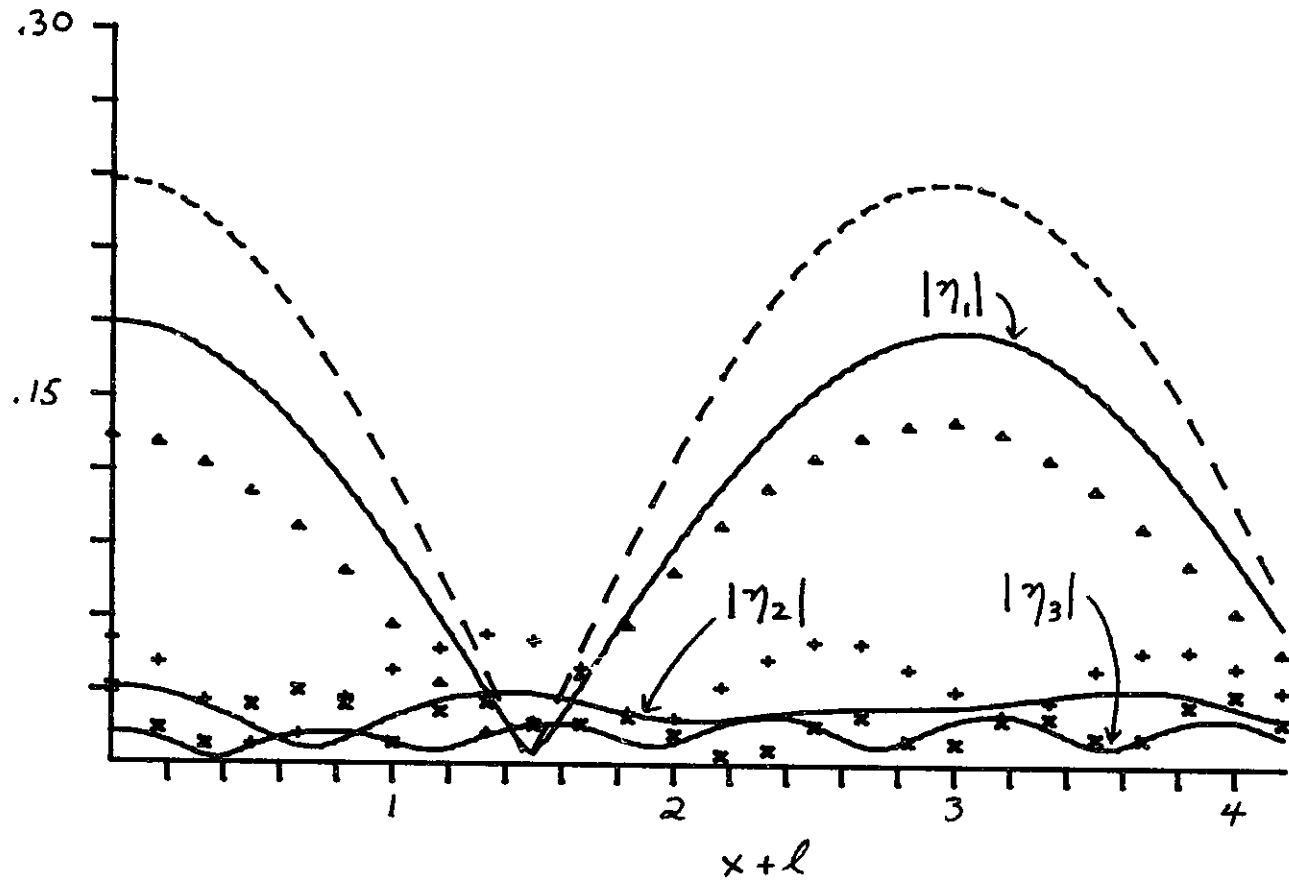


Fig. 5.1f. $L = 4.173$ ft., $A_1 = .040$ (See Fig. 5.1a).

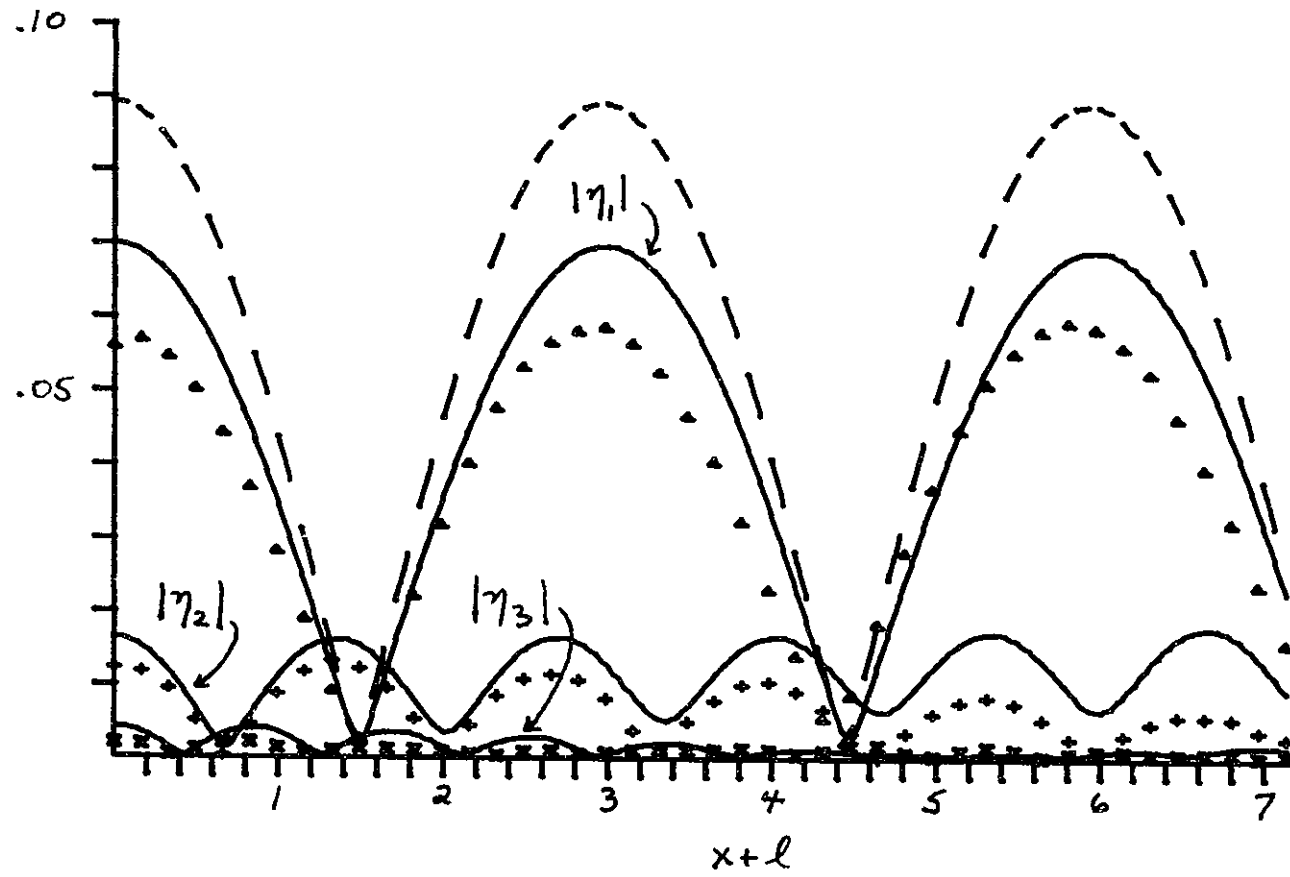


Fig. 5.1g. $L = 7.136$ ft., $A_1 = .015$ (See Fig. 5.1a).

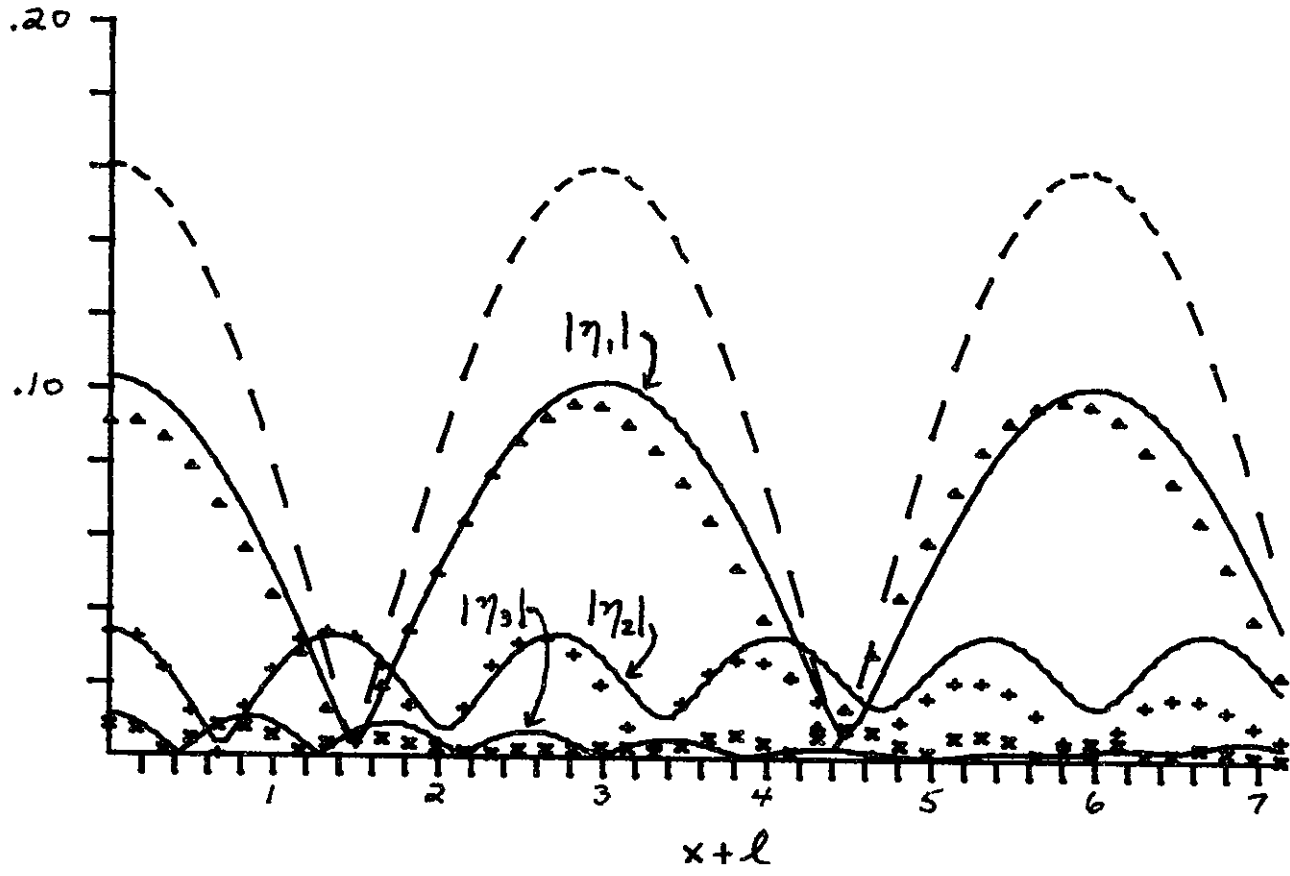


Fig. 5.1h. $L = 7.136$ ft., $A_1 = .027$ (See Fig. 5.1a).

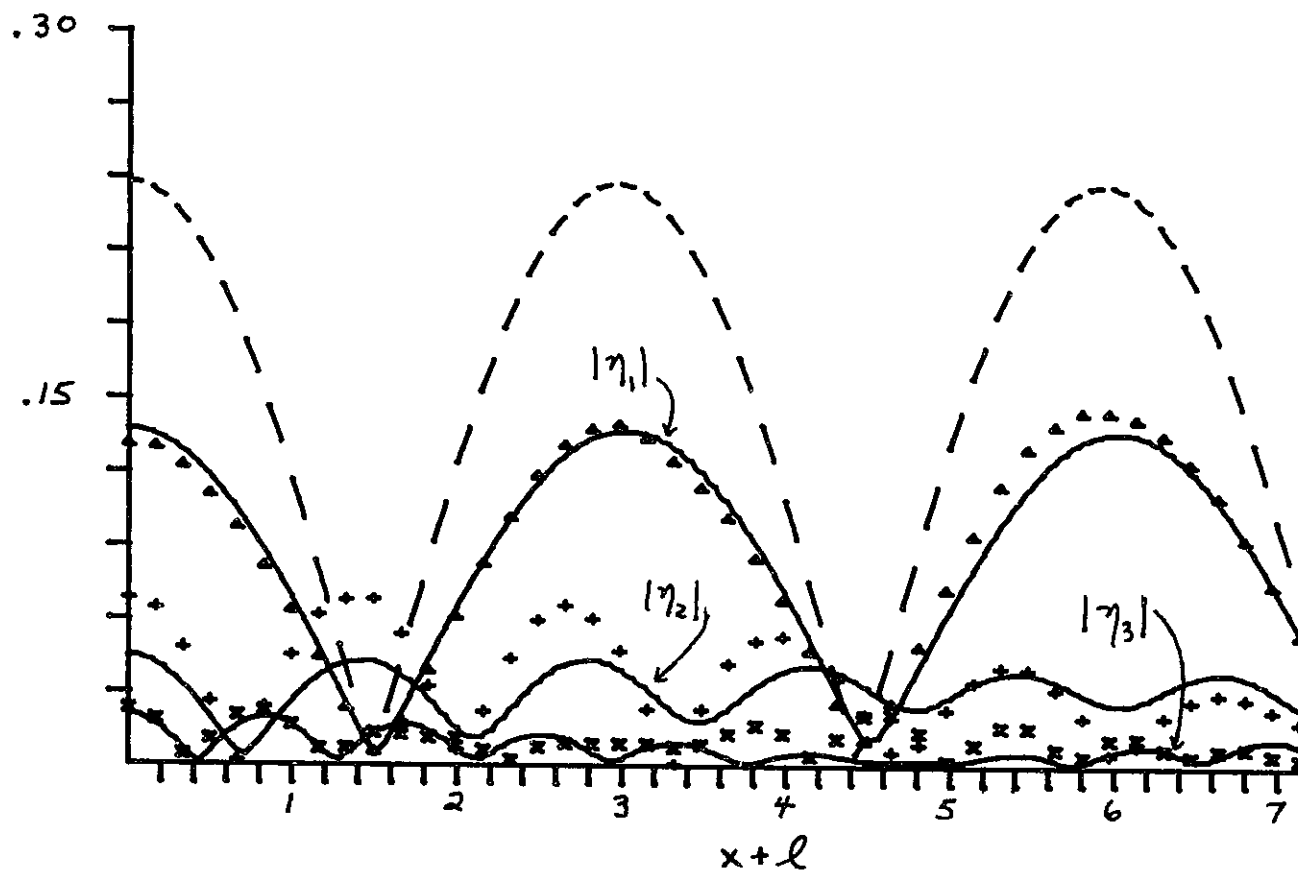


Fig. 5.1i. $L = 7.136$ ft., $A_1 = .040$ (See Fig. 5.1a).

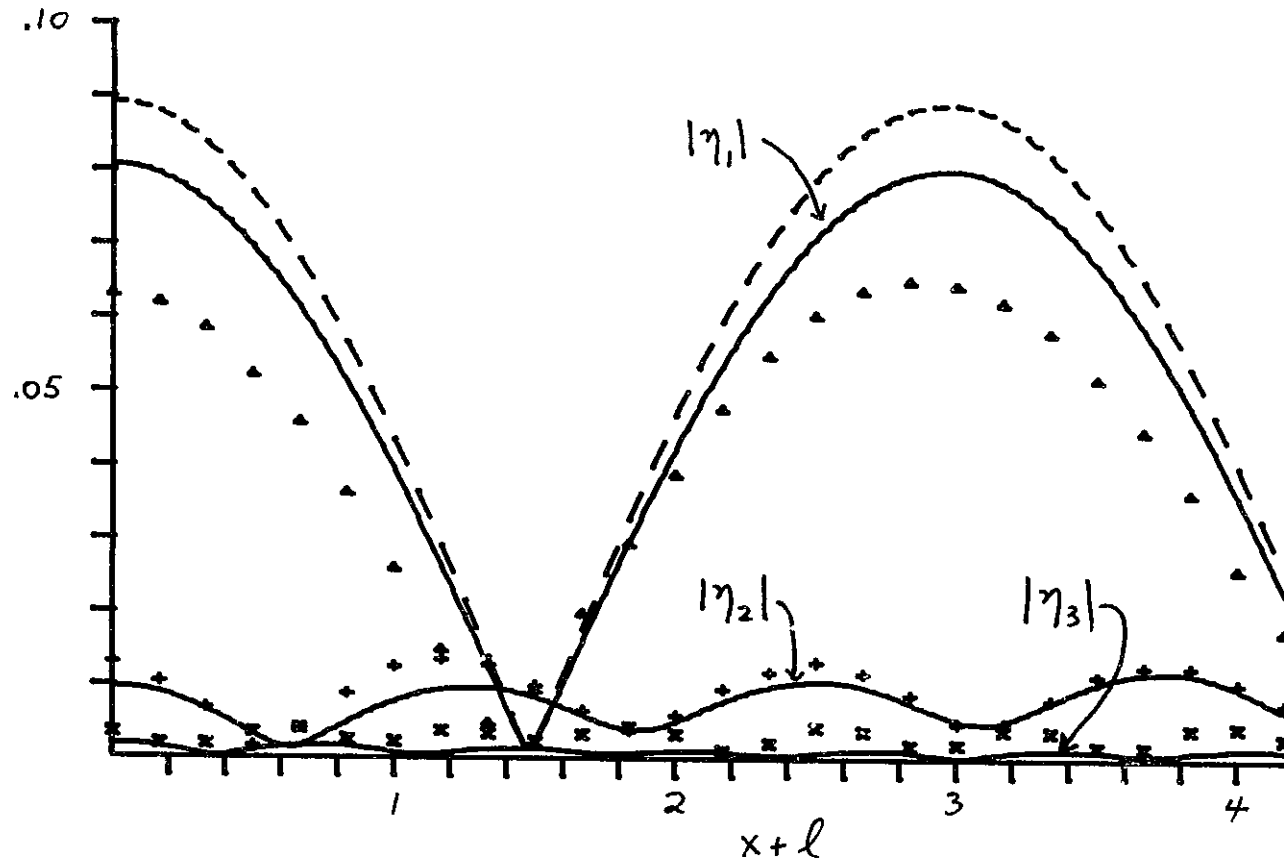


Fig. 5.2a. Experiment vs. inviscid nonlinear theory ($\bar{f} = 0$) with exact dispersion relation. ($\Delta, +, \times$): measured first, second, and third harmonic amplitudes. (—): nonlinear theory. (----): linear theory for first harmonic amplitude. $L = 4.173$ ft., $A_1 = .015$.

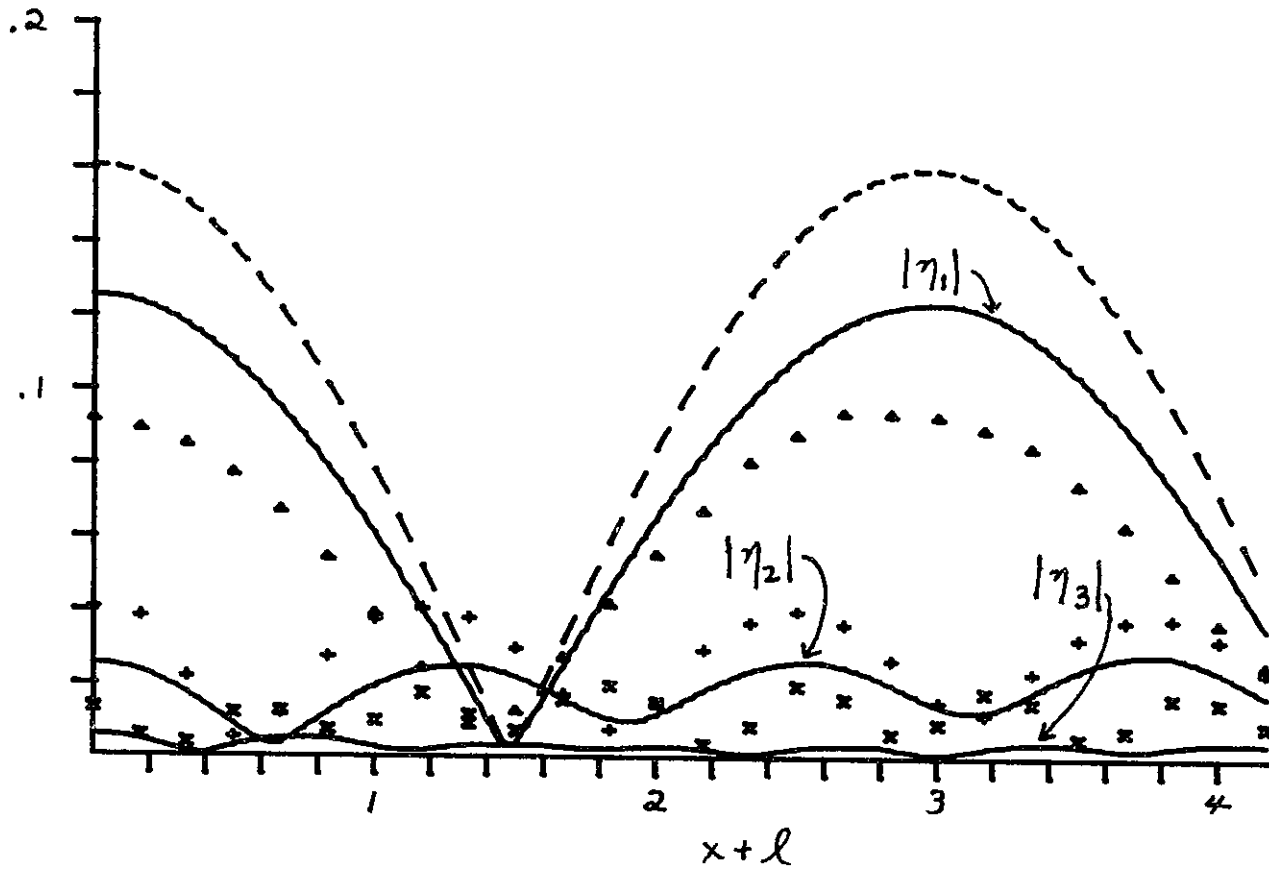


Fig. 5.2b. $l = 4.173$ ft., $A_7 = .027$ (See Fig. 5.2a).

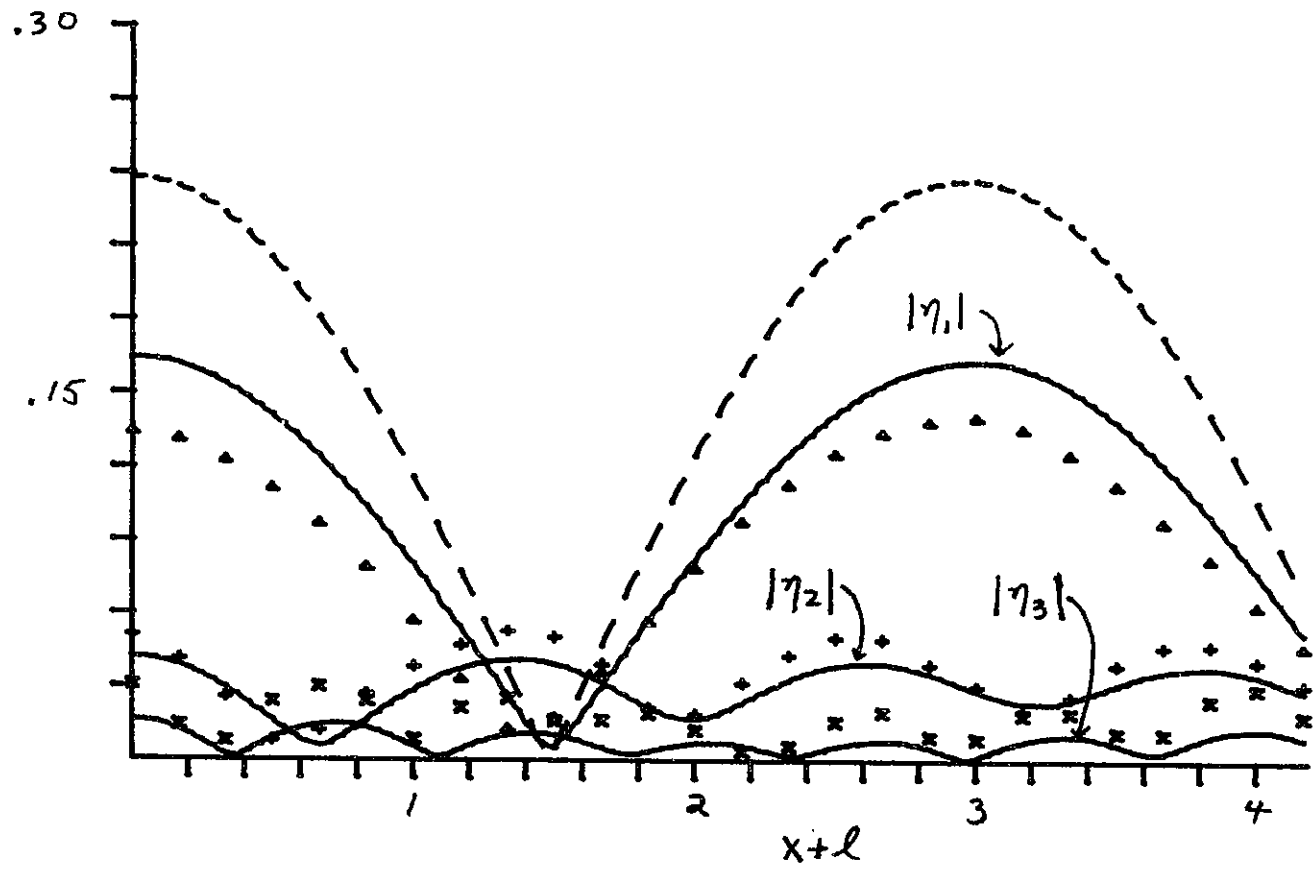


Fig. 5.2c. $L = 4.173$, $A_1 = .040$ (See Fig. 5.2a).

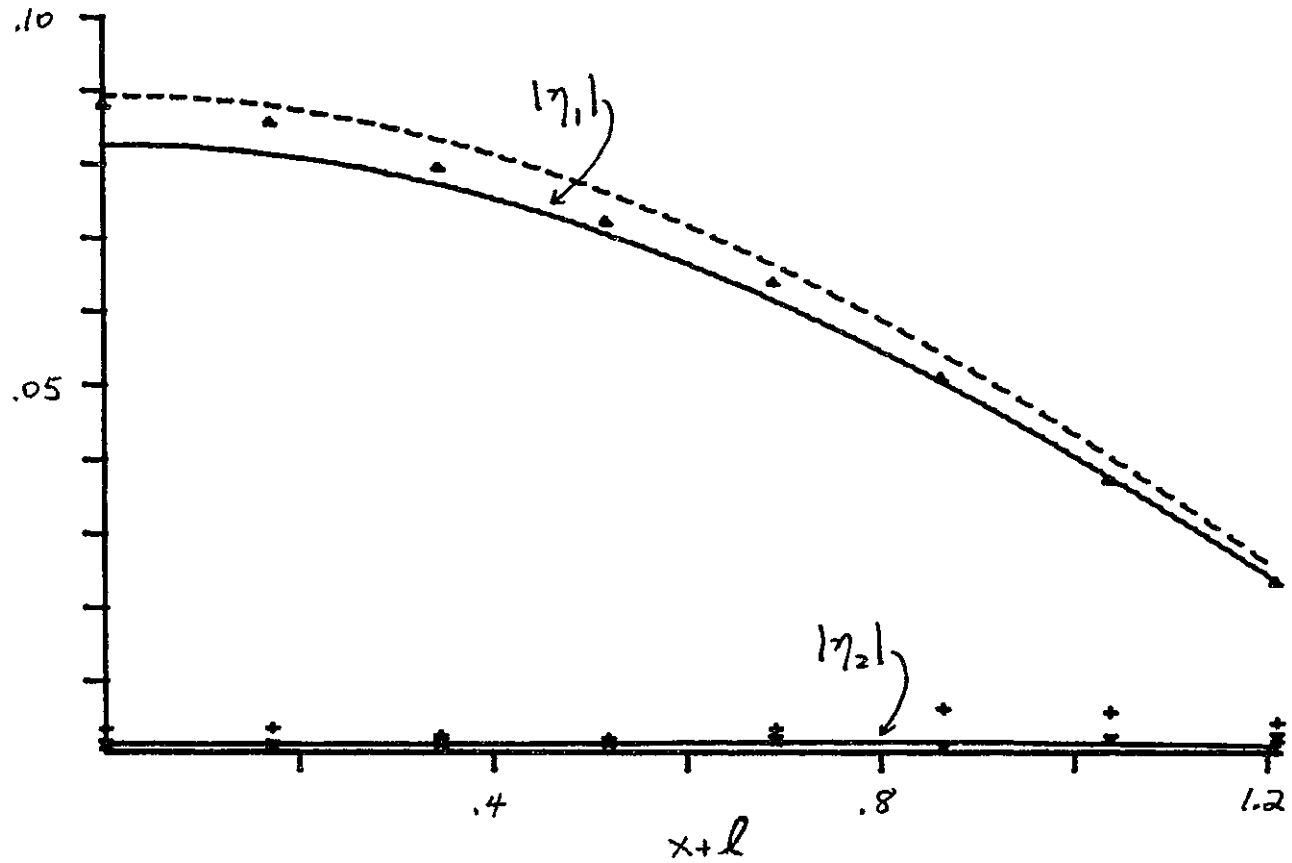


Fig. 5.3a. Experiment vs. nonlinear theory with separation loss ($\bar{f} = .35$). ($\Delta, +, x$): measured first, second, and third harmonic amplitudes. (—): nonlinear theory. (----): linear theory for first harmonic amplitude. $L = 1.211$ ft., $A_1 = .015$.

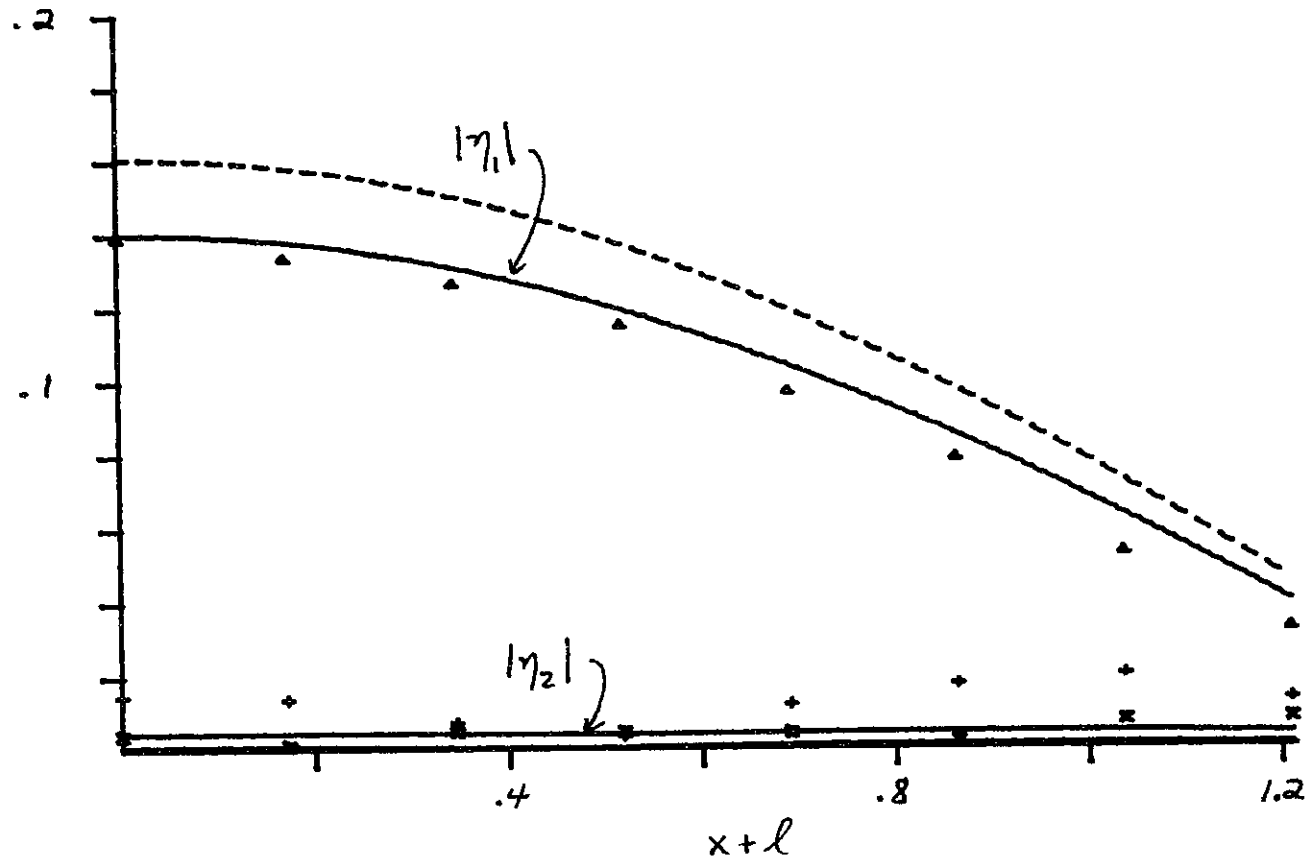


Fig. 5.3b. $L = 1.211$ ft., $A_1 = .027$ (See Fig. 5.3a).

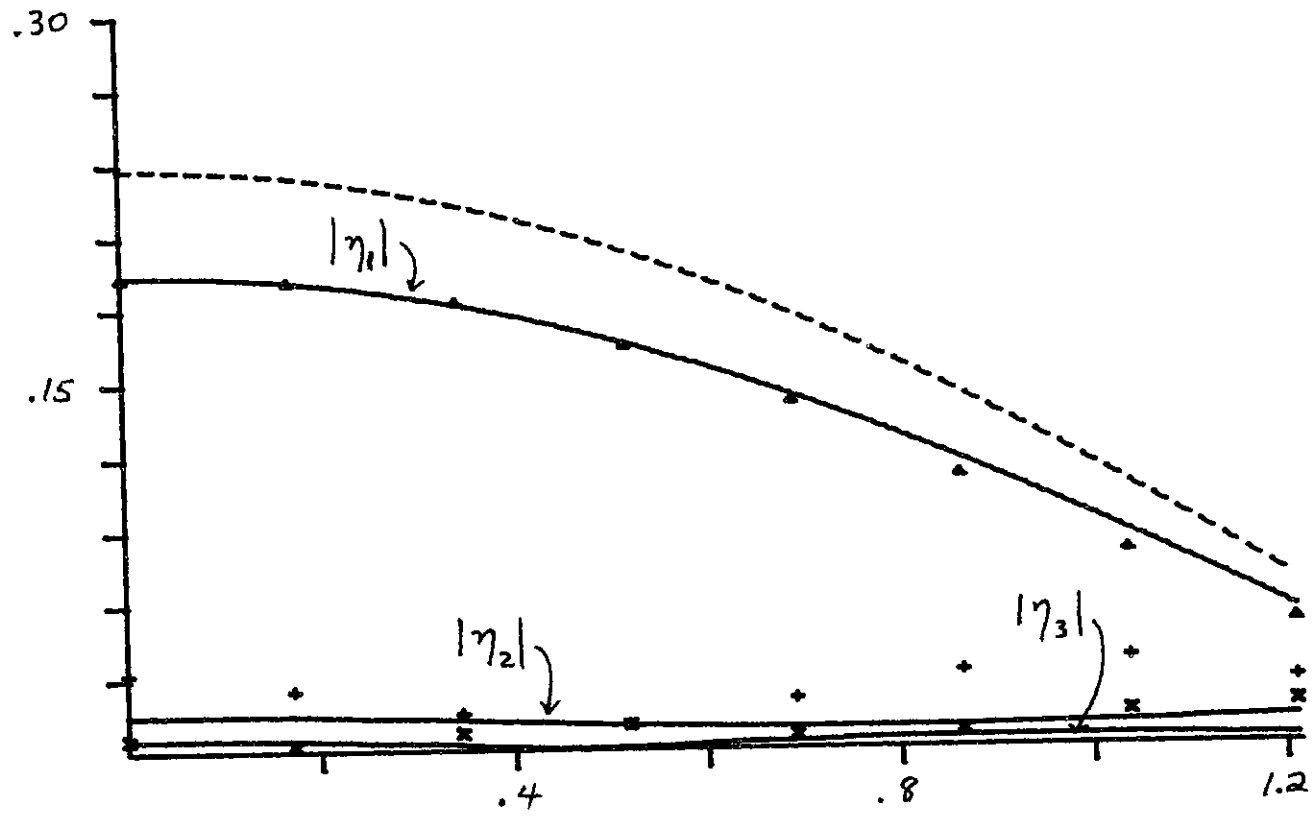


Fig. 5.3c. $L = 1.211$ ft., $A_1 = .040$ (See Fig. 5.3a).

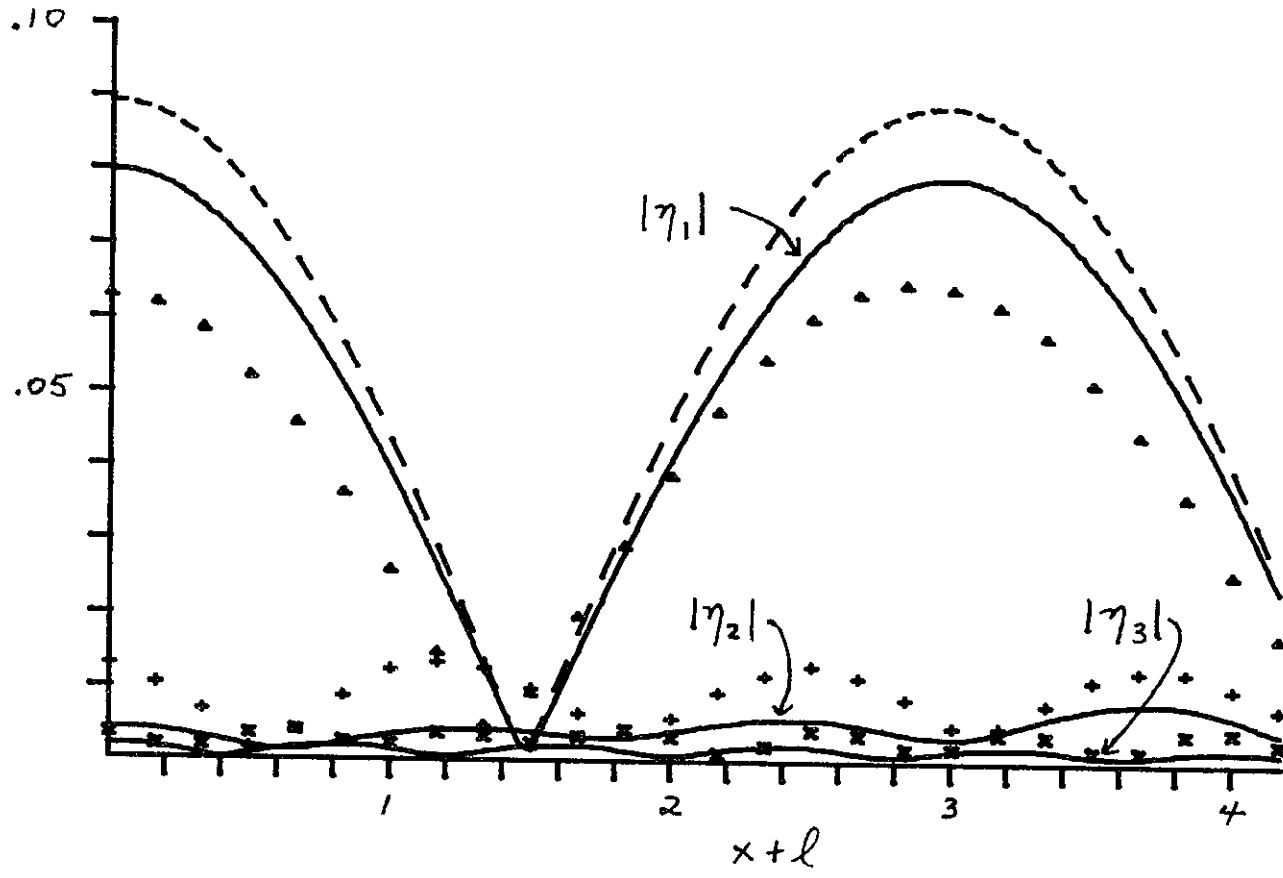


Fig. 5.3d. $L = 4.173$ ft., $A_1 = .015$ (See Fig. 5.3a).

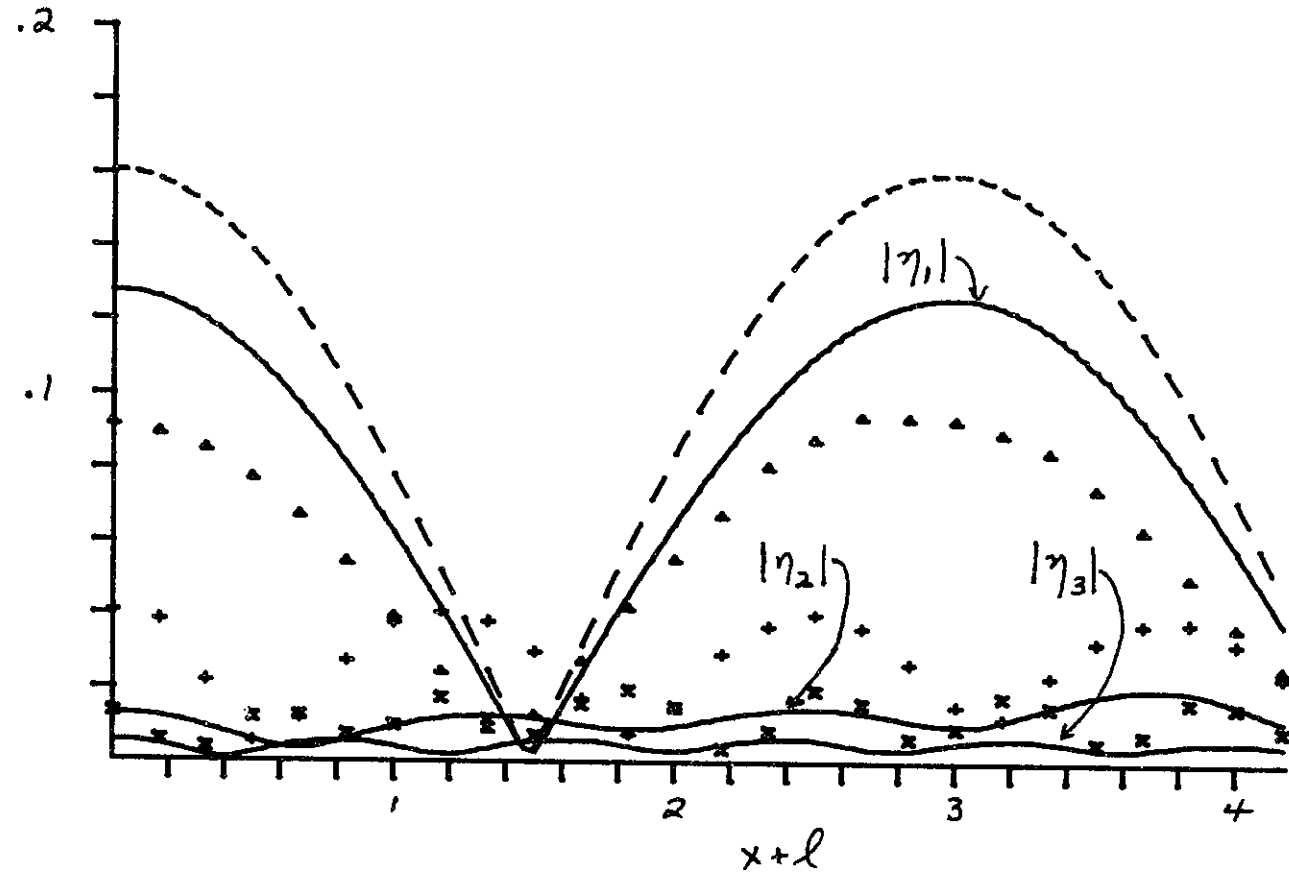


Fig. 5.3e. $L = 4.173$, $A_1 = .027$ (See Fig. 5.3a).

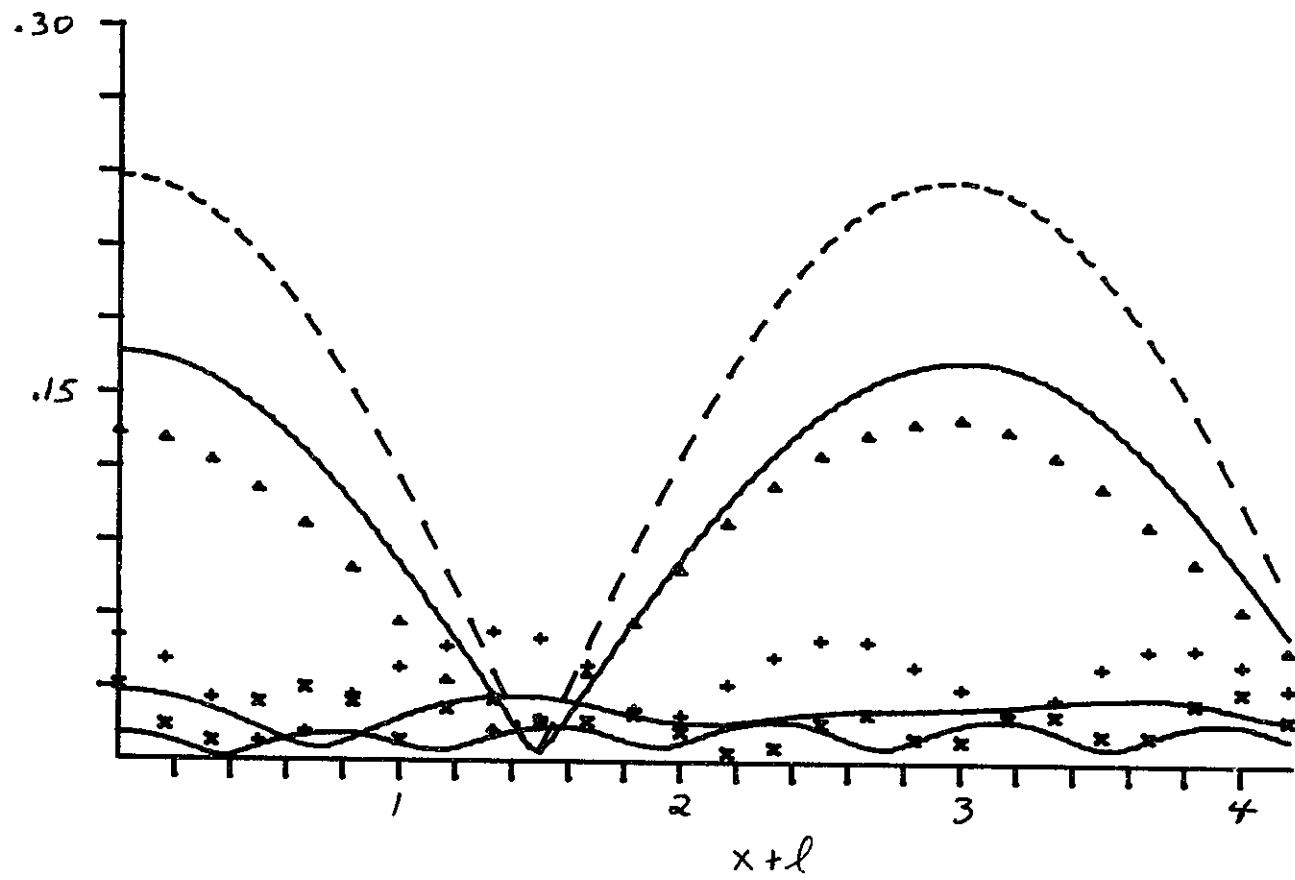


Fig. 5.3f. $L = 4.173$ ft., $A_1 = .040$ (See Fig. 5.3a).

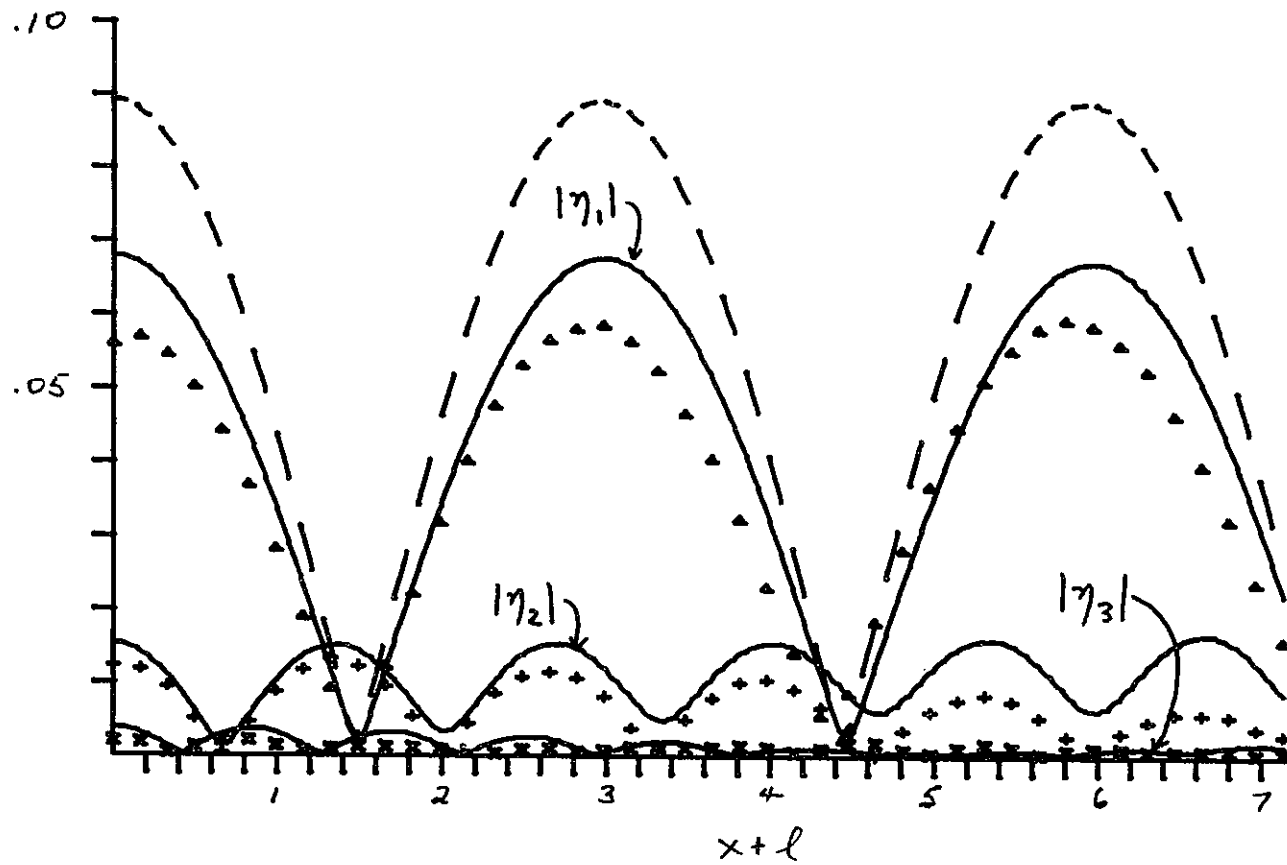


Fig. 5.3g. $L = 7.136$ ft., $A_7 = .015$ (See Fig. 5.3a).

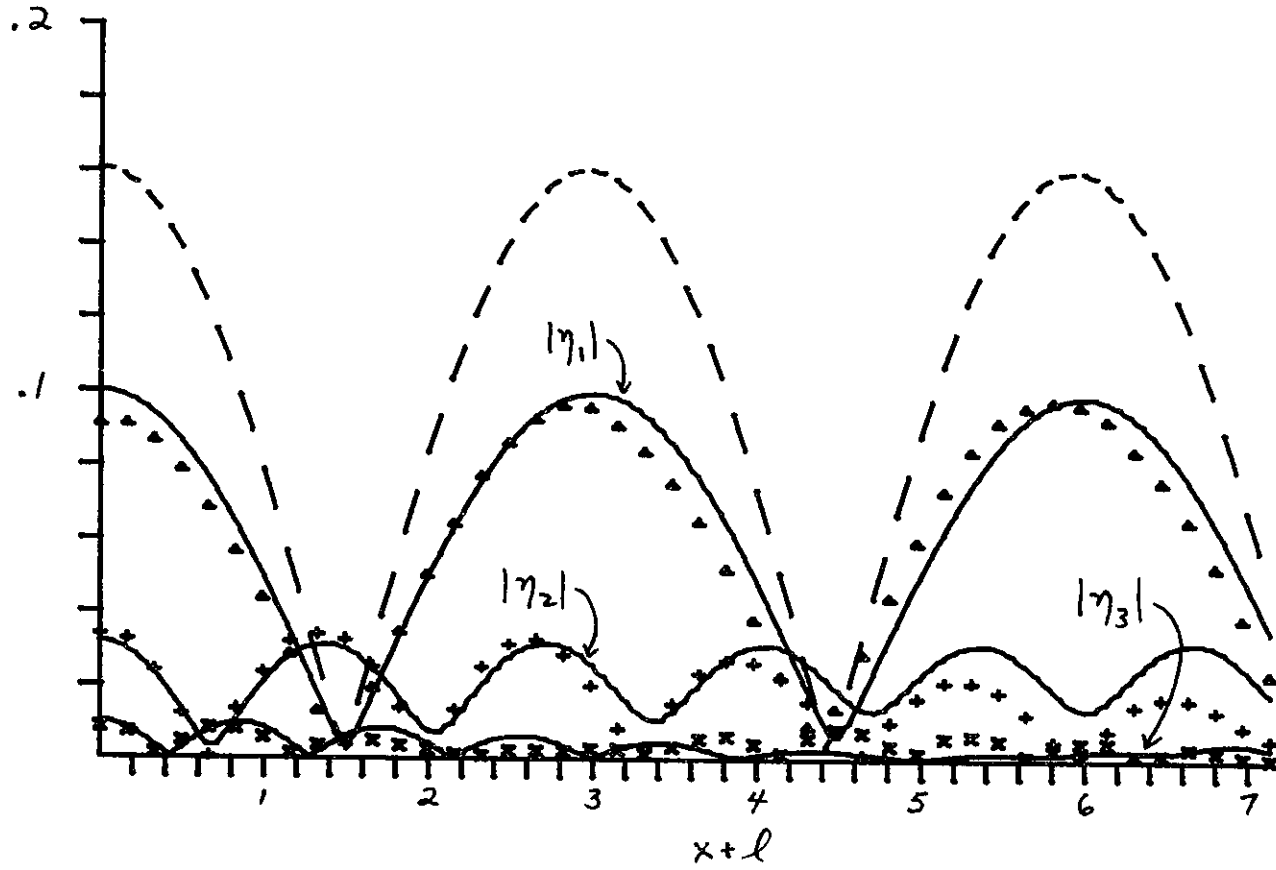


Fig. 5.3h. $L = 7.136$ ft., $A_1 = .027$ (See Fig. 5.3a).

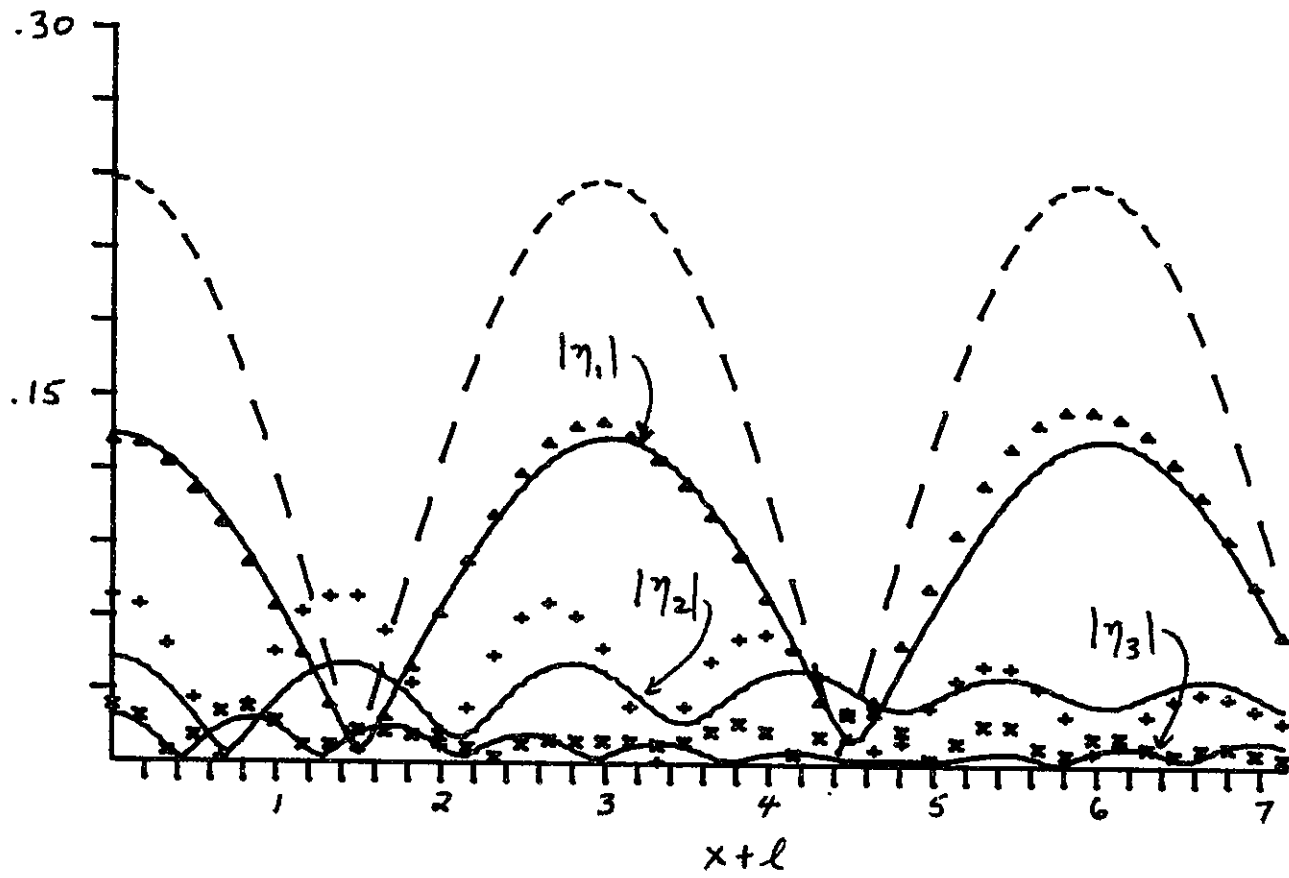


Fig. 5.3i. $L = 7.136$ ft., $A_1 = .040$ (See Fig. 5.3a).

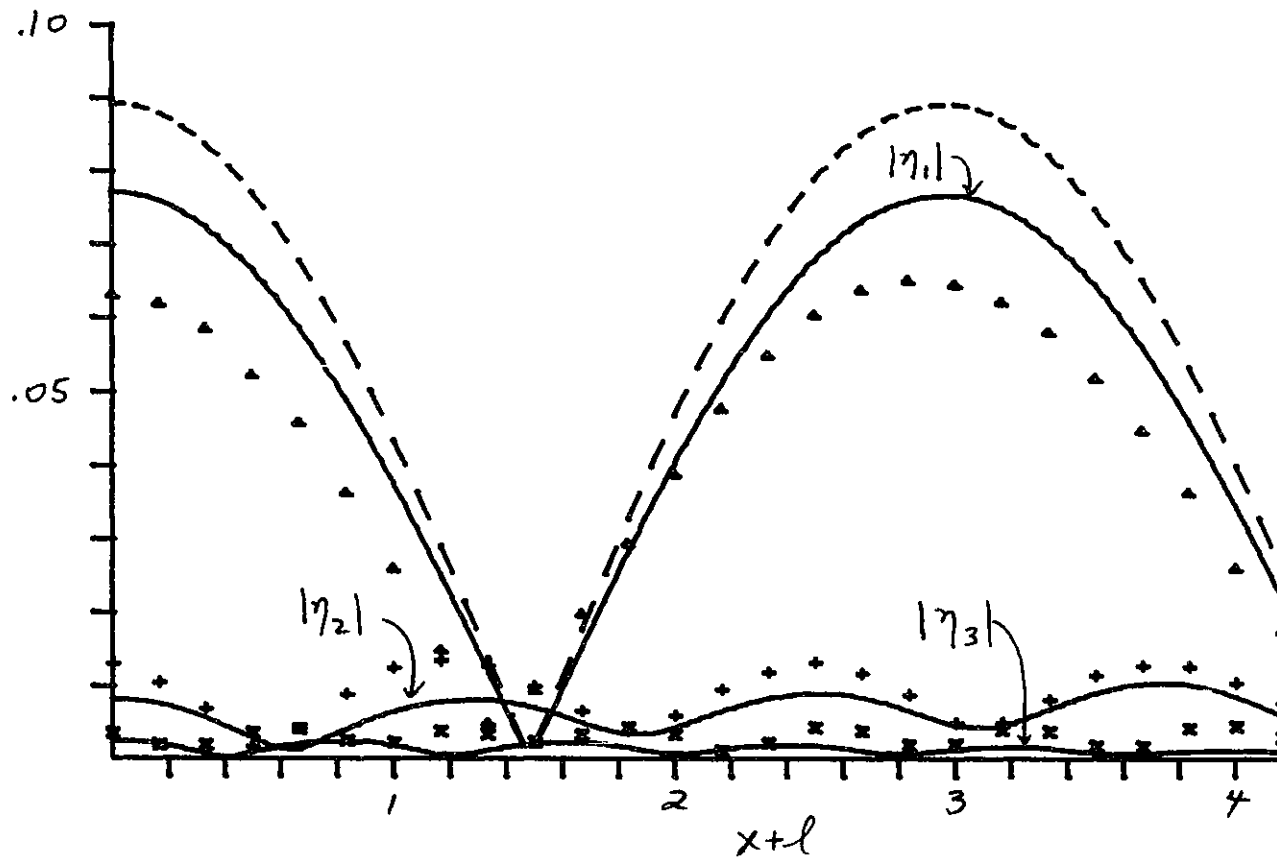


Fig. 5.4a. Experiment vs. nonlinear theory with separation loss ($\bar{f} = .35$) and exact dispersion relation. ($\Delta, +, x$): measured first, second, and third harmonic amplitudes. (—): nonlinear theory. (----): linear theory for first harmonic amplitude. $L = 4.173$ ft., $A_1 = .015$.

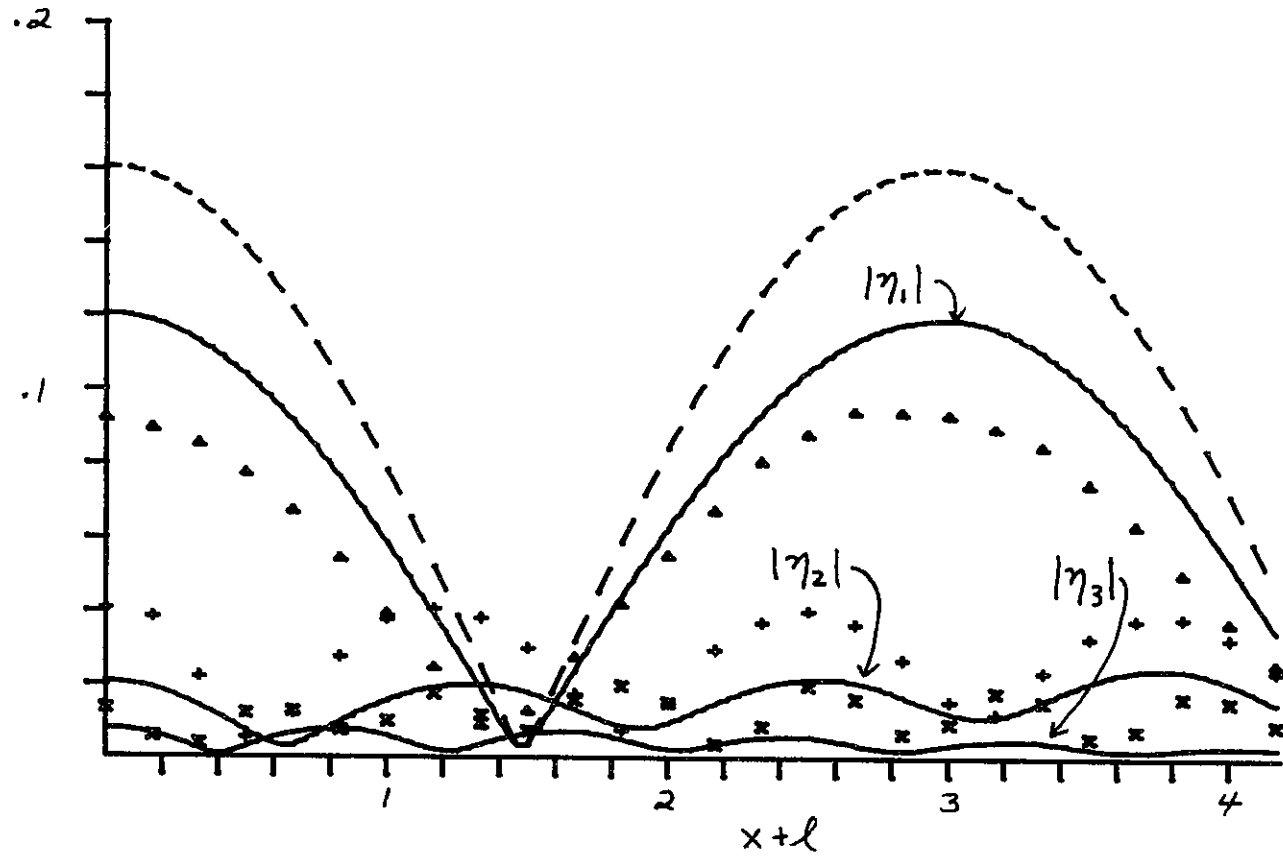
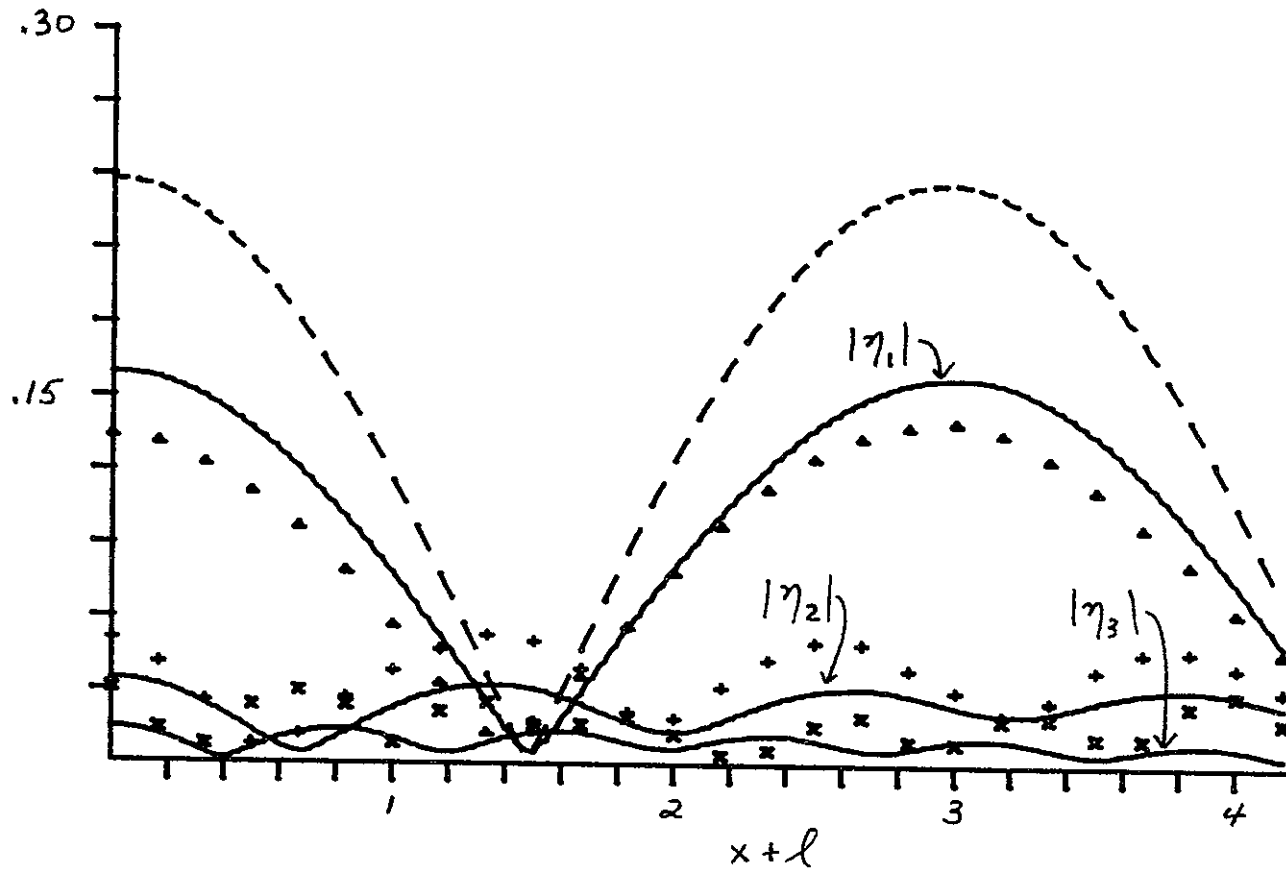


Fig. 5.4b. $L = 4.173$ ft., $A_1 = .027$ (See Fig. 5.4a).



5.4c. $L = 4.173$ ft., $A_1 = .040$ (See Fig. 5.4a).

5.2 Some Theoretical Predictions for a Large Scale Harbor

Having obtained some experimental confirmation of the nonlinear theory, we shall investigate theoretically the response of a harbor having the practical dimensions $2a = 100$ m, $h = 20$ m, and $L = 1000$ m. The first three linear resonant modes occur for $\lambda = \omega L / \sqrt{gh} = 1.41, 4.36,$ and 7.36 corresponding to wave periods of 5.305, 1.716, and 1.016 minutes, respectively. Table 5.3 summarizes the linear results pertaining to these harbor modes.

Table 5.3

λ	μ^2	δ	<u>Amplification</u> ($\eta_1(-\lambda)/A_1$)
1.41	7.95×10^{-4}	.0705	14.35
4.36	7.60×10^{-3}	.218	4.83
7.36	2.17×10^{-2}	.368	2.99

Note that each value of μ^2 is much smaller than the corresponding value of δ ; this is typical for large scale harbors. In practice then, the assumption $\delta \ll 1$ is likely to be more restrictive than the assumption $\mu^2 \ll 1$.

Consider the response of the harbor to monochromatic incident waves, with normalized amplitude $A_1 = .03, A_2 = A_3 = A_4 \dots = 0$. Linearized theory predicts that, for the first resonant mode ($\lambda = 1.41$), the normalized wave amplitude at the back wall of the harbor will be $\eta_1(-\lambda) = .430$. This corresponds to a peak-to-trough wave height of .86 times the depth, which is greater than the value at which waves break in

shallow water.

The predictions of inviscid nonlinear theory are shown in Figs. 5.5(a) through 5.5(d), for the case $A_1 = .03$. Fig. 5.5(a) shows the number of harmonics required in the numerical solution, N^* , versus the normalized incident wave frequency, $\ell = \omega L / \sqrt{gh}$. As expected, the greatest number of harmonics are required at values of ℓ corresponding to resonant harbor modes, for which the wave amplitude in the harbor is large.

Fig. 5.5(b) shows the variation of the first harmonic amplitude at the back wall, $(\eta_1(-\ell))$, with incident wave frequency, ω . The solid line is the prediction of linearized theory (and regular perturbation theory, also); the points are nonlinear results. According to nonlinear theory, the first resonant mode occurs at $\ell = 1.37$ and has a peak height of .382; as compared with $\ell = 1.41$ and a peak height of .430 in linearized theory. For the second and third resonant modes, the resonant amplification is smaller, and the discrepancy between nonlinear and linear theory is therefore smaller.

Fig. 5.5(c) shows second harmonic generation due to nonlinearity. The solid line is calculated from the regular perturbation theory of section 3.3; the points are numerically-generated results. From Table 5.3, we see that, in the range of ℓ covering the first three resonant modes, $\ell \ll 1/\mu^2$. Therefore, we expect that regular perturbation will adequately describe second harmonic generation so long as the wave amplitudes are not too large. Comparing 5.5(c) and 5.5(a), we see that the major discrepancies between regular perturbation and numerical theory occur where the numerical solution required many more

than two harmonics. The various peaks in second harmonic generation have been discussed in Section 3.3; here we simply recall that the three central peaks correspond to linear resonance of the first harmonic, whereas the two small peaks flanking each central peak correspond to linear resonance of the second harmonic. The effect of dispersion increases with increasing ℓ and tends to shift the small peaks to the right relative to the central peak. At $\ell = 7.36$, one of the small peaks has almost overlapped its adjacent central peak; this corresponds to a situation in which both the first and second harmonics are resonated simultaneously. As a result of this phenomenon, the peaks in Fig. 5.5(c) do not diminish with ℓ as fast as the first harmonic peaks of Fig. 5.5(b).

The variation of $|\eta_3(-\ell)|$ with ℓ is shown in Fig. 5.5(d). Note that the largest peak in $|\eta_3(-\ell)|$ occurs at $\ell = 1.41$, corresponding to the first resonant harbor mode, and has a magnitude of .023, which is comparable to the magnitude of $\eta_2(-\ell)$. This is contrary to the usual situation in which the higher harmonics are progressively smaller. The reason for this can be seen from Table 5.3. Since the second resonant harbor mode ($\ell = 4.36$) occurs at a frequency very nearly three times that of the first resonant harbor mode ($\ell = 1.41$), we see that, when $\ell = 1.41$, both the first and third harmonics are resonated simultaneously. This is quite generally true for the long, narrow bay, because its resonant modes appear at roughly odd multiples of $\pi/2$. This resonance mechanism for the third harmonic is similar to the one occurring at $\ell = 7.36$ for the second harmonic, though the underlying reasons are different for the two cases.

Fig. 5.5(e) shows the mean set-up at the back wall, $\eta_0(-\ell)$, vs. ℓ . The solid line is the prediction of regular perturbation theory, cf. Fig. 3.1(c); the points are calculated from the numerical solutions using (3.2.17). Note that the peaks occur at values of ℓ for which the first harmonic is linearly resonated. Since η_0 depends primarily on the square of η_1 , the peaks of η_0 diminish in height more rapidly than those of η_1 .

The numerically-predicted spatial dependence of the harbor response is shown in Figs. 5.6(a)-(c), 5.7(a)-(c), and 5.8(a)-(c) for each of the first three resonant modes. These figures may be compared with the predictions of regular perturbation theory, shown in Figs. 3.2, 3.3, and 3.4. Note that the higher harmonics are progressively smaller; this is the a posteriori justification for truncating the numerical solution at a finite number of harmonics. The differences between the numerical solutions and regular perturbation theory are mainly due to the fact that the latter overestimates the first harmonic amplitude.

For incident waves with amplitudes greater than $A_1 = .03$, the numerical scheme frequently requires more than ten harmonics to achieve convergence. This is not entirely satisfactory because the value of δ associated with the tenth harmonic, at say $\ell = 4.36$, is 2.18. This exceeds the value $\delta = \pi/2 = 1.5708$ at which cross modes first appear in the bay. Thus, at larger amplitudes, the assumption of one-dimensionality in the far field of the harbor is no longer tenable. Furthermore, the peak-to-trough wave heights predicted by the nonlinear theory exceed half the depth. At such large amplitudes, the waves are no longer correctly described by the Boussinesq equations.

Thus far, we have not accounted for entrance loss due to separation, whose primary effect is to reduce the resonant amplitude of the first harmonic. The magnitude of this reduction depends upon the average friction factor \bar{f} , which in turn depends strongly upon the particular shape of the harbor entrance. As argued in Section 4.3.2, we expect \bar{f} to be less than .7 for the long narrow bay. To estimate the influence of separation, we shall use the conservative value $\bar{f} = .35$, which coincides with the value chosen for the laboratory experiments.

Of practical interest is the relative importance of nonlinearity and separation in reducing the resonant amplitudes of the first harmonic. Fig. 5.9 shows the variation of $|\eta_1(-\ell)|$ with increasing incident wave amplitudes, $|A_1|$, for each of the first three resonant harbor modes. The dashed lines represent linearized theory; their slopes are just the amplification factors of Table 5.3. The symbols " Δ " and " x " indicate the values of $|\eta_1(-\ell)|$ according to inviscid nonlinear theory ($\bar{f} = 0$) and nonlinear theory with separation ($\bar{f} = .35$), respectively. Note that, for the first resonance mode ($\ell = 1.41$), the combined reduction due to both separation and nonlinearity is roughly twice that due to nonlinearity alone; thus both effects are of roughly equal importance. For the second and third harbor modes ($\ell = 4.37$ and 7.36), the effect of nonlinearity dominates the effect of separation. This is reasonable since nonlinearity increases with increasing ℓ , whereas separation does not.

The spatial dependence of the harbor response according to numerical theory with $\bar{f} = .35$ and $|A_1| = .03$ is shown in Figs. 5.10(a)-(c), 5.11(a)-(c), and 5.12(a)-(c), for each of the first three resonant

modes. These figures may be compared with the predictions of inviscid nonlinear theory, shown in Figs. 5.6, 5.7, and 5.8. As expected, the inclusion of separation losses leads to a reduction in the predicted wave heights. For the first resonant mode, this reduction is substantial; for the second and third resonant modes, the viscous theory agrees fairly closely with the inviscid theory.

When the incident wave is not monochromatic, nonlinear interactions generate a great many new frequencies, some of which may be resonated by the linear mechanism. Consider, for example, an incident wave having $A_1 = 0$ but A_2 and A_3 nonzero, as in Fig. 5.13(a). The incident wave spectrum is dominated by two frequencies, 2ω and 3ω , where ω coincides with the first resonant harbor mode, viz. $\lambda = \omega L / \sqrt{gh} = 1.41$. The harbor response according to linearized theory is simply an amplification of A_3 , corresponding to the resonant mode with $\lambda = 4.36$, and is shown in Fig. 5.13(b). However, nonlinear theory allows for the generation of additional harmonics; among them the first and fifth harmonics, both of which coincide with resonant harbor modes. Fig. 5.13(c) shows the harbor response at $x = -\lambda$ predicted by inviscid nonlinear theory. Nine harmonics are present in the numerical solution. This means that the wave spectrum of an incident wave can be significantly changed by nonlinearity. This possibility, somewhat similar to subharmonic resonance in simpler physical systems, can be important to the design of mooring systems for ships in the harbor.

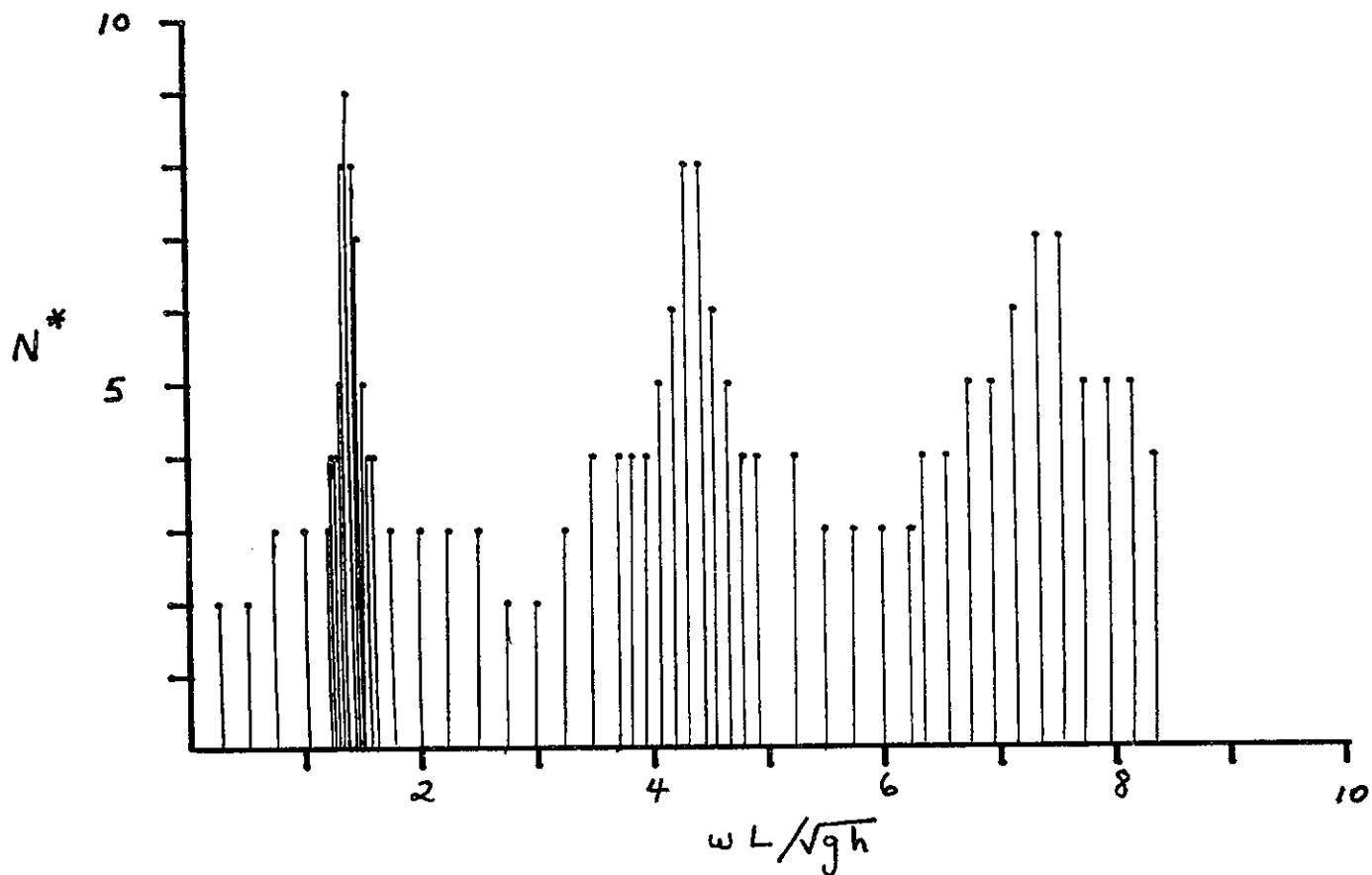


Fig. 5.5a. Inviscid nonlinear theory ($\bar{\tau} = 0$): Frequency response of large-scale harbor ($h = 20$ m., $2a = 100$ m., $L = 1000$ m., $A_1 = .03$). Number of harmonics, N^* , required in the numerical solutions.

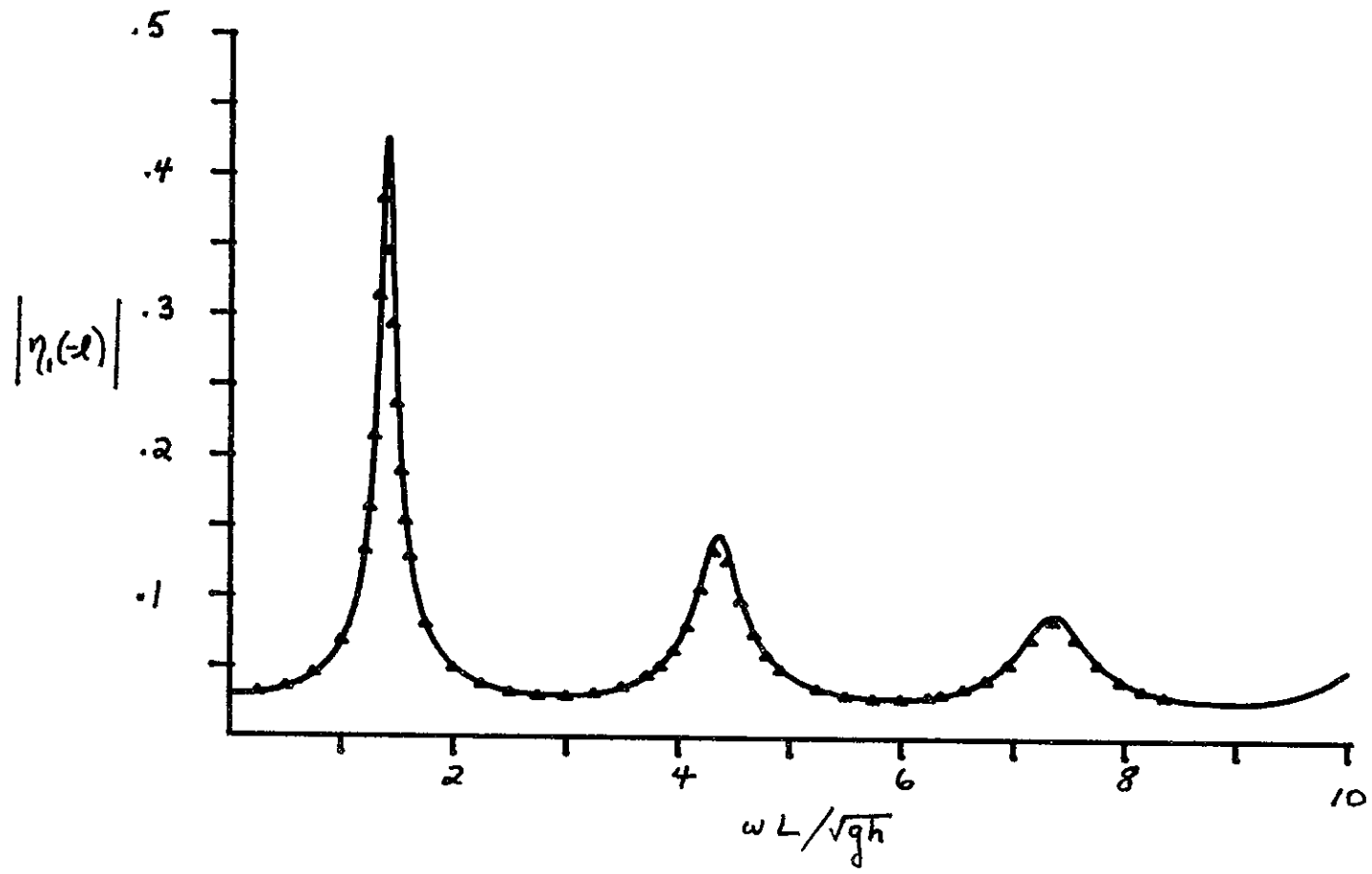


Fig. 5.5b. First harmonic amplitude at the back wall according to nonlinear theory (Δ) and regular perturbation theory (---). (See Fig. 5.5a).

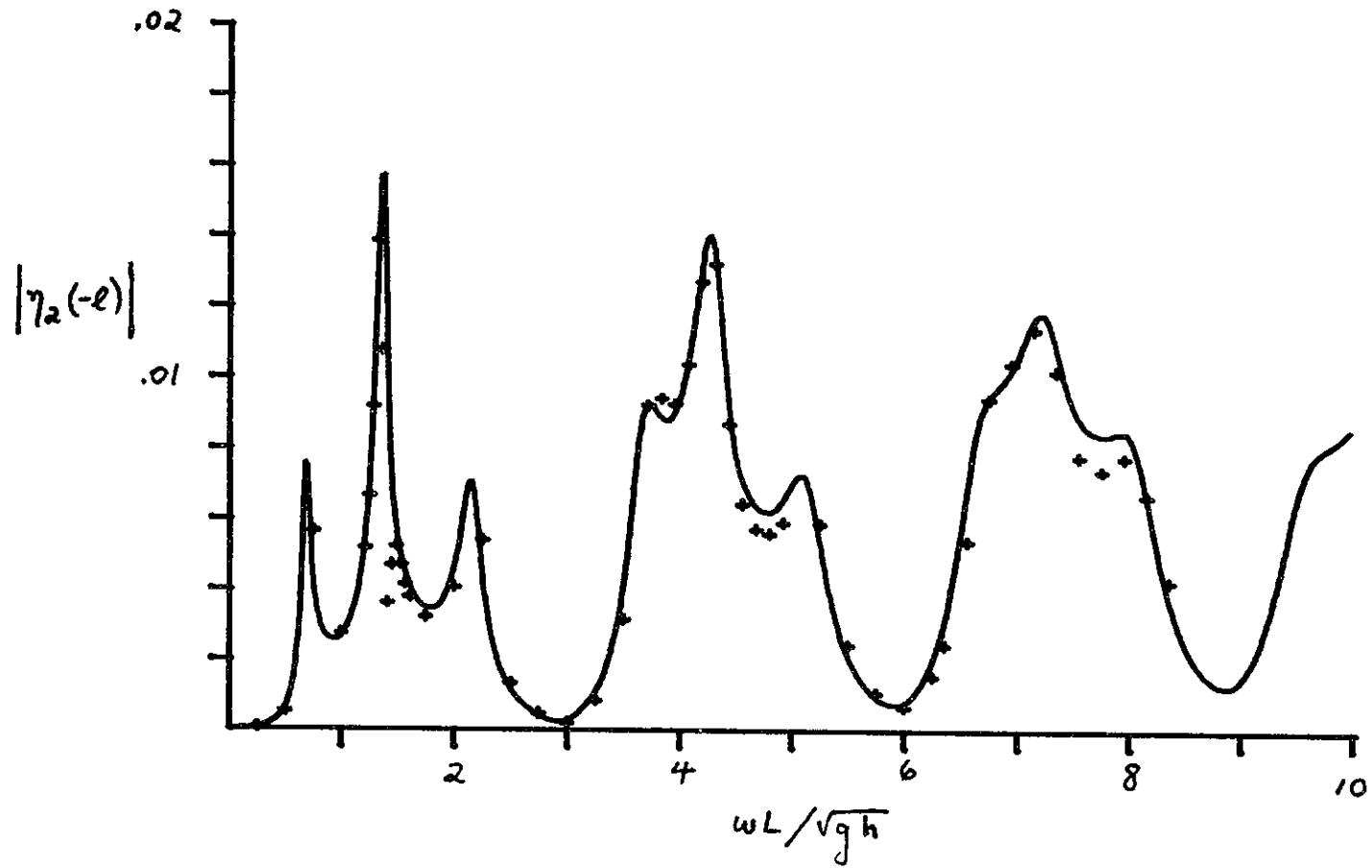


Fig. 5.5c. Second harmonic amplitude at the back wall according to nonlinear theory (+) and regular perturbation theory (—). (See Fig. 5.5a).

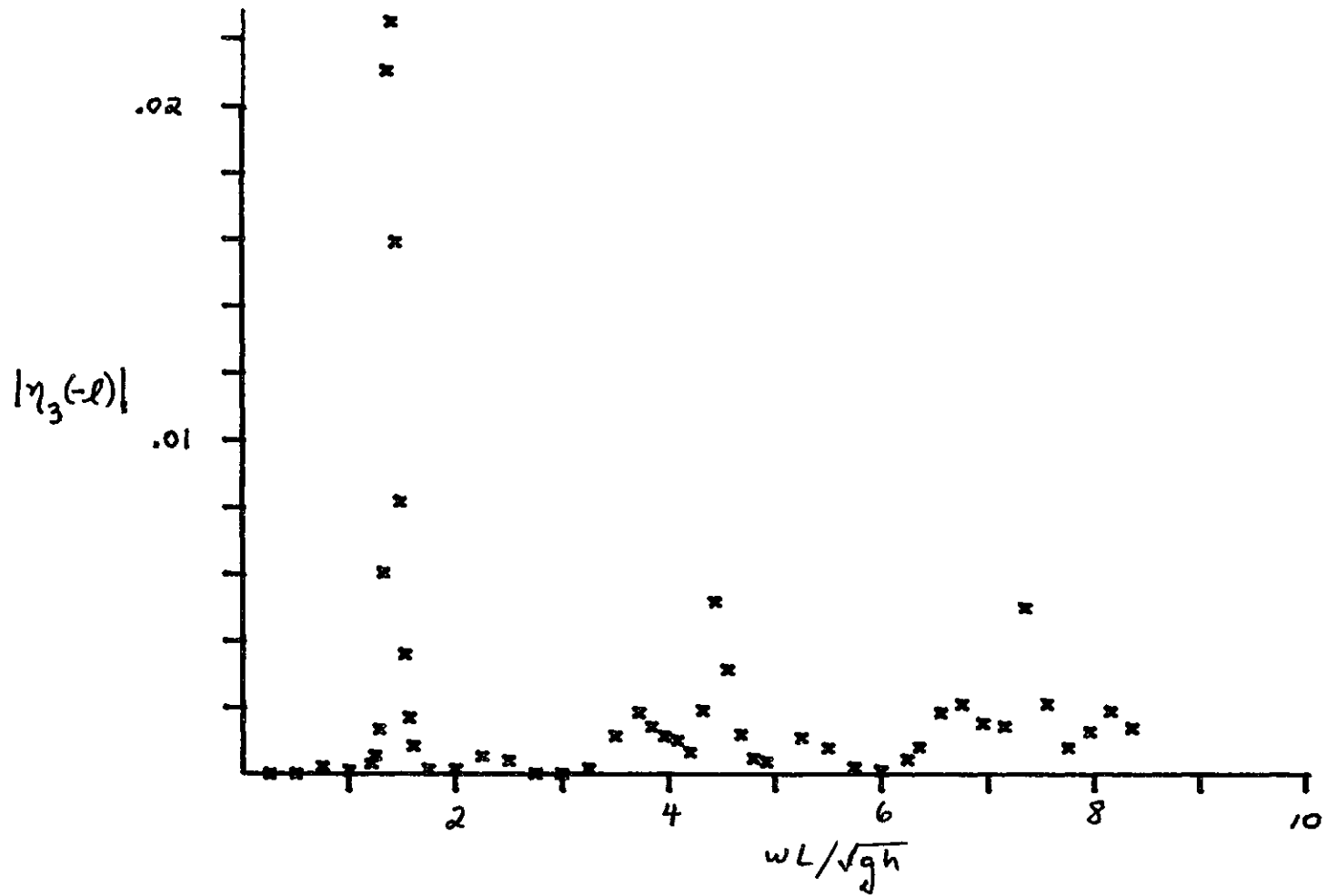


Fig. 5.5d. Third harmonic amplitude at the back wall according to nonlinear theory (x).
(See Fig. 5.5a).

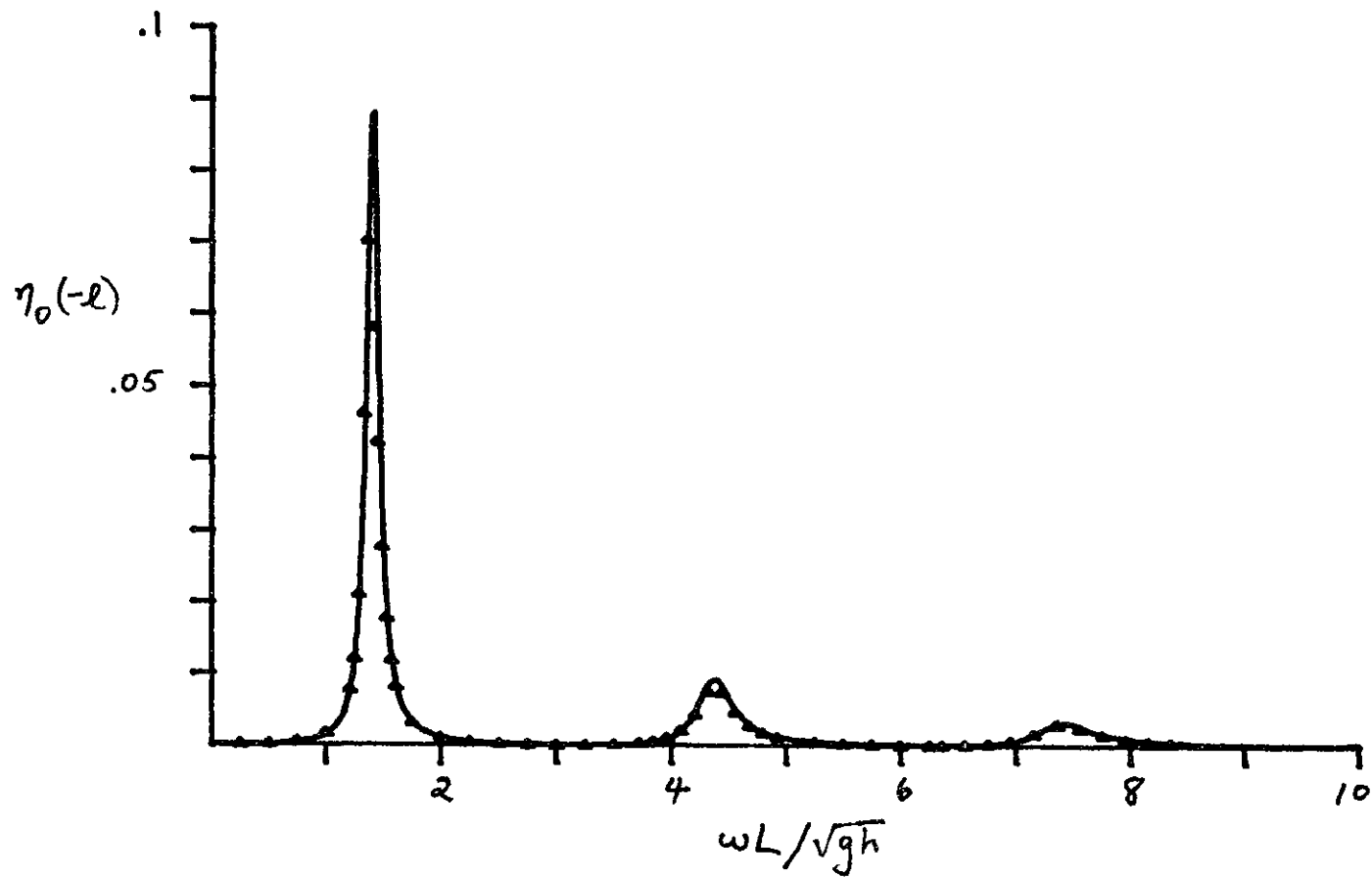


Fig. 5.5e. Zeroth harmonic at the back wall according to nonlinear theory (Δ) and regular perturbation theory (—). (See Fig. 5.5a).

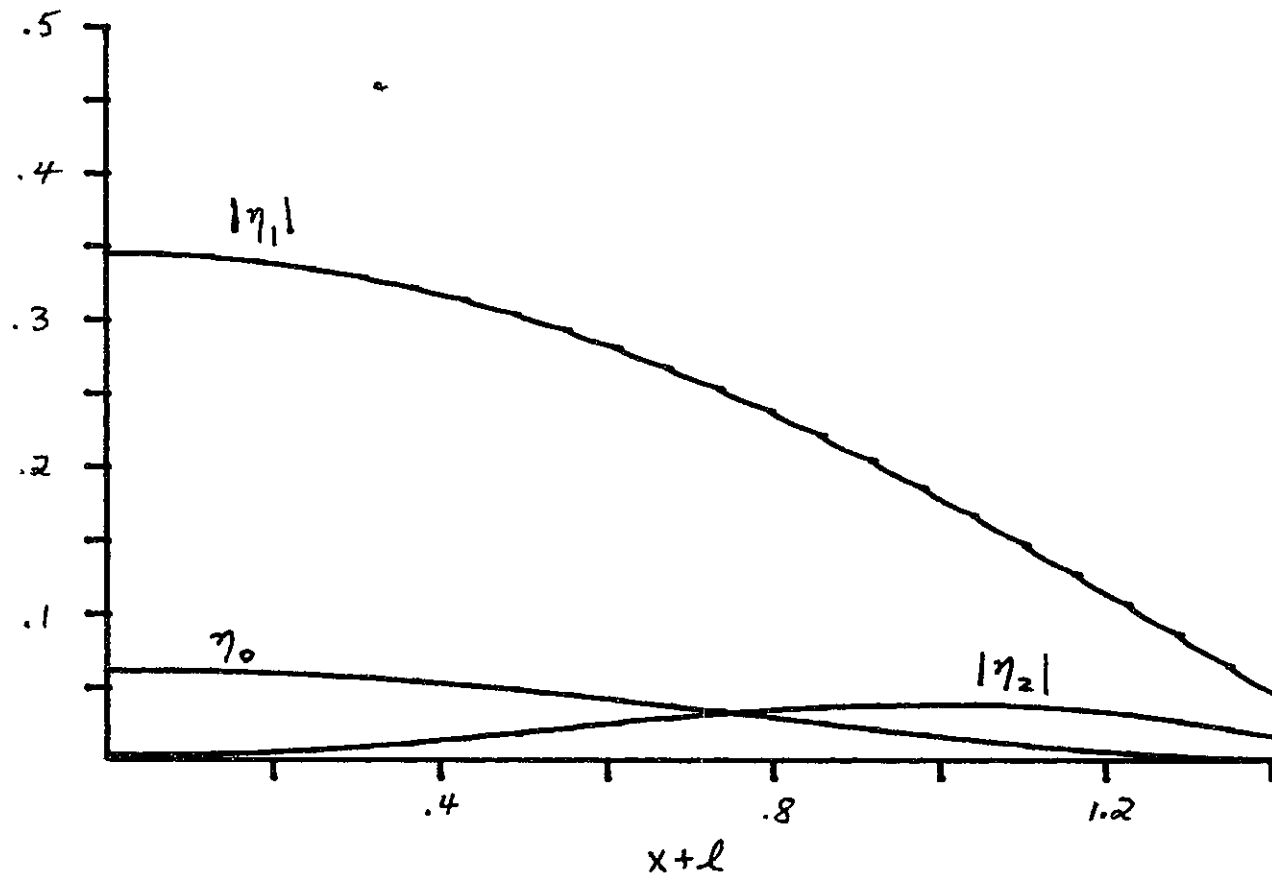


Fig. 5.6a. Inviscid nonlinear theory ($\bar{f} = 0$): First resonant mode of large-scale harbor ($h = 20$ m., $2a = 100$ m., $L = 1000$ m., $A_1 = .03$, $\epsilon = 1.41$). Spatial variation of the lower harmonics.

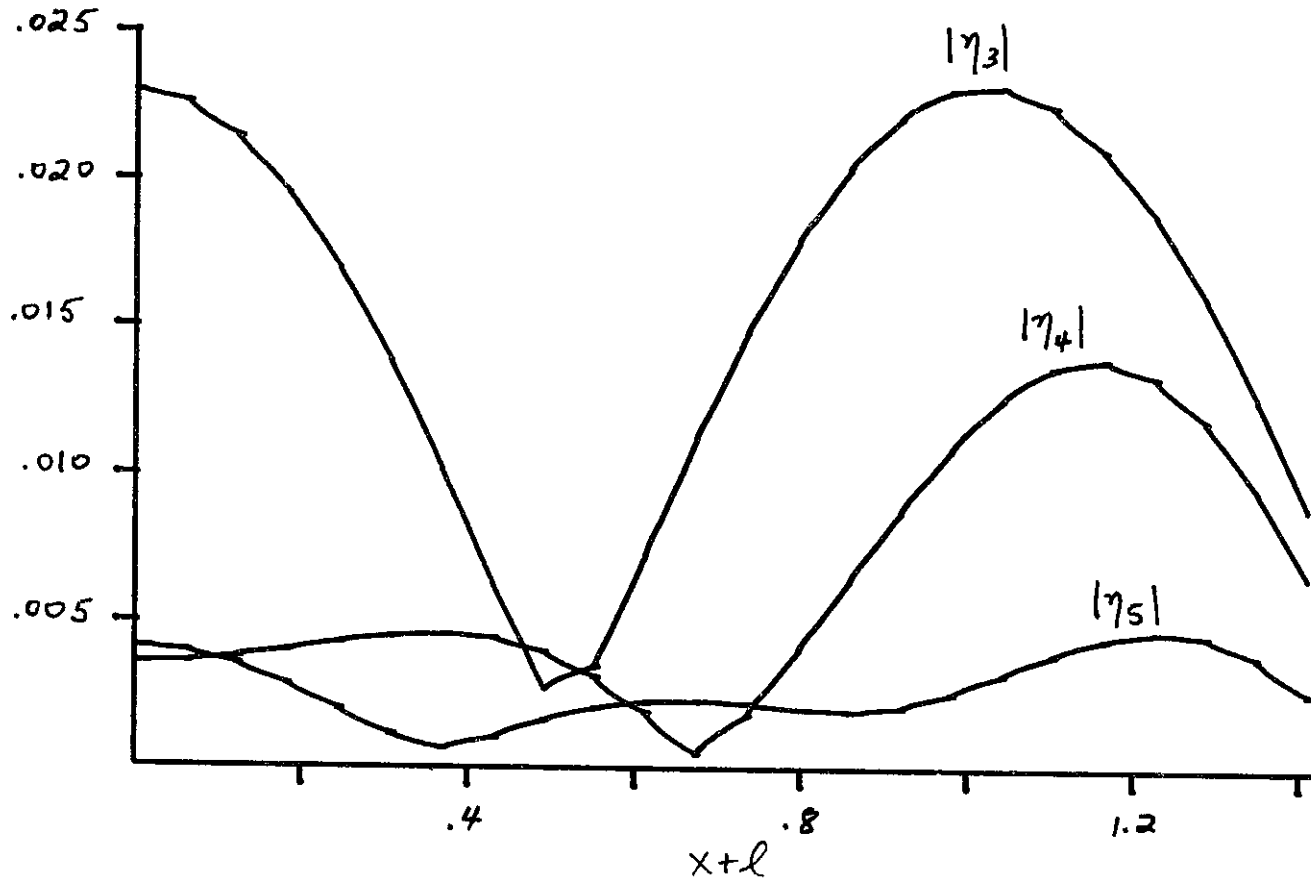


Fig. 5.6b. Spatial variation of the higher harmonics. (See Fig. 5.6a).

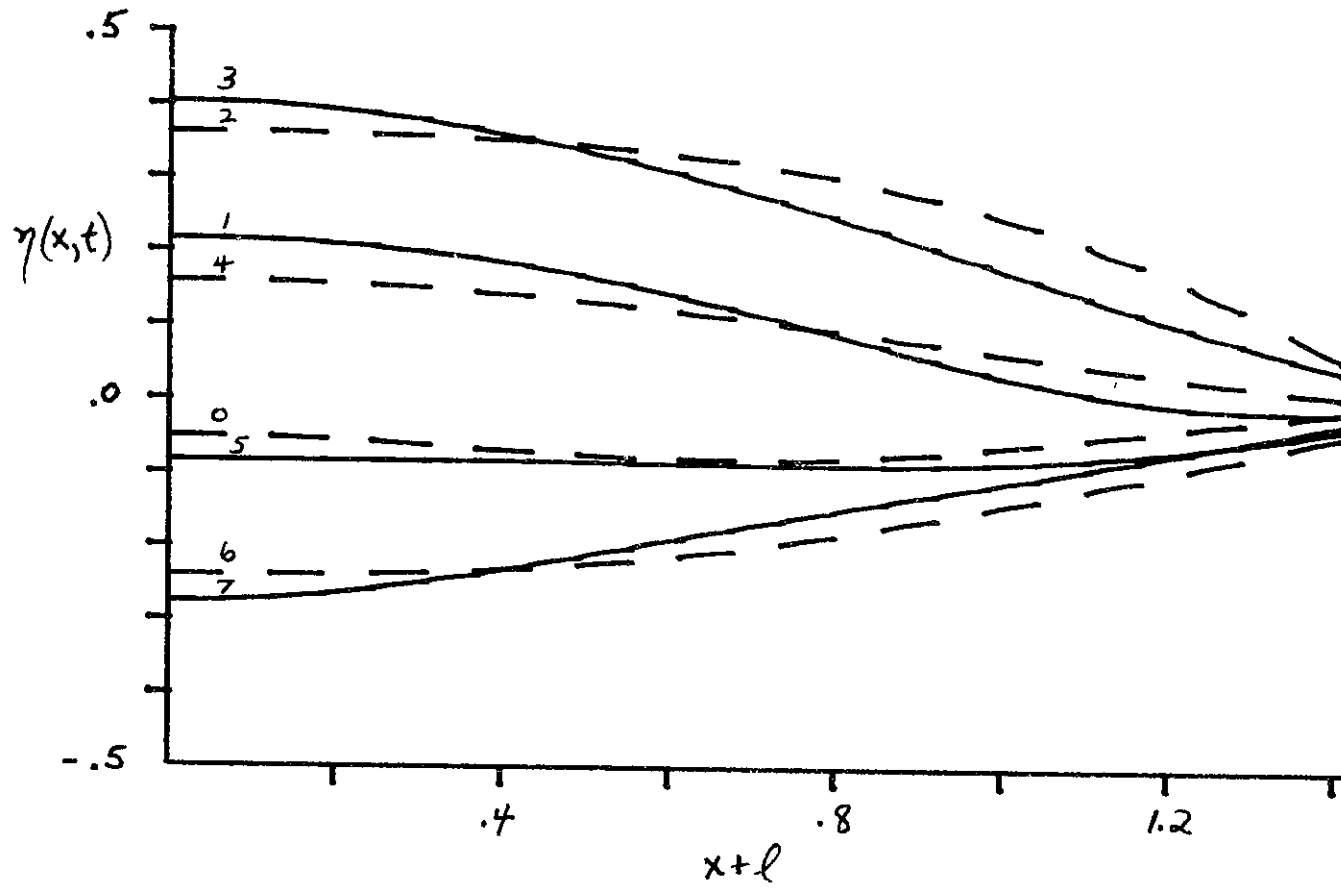


Fig. 5.6c. Surface profiles at times $t = m\pi/4$, $m = 0,1,2\dots7$.

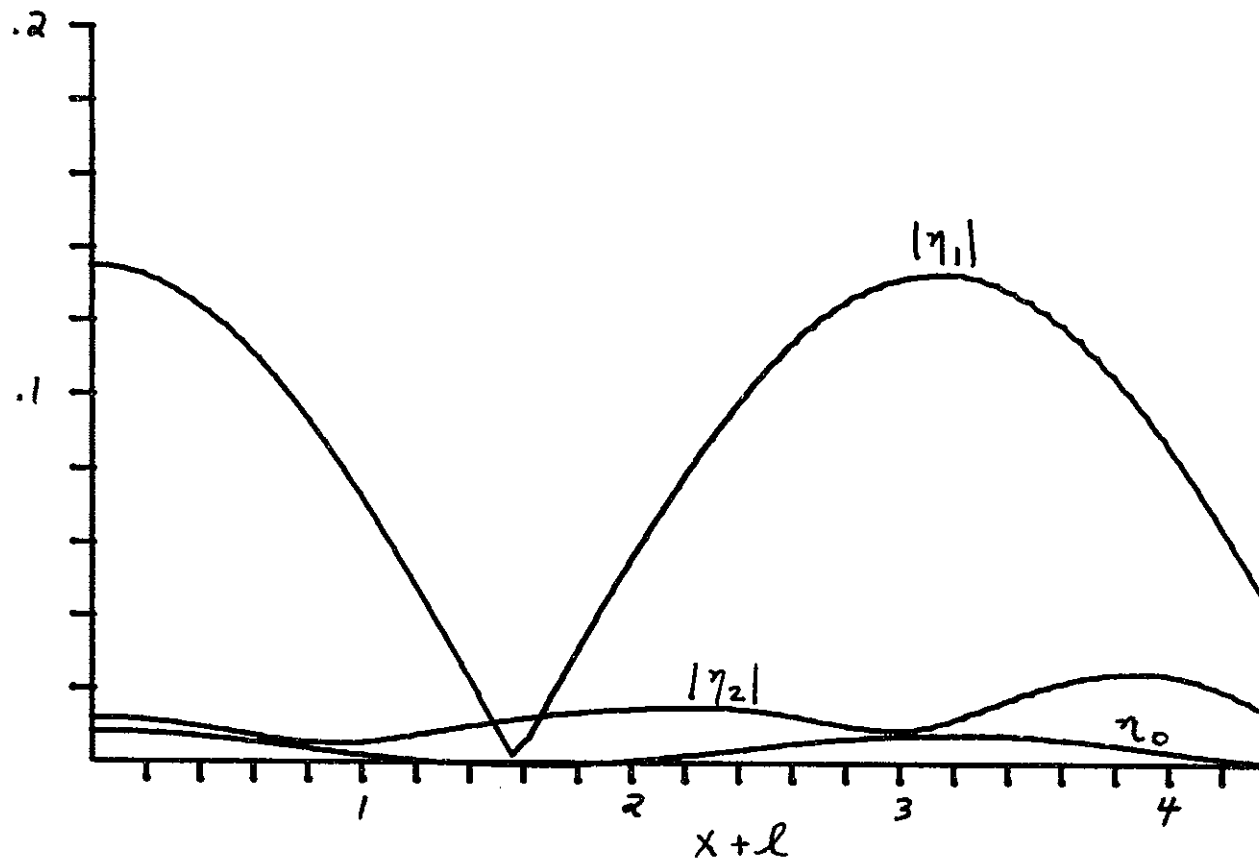


Fig. 5.7a. Inviscid nonlinear theory ($\bar{f} = 0$): Second resonant mode of large-scale harbor ($h = 20$ m., $2a = 100$ m., $L = 1000$ m., $A_1 = .03$, $\lambda = 4.36$). Spatial variation of the lower harmonics.

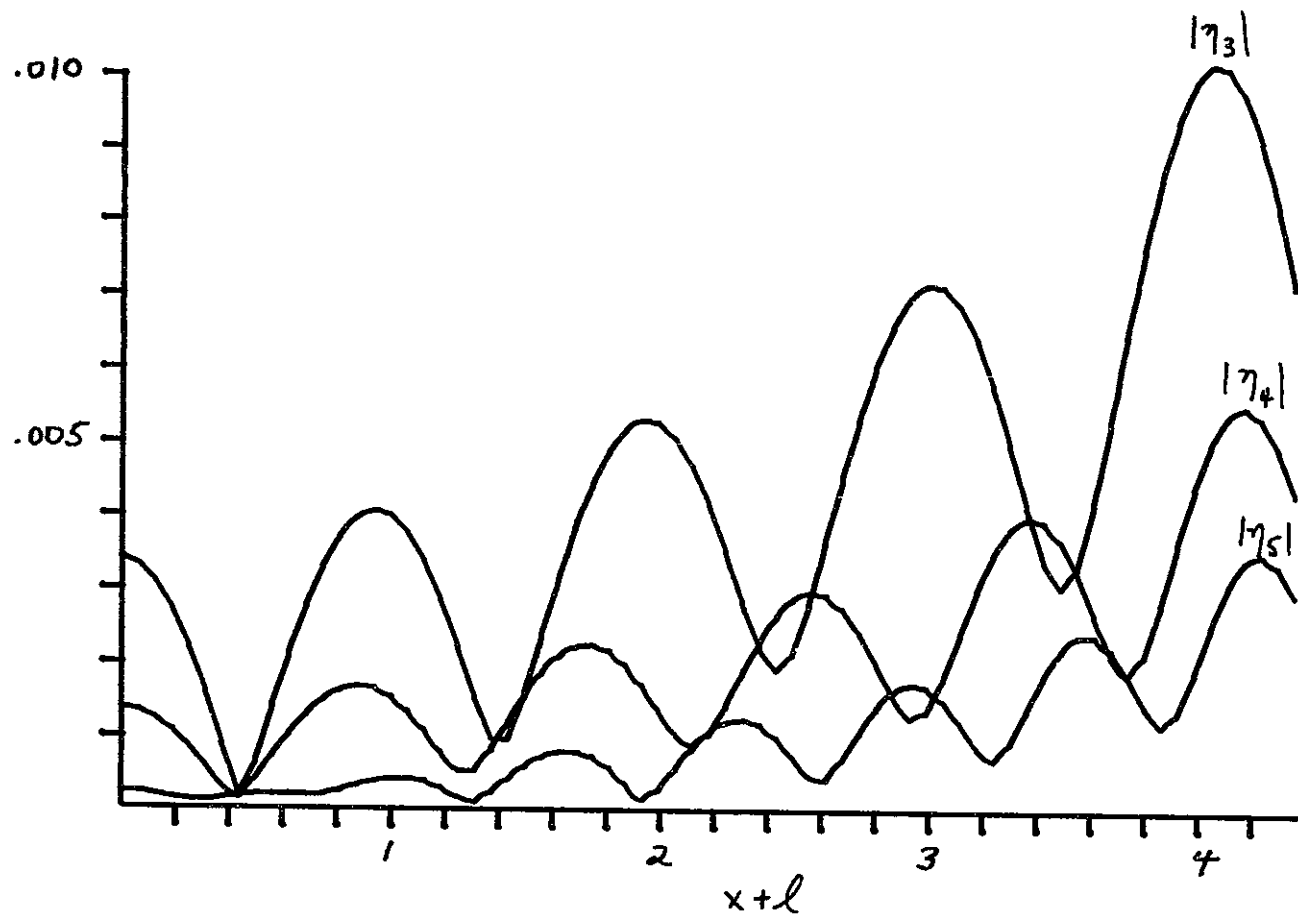


Fig. 5.7b. Spatial variation of the higher harmonics. (See Fig. 5.7a).

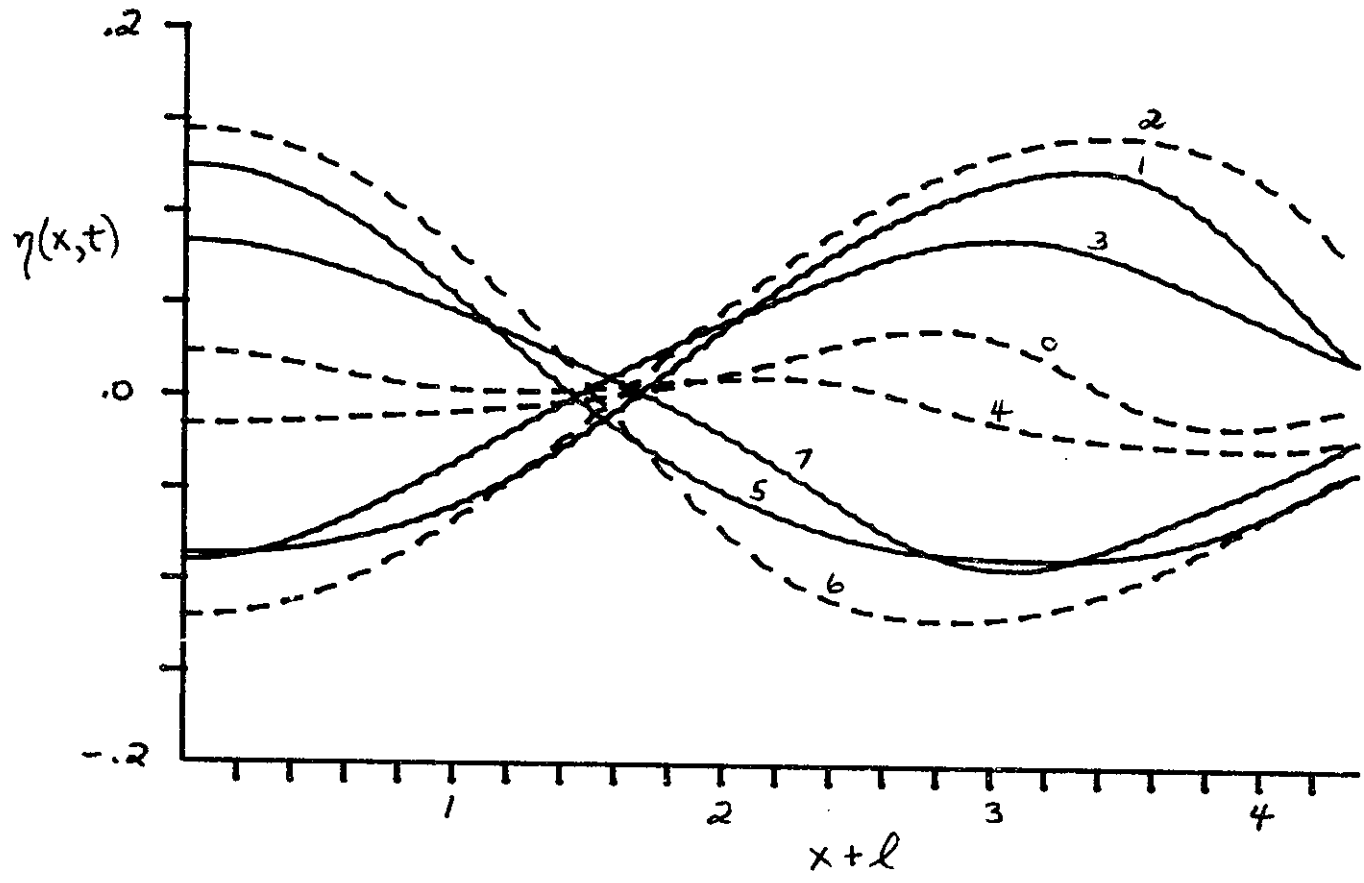


Fig. 5.7c. Surface profiles at times $t = m\pi/4$, $m = 0, 1, 2, \dots, 7$. (See Fig. 5.7a).

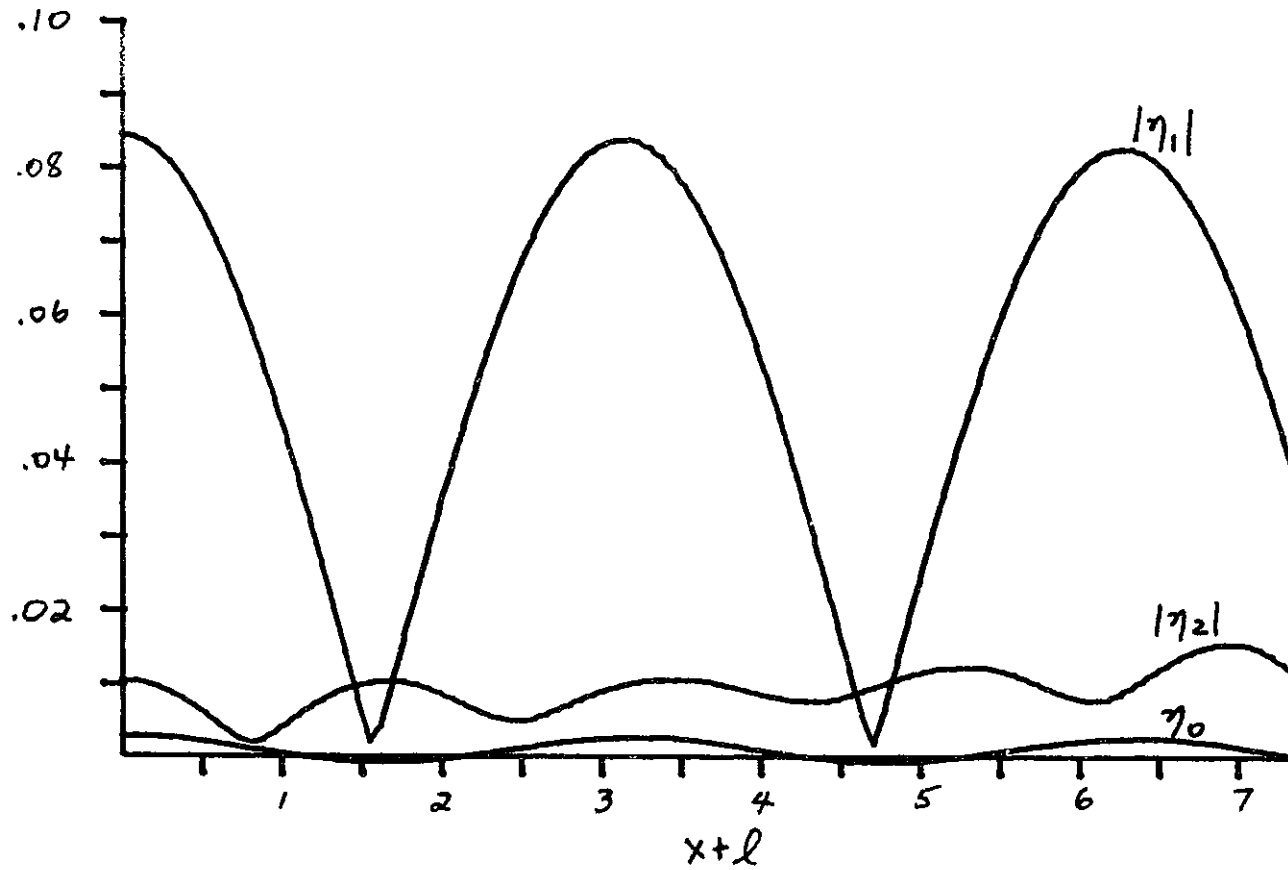


Fig. 5.8a. Inviscid nonlinear theory ($\bar{f} = 0$): Third resonant mode of large-scale harbor ($h = 20$ m., $2a = 100$ m., $L = 1000$ m., $A_1 = .03$, $\epsilon = 7.36$). Spatial variation of the lower harmonics.

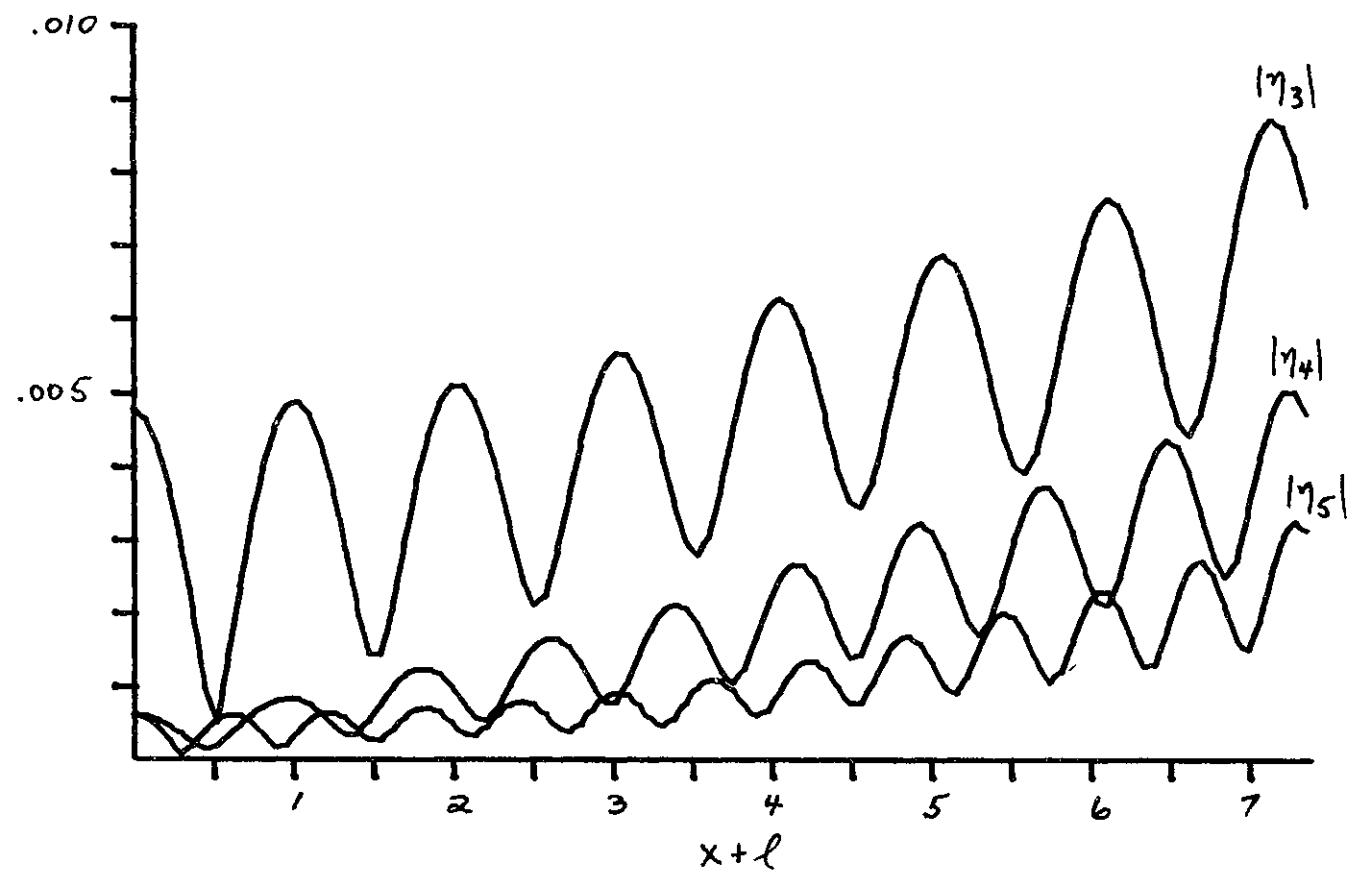


Fig. 5.8b. Spatial variation of the higher harmonics. (See Fig. 5.8a).

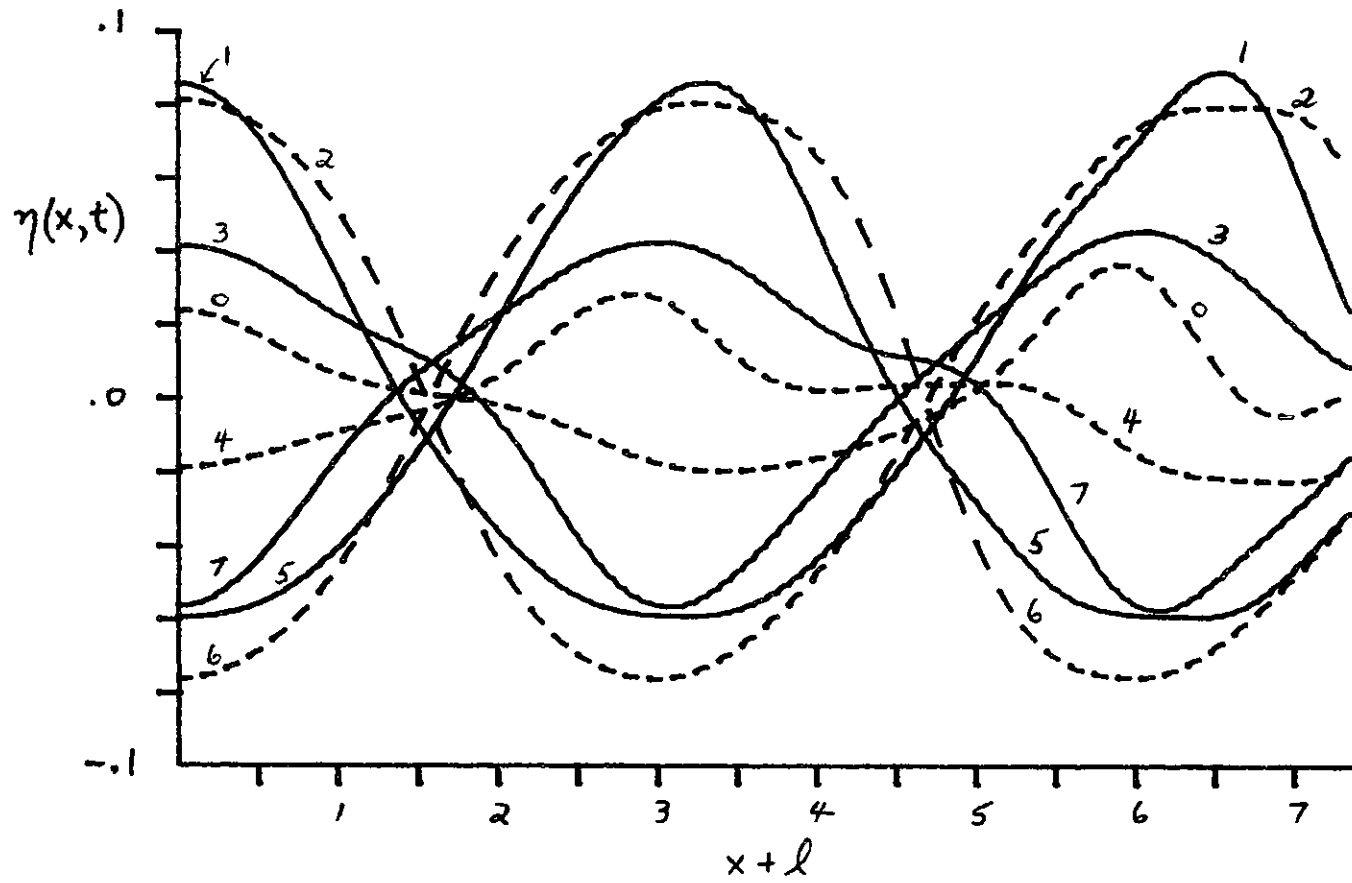


Fig. 5.8c. Surface profiles at times $t = m\pi/4$, $m = 0, 1, 2, \dots, 7$. (See Fig. 5.8a).

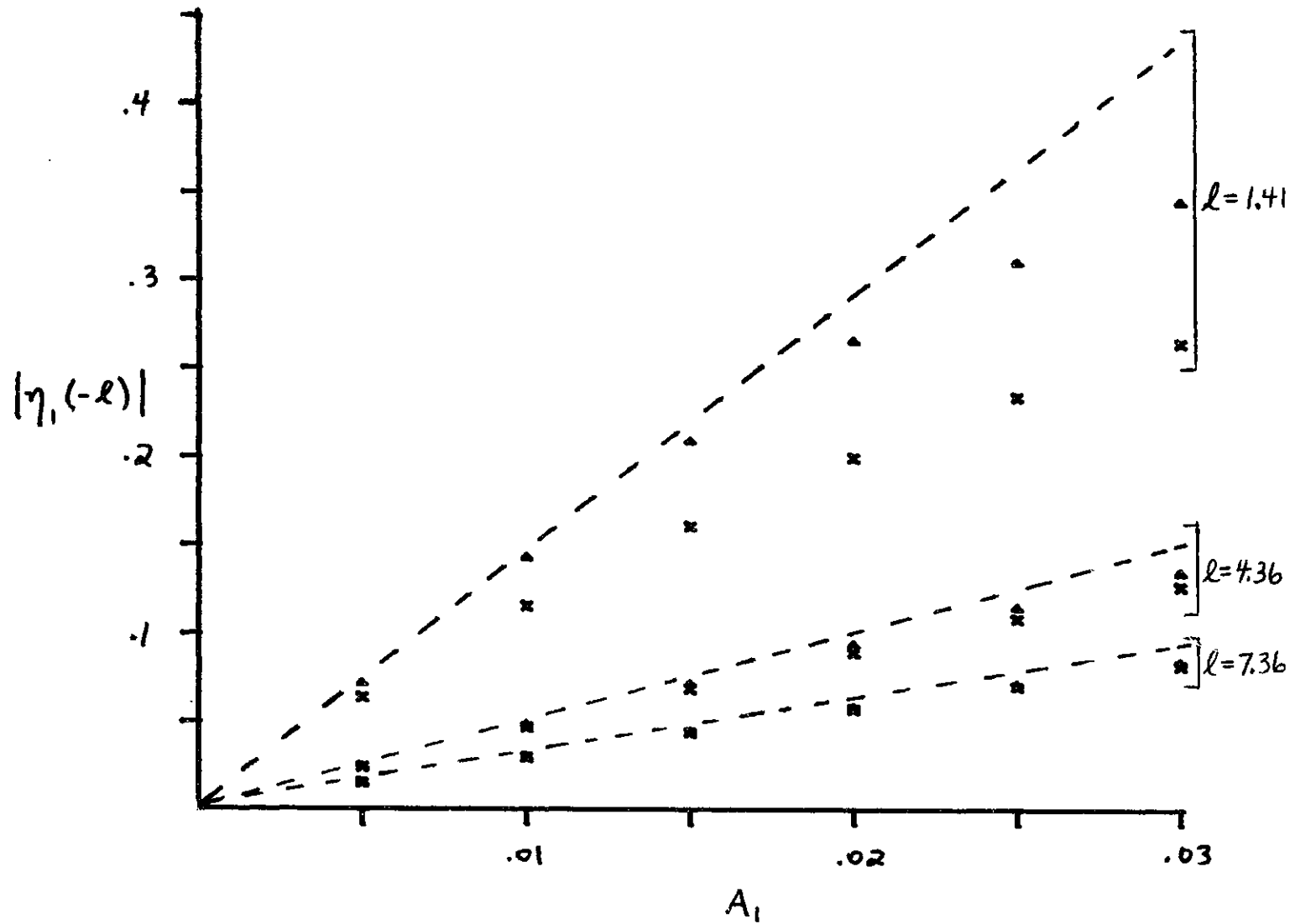
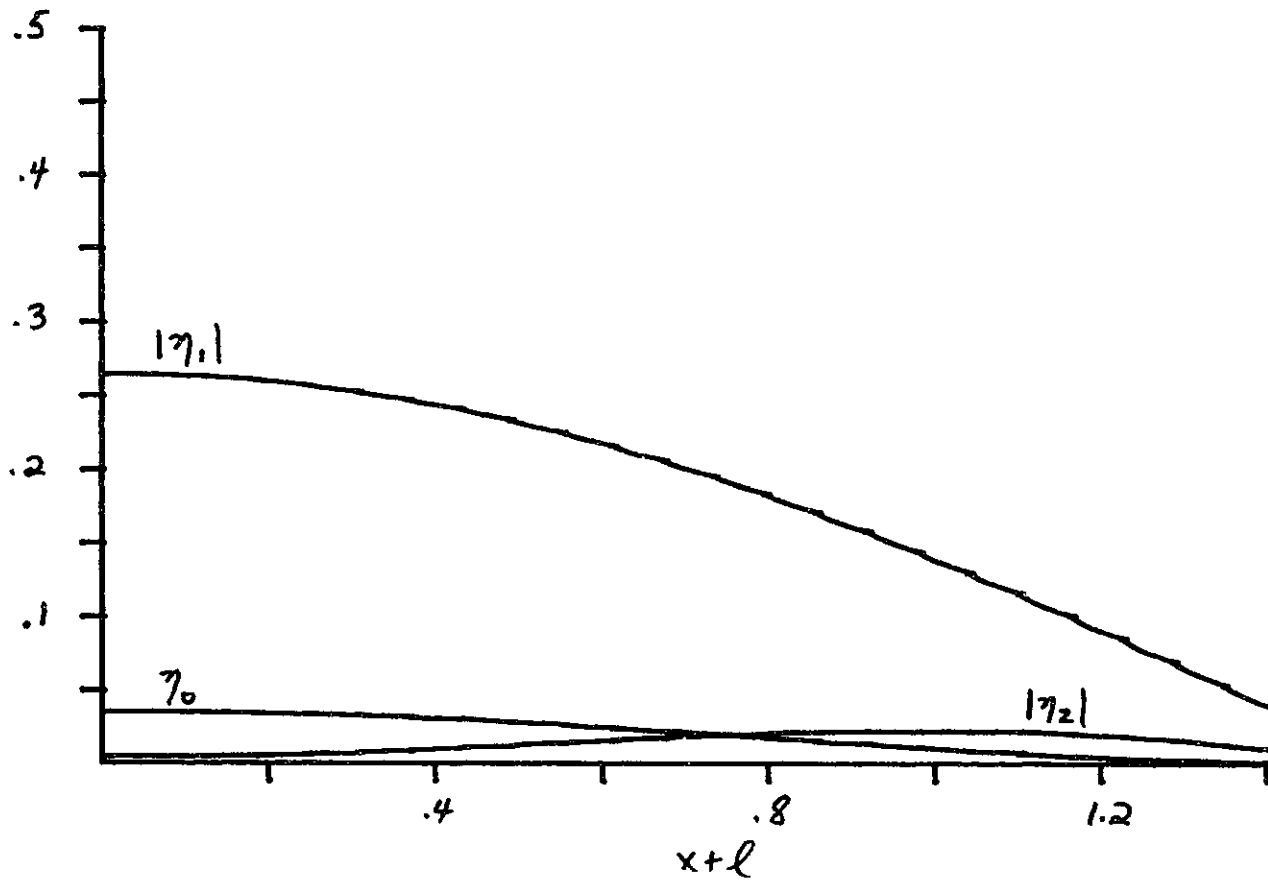
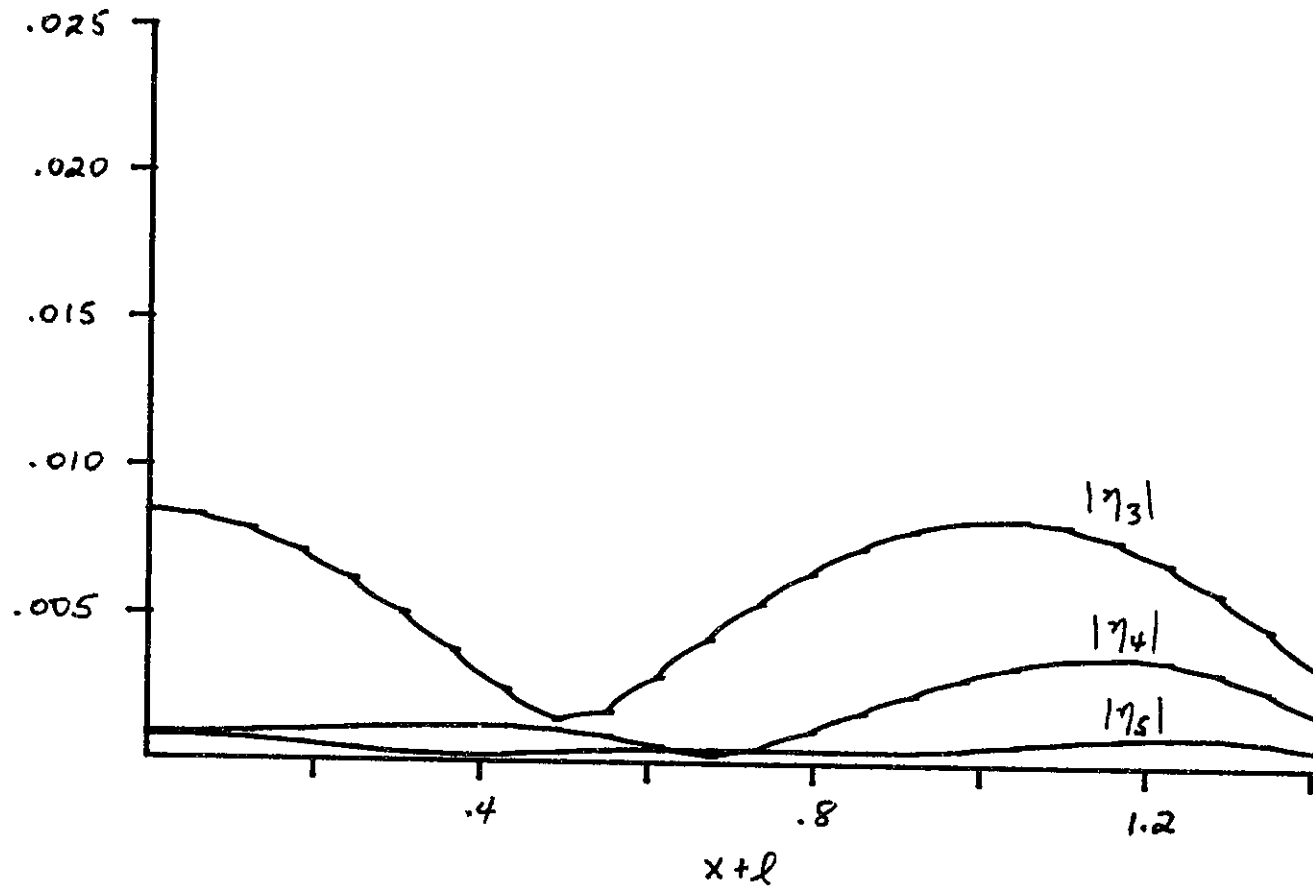


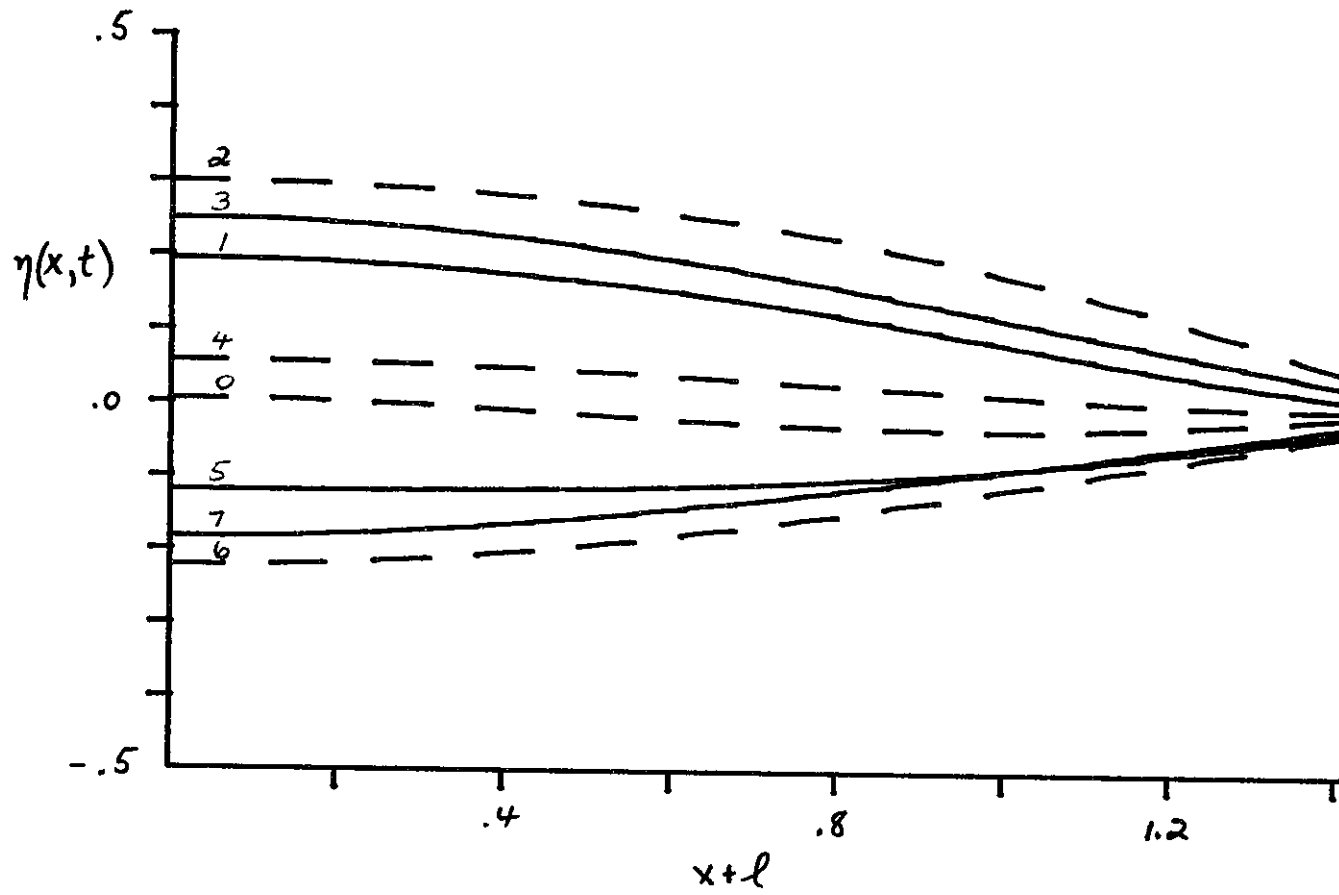
Fig. 5.9. First harmonic amplitude at the back wall of the large-scale harbor vs. incident wave amplitude. (----): linear theory. (): inviscid nonlinear theory ($\bar{f} = 0$). (x): nonlinear theory with separation loss ($\bar{f} = .35$).



5.10a. Nonlinear theory with separation loss ($\bar{f} = .35$): First resonant mode of large-scale harbor ($h = 20$ m., $2a = 100$ m., $L = 1000$ m., $A_1 = .03$, $\epsilon = 1.41$). Spatial variation of the lower harmonics.



5.10b. Spatial variation of the higher harmonics. (See Fig. 5.10a).



5.10c. Surface profiles at times $t = m\pi/4$, $m = 0,1,2\dots7$. (See Fig. 5.10a).

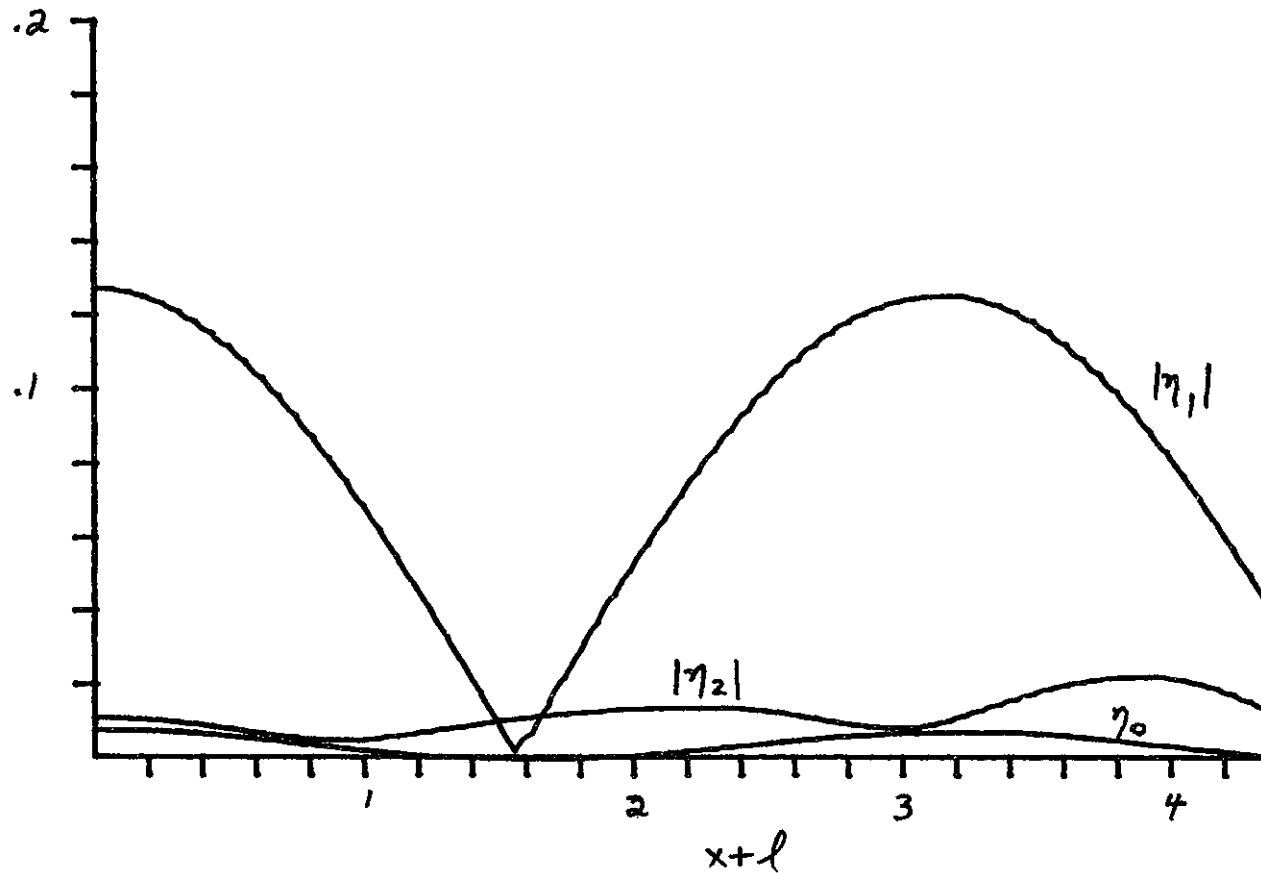


Fig. 5.11a. Nonlinear theory with separation loss ($\bar{f} = .35$): Second resonant mode of large-scale harbor ($h = 20$ m., $2a = 100$ m., $L = 1000$ m., $A_1 = .03$, $\epsilon = 4.36$). Spatial variation of the lower harmonics.

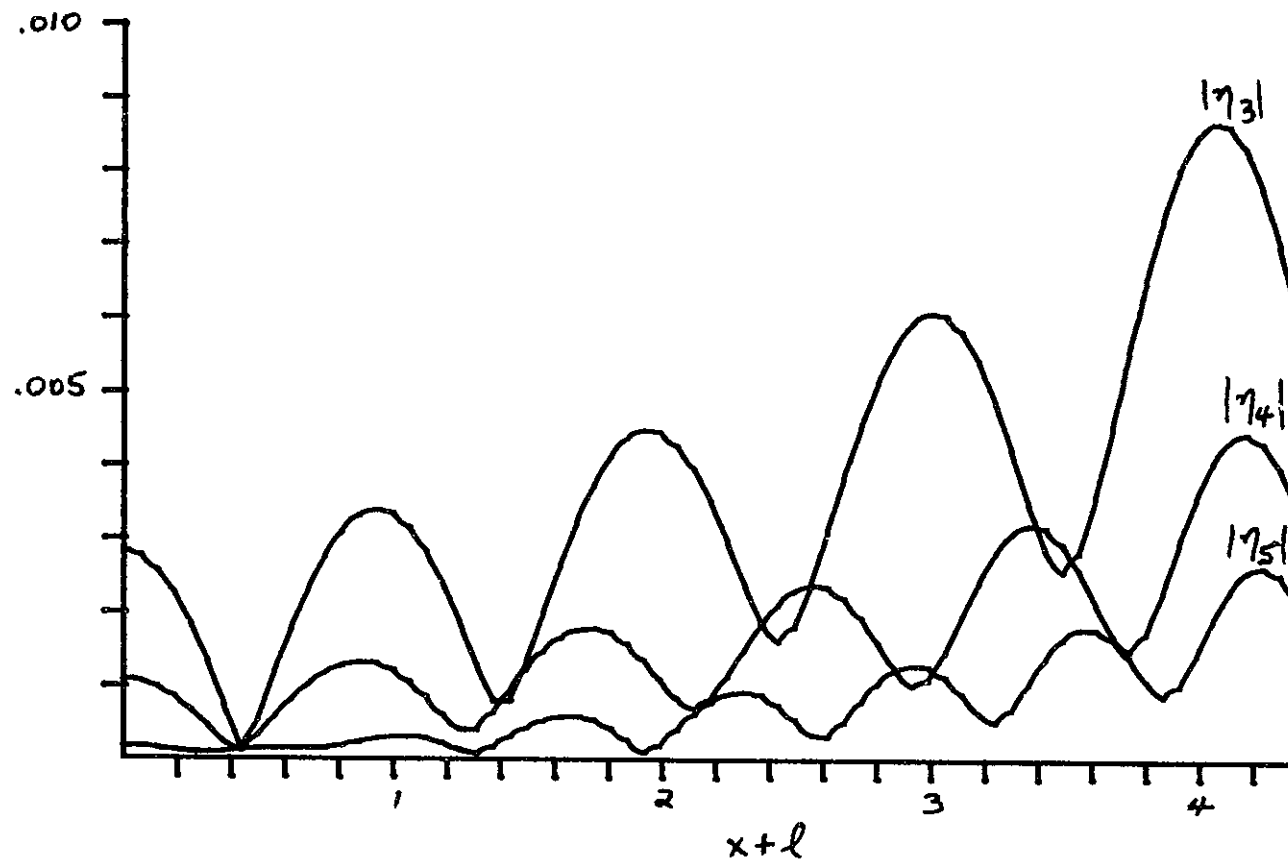


Fig. 5.11b. Spatial variation of the higher harmonics. (See Fig. 5.11a).

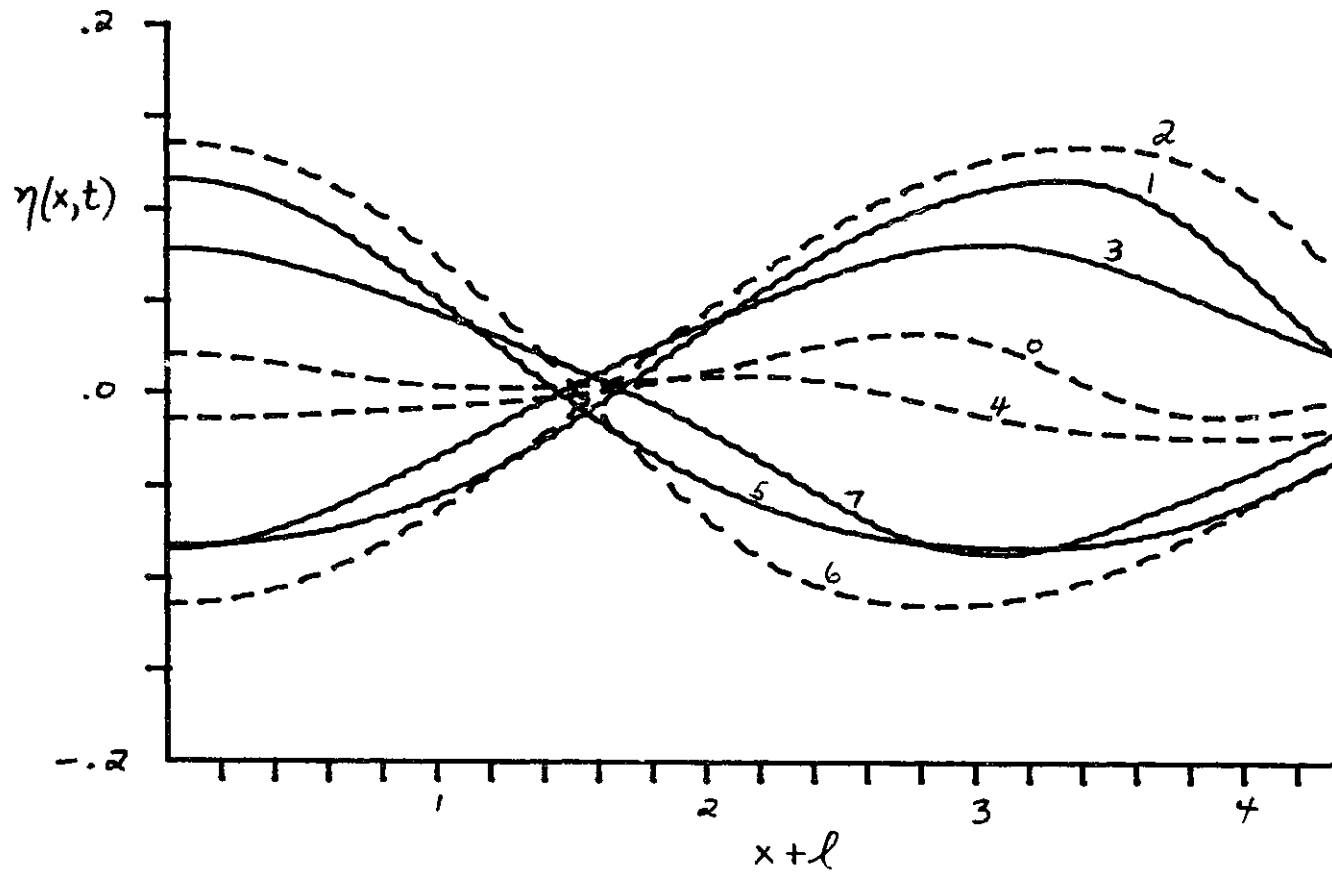


Fig. 5.11c. Surface profiles at times $t = m\pi/4$, $m = 0, 1, 2, \dots, 7$. (See Fig. 5.11a).

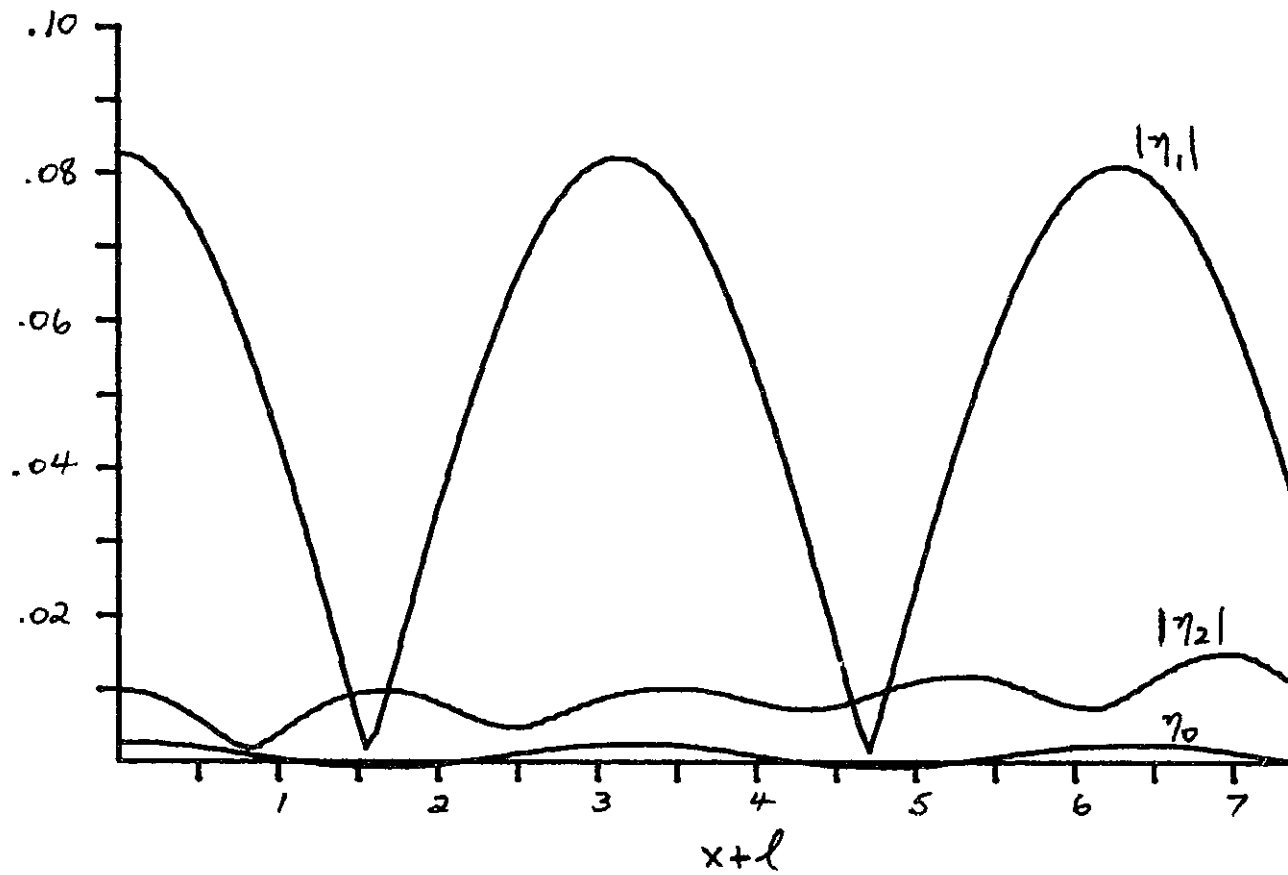


Fig. 5.12a. Nonlinear theory with separation loss ($\bar{f} = .35$): Third resonant mode of large-scale harbor ($h = 20$ m., $2a = 100$ m., $L = 1000$ m., $A_1 = .03$, $\lambda = 7.36$). Spatial variation of the lower harmonics.

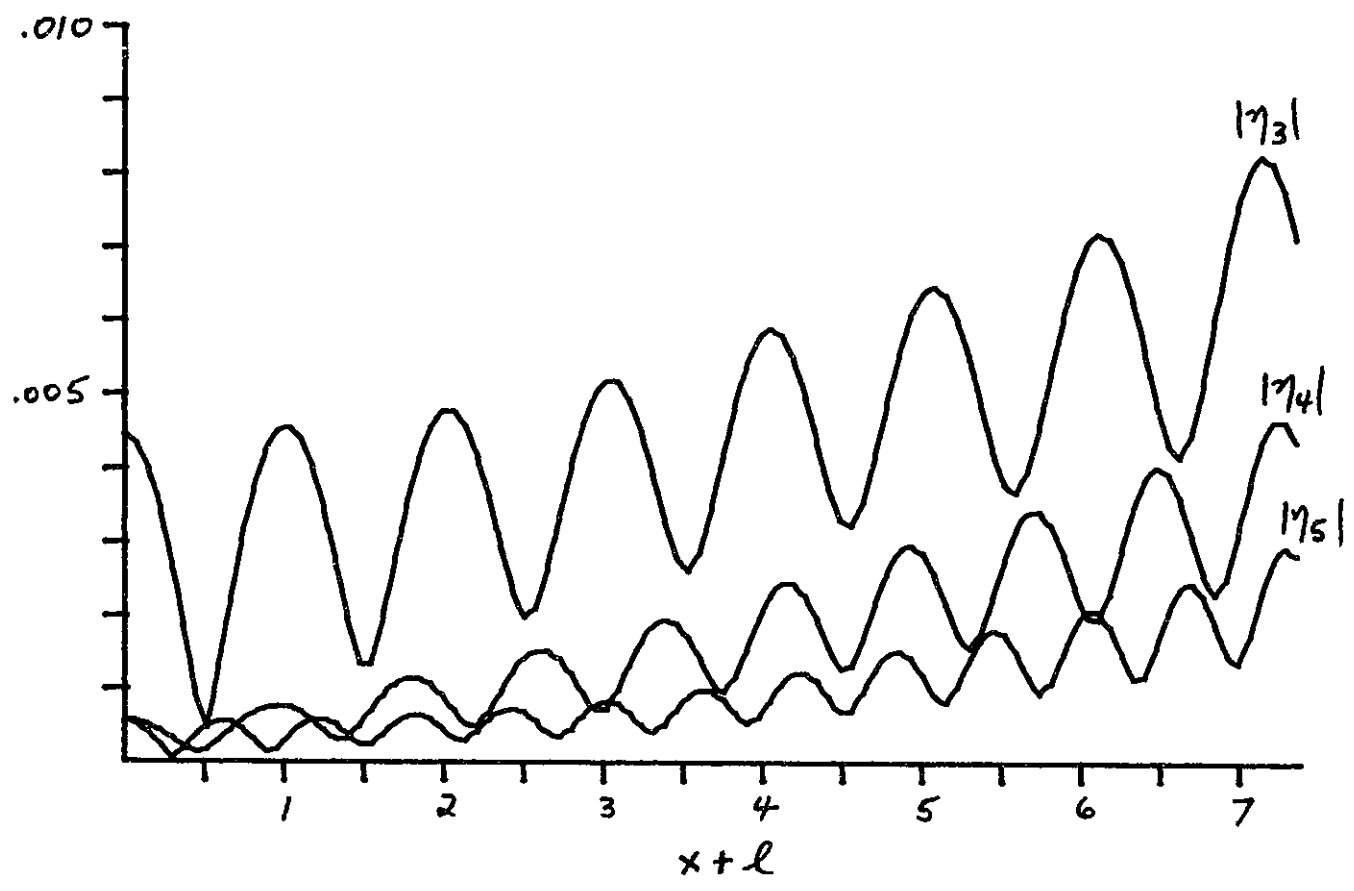


Fig. 5.12b. Spatial variation of the higher harmonics. (See Fig. 5.12a).

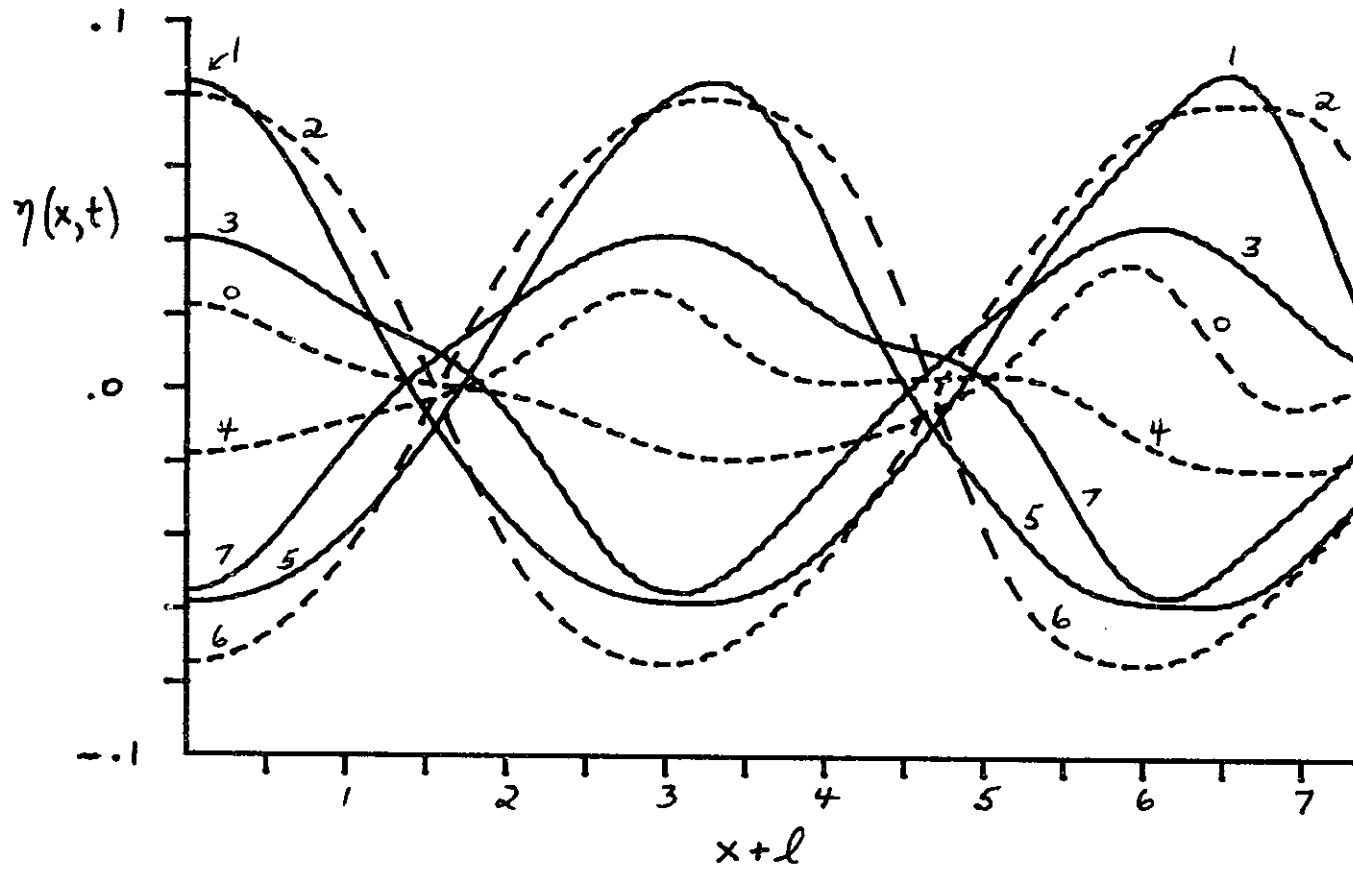


Fig. 5.12c. Surface profiles at times $t = m\pi/4$, $m = 0, 1, 2, \dots, 7$. (See Fig. 5.12a).

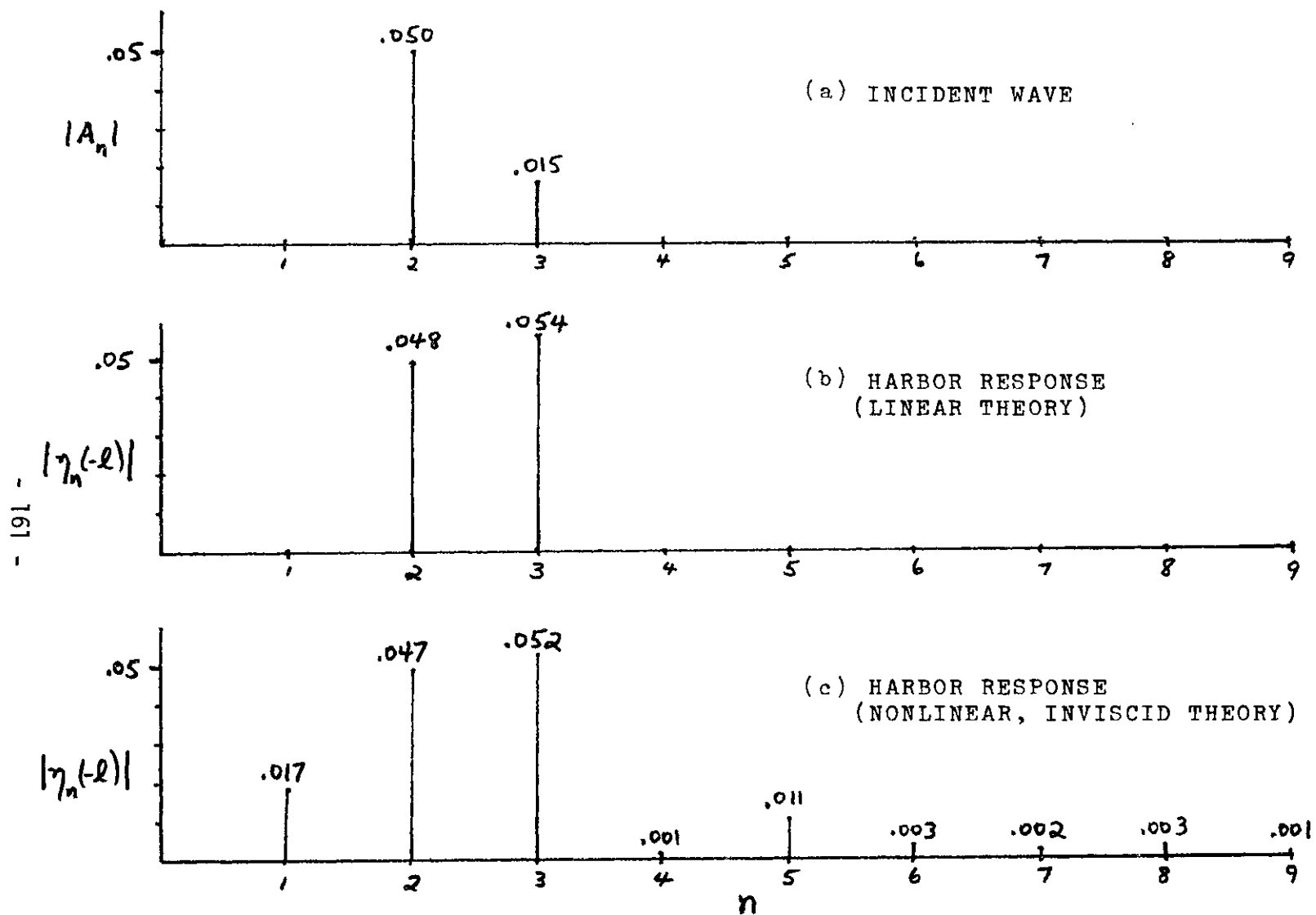


Fig. 5.13. Response of large-scale harbor to nonmonochromatic incident wave ($h = 20$ m., $2a = 100$ m., $L = 1000$ m., $A_2 = .050$, $A_3 = .015$, $\epsilon = 1.41$).

CHAPTER VI
CONCLUDING REMARKS

6.1 Validity of the Various Approximations

The proposed nonlinear theory for harbor resonance hinges on the smallness of three parameters-- ϵ , μ^2 , and δ --corresponding to the assumptions of weak nonlinearity, weak dispersion, and a narrow harbor entrance. The assumption $\epsilon \sim \mu^2 \ll 1$ is required by the depth-averaged Boussinesq equations; the smallness of δ permits a linear treatment of the radiated wave in the ocean and a one-dimensional treatment of the nonlinear response in the long, narrow bay.

Two major approximations are made in the present work, namely to decompose the solution into a finite number of harmonics and to use an impedance boundary condition at the harbor entrance. The impedance boundary condition is, however, only valid for the lowest few harmonics, hence the calculated higher harmonics may be quantitatively unreliable even if numerical convergence is achieved by including many harmonics. Nonetheless, the lowest few harmonics are expected to be substantially correct.

In a large scale harbor, the depth is usually comparable to or smaller than the entrance width, so that $\mu^2 \leq \delta^2 \ll \delta$. Therefore the condition $\delta \ll 1$ is generally more restrictive than the condition $\mu^2 \ll 1$; in other words, the assumption $\delta \ll 1$ is likely to break down before the assumption $\mu^2 \ll 1$. For this reason, future efforts should first be directed at removing the restriction on δ , rather than on μ^2 .

More will be said about this in Section 6.3.

6.2 On the Importance of Nonlinear and Frictional Effects

For monochromatic waves incident on a long, narrow bay, the principal effect of nonlinearity is to transfer energy from the linearly resonated first harmonic to higher harmonics. The efficiency with which higher harmonics are generated depends upon ϵ for a harbor having $\ell \ll 1/\mu^2$ and upon ϵ/μ^2 for a harbor with $\ell \geq 1/\mu^2$. In some cases, harmonic generation is enhanced by linear resonance occurring at an integral multiple of the fundamental frequency. For example, when the quarter-wave mode is excited by the incident wave, odd harmonics of the incident wave frequency generally lie close to the higher harbor modes and are therefore amplified. Similarly, when the fundamental frequency resonates one of the higher harbor modes, the influence of dispersion may cause the second harmonic to be linearly resonated also. This phenomenon gives partial explanation for some observed features in the experiments, for the second and third harbor lengths studied.

The energy relation of Section 3.4 indicates that energy is transferred to the higher harmonics at the expense of the first harmonic. The resonant amplification of the first harmonic, $|n_1(-\ell)/A_1|$, is therefore found to decrease with increasing incident wave amplitudes. Thus, linearized theory overestimates the resonant response of a harbor subject to monochromatic incident waves.

When the incident wave is not monochromatic, the difference tone of two high frequency components may excite a highly resonant harbor

mode occurring at a low frequency. In this case, nonlinear theory indicates that the harbor response may in fact be more severe than that predicted by linearized theory.

In all cases, harmonic distortion is to be expected from nonlinearity. In particular, the existence of a mean set-up, $\eta_0(x)$, which is highest at the back wall of the bay, is of practical importance, even though it is usually quite small. Further, the details of the frequency spectrum in the harbor may be important in designing mooring systems for ships in the harbor.

The primary effect of friction is to increase the total damping in the harbor. Boundary-layer dissipation is shown to be small compared to radiation damping, except in unusually long harbors. The effect of separation loss depends largely on the shape of the harbor entrance. For an entrance with sharp corners, separation loss may be as important as nonlinearity in damping the fundamental harmonic. For an asymmetrical harbor entrance, separation may contribute substantially to the mean set-up, $\eta_0(x)$; however, the generation of higher harmonics is usually much less than that due to nonlinearity in the far field of the harbor. Finally, separation is known to reduce the mass reactance of the entrance and this may slightly increase the characteristic frequencies of the resonant harbor modes.

6.3 Suggestions for Future Research

In this investigation, the long, narrow bay was chosen for its simplicity, and certain assumptions were made for convenience in the

mathematical formulation. Below we sketch how some of these limitations might be removed:

(1) Extension to harbors of arbitrary shape:

For a two-dimensional harbor, there is a greater variety of possible nonlinear interactions than in the one-dimensional, long, narrow bay. In particular, nonlinearity will couple waves intersecting at oblique angles. Since the density of linearly resonant modes (in frequency space) is greater in a two-dimensional harbor, harmonics generated by nonlinearity are more likely to be linearly resonated. Thus, nonlinear effects are expected to be even more important in a two-dimensional harbor than in the long, narrow bay.

At present, numerical procedures exist for solving the linear theory for harbors of arbitrary shape, see Lee (1971) and Chen and Mei (1975). The latter employ a hybrid analytical-finite element technique which is based upon a variational principle; in this regard, it may be useful to note that the Boussinesq equation can also be cast in variational form; see Whitham (1967b).

(2) Extension to slowly varying depth:

This involves a slight modification of the constant-depth Boussinesq equations and should present no theoretical difficulty; see Peregrine (1972).

The extension of the present theory to water of arbitrary depth involves the complete, three-dimensional theory sketched in Section 1.2. This is both difficult and unnecessary for most large harbors, which

typically resonate at frequencies that are well covered by the shallow-water approximation.

(3) Extension to harbor with wide entrances:

In the present theory, the matching conditions at the entrance are satisfied in an average way using an effective radiation impedance. This is unsuitable for wide entrances or for high frequency waves, such as might be generated through nonlinearity. A numerical procedure could be used to ensure exact matching at every point in the entrance.

(4) Entrance Loss:

When flow separation at sharp corners is significant, inviscid theory cannot be used to describe the flow field in the entrance. At present, an understanding of separation is perhaps more accessible through experiment than theory.

LIST OF REFERENCES

- Batchelor, G.K., *An Introduction to Fluid Dynamics*, Cambridge University Press, Cambridge, England, 1974, pp. 353-358.
- Benney, D.J. and Luke, J. C., "On the Interactions of Permanent Waves of Finite Amplitude", *J. of Mathematics and Physics*, Vol. 43, 1964, pp. 309-313.
- Benney, D. J. and Niell, A. M., "Apparent Resonances of Weakly Nonlinear Standing Waves", *J. of Mathematics and Physics*, Vol. 41, 1962, pp. 254-263.
- Biesel, F., "The Similitude of Scale Models for the Study of Seiches in Harbors", *Proc. of the Fifth Conference on Coastal Engineering*, Grenoble, France, 1954; Council Wave Research, Berkeley, California, 1955, pp. 95-118.
- Biesel, F., "Radiating Second-Order Phenomena in Gravity Waves", *Proc. of Tenth Congress of the International Association for Hydraulic Research*, Vol. 1, London, England, 1963, pp. 197-203.
- Bryant, P. J., "Periodic Waves in Shallow Water", *J. of Fluid Mechanics*, Vol. 59, Part 4, 1973, pp. 625-644.
- Chen, H. S. and Mei, C. C., "Oscillations and Wave Forces in a Man-Made Harbor in the Open Sea", *Proc. of the Tenth Symposium on Naval Hydrodynamics*, June, 1974 (in press).
- Chu, V. H. and Mei, C. C., "On Slowly Varying Stokes Waves", *J. of Fluid Mechanics*, Vol. 41, Part 4, 1970, pp. 873-887.
- Daily, J. W. and Harleman, D. R. F., *Fluid Dynamics*, Addison-Wesley, Reading, Mass., 1966, pp. 314-319.
- Gaillard, P., "Des Oscillations Non Lineaires des Eaux Portuaires", *Houille Blanche*, Vol. 15, 1960, pp. 164-172.
- Hwang, L. S. and Tuck, E. O., "On the Oscillations of Harbours of Arbitrary Shape", *J. of Fluid Mechanics*, Vol. 42, Part 3, 1970, pp. 447-464.
- Ingard, U., "Nonlinear Distortion of Sound Transmitted through an Orifice", *J. of the Acoustical Society of America*, Vol. 48, No. 1 (Part 1), 1970, pp. 32-33.
- Ingard, U. and Ising, H., "Acoustical Nonlinearity of an Orifice", *J. of the Acoustical Society of America*, Vol. 42, 1967, pp. 6-17.

- Ippen, A. T. and Goda, Y., "Wave Induced Oscillations in Harbours: The Solution for a Rectangular Harbour Connected to the Open Sea", Technical Report No. 59, Ralph M. Parsons Laboratory for Water Resources and Hydrodynamics, Dept. of Civil Engineering, M.I.T., Cambridge, Mass., July 1963.
- Ippen, A. T. and Raichlen, R., "Wave Induced Oscillations in Harbors: The Problem of Coupling of Highly Reflective Basins", Technical Report No. 49, Ralph M. Parsons Laboratory for Water Resources and Hydrodynamics, Dept. of Civil Engineering, M.I.T., Cambridge, Mass., 1962.
- Ito, Y., "On the Effect of Tsunami-Breakwater", *Coastal Engineering in Japan*, Vol. 13, 1970, pp. 89-102.
- Jarlan, G. E., "The Application of Acoustic Theory to the Reflective Properties of Coastal Engineering Structures", *Quarterly Bulletin*, National Research Council of Canada, Ottawa, Canada, No. 1965, 1 (Apr.), pp. 23-63.
- Jonsson, I. G. and Carlsen, N. A., "Experimental and Theoretical Investigation in an Oscillatory Turbulent Boundary Layer", *J. of Hydraulic Research*. Vol. 14, No. 1, 1976, pp. 45-60.
- Kim, Y. Y. and Hanratty, J. J., "Weak Quadratic Interactions of Two-Dimensional Waves", *J. of Fluid Mechanics*, Vol. 50, Part 1, 1971, pp. 107-132.
- Lee, J. J., "Wave-Induced Oscillations in Harbors of Arbitrary Geometry", *J. of Fluid Mechanics*, Vol. 45, Part 2, 1971, pp. 375-394.
- Longuet-Higgins, M. S., "Resonant Interaction Between Two Trains of Gravity Waves", *J. of Fluid Mechanics*, Vol. 12, 1962, pp. 321-332.
- Mei, C. C. and Chen, H. S., "Hybrid-Element Method for Water Waves", *Proc. of the Symposium on Modeling Techniques*, American Society of Civil Engineers, 1975.
- Mei, C. C., Lui, P. L-F., and Ippen, A. T., "Quadratic Loss and Scattering of Long Waves", *J. of the Waterways, Harbors, and Coastal Engineering Division*, WW3, 1974, pp. 217-239.
- Mei, C. C. and Unluata, U., "Harmonic Generation in Shallow Water Waves", *Waves on Beaches and Resulting Sediment Transport*, Academic Press, New York, 1972, pp. 181-202.
- Mei, C. C. and Unluata, U., "Resonant Scattering by a Harbor with Two Coupled Basins", *J. of Engineering Mathematics*, Vol. 10, No. 4, 1976, pp. 333-353.

- Miles, J. W. and Munk, W. H., "Harbor Paradox", *J. of the Waterways and Harbors Division*, Proc. of the American Society of Civil Engineers, Vol 87, 1961, pp. 111-130.
- Morse, P. M. and Feshback, H., *Methods of Theoretical Physics*, Vol. I, McGraw-Hill, New York, 1953, pp. 814-815.
- Peregrine, D. H., "Equations for Water Waves and the Approximations behind Them", *Waves on Beaches and Resulting Sediment Transport*, Academic Press, New York, 1972, pp. 95-121.
- Phillips, O. M., "On the Dynamics of Unsteady Gravity Waves of Finite Amplitude. Part I. The Elementary Interactions", *J. of Fluid Mechanics*, Vol. 9, 1960, pp. 193-217.
- Phillips, O. M., *The Dynamics of the Upper Ocean*, Cambridge University Press, Cambridge, 1966, pp. 42-43.
- Phillips, O. M., "Nonlinear Dispersive Waves", *Annual Review of Fluid Mechanics*, Vol. 6, Annual Reviews, Inc., Palo Alto, California, 1974, pp. 93-110.
- Raichlen, F. and Ippen, A. T., "Wave Induced Oscillations in Harbours", *J. of the Hydraulics Division*, American Society of Civil Engineers, Vol. 91, No. HY2, 1965, pp. 1-26.
- Stoker, J. J., *Water Waves*, Interscience Publishers, Inc., New York, 1957, pp. 174-181.
- Tadjbakhsh, I. and Keller, J. B., "Standing Surface Waves of Finite Amplitude", *J. of Fluid Mechanics*, Vol. 8, 1960, pp. 442-451.
- Terrett, F. L., Osorio, J. D. C., and Lean, G. H., "Model Studies of a Perforated Breakwater", *Proc. of the Eleventh Conference on Coastal Engineering*, 1968, pp. 1104-1109.
- Unluata, U. and Mei, C. C., "Long Wave Excitation in Harbours--An Analytical Study", Technical Report No. 171, Ralph M. Parsons Laboratory for Water Resources and Hydrodynamics, Dept. of Civil Engineering, M.I.T., Cambridge, Mass., 1973.
- Unluata, U. and Mei, C. C., "Effects of Entrance Loss on Harbor Oscillations", *J. of the Waterways, Harbors and Coastal Engineering Division*, Proc. of the American Society of Civil Engineers, Vol. 101, No. WW2, 1975.
- Ursell, F., "Edge Waves on a Sloping Beach", *Proc. Royal Soc. A*, Vol. 214, 1952, p. 79.
- Verhagen, J. and van Wijngaarden, L., "Nonlinear Oscillations of Fluid in a Container", *J. of Fluid Mechanics*, Vol. 22, 1965, pp. 737-751.

- Whitham, G. B., "A General Approach to Linear and Non-Linear Dispersive Waves Using a Lagrangian", *J. of Fluid Mechanics*, Vol. 22, 1965, pp. 273-283.
- Whitham, G. B., "Nonlinear Dispersion of Water Waves", *J. of Fluid Mechanics*, Vol. 27, 1967, pp. 399-412.
- Whitham, G. B., "Variational Methods and Applications to Water Waves", *Proc. Roy. Soc. of London, Series A*, Vol. 299, 1967, pp. 6-25.
- Wilson, B. N., *XIX International Navigation Congress*, Section II, Communication 1, London, 1957, pp. 13-61.

APPENDIX A
NUMERICAL ITERATION PROCEDURE FOR SOLVING A NONLINEAR,
TWO-POINT BOUNDARY VALUE PROBLEM

The following is a FORTRAN IV computer program which solves the boundary value problem posed in Section 3.5. The variable names follow closely the notation used in Section 3.5. The principal variables are:

- XLONG -- harbor length (L)
- XWIDE -- Harbor width (2a)
- XDEEP -- harbor depth (h)
- FRICT -- friction factor (\bar{f}) in separation loss theory
- NHMAX -- maximum number of harmonics
- NH -- number of harmonics at a given point in the iteration procedure. $NH \leq NHMAX$.
- Z -- an array of size NHMAX containing the radiation impedance for each harmonic
- A -- an array of size NHMAX containing twice the incident wave amplitude for each harmonic
- R,DR -- arrays of size $(NHMAX)^2$ containing the coupling constants for the nonlinear equations
- B -- an array of size $(NPT)(NHMAX)$ containing the current solution for $\eta_n(x_j)$, $n = 1, 2, \dots, NH$, $J = 1, 2, \dots, NPT$
- E -- an array of size $(NPT)(NHMAX)^2$ containing the NH basis solutions $e_n(x_j)$, $n = 1, 2, \dots, NH$, $J = 1, 2, \dots, NPT$

On the IBM 370 computer at the M.I.T. Information Processing Center, the total storage required by the program was found to be

$$\text{Storage (in Kilobytes)} = 52 + 8(NPT)(NHMAX)(NHMAX + 1)/1024$$

The execution time for an iteration with NH harmonics was found to be approximately

$$\text{Time (in } \mu\text{sec)} = 8 (\text{NPT})(\text{NH})^3$$

For example, with NPT = 135 and NH = NHMAX = 10, the total storage required is 168 kilobytes, and the execution time per iteration is approximately 1.08 seconds.

C*****	MAIN PROGRAM: COMPUTES INPUTS TO SUBROUTINE BVP	MAIN0001
	CCOMPLEX A(20),Z(20)	MAIN0002
	REAL W(20)	MAIN0003
	CCOMCN /AREA1/A,Z,W,H,NPT,NHMAX,FRICT	MAIN0004
	DATA XDEEP,XWIDE,XLONG/20.,100.,1000./	MAIN0005
	CALL TIMING(ISTART)	MAIN0006
	READ(5,*) ITIME	MAIN0007
	ISTART=ISTART+6000*ITIME	MAIN0008
	NHMAX=10	MAIN0009
	WRITE(6,902) NHMAX,XDEEP,XWIDE,XLONG	MAIN0010
	WRITE(7,902) NHMAX,XDEEP,XWIDE,XLONG	MAIN0011
902	FORMAT(' NHMAX,XDEEP,XWIDE,XLONG=',I3,3F10.1)	MAIN0012
	DO 1 I=2,NHMAX	MAIN0013
1	A(I)=(0.,0.)	MAIN0014
	CALL COUPLE	MAIN0015
5	READ(5,*) XL1,XL2,NXL,XHIGH,IPT,NH1,FRICT	MAIN0016
	IF (NXL .LT. 0) GO TO 999	MAIN0017
	FRICT=FRICT*4./ (3.*3.1415926)	MAIN0018
	A(1)=(1.,0.)*XHIGH/XDEEP	MAIN0019
	DO 20 J=1,NXL	MAIN0020
	XL = XL1+(J-1)*XL2	MAIN0021
	XA = XL*.5*XWIDE/XLONG	MAIN0022
	XH = XL*XDEEP/XLONG	MAIN0023
	NPT=2+IPT*XL/.0628	MAIN0024
	H=XL/(NPT-1)	MAIN0025
	WRITE(6,901) NPT,XHIGH,XL,XA,XH,H,FRICT	MAIN0026
	WRITE(7,901) NPT,XHIGH,XL,XA,XH,H,FRICT	MAIN0027
901	FORMAT(' NPT,XHIGH,XL,XA,XH,H=',I3,F6.2,4F10.6/' FRICT='F10.6)	MAIN0028
	DO 10 I=1,NHMAX	MAIN0029
	Q=I*SQRT(1.+I*I*XH*XH/3.)	MAIN0030
	Z(I)=(0.,-1.)*XA+.637*XA*(ALOG(Q*XA)-.875)	MAIN0031
	W(I)=1.+ .5*H*H*Q*Q	MAIN0032
	Q=1./CABS(COS(Q*XL)+Q*Z(I)*SIN(Q*XL))	MAIN0033
10	WRITE(6,900) I,Q	MAIN0034
900	FORMAT(' AMPLIFICATION OF HARMONIC ',I2,'=',F8.4)	MAIN0035
	CALL BVP(NH1,ISTART)	MAIN0036

- 173 -

```
20 IF (NPT .LT. 0) GO TO 999
CONTINUE
GC TO 5
999 STOP
END
```

```
MAIN0037
MAIN0038
MAIN0039
MAIN0040
MAIN0041
```

```

SUBROUTINE COUPLL
C*****COMPUTES COUPLING CONSTANTS FOR THE NONLINEAR EQUATIONS
REAL R(20,20),DR(20,20)
COMMON /AREA2/R,DR
DO 10 I=1,20
DO 5 L=1,20
IF (L .EQ. I) GO TO 5
Q=.5-.25*(1/(1+3*(2*L-I)))
R(I,L)=Q*(I*I-2*L*L+2*I*L)
DR(I,L)=- (I+L)*Q/(I-L) - (2*I-L)*Q/L
5 CONTINUE
10 CONTINUE
RETURN
END

```

```

COUP0001
COUP0002
COUP0003
COUP0004
COUP0005
COUP0006
COUP0007
COUP0008
COUP0009
COUP0010
COUP0011
COUP0012
COUP0013
COUP0014

```

	SUBROUTINE BVP(NH1,ISTART)	BVP 0001
	C*****SOLVES A BOUNDARY VALUL PROBLEM CONSISTING OF N COUPLED,	BVP 0002
	C*****NONLINEAR, SFCOND-CREEP DIFFERENTIAL EQUATIONS SUBJECT TO	BVP 0003
	C*****TWO-POINT BOUNDARY CONDITIONS	BVP 0004
	COMPLEX B(1350),E(13500)	BVP 0005
	COMPLEX S(20,20),C(20),Z(20),CCNJG,CQ,A(20)	BVP 0006
	REAL W(20),R(20,20),DR(20,20)	BVP 0007
	REAL BPRINT(10)	BVP 0008
	COMMON /AREA1/A,Z,W,H,NPT,NHMAX,FRICT/AREA2/R,DR/AREA3/S,C	BVP 0009
	IF (NH1 .GT. 0) GC TO 5	BVP 0010
	DC 10 J=1,NPT	BVP 0011
	JX=(J-1)*NHMAX	BVP 0012
	DC 10 I=1,NHMAX	BVP 0013
10	B(I+JX)=(0.,0.)	BVP 0014
5	NP=NPT-1	BVP 0015
.	NHP=NHMAX*NPT	BVP 0016
176	DC 80 NH=1,NHMAX	BVP 0017
-	QRELAX=1.	BVP 0018
15	ITER=0	BVP 0019
	ITER=ITER+1	BVP 0020
	IF (ITER .GT. 50) GO TO 82	BVP 0021
	CALL TIMING(ISTCP)	BVP 0022
	ILEFT=ISTART-ISIOP	BVP 0023
	WRITE(6,899) ILEFT,NH	BVP 0024
899	FORMAT(115X,I10,2X,I3)	BVP 0025
	IF (ILEFT .LT. 1000) GC TO 81	BVP 0026
	DC 50 K=1,NH	BVP 0027
	KX=NHP*(K-1)	BVP 0028
	DC 20 I=1,NH	BVP 0029
20	E(I+KX)=1/(1+3*(I-K))	BVP 0030
	DC 35 J=1, NP	BVP 0031
	JX=(J-1)*NHMAX	BVP 0032
	KX=NHMAX*(1-1/J)	BVP 0033
	DC 35 I=1,NH	BVP 0034
	IX=I+JX+KX	BVP 0035
	CQ=(C.,0.)	BVP 0036

	I2=I/2	BVP 0037
	DC 300 L=1, NH	BVP 0038
	IF ((I2/L) - (L/(I+1))) 200, 300, 100	BVP 0039
100	CQ=CQ+R(I, L)*B(L+JX)*E(IX-L)+DR(I, L)*(B(L+JX)-B(L+JX-NX))*(E(IX-L)	BVP 0040
	* -E(IX-L-NX))/(H*H)	BVP 0041
	GO TO 300	BVP 0042
200	LX=L+JX	BVP 0043
	CQ=CQ+R(I, L)*CONJG(B(LX-I))*E(LX+KX)	BVP 0044
	* +DR(I, L)*CONJG(B(LX-I)-B(LX-I-NX))*(E(LX+KX)-E(LX+KX-NX))/(H*H)	BVP 0045
300	CONTINUE	BVP 0046
	CQ=(.5*H*H*CQ+E(IX))/W(I)	BVP 0047
35	E(IX+NHMAX)=CQ+(NX/NHMAX)*(CQ-F(IX-NX))	BVP 0048
	C(K)=A(K)	BVP 0049
	DO 50 I=1, NH	BVP 0050
	JX=I+NHP-NHMAX	BVP 0051
	IX=JX+(K-1)*NHP	BVP 0052
	CQ=Z(I)+FRICT*(0., -1.)*CABS(B(JX)-B(JX-NHMAX))/(H*I*I)	BVP 0053
50	S(I, K)=E(IX)-CQ*(E(IX)-E(IX-NHMAX))/H	BVP 0054
	CALL SYSN(NH)	BVP 0055
	Q=QRELAX	BVP 0056
	ICVRG=0	BVP 0057
	IGOOD=0	BVP 0058
	DO 70 J=1, NPT	BVP 0059
	JX=(J-1)*NHMAX	BVP 0060
	DC 65 I=1, NH	BVP 0061
	IX=I+JX	BVP 0062
	CQ=-Q*B(IX)+Q*C(1)*E(IX)	BVP 0063
	IF (NH.LT. 2) GO TO 61	BVP 0064
	DC 60 K=2, NH	BVP 0065
60	CQ=CQ+Q*C(K)*F(IX+(K-1)*NHP)	BVP 0066
61	ICVRG=ICVRG+CABS(CQ)/.001	BVP 0067
65	B(IX)=B(IX)+CQ	BVP 0068
70	IGOOD=IGOOD+CABS(B(NH+JX))/.001	BVP 0069
	WRITE(6, 900) (B(I), I=1, NH)	BVP 0070
900	FORMAT(1X, 3P10F12.6)	BVP 0071
	QRELAX=.5	BVP 0072

	IF (ICVRG .GT. 0) GC TO 15	BVP 0073
	IF (IGCOD .EQ. 0) GC TO 85	BVP 0074
30	CONTINUE	BVP 0075
	NH=NHMAX	BVP 0076
	WRITE(6,980)	BVP 0077
	WRITE(7,980)	BVP 0078
980	FORMAT(' MORE HARMONICS NEEDED')	BVP 0079
	GO TO 85	BVP 0080
81	WRITE(6,981)	BVP 0081
	WRITE(7,981)	BVP 0082
981	FORMAT(' TIME RAN OUT')	BVP 0083
	NPT=-1	BVP 0084
	GC TO 85	BVP 0085
82	WRITE(6,982)	BVP 0086
	WRITE(7,982)	BVP 0087
982	FORMAT(' NOT CONVERGENT')	BVP 0088
85	WRITE(6,901) NH	BVP 0089
	WRITE(7,901) NH	BVP 0090
901	FORMAT(' NH=',I3)	BVP 0091
	DO 90 J=1,NPT	BVP 0092
	DO 91 I=1,NH	BVP 0093
91	BPRINT(I)=CAES(B(I+(J-1)*NHMAX))	BVP 0094
	WRITE(6,902) (BPRINT(I),E(I+(J-1)*NHMAX), I=1,NH)	BVP 0095
902	FORMAT(1X,3P15F8.3)	BVP 0096
90	CONTINUE	BVP 0097
	WRITE(6,903)	BVP 0098
903	FORMAT(1H1)	BVP 0099
	RETURN	BVP 0100
	END	BVP 0101

```

SUBROUTINE SYSN (NH)
C*****SOLVES A SYSTEM OF N LINEAR ALGEBRAIC EQUATIONS
COMPLEX S (20,20) ,C (20) ,PVT
COMMON /AREA3/S,C
DO 50 K=1,NH
PVT=S (K,K)
IF (CABS (PVT) .LT. 1.E-5) WRITE (1,90)
C (K)=C (K)/PVT
DO 20 J=K,NH
20 S (K,J)=S (K,J)/PVT
DO 40 I=1,NH
IF (I .EQ. K) GO TO 40
PVT=S (I,K)
C (I)=C (I)-PVT*C (K)
DO 30 J=K,NH
30 S (I,J)=S (I,J)-PVT*S (K,J)
40 CONTINUE
50 CONTINUE
90 FORMAT (' **SYSN SINGULAR**')
RETURN
END

```

```

SYSN0001
SYSN0002
SYSN0003
SYSN0004
SYSN0005
SYSN0006
SYSN0007
SYSN0008
SYSN0009
SYSN0010
SYSN0011
SYSN0012
SYSN0013
SYSN0014
SYSN0015
SYSN0016
SYSN0017
SYSN0018
SYSN0019
SYSN0020
SYSN0021

```

C*****SAMPLE INPUT DATA

20
.25 .25 4 .6 1 -1 .35
1.21 .04 11 .6 1 -1 .35
1.75 .25 8 .6 1 -1 .35
3.72 .12 11 .6 1 -1 .35
5.25 .25 5 .6 1 -1 .35
6.36 .20 11 .6 1 -1 .35
1.41 1. 1 .6 1 -1 0.
1.41 1. 1 .5 1 -1 0.
1.41 1. 1 .4 1 -1 0.
1.41 1. 1 .3 1 -1 0.
1.41 1. 1 .2 1 -1 0.
1.41 1. 1 .1 1 -1 0.
1.41 1. 1 .6 1 -1 .35
1.41 1. 1 .5 1 -1 .35
1.41 1. 1 .4 1 -1 .35
1.41 1. 1 .3 1 -1 .35
1.41 1. 1 .2 1 -1 .35
1.41 1. 1 .1 1 -1 .35
4.36 1. 1 .6 1 -1 0.
4.36 1. 1 .5 1 -1 0.
4.36 1. 1 .4 1 -1 0.
4.36 1. 1 .3 1 -1 0.
4.36 1. 1 .2 1 -1 0.
4.36 1. 1 .1 1 -1 0.
4.36 1. 1 .6 1 -1 .35
4.36 1. 1 .5 1 -1 .35
4.36 1. 1 .4 1 -1 .35
4.36 1. 1 .3 1 -1 .35
4.36 1. 1 .2 1 -1 .35
4.36 1. 1 .1 1 -1 .35
7.36 1. 1 .6 1 -1 0.
7.36 1. 1 .5 1 -1 0.
7.36 1. 1 .4 1 -1 0.
7.36 1. 1 .3 1 -1 0.

(output for this case on p. 181)

DATA0001
DATA0002
DATA0003
DATA0004
DATA0005
DATA0006
DATA0007
DATA0008
DATA0009
DATA0010
DATA0011
DATA0012
DATA0013
DATA0014
DATA0015
DATA0016
DATA0017
DATA0018
DATA0019
DATA0020
DATA0021
DATA0022
DATA0023
DATA0024
DATA0025
DATA0026
DATA0027
DATA0028
DATA0029
DATA0030
DATA0031
DATA0032
DATA0033
DATA0034
DATA0035
DATA0036

APPENDIX B

FOURIER ANALYSIS OF EXPERIMENTAL DATA

The following is a BASIC computer program which Fourier analyzes the experimental data, while the experiment is in progress. The execution of the program is remotely controlled by a switch, as explained in section 4.1.3. The principal variables in the program are:

T -- number of voltage readings taken in one complete wave period

K1 -- number of harmonics analyzed

C -- a calibration factor

F -- an array containing (T+1) voltage readings

A -- a discrete Fourier cosine transform

B -- a discrete Fourier sine transform

The instruction CALL(1,D,F) reads the external Hewlett Packard 3450A Multi-Function Meter and stores the voltage reading under the variable name D.

```

10 DIM F[30]
20 READ T,K1,C
30 DATA 22,4,1
40 LET T1=T+1
50 LET I=-2
55 LET I=I+2
60 GOSUB 1000
70 FOR J=1 TO T1
80 CALL (I,D,F)
90 LET F[J]=D
100 NEXT J
110 GOSUB 3000
120 GOTO 55
130 STOP
1000 REM ***** SWITCHING ROUTINE *****
1010 CALL (I,D,F)
1020 IF D >= 5 THEN 1040
1030 GOTO 1010
1040 CALL (I,D,F)
1050 IF D <= 5 THEN 1070
1060 GOTO 1040
1070 WAIT (500)
1080 RETURN
3000 REM ***** FOURIER ANALYSIS *****
3010 PRINT I
3020 LET F[1]=(F[1]+F[T1])/2
3030 LET H=6.28318/T
3040 FOR K=1 TO K1
3050 LET A=B=0
3060 FOR J=1 TO T1-1
3070 LET A=A+F[J]*COS((J-1)*K*H)
3080 LET B=B+F[J]*SIN((J-1)*K*H)
3090 NEXT J
3100 PRINT 2*SQR(A*A+B*B)/T/C,
3110 LET P[K]=ATN(B/A)+(1-SGN(A))*1.5708
3120 NEXT K
3130 PRINT
3140 PRINT " ",
3150 FOR K=2 TO K1
3160 LET P=P[K]-K*P[1]
3170 PRINT P-6.28318*INT(P/6.28318),
3180 NEXT K
3190 PRINT
3200 RETURN
9999 END

```

BIOGRAPHY

Steven R. Rogers was born on February 28, 1952, in Washington, D. C. . His primary education was received at the Hebrew Academy of Washington and his secondary education at the Talmudical Academy of Baltimore and Montgomery Blair High School of Silver Spring.

He was awarded a Bachelor of Science degree in physics by M. I. T. in June, 1972. His bachelor's thesis, "Ising Chain with Random Magnetic Moments", appears in *Studies in Applied Mathematics*, Vol. 52, No. 2, 1973, pp. 163-173. A fellowship from the Fannie and John Hertz Foundation of Los Angeles, California, has enabled him to pursue graduate studies at M. I. T. .

His employment experience includes work at the Technion-- Israel Institute of Technology (1974), the Weizmann Institute of Science (1972), and the X-ray Exposure Control Laboratory (1970 and 1971), where he served as a commissioned officer in the U. S. Public Health Service.

The author is a member of the American Physical Society and the American Geophysical Union, and is a licensed amateur radio operator. He is also a member of Phi Beta Kappa and Sigma Xi honorary associations.